Role of the Arctic snow cover in high-latitude hydrological cycle asrevealed by climate model simulations

María Santolaria Otín

Communauté UNIVERSITÉ Grenoble Alpes

THÈSE

Pour obtenir le grade de

DOCTEUR DE LA COMMUNAUTÉ UNIVERSITÉ GRENOBLE ALPES

Spécialité : Sciences de la Terre et de l'Univers et de l'Environnement (CESTUE)

Arrêté ministériel : 25 mai 2016

Présentée par

María SANTOLARIA OTIN

Thèse dirigée par **Olga ZOLINA**, Enseignant-chercheur, Communauté Université Grenoble Alpes

préparée au sein du **Laboratoire Institut des Géosciences de l'Environnement**
dans **l'École Doctorale Terre, Univers, Environnement**

Le rôle de la couverture de neige de l'Arctique dans le cycle hydrologique de hautes latitudes révélé par les simulations des modèles climatiques

Role of the Arctic snow cover in high-latitude hydrological cycle as revealed by climate model simulations

Thèse soutenue publiquement le **4 novembre 2019**,
devant le jury composé de :

Madame OLGA ZOLINA
MAITRE DE CONFERENCES, UNIVERSITE GRENOBLE ALPES, Directeur de thèse
Monsieur PAVEL GROISMAN
DOCTEUR EN SCIENCES, SCIENCES & SCE. D'HYDROLOGIE-ASHEVILLE, Rapporteur
Monsieur NOEL KEENLYSIDE
PROFESSEUR, UNIVERSITE BERGEN - NORVEGE, Rapporteur
Monsieur GERHARD KRINNER
DIRECTEUR DE RECHERCHE, CNRS DELEGATION ALPES, Président
Monsieur MARTIN WEGMANN
DOCTEUR EN SCIENCES, INSTITUT ALFRED WEGENER ALLEMAGNE, Examinateur
Monsieur SERGEY GULEV
PROFESSEUR, ACADEMIE DES SCIENCES DE RUSSIE, Examinateur

'La filosofía está escrita en ese libro enorme que tenemos continuamente abierto delante de nuestros ojos (hablo del universo), pero que no puede entenderse si no aprendemos primero a comprender la lengua y a conocer los caracteres con que se ha escrito. Está escrito en lengua matemática, y los caracteres son triángulos, círculos y otras figuras geométricas sin los cuales es humanamente imposible entender una palabra ; sin ellos se deambula en vano por un laberinto oscuro."

"Il saggiatore", Galileo Galilei (1623)

Remerciements

During these three years, ma vie s'est déroulée toujours dans trois langues. Así que en mis agradecimientos vais a tener que entrar en mi cabeza . . .

First, I would like to thank my supervisor, Olga Zolina, for the trust and confidence that she has put in me during these three years. I have felt free and guided to fully explore the Arctic. I am very thankful to the rapporteurs of this PhD, Noel Keenlyside and Pavel Groisman, for accepting the review of the manuscript. In particular, I would like to thank Noel Keenlyside for inviting me to Bergen, and to give me such a warm welcome in his team. I acknowledge the serenity and the wise advice of Pavel Groisman, they have been always very pertinent and useful for my research. I am very thankful to rest of jury : Gerhard Krinner, for sharing his endless wisdom of the CMIP world ; Sergey Gulev, for looking after my PhD since the very beginning and Martin Wegmann, for all his support and motivation over these three years. I would like to thank also the members of the ARCTIC-ERA Project, it has been always a pleasure to meet them all over the world. In particular, I thank Dmitry Streletskiy to make me discover the real permafrost of the Arctic Tundra.

Il me tient à cœur de remercier Martin Ménégoz, qui m'a aidée à faire les premiers pas au BSC et qui m'a introduite à ce merveilleux monde de la cryosphere.

Je dédie un grand remerciement à Ambroise Dufour, pour les trois années partagées entre lignes de code, transmission d'expérience et savoir et surtout, pour sa sérénité et sa précieuse et incalculable aide sur la fin.

Ça a été un grand plaisir d'avoir été entouré de glaciologues, climatologues, nivologues et même des sismologues pendant ces trois ans. Dans ce labo, on sent que les différents chemins de recherche se croisent ainsi que les différentes passions. Je voudrais remercier tous les gens du labo qui m'ont encouragée surtout dans la dernière ligne droite avec des petits mots echangés dans les couloirs. Les sourires du publique de la Salle Llibourty le jour de ma soutenance, toutes les félicitations et les discussions d'après donnent vraiment envie de partager ton travail, elles te font sentir que, en fait, tu appartiens aussi à cette communauté scientifique.

"Les jours passent vite quand on s'amuse" et c'est ce qui s'est passé : les midis à EVE, les soirées au Labo ("le bon"), les weekends en montagne, dans les Calanques ou n'importe où mais haut, donnent des très bons souvenirs, et tout ça c'est grâce à la bonne ambiance entre tous les

doctorants (et pas que) du labo. C'était un grand plaisir de partager ces trois ans avec mes collègues de promo : Jai, Marion, Lucas et Kévin. On l'a super bien réussi, bravo à nous tous ! Je pense que chacun a apporté son truc à cette mini équipe. Aussi, je tiens à remercier les "anciens" doctorants qui nous balisent le chemin (Etienne, Olivier, Fanny, Ilan, Cédric, Julien Beaumet, Joseph . . .) ainsi qu'aux "nouveaux" doctorants qui apportent de la fraîcheur dans le laboratoire (Ugo, Jordi, Sarah. . .). Quelques mots spéciaux pour mes très chères co-bureaux Jinhwa Shin et Albane Barbero : j'ai eu une chance énorme d'être tombée dans ce bureau (même si ça caille en hiver) et d'avoir pu partager avec vous nos intimes inquiètudes et joies ("Wait wait, close the door !"). Gabi, mi querida menina, no sé que hubiese hecho sin ti. También va para ti Marta, por esos vinitos a -2 °C en la terraza de Place Saint Eynard, arreglando el mundo así como si nada.

Esta tesis también va dedicada a todas mis amigas de Huesca, que han escuchado mis chapadas sobre el cambio climático y el Ártico con los ojos y oídos abiertos durante todos estos años. Y sobre todo, durante este largo verano, por hacerme olvidar el manuscrito durante un ratito en compañía de unos buenos kikos y una caña fresquita en el Candolias. Todo este esfuerzo no hubiese sido posible sin mi familia. Mil gracias a mi Tía Chus, a Jota y a Santi por venir a verme a esta ciudad lejana entre montañas. Muchas gracias a Laura por la ayuda logística y culinaria. Es fácil volar sin alas cuando tienes un buen paracaídas, y eso es lo que son mi madre, mi padre y mi hermano. Quizás sin saberlo, cada uno ha aportado su grano de arena a este trabajo y a su autora : la pasión y la alegría de mi madre, la razón y calma de mi padre y la experiencia y creatividad científica de mi hermano. Con todo esto no se puede fallar. Y por último pero no menos importante, merci Julien Brondex, tu m'a toujours apporté la lumière dans cette longue course.

En fin, *tout est bien qui finit bien* !

Résumé

La neige est une composante essentielle du système climatique arctique. Au nord de l'Eurasie et de l'Amérique du Nord, la couverture neigeuse est présente de 7 à 10 mois par an et son extension saisonnière maximale représente plus de 40% de la surface terrestre de l'hémisphère nord. La neige affecte une variété de processus climatiques et de rétroactions aux hautes latitudes. Sa forte réflectivité et sa faible conductivité thermique ont un effet de refroidissement et modulent la rétroaction neige-albédo. Sa contribution au bilan radiatif de la Terre est comparable à celle de la banquise. De plus, en empêchant d'importantes pertes d'énergie du sol sous-jacent, la neige limite la progression de la glace et le développement du pergélisol saisonnier. Réserve d'eau naturelle, la neige joue un rôle essentiel dans le cycle hydrologique aux hautes latitudes, notamment en ce qui concerne l'évaporation et le ruissellement. La neige est l'une des composantes du système climatique présentant la plus forte variabilité. Le réchauffement de l'Arctique étant deux fois plus rapide que celui du reste du globe, la variabilité présente et future des caractéristiques de la neige est cruciale pour une meilleure compréhension des processus et des changements climatiques. Cependant, notre capacité à observer l'Arctique terrestre étant limitée, les modèles climatiques jouent un rôle clé dans notre aptitude à comprendre les processus liés à la neige. À cet égard, la représentation des rétroactions associées à la neige dans les modèles climatiques, en particulier pendant les saisons intermédiaires (lorsque la couverture neigeuse de l'Arctique présente la plus forte variabilité), est primordiale.

Notre étude porte principalement sur la représentation de la neige terrestre arctique dans les modèles de circulation générale issus du projet CMIP5 (Coupled Model Intercomparison Project) au cours du printemps (mars-avril) et de l'automne (octobre-novembre) de 1979 à 2005. Les caractéristiques de la neige des modèles de circulation générale ont été validées par rapport aux mesures de neige in situ, ainsi qu'à des produits satellitaires et à des réanalyses.

Nous avons constaté que les caractéristiques de la neige dans les modèles ont un biais plus marqué au printemps qu'en automne. Le cycle annuel de la couverture neigeuse est bien reproduit par les modèles. Cependant, les cycles annuels d'équivalent en eau de la neige et de sa profondeur sont largement surestimés par les modèles, notamment en Amérique du Nord. Il y a un meilleur accord entre les modèles et les observations dans la position de la marge de neige au printemps plutôt qu'en automne. Les amplitudes de variabilité interannuelle pour toutes les variables de la neige sont nettement sous-estimées par la plupart des modèles CMIP5. Pour les deux saisons, les tendances des variables de la neige dans les modèles sont principalement négatives, mais plus faibles et moins significatives que celles observées. Les distributions spatiales des tendances de la couverture neigeuse sont relativement bien reproduites par les modèles, toutefois, la distribution spatiale des tendances en équivalent-eau et en profondeur de la neige présente de fortes hétérogénéités régionales.

Enfin, nous concluons que les modèles CMIP5 fournissent des informations précieuses sur les caractéristiques de la neige en Arctique terrestre, mais qu'ils présentent encore des limites. Il y a un manque d'accord entre l'ensemble des modèles sur la distribution spatiale de la neige par rapport aux observations et aux réanalyses. Ces écarts sont particulièrement marqués dans les régions où la variabilité de la neige est la plus forte. Notre objectif dans cette étude était d'identifier les circonstances dans lesquelles ces modèles reproduisent ou non les caractéristiques observées de la neige en Arctique. Nous attirons l'attention de la communauté scientifique sur la nécessité de prendre compte nos résultats pour les futures études climatiques.

Mots clés : Caractéristiques de la neige, climat arctique, modèles CMIP5, réanalyses, stations de neige.

Abstract

Snow is a critical component of the Arctic climate system. Over Northern Eurasia and North America the duration of snow cover is 7 to 10 months per year and a maximum snow extension is over 40% of the Northern Hemisphere land each year. Snow affects a variety of high latitude climate processes and feedbacks. High reflectivity of snow and low thermal conductivity have a cooling effect and modulates the snow-albedo feedback. A contribution from terrestrial snow to the Earth's radiation budget at the top of the atmosphere is close to that from the sea ice. Snow also prevents large energy losses from the underlying soil and notably the ice growth and the development of seasonal permafrost. Being a natural water storage, snow plays a critical role in high latitude hydrological cycle, including evaporation and run-off. Snow is also one of the most variable components of climate system. With the Arctic warming twice as fast as the globe, the present and future variability of snow characteristics are crucially important for better understanding of the processes and changes undergoing with climate. However, our capacity to observe the terrestrial Arctic is limited compared to the mid-latitudes and climate models play very important role in our ability to understand the snow-related processes especially in the context of a warming cryosphere. In this respect representation of snow-associated feedbacks in climate models, especially during the shoulder seasons (when Arctic snow cover exhibits the strongest variability) is of a special interest.

The focus of this study is on the representation of the Arctic terrestrial snow in global circulation models from Coupled Model Intercomparison Project (CMIP5) ensemble during the melting (March-April) and the onset (October-November) season for the period from 1979 to 2005. Snow characteristics from the general circulation models have been validated against in situ snow measurements, different satellite-based products and reanalyses.

We found that snow characteristics in models have stronger bias in spring than in autumn. The annual cycle of snow cover is well captured by models in comparison with observations, however, the annual cycles of snow water equivalent and snow depth are largely overestimated by models, especially in North America. There is better agreement between models and observations in the snow margin position in spring rather than in autumn. Magnitudes of interannual variability for all snow characteristics are significantly underestimated in most CMIP5 models compared to observations. For both seasons, trends of snow characteristics in models are primarily negative but weaker and less significant than those from observations. The patterns of snow cover trends are relatively well reproduced in models, however, the spatial distribution of trends for snow water equivalent and snow depth display strong regional heterogeneities.

Finally, we have concluded CMIP5 general circulation models provides valuable information about the snow characteristics in the terrestrial Arctic, however, they have still limitations. There is a lack of agreement among the ensemble of models in the spatial distribution of snow compared to the observations and reanalysis. And these discrepancies are accentuated in regions where variability of snow is higher in areas with complex terrain such as Canada and Alaska and during the melting and the onset season. Our goal in this study was to identify where and when these models are or are not reproducing the real snow characteristics in the Arctic, thus we hope that our results should be considered when using these snow-related variables from CMIP5 historical output in future climate studies.

Keywords : Snow characteristics, Arctic climate, CMIP5 models, reanalyses, rnow stations.

Table of contents

Notations

The acronyms and the main abbreviations used in this PhD are shown below.

Acronyme	**Signification**
ACIA	Arctic Climate Impact Assessment
AMIP	Atmosphere Model Intercomparison Project
AMO	Atlantic Multidecadal Oscillation
AO	Arctic Oscillation
AOGCM	Atmosphere-Ocean General Circulation Model
AVHRR	Advanced Very High Resolution Radiometer
CAVM	Circumpolar Arctic Vegetation Map
CDO	Climate Data Operator
CDR	Climate Data Record
CIRES	Cooperative Institute for Research in Environmental Sciences
CLM	Community Land Model
CMIP5	Coupled Model Intercomparison Project 5
CMOR	Climate Model Output Rewriter
DAS	Data Assimilation System
ECMWF	European Centre for Medium-Range Weather Forecasts
EDLB	Eurasian Dry Land Band
ESM	Earth System Model
GCM	General Circulation Model
GEOS-5	Goddard Earth Observing System
GHCN	Global Historical Climatology Network
GHG	GreenHouse Gases
GLDAS	Global Land Data Assimilation System

ID	Identification Number
IMH	Institute of Meteorology and Hydrology
IMS	Ice Mapping System
IPA	International Permafrost Association
IPCC	Intergovernmental Panel on Climate Change
ISBA	Interaction Sol-Biosphère-Atmosphère
JMA	Japanese Meteorological Agency
LiDAR	Light Detection And Ranging
LIMon	Land Ice Monthly
NAO	North Atlantic Oscillation
NASA	National Aeronautics and Space Administration
NCEI	National Center for Environmental Information
NOAA	National Oceanic and Atmospheric Administration
PNA	Pacific North American
QBO	Quasi-Biennal Oscillation
RCP	Representative Concentration Pathways
RIHMI-WDC	Russian Research Institute for Hydrometeorological Information - World Data Center
ROS	Rain-On-Snow
SAF	Snow Albedo Feedback
SWIPA	Snow, Water, Ice, Permafrost in the Arctic
UCAR	University Corporation for Atmospheric Research
VHRR	Very High Resolution Radiometer
WCRP	World Climate Research Program
WGSIP	Working Group on Seasonal to Interannual Prediction
WMO	World Meteorological Organization

Notation	**Description**	**Units**
SCD	Snow cover duration	[*days*]
SCE	Snow cover extent	[%]
Sftgif	Land ice area fraction	[%]
Sftlf	Land area fraction	[%]
SIC	Sea ice concentration	[%]
SNC	Snow area fraction (same as SCE)	[%]
SND	Snow depth	[cm] *or* [m]
SNW	Surface snow amount	[$\mathrm{kg\,m^{-2}}$]
SST	Sea surface temperature	[°C]
SWE	Snow water equivalent (same as SNW)	[$\mathrm{kg\,m^{-2}}$]

Chapter 1

Introduction

1.1 Arctic climate system

There are several ways to define the Arctic region. The geographical definition is based on solar-Earth motion considering the Arctic as the region above the 66°34′ N parallel, the *Arctic Circle*. When defined in this way, its most fundamental characteristic is continuous daylight during the summer solstice and its absence during winter solstice (polar night). The duration of the daylight hours depends on the latitude. In the extreme case of the North Pole, the sun never sets between spring and autumn equinoxes and never rises during the rest of the year. Another way to set the boundaries of the Arctic is to consider it as the region north of the tree line, where vegetation is mainly dotted shrubs and lichens (Figure 1.1a). Arctic conditions, such as extreme winter cold, widespread permafrost and seasonal snow cover are present south of the limits of the Arctic circle and the tree line delimitation. Therefore, we consider the Arctic domain as the area north of 50° latitude and we focused on the ice-free land portion of the Arctic since the aim of this study is to evaluate terrestrial snow characteristics (Figure 1.1b ; see Chapter 3 for further details). Along the Arctic area, for some analysis, we consider separately the North American sector ["NAm"] and the Eurasian sector ["EURA"] separated by the 180°E meridian (blue and red hemispheres, respectively, in Figure 1.1b ; Table 1.1). Eurasian sector is also split into the Western ["EURAWest"] and the Eastern ["EURAEast"] Eurasian sectors by 90°E meridian (Table 1.1).

(a) (b)

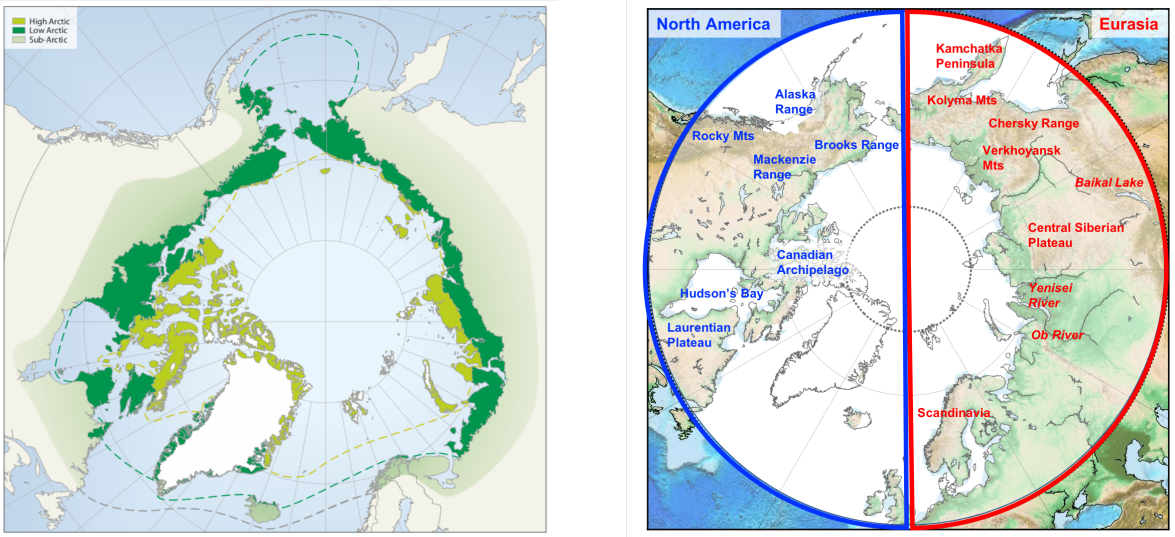

FIGURE 1.1 – (a) Map of high and low Arctic zones delineated according to the Circumpolar Arctic Vegetation Map (CAVM Team 2003). Tree line corresponding to the southern limit of Sub-Arctic zones (extracted from SWIPA (2017)). (b) Arctic domain defined north of 50 degrees latitude (in circle). The terrestrial ice-free Arctic (topographic in color) and the ocean and permanent ice areas (masked in white) are distinguished. Geographical features are labeled to facilitate the spatial description of snow characteristics in the text.

Domain (50°N – 90°N)	**Acronym**	**Longitude**
Arctic	ARC	0°E – 360°E
Eurasia	EURA	0°E – 180°E
Western Eurasia	EURAWest	0°E – 90°E
Eastern Eurasia	EURAEast	90°E – 180°E
North America	NAm	180°E – 360°E

TABLE 1.1 – Arctic domains.

The Arctic climate system is characterized by its low thermal energy state and by its strong couplings between the atmosphere, ocean and land (Serreze and Barry, 2014). Arctic encompasses extreme climate differences which varies largely by location and season. Surface air temperature (2 m above ground) presents a marked regional and seasonal variability. The mean temperature of January is less than −35°C in some parts of Siberia and the Canadian Archipelago, whereas over the central Arctic Ocean, temperature is typically around −25°C in January (Figure 1.2a). The presence of relatively warm and ice-free ocean water, and the atmospheric heat transport by the North Atlantic cyclones allows Iceland to have a mean temperature in January around 0°C

(Figure 1.2a). In July, mean temperature over land may vary from 10°C to 20°C (Figure 1.2b). Precipitation over the Arctic is quite scarce compare to other regions of the globe. Some parts of the Arctic, such the Canadian Archipelago, can be compared to arid regions elsewhere, with an annual mean precipitation of 200 mm or less ; whereas in the Atlantic sector, where Atlantic cyclones transport the moisture, it can reach 1000 mm (ACIA, 2004; Serreze and Hurst, 2000). Over a considerable part of the terrestrial Arctic, precipitation has maxima in summer but, for the Atlantic sector of the Arctic, maximum occurs in winter due to increase of cyclone activity in the cold season.

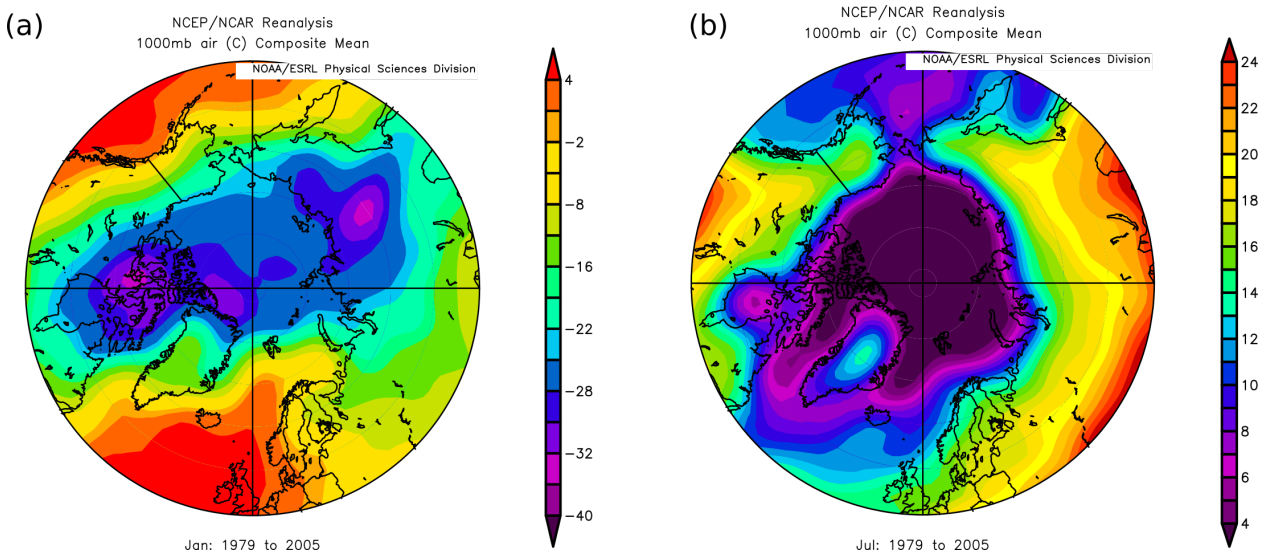

FIGURE 1.2 – Surface air temperature climatology in (a) January and (b) July during 1979-2005 using NCEP/CFSR Reanalysis from ESRL (Earth System Research Laboratory) Monthly/Seasonal Climate Composites https://www.esrl.noaa.gov/psd/cgi-bin/data/composites/printpage.pl .

The main feature of the Arctic is its cryosphere, whether sea ice, ice sheets, mountain glaciers and ice caps, permafrost, river and lake ice, and snow (Figure 1.3). The Arctic Ocean occupies most of the surface north of 70° latitude and is covered by floating sea ice throughout the year. Summer Arctic sea ice extent has been decreasing since the beginning of the satellite era in the late 70s by -13.3 % per decade (1979-2014) (Serreze and Stroeve, 2015). The alarming record minima of sea ice extent of $4.1 \times 10^6\,\mathrm{km}^2$ on 14th September 2007 (Comiso *et al.*, 2008) was overtaken on 13th September 2012 reaching $3.4 \times 10^6\,\mathrm{km}^2$ (Parkinson and Comiso, 2013) (Figure 1.4). Overall, the decline of Arctic annual sea ice extent maximum and minimum has been $-2.41 \pm 0.56\,\%$ per decade and $-13.5 \pm 2.93\,\%$ change relative to the 1979-2015 climate average (Peng and Meier, 2018). Sea

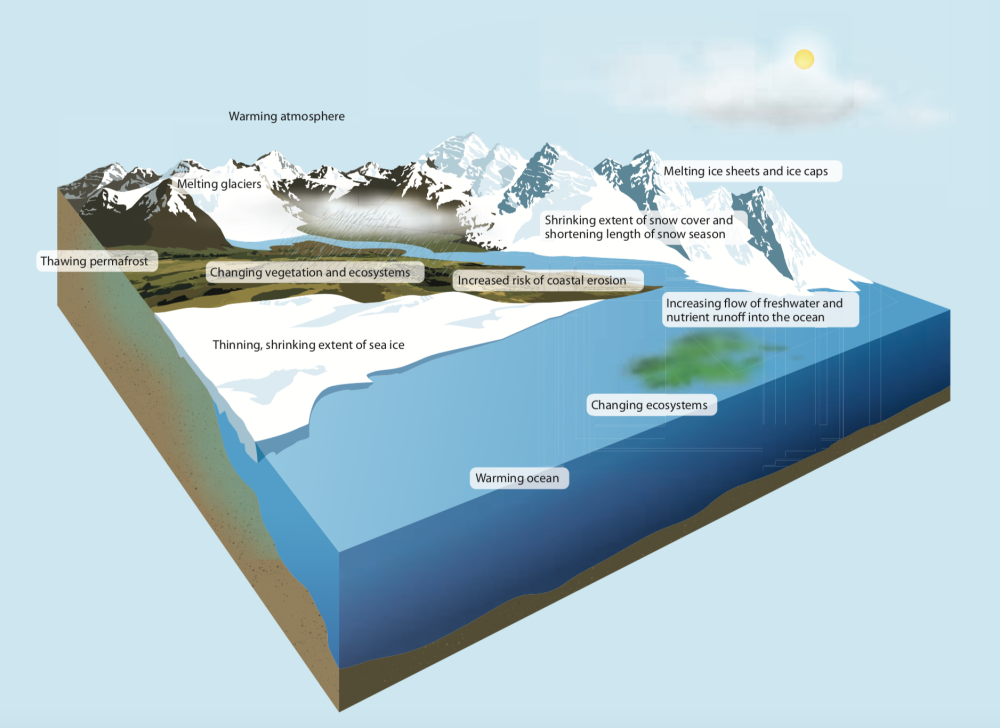

FIGURE 1.3 – Schematic representation of the components of the Arctic Cryosphere and their associated observed changes caused by global warming (graphic extracted from SWIPA (2011) and has been adapted from an image created by the U.S. National Center for Atmospheric Research).

ice extent decline is projected to continue during the twenty-first century under different emission scenarios (Collins *et al.*, 2013).

The Greenland ice sheet represents the largest mass of permanent land ice in the Arctic and it has been losing 171 Gt/year in average computed over 1991-2015 (Van den Broeke *et al.*, 2016) with a stronger mass loss of 286 ± 20 Gt/year over the last decade (2010-2018) (Mouginot *et al.*, 2019). Sub-polar ice caps and mountain glaciers are concentrated in the mountainous parts of Siberia and Canadian archipelagos, in Svalbard and Iceland. The monitored Arctic glaciers and ice caps are out of balance with present day climate, which means that they are committed to lose additional mass in the coming decades even if the climate was stabilized in its present state (Mernild *et al.*, 2013). Only 25 ± 35 % of the attributed loss of glacier mass was due to anthropogenic causes during the period from 1851 to 2010, whereas from 1991 to 2010 it has risen to 69 ± 24 % (Marzeion *et al.*, 2014). Permafrost is defined as ground (soil or rock and included ice or organic material) that remains at or below 0°C for at least two consecutive years (IPA, 2008). It occupies approximately 25% of the Northern Hemisphere land (Biskaborn *et al.*, 2019) and it is also present in sub-sea sediments. Permafrost soils store a large amount of carbon. As temperature increases and permafrost thaws,

the carbon contained in permafrost can be released and emitted to the atmosphere as greenhouse gases such as carbon dioxide CO_2 and methane CH_4 (McGuire *et al.*, 2016; Schuur *et al.*, 2015), which in turn increases the pace of future climate change (Schuur *et al.*, 2008).

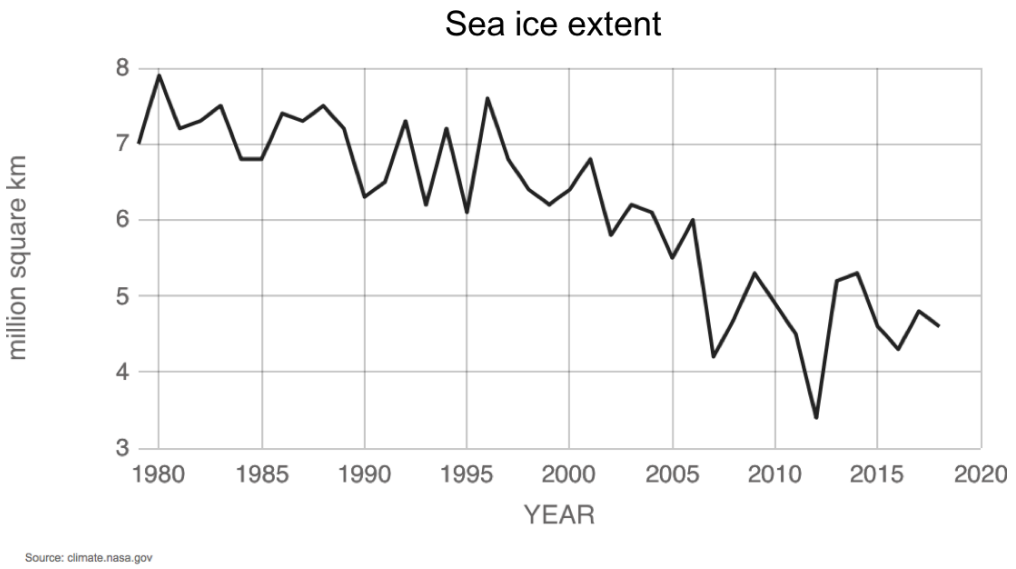

FIGURE 1.4 – Time series of annual Arctic sea ice minimum since 1979 to present based on satellite observations. Data from : NSIDC/NASA (https://climate.nasa.gov/vital-signs/arctic-sea-ice/).

1.2 Snow and climate

1.2.1 Snow formation

Snow is crucially important component of the Arctic climate system. Snow originates in cold clouds when two particular conditions are present : supersaturation and supercooling. By definition, an air mass that contains more water vapor than 100% of relative humidity is supersaturated. The higher the temperature, the more water vapor it can hold. As moist air rises, it expands and cools. When supersaturated air cools, the excess of water vapor crystallizes out into water or cloud droplets of the size of $\sim$10 microns in radius (Armstrong and Brun, 2008). When cooled below 0°C, such small droplets do not necessarily freeze and may "super cool" (i.e. lowering the temperature of gas/liquid below its freezing point without becoming a solid) to a temperature bellow -20°C and occasionally bellow -40°C (Armstrong and Brun, 2008). Once a droplet has already frozen, it will grow rapidly at the expense of the remaining water droplets as they condense onto the surface of the ice crystal because of the difference in saturation vapor pressure between ice and water. The shape of the initial ice crystal (columnar, platelike, dendritic etc.) depends on the temperature at formation, but

subsequent growth and structural detail also depend on the degree of saturation (Hobbs, 1974). As snow crystals fall down to the ground, they may experience considerable changes since temperature and humidity vary with altitude. The constitution of the surface snow layer depends on the original form of the crystal and the weather conditions during the fall and deposition. Snow on the ground may dissipate quickly through melting or sublimation or may persist for a longer time. In the second case, the snow will undergo metamorphism, changing its grain texture, size, and shape, primarily as a result of temperature and overburden pressure when buried by subsequent snowfalls (Armstrong and Brun, 2008).

Snowpack is described by three basic parameters : snow depth, snow water equivalent (SWE) and snow density. The *snow depth* is the thickness or the height of snow, usually expressed in cm. The *snow water equivalent* is the thickness of water resulting from the melting of the initial mass of the snow, which is usually expressed in $\mathrm{kg\,m^{-2}}$ or mm. Both variables are linked by the *snow density*, that is the ratio of mass to volume for a given sample, the standard units are $\mathrm{kg\,m^{-3}}$. For example, considering a maximum seasonal snowpack with a density of $\sim 400\,\mathrm{kg\,m^{-3}}$ and a height of 50 cm, the resulting SWE will be 200 mm or 200 $\mathrm{kg\,m^{-2}}$ (see further details in Chapter 2).

1.2.2 Snow properties

Snow is one of the basic elements of the Arctic system, with a duration of snow cover for 7 to 10 months over the year (Figure 1.5) and with a maximum extension of 40% of the Northern Hemisphere land surface (approximately $47 \times 10^6\,\mathrm{km^2}$) each year (Robinson and Frei, 2000; Lemke *et al.*, 2007). The unique properties of snow have an important impact on climate (Cohen and Rind, 1991; Groisman *et al.*, 1994, ; Figure 1.6). Snow has a strong direct influence on the overlying low troposphere as has been shown by observations (e.g., Dewey, 1977) and by models (Walsh and Ross, 1988; Vavrus, 2007) ; the impact is also present in the upper atmosphere (e.g., Alexander *et al.*, 2010). Snow has high reflectivity and this leads to influence on climate through the snow-albedo feedback (Qu and Hall, 2007; Fletcher *et al.*, 2015), which is a climate feedback mechanism whereby land surface warming is enhanced through reductions in snow cover and surface albedo, and subsequently increased radiation absorbed at the surface (Thackeray *et al.*, 2018). The contribution of terrestrial snow to the Earth radiation budget at the top of the atmosphere through the snow-albedo feedback is nearly equal to that from sea ice, the so-called cryosphere radiative forcing (Flanner *et al.*, 2011; Singh *et al.*, 2015).

The high albedo of snow (0.8-0.9 for dry snow) together with its low thermal conductivity favors low surface air temperatures. This last property is crucial for the insulation of the underlying soil from large energy losses and notably for the ice growth rate and the development of seasonal permafrost (Lawrence and Slater, 2009; Gouttevin *et al.*, 2012; Koven *et al.*, 2013; Slater *et al.*, 2017). The impact of snow on permafrost depends on its duration, thickness, accumulation and melting processes, structure, density, and thermal properties (Zhang *et al.*, 1996). In summer, late-lying snow cover increases surface albedo and thus, surface air temperature decreases which prevents permafrost from thawing. In spring, a late snow melt delays warming of the soil surface while it is close to 0°C, even if the air temperature is positive (Romanovsky and Osterkamp, 1997; Streletskiy *et al.*, 2015). During the snow season, a thick snow cover insulates the soil from air temperatures below 0°C which hampers the development of permafrost and ice growth. Changes in permafrost temperature are largely attributed to variations on the thickness of snow cover (Streletskiy *et al.*, 2015). Sherstyukov *et al.* (2008) found that changes in mean annual ground temperature in Siberia are more dependent on snow-cover thickness rather than on changes in air temperature. This relationship has also been found in the Northern Hemisphere discontinuous zone of permafrost, where ground warming results from the increase of snow thickness, while air temperature remains statistically invariant (Biskaborn *et al.*, 2019).

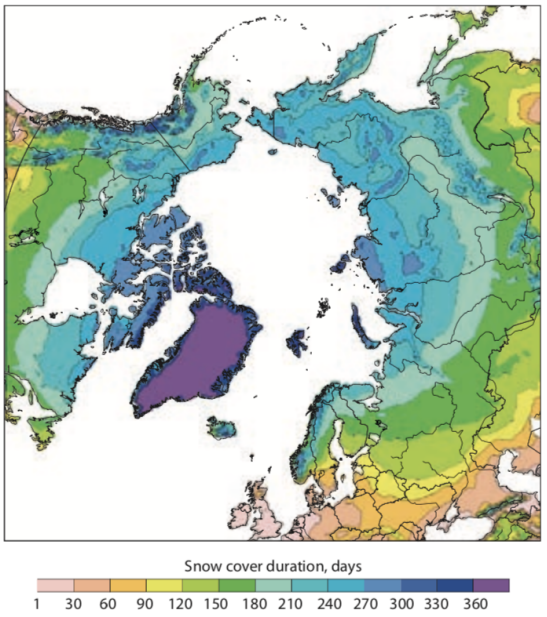

FIGURE 1.5 – Mean annual snow cover duration over Arctic land areas from the NOAA IMS-24 daily snow cover analysis for the snow seasons 1998/99 to 2013/14. Extracted from SWIPA (2017).

Snow is a natural store of water, playing a critical role in energy fluxes (release of latent heat), run-off (peak of flow) and evaporation (Groisman *et al.*, 2017). As a natural water reservoir, snow affects the water availability for a substantial part of humanity (Barnett *et al.*, 2005). In the early 1980s, Woo stated that the run-off generated by snow in the Arctic drainage basin accounts for 75% of the total annual flow in the Northwest Territories in Canada. Mankin *et al.* (2015) found that

the 68 Northern Hemisphere river basins providing water availability to around 2 billion people are exposed to a significant risk of a decrease in snow potential supply in this century.

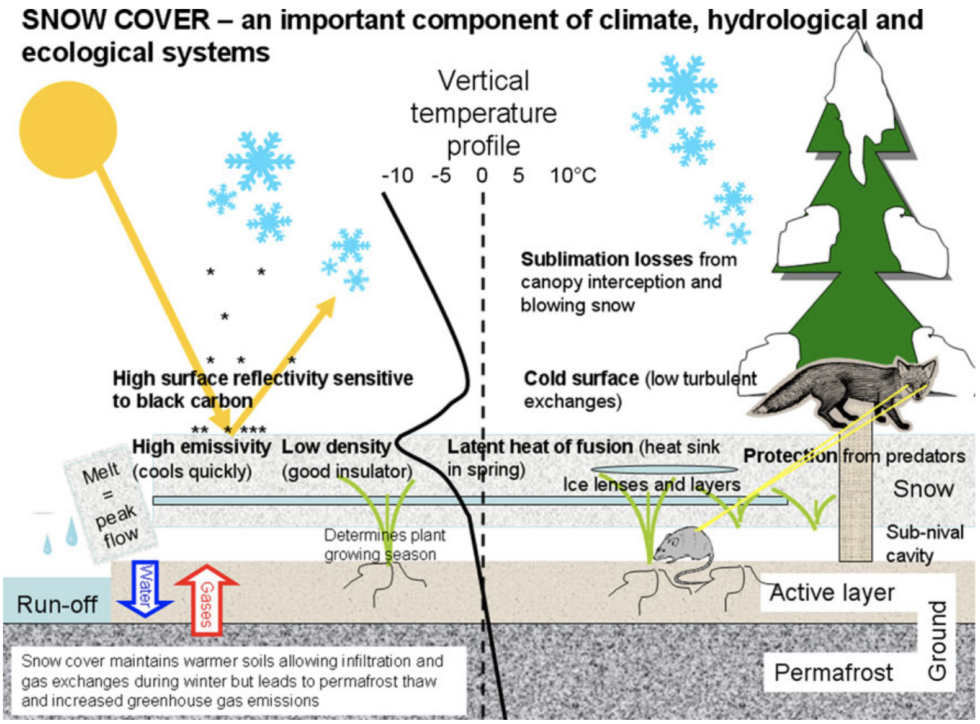

FIGURE 1.6 – Schematic illustration outlining the importance of snow on the strong temperature gradients occurring near the snow surface. The solid black line represents an idealized ground-snow-atmosphere temperature profile. Source R. Brown and T. V. Callaghan. Extracted from Callaghan *et al.* (2011b).

1.3 Arctic amplification and its influence on snow

The Arctic has warmed at a pace twice faster than the global average over the past 50 years, a phenomenon known as the Arctic Amplification (Serreze and Barry, 2011). Already in 1896, Svante Arrhenius argued that changes in the concentration of CO_2 will influence the global temperature with a strong impact in polar latitudes. Global warming has a direct impact on the loss of ice cover driving a cascading effect on atmospheric circulation changes (Francis and Skific, 2015; Ma *et al.*, 2018) as well as on moisture budgets, evaporation and precipitation (Dufour *et al.*, 2016; Liu *et al.*, 2012; Kattsov and Walsh, 2000). However, the inherent complexity of processes involved hinders a proper understanding of the water cycle feedback (e.g., Bintanja and Selten, 2014) and specifically, the snow response to a changing climate (Brown and Mote, 2009; Henderson *et al.*, 2018).

Arctic warming affects the timing and duration of snow cover, the snow accumulation and the fraction of precipitation that falls as snow. Snow cover duration is reduced by 2 to 4 days per decade (1972-2014) (Brown *et al.*, 2017) because snow melt occurs earlier in spring (Cayan *et al.*, 2001; Stewart, 2009). This phenomena is not uniform over the whole region : satellite data collected over the period 1979-2011 have highlighted an averaged reduction of snow cover duration of 1.6 days per decade in the Northern American sector, whereas it reaches 3.3 days per decade in the Eurasian continental sector (Wang *et al.*, 2013). This large reduction of the snow cover season has an immediate impact on the vegetation growth. Barichivich *et al.* (2013) stated that the Eurasian Arctic has experienced a larger reduction of the vegetation growing season (12.6 days) compared to the North American Arctic region (6.2 days) from 1982 to 2011. As for the snow cover duration, this non-uniform spatial trend distribution has also been observed for other snow characteristics, such as snow depth (Zhong *et al.*, 2018) or snow water equivalent (Mudryk *et al.*, 2015). Using around 820 stations spread all over the Russian Federation during the period from 1966 to 2007, Bulygina *et al.* (2009) found that the winter-averaged snow depth decreased in the mountainous regions of Southern Siberia ($-$ 8-12 cm/dec) ; whereas in the western part of the Russian Federation it increased (around +4-6 cm/dec), with the maximum trends being observed in Northern West Siberia (+8.1 cm/dec at meteorological station Turukhansk at 38 m elevation). Brown *et al.* (2017) reported a non-significant trend of annual snow depth accumulation of -0.6 cm/dec from 1950 to 2013 in the North American Arctic sector. This trend was computed using 56 stations from the Global Historical Climatology Network (GHCM) which recorded daily snow observations north of 60°N. Significant decreasing trends in snow depth maximum were found in Yukon and the MacKenzie Basin from 1950 to 2012 ; however, over the rest of the Canadian Arctic, no significant trend could be found (Vincent *et al.*, 2015). Notwithstanding the regional heterogeneities found in the Arctic system, which highlights its complexity, there is multi-dataset evidence that, on average, snow accumulation is decreasing (Brown, 2000; Park *et al.*, 2012).

Arctic atmospheric moistening is another consequence of the anthropogenic warming (Min *et al.*, 2008). The local loss of ice cover (Holland *et al.*, 2007; Bintanja and Selten, 2014) and the local intensification of water cycle (Rawlins *et al.*, 2010; Dufour *et al.*, 2016) affects Arctic land areas with an increase in precipitation. At midlatitudes with a milder climate, snowfall (solid precipitation) is projected to decrease as the precipitation phase changes to liquid with increasing temperatures ; whereas, in high latitudes with a colder climate, snowfall is projected to increase

(Räisänen, 2008). The increase in snowfall in deep snowpack regions (i.e. colder regions) may offset the current global reduction in snowfall during a shorter snow season (Wu *et al.*, 2018). In a warmer climate, the timing or amount of snowmelt is associated with a reduction in the peak of stream flow (Musselman *et al.*, 2017) and an earlier onset of soil moisture drying (Mahanama *et al.*, 2012), as a larger proportion of snow would melt earlier in the season. The direct consequences are unseasonal thaws (Liston and Hiemstra, 2011; Mishra *et al.*, 2010) and an increase of fire risk due to drier soils (Westerling *et al.*, 2006). Likewise, the decrease in the fraction of precipitation falling as snow leads to reduced overall stream flow (Berghuijs *et al.*, 2014) and increases the potential for rain-on-snow events (ROS) that even if rare and regional (Cohen *et al.*, 2015) can cause large flooding when they occur (Berghuijs *et al.*, 2016).

1.4 PhD rationale : Snow representation and objectives

The paucity of observational data sets in the Arctic makes it difficult to distinguish with confidence the climate forcing signal from the background noise of natural variability in snow evolution (Brown, 2000; Mudryk *et al.*, 2014; Najafi *et al.*, 2016). The spatial distribution of *in situ* measurements is quite scarce and few long term snow stations exist (Brown and Braaten, 1998; Bulygina *et al.*, 2011). Satellite derived products provide valuable information of snow characteristics (e.g., Riggs *et al.*, 2006) but their temporal extent is usually not sufficient for climatological research. Models are needed to help us to understand snow-related processes, namely, in the context of a warming cryosphere. Land surface models are employed to reproduce the temporal evolution of snow characteristics and its implications for different fields (e.g. hydrology, meteorology, climatology, glaciology and ecology). Snow models have been developed with a wide range of complexity. Some models are quite sophisticated with a detailed snow stratigraphy, others with an intermediate degree of complexity using 2-3 layers, and simple, zero-layer (combined with soil) or single layer-snow models (Slater *et al.*, 2001). Generally, in Earth System Models (ESMs), the snow modules are zero- and single-layer configurations. These simple models require fewer parameterizations, leading to faster computation ; however, they experience some limitations (Bokhorst *et al.*, 2016; Krinner *et al.*, 2018).

In this research we focus on the evaluation of General Circulation Models (GCMs) from the Coupled Model Intercomparison Project 5 (CMIP5). CMIP5 is a standard framework from the World Climate Research Program (WRCP) aiming at improving our collective knowledge about

the climate system. Currently, there have already been many studies evaluating the GCMs from the CMIP5 project (Flato *et al.*, 2013). Our work builds upon previous studies assessing snow characteristics in general circulation models where some progress and faults have been identified (Flato *et al.*, 2013; Brutel-Vuilmet *et al.*, 2013; Kapnick and Delworth, 2013; Terzago *et al.*, 2014). One of the main results was that the observed decreasing trend in spring snow cover in the Northern Hemisphere over the period 1979-2015 (Derksen and Brown, 2012) is largely underestimated in CMIP5 models due to an underestimation of the boreal temperature (Brutel-Vuilmet *et al.*, 2013). Also, the spread in snow-albedo feedback (SAF) was not reduced from CMIP3 likely due to a wide spread in the different treatment of vegetation in models (Qu and Hall, 2013). Recently, Thackeray *et al.* (2018) found that indeed, the structural differences in the snowpack, vegetation and albedo parametrizations drive most of the spread. Notably, models displaying the largest bias in SAF, also show clear structural and parametric errors. However, snow regimes in autumn have received less attention compared to spring.

In this respect, representation of snow-associated feedbacks in climate models, especially during the mid seasons (when Arctic snow cover exhibits the strongest variability) is of a special interest. At the offset of the snow season, down-welling shortwave and longwave radiation fluxes provide most of the energy enabling snow melt ; at the onset, temperatures are sufficiently cold to favor solid precipitation and snow accumulation (Sicart *et al.*, 2006). In spring, the snow albedo feedback is stronger as snow cover starts to age and recede due to increasing temperature and insolation (Qu and Hall, 2013; Thackeray *et al.*, 2016). In addition, positive (negative) snow cover anomalies in Eurasia from winter to spring may be followed by negative (positive) anomalies in the rainfall during the Indian summer moonson (Prabhu *et al.*, 2017; Senan *et al.*, 2016) but this snow-teleconnection is still controversial (Peings and Douville, 2010; Zhang *et al.*, 2019). While variations in snow characteristics are smaller in autumn than in spring, they also experience changes which have links to atmospheric circulation (Henderson *et al.*, 2018). Observational (Cohen *et al.*, 2007) and modeling (Peings *et al.*, 2012) studies linked the increase in Eurasian snow cover with the winter phase of the Arctic Oscillation (AO) and North Atlantic Oscillation (NAO). However, Gastineau *et al.* (2017) using an ensemble of CMIP5 models, demonstrated that this relationship is simulated by only four models and is largely underestimated by the majority of the ensemble. Douville *et al.* (2017) have questioned the robustness of the snow-NAO relationship and also argued for the importance of eastward phases of the Quasi-Biennial Oscillation (QBO) in modulation of snow cover variability.

To summarize, there is a need for comprehensive evaluation and validation of snow characteristics in climate models using available observations over the last decades in order to demonstrate which Arctic snow features are more robust across different models and which are not captured effectively. The focus of this PhD is on the representation of Arctic terrestrial snow in global circulation models from the CMIP5 ensemble in the mid seasons. Our goal is to make an evaluation of individual models to provide reliable information for the scientific community and hopefully help to improve the snow representation in future general circulation models. This thesis is organized as follows. Chapter 2 describes the snow data sources –namely, CMIP5 models, reanalyses and observations. Chapter 3 is dedicated to the description of the methodology, the treatment of data to provide comparability and the statistical tools employed. Chapter 4 presents the analysis of the spatial structure of snow characteristics. In Chapter 5 we study the temporal evolution and variability of snow characteristics. Finally, Chapter 6 offers the main conclusions and some perspectives for future research.

Chapter 2

Data

Contents

2.1 Overview

Our capacity to observe the terrestrial Arctic is limited compared to the mid-latitudes. Conditions are not ideal for continuous monitoring of snow characteristics due to inclement weather conditions, the polar night and the wind transport of snow. Moreover, the uneven spatial distribution of snow stations concentrated at 55°N in Canada (Brown and Braaten, 1998) or the lack of data in northern Siberia (Bulygina *et al.*, 2011) make challenging the up-scaling to larger regions. The snow stations are key for climatological research of snow characteristics as they are a unique record and the longest existing data in time. The temporal extent of the satellite era usually limits the study of the climate variability of snow (Maurer *et al.*, 2003; Riggs *et al.*, 2006). Even if both the *in situ* measurement and satellite data provide valuable information for snow and environment (Groisman and Davies, 2001), they present the aforementioned spatial and temporal limitations.

Reanalyses are a combination of observations and numerical models proving a synthesized estimate of the Earth system. They can reproduce the state of the climate and extend over several decades, as is the case for the NCEP/CFSR (Saha *et al.*, 2010) and ERA-Interim (Dee *et al.*, 2011) reanalyses ; or longer time periods, as the NOAA-CIRES 20th reanalysis (Compo *et al.*, 2011). Typically, reanalysis products cover the entire globe from the surface to well above the stratosphere.

Land snow-cover models are used to simulate the temporal evolution of snow in multiple applications (e.g. hydrology, meteorology, climatology, glaciology and ecology). There exist a wide variety of empirical and physically-based snow models whose degree of complexity may be adjusted to the intended application (Magnusson *et al.*, 2015). The sophistication of snow models ranges from the more complex with a detailed snow stratigraphy (e.g., CROCUS ; Brun *et al.*, 1992, 1997; Vionnet *et al.*, 2012), i.e vertical evolution of snow properties like snowpack compaction, liquid water percolation, snow interception etc., through the intermediate model complexity (2-3 layers) and to the simplest, with zero-layer (combined with soil) or single layer-snow models (Slater *et al.*, 2001). The modules used in Earth System Models (ESMs) are usually zero- and single-layer snow model configurations, having fewer parameterizations leading to fast computations, however, they involve some limitations (Bokhorst *et al.*, 2016; Krinner *et al.*, 2018). Some of the flaws in ESMs have been linked to the representation of the vegetation (Essery, 2013; Thackeray *et al.*, 2015), thermal conductivity (Cook *et al.*, 2008; Gouttevin *et al.*, 2012) and radiative processes (Thackeray *et al.*, 2016). However, even in detailed physically-based models, there are snow related processes that are not well captured, particularly in cold conditions (Domine *et al.*, 2016). The uncertainty of the underlying physics remains a drawback in the advance of snow modeling (Lafaysse *et al.*, 2017).

This chapter describes the wide variety of data used, from general circulation models to snow stations through the different satellite-based products and reanalyses, in order to bridge the gaps between the representations of snow characteristics in such a variety of data sets.

2.2 General Circulation Models (GCMs)

2.2.1 Coupled Model Intercomparison Project 5 : CMIP5

As a part of the World Climate Research Program (WCRP), CMIP5 (Taylor *et al.*, 2012, Coupled Model Intercomparison Project Phase 5) is a standard framework for studying the output of coupled atmosphere-ocean general circulation models ("AOGCMs"). CMIP5 builds on the accomplishment of previous CMIP phases (Meehl *et al.*, 2000, 2005) and aims at advancing our collective understanding of climate variability and climate change. The CMIP5 framework includes simulations on several timescales, ranging from seasonal to multidecadal. All simulations included in the CMIP5 framework (Figure 2.1) are classified by "core" and by one or two surrounding "tiers"

according to a consensus of prioritization. The "core" simulations (shaded in pink, Figure 2.1) are crucial for the evaluation of climate models and they produce information of keen interest about future projections. The "tier1" (shaded in yellow, Figure 2.1) researches specific aspects of climate model forcing, responses and processes that are examined in further depth in "tier2" (shaded in green, Figure 2.1). The strategy of CMIP5 encompasses two type of climate experiments (Figure 2.1a,b) that we briefly describe below :

1. ***Long-term integrations (century time scale)*** (Figure 2.1a) are usually started from multicentury preindustrial control (quasi equilibrium). These simulations follow the protocol of the previous phases of CMIP, but they add some additional runs to supply a more exhaustive understanding of climate change and variability. The core of long-term simulations (Figure 2.1a) involve an AMIP run, a coupled control run and a "historical" run. The latter are forced by observed atmospheric composition and reflect both the anthropogenic and the natural evolution of the climate system. The historical runs, also called "twentieth century" simulations, cover the time period from 1850 to 2005. The new addition with respect to previous phases is that in CMIP5, the historical runs include a time-evolving land cover.

   Within the long-term simulations, there are also future projections forced with specified concentrations of greenhouse gases, which are referred to as "representative concentration pathways" (RCPs) described in Moss *et al.* (2010). In CMIP5, there are four RCPs which are based on estimations of future population growth, technological development and societal responses (Figure 2.2). The denomination of each RCP provides an approximate estimate of the radiative forcing in the year 2100 (relative to preindustrial conditions). Unlike phase 3, in CMIP5, these RCPs take policy interventions into account, meaning that the RCPs are mitigation scenarios where actions to curb emissions are considered. The four future scenarios are : RCP8.5, referred to as the "high scenario", the two "intermediate scenarios" RCP4.5 and RCP6, and the so called "peak-and-decay" scenario RCP2.6.

2. ***Near-term integrations (10-30 yr)*** (Figure 2.1b), also called decadal prediction experiments (Meehl *et al.*, 2009). The near-term prediction experiments are a novelty of CMIP. Decadal prediction experiments are organized by the WGCM and the Working Group on Seasonal to Interannual Prediction (WGSIP). These near-term simulations are initialized with observed ocean and sea ice conditions. There are two collections of core simulations (Figure

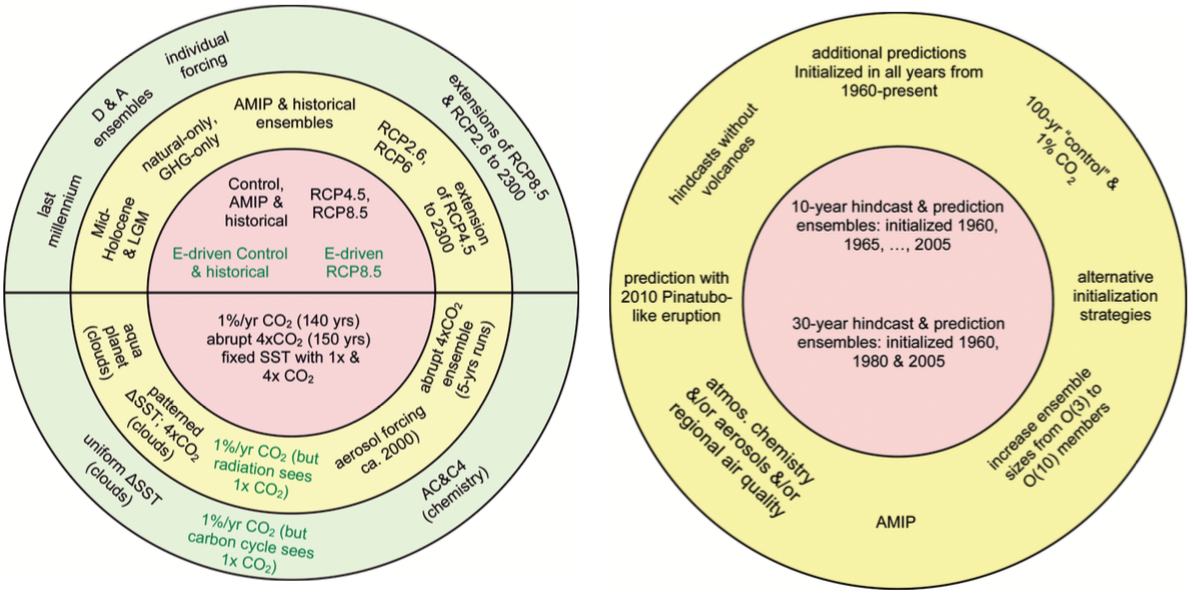

(a) (b)

FIGURE 2.1 – (a) Schematic summary of CMIP5 long-term experiments. Upper hemisphere experiments are suitable for validation with observations or provide projections. Green fonts refer to simulations performed only by models with carbon cycle representations. (b) Schematic summary of CMIP5 decadal prediction integrations. Extracted from Taylor *et al.* (2012).

2.1b) : i) a set of 10 year hindcasts initialized from observed climate states near every five years from 1960 to 2005 ; ii) two 30-year hindcasts initialized in 1960 and 1980, and one 30 year prediction initialized in 2005, ending in 2035. In the first one, we can asses the skill of the climate forecast when initial climate conditions exert some detectable influence, whereas in the second one, with a longer time scale, the external forcing of an increase in GHGs will dominate the response of the system even if some residual influence of the difference in initial conditions prevail. Thus, in the near-term simulations models are not only responding to climate forcing (e.g. increase in CO_2 concentration) but they may also reproduce the climate change evolution, including the unforced component.

Climate models involved in CMIP5 have a twofold mission. First, purely scientific, aims at advancing in our knowledge of the Earth Climate System, its past, present and future evolution. The second is to contribute to the IPCC (Intergovernmental Panel on Climate Change) reports to mitigate climate change and adapt to its effects (Edenhofer *et al.*, 2014; Field *et al.*, 2014).

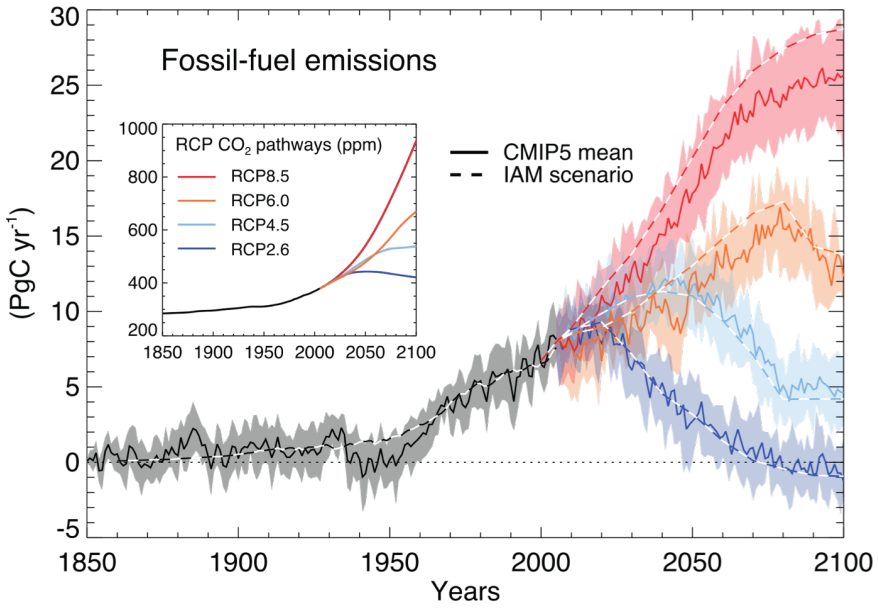

FIGURE 2.2 – Time series of compatible emission rate (PgC yr^{-1}) of fossil fuel emissions simulated by the CMIP5 ESMs for the four RCP scenarios. Dashed lines represent the historical estimates and emissions calculated by the Integrated Assessment Models (IAMs) used to define the RCP scenarios ; solid lines and shading show results from CMIP5 ESMs (model mean, with 1 standard deviation shaded). Extracted from Ciais *et al.* (2014).

The straightforward approach to model evaluation is to compare the model output with existing observations to identify its strengths and weaknesses. The core of this PhD is to contribute to this vast task by analyzing the snow characteristics in CMIP5 models. For this purpose, we evaluate the most realistic simulations from CMIP5, the "historical runs" from the "long-term integration" type climate experiments. They are forced by observed atmospheric composition and exhibit the anthropogenic forcing as well as the natural evolution of the climate system.

Model name	**Modeling Center (Institut ID)**	**Resolution**	**Nb members**	Reference
bcc-csm1-1	Beijing Climate Center, China Meteorological Administration (BCC)	2.8° × 2.8°	3	Wu *et al.* (2013)
CanESM2	Canadian Center for Climate Modeling and Analysis (CCCMA)	2.8° × 2.8°	5	Arora *et al.* (2011)
CCSM4	National Center for Atmospheric Research (NCAR)	0.9° × 1.2°	8	Gent *et al.* (2011)
CNRM-CM5	Centre National de Recherches Météorologiques/Centre Européen de Recherche et Formation Avancée en Calcul Scientifique (CNRM-CERFACS)	1.4° × 1.4°	10	Voldoire *et al.* (2012)
CSIRO-Mk3-6-0	Commonwealth Scientific and Industrial Research Organization in collaboration with Queensland Climate Change Center of Excellence (CSIRO-QCCCE)	1.8° × 1.8°	10	Collier *et al.* (2011)
GISS-E2-H	NASA Goddard Institute for Space Studies (NASA GISS)	2.0° × 2.5°	6	Schmidt *et al.* (2006)
GISS-E2-R			6	Schmidt *et al.* (2006)
inmcm4	Institute for Numerical Mathematics (INM)	1.5° × 2.0°	1	Volodin *et al.* (2010)
MIROC-ESM-CHEM	Japan Agency for Marine-Earth Science and Technology, Atmosphere and Ocean Research Institute (The University of Tokyo), and National Institute for Environmental Studies (MIROC)	2.8° × 2.8°	1	Watanabe *et al.* (2011)
MIROC-ESM		2.8° × 2.8°	3	Watanabe *et al.* (2011)
MIROC5		1.4° × 1.4°	5	Watanabe *et al.* (2010)
MPI-ESM-LR	Max Planck Institute for Meteorology (MPI-M)	1.8° × 1.8°	3	Giorgetta *et al.* (2013)
MPI-ESM-P			2	Giorgetta *et al.* (2013)
MRI-CGCM3	Meteorological Research Institute (MRI)	1.1° × 1.1°	5	Yukimoto *et al.* (2012)
NorESM1-M	Norwegian Climate Center (NCC)	1.8° × 2.5°	3	Bentsen *et al.* (2013)
NorESM1-ME			2	Bentsen *et al.* (2013)

TABLE 2.1 – CMIP5 models, modeling center and institute acronym (https://cmip.llnl.gov/cmip5/), resolution and number of ensemble members considered.

2.2.2 Snow Variables in CMIP5

In the introduction it was mentioned that the snowpack can be described by snow depth or snow water equivalent, and that both characteristics are related by the snow density. From the *in situ* point of view, snow depth usually refers to the total height of snow on the ground at the time of observation and it is measured with a snow ruler or similar graduated rod which is pushed down through the snow to the ground surface (Jarraud, 2008). Snow water equivalent is the thickness of the water that would be obtained by melting the snow sample and it can be measured directly by melting the sample and measuring its liquid content, or indirectly by inferring the water equivalent using an appropriate specific snow density (Jarraud, 2008). Returning to the example from the introduction, for a snow sample of 50 cm height with a maximum seasonal snow density of 400 $kg\,m^{-3}$, the resulting snow water equivalent would be 200 mm following this relationship :

$$m_{liquid\,water} = m_{snow}$$
$$\rho_{liquid\,water} \cdot h_{liquid\,water} \cdot S = \rho_{snow} \cdot h_{snow} \cdot S$$

$$\rightarrow h_{liquid\,water} = \frac{\rho_{snow=400\,kg\,m^{-3}}}{\rho_{liquid\,water=1000\,kg\,m^{-3}}} \cdot h_{snow=0.5\,m} = 200\,mm$$

However, when moving from the *in situ* representation to large scale, the concept of snow characteristics is slightly nuanced. From the model perspective, there is no one observation point ; instead, space is discretized in grid cells which makes the conversion of snow depth to snow water equivalent much more complex. Indeed, in CMIP5 models, the spatial resolution of grid cells varies from $\sim 100\,\mathrm{km}^2$ to $\sim 300\,\mathrm{km}^2$. The snow surface representation also depends on the different canopies within the grid cells, that is, the type of vegetation (e.g. trees, shrubs), topography, land use, presence of lakes and rivers etc. which are in the land-surface model of the GCM. The variables that represent terrestrial snow characteristics in CMIP5 models are described in the document "standard_output.pdf" accessible via https://pcmdi.llnl.gov/mips/cmip5/docs/ :

- **Snow Area Fraction** ("snc", %) : Fraction of each grid cell that is occupied by snow that rests on the land portion of the cell. "Snow Area Fraction" is usually called "Snow Cover Extent" ; throughout the manuscript we will refer it as **"SCE"**.
- **Surface Snow Amount** ("snw", $kg\,m^{-2}$) : Computed as the mass of surface snow on the land portion of the grid cell divided by the land area in the grid cell ; reported as 0.0 where the land fraction is 0 ; snow on vegetation canopy or on sea ice is excluded. "Surface Snow

Amount" corresponds to the snow water equivalent definition (h_w in Figure 2.3) ; hereafter we will refer to it as **"SWE"**.

- **Snow Depth** ("snd", m) : when over land, this is computed as the mean thickness of snow in the land portion of the grid cell (averaging over the entire land portion, including the snow-free fraction). Reported as 0.0 where the land fraction is 0. Snow depth (**"SND"**) is represented by h_{snow} as in Figure 2.3.

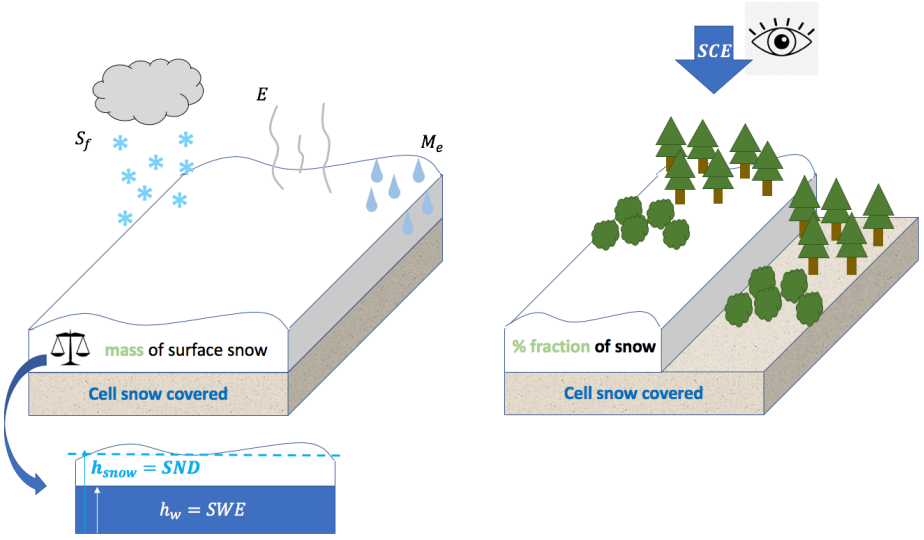

FIGURE 2.3 – Diagram of snow characteristics in general circulation models.

In the CMIP5 models considered in this study (Table 2.1), the snow water equivalent (SWE) is a prognostic variable (ES-DOC, https://es-doc.org) resulting from the balance between snowfall, evaporation and snowmelt rates (Equation 2.1 ; Manabe, 1969; Thackeray *et al.*, 2016). Snow depth (SND) is usually a diagnostic variable depending on SWE by means of the snow density.

$$\frac{d}{dt}(SWE) = S_f - E - M_e \tag{2.1}$$

where S_f is the rate of snowfall, E is the evaporation rate and M_e is the rate of snow melt which can be computed by the heat balance (E_x) condition of a snow covered surface, that is, $M_e = E_x/L_f$ when $E_x > 0$ and $M_e = 0$ when $E_x <= 0$ (Manabe, 1969). Snow cover fraction or extent (SCE) is usually diagnosed from SWE by means of a monotonic function using different parametrizations depending on the model (Liston, 2004; Wu *et al.*, 2018). Models also present different conservation

properties (e.g. water discharge-storage), couplings with atmosphere and land cover types which depend essentially on the land model integrated in the GCM. For example, to diagnose SCE, the ISBA surface model, a component of CNRM-CM5, uses an asymptotic function of SWE (Equation 2.2 ; Douville *et al.*, 1995) :

$$p_{ng} = \frac{W_n}{W_n + W_{crn}(= 10mm)} \tag{2.2}$$

where W_n is the mean snow water equivalent (SWE), W_{crn} the critical water equivalent of snow necessary to the estimation of p_{ng} which represents the fraction of snow covering the soil (SCE) (Douville *et al.*, 1995). Conversely, the CLM 3.5 land model from CCSM4 uses a tangential hyperbolic function (Equation 2.3 ; Niu and Yang, 2007; Xu and Dirmeyer, 2013).

$$SCE = \tanh\left[\frac{h_{snow}}{\alpha z_{0g}(\rho_{snow}/\rho_{new})^{\beta}}\right] \tag{2.3}$$

where h_{snow} is the spatially averaged snow depth (expressed as a function of SWE and snow density), and z_{0g} is the surface roughness length. The ρ_{snow} is the model-calculated snow density and ρ_{new} is a prescribed fresh snow density of 100 $kg\,m^{-3}$, β is a tunable parameter depending on several factors (e.g. vegetation, orography) and α is fixed to 2.5 for simplicity in the global model (Xu and Dirmeyer, 2013).

CMIP5 Snow Data Archive In order to facilitate the model output, the CMOR2 software library was created where variables are stored following this standard filename format (https://cmip.llnl.gov/cmip5/docs/CMIP5_output_metadata_requirements.pdf, Taylor *et al.*, 2011) :

```
filename = <variable name>_<MIP table>_<model>_<experiment>_<ensemble
           member>_<temporal subset>].nc
```

The snow land variables such as SCE, SWE and SND are stored as “Monthly Mean Land Cryosphere Fields” with the corresponding filename encoding :

```
snow_filename = snow_LImon_<model>_historical_<ensemble member>_<period>.nc
```

The <MIP table> provides information about the *modeling realm*, the high level modeling component relevant for the variable such as “LandIce” for snow or “Atmosphere” for snowfall, and also the *frequency*, “Monthly” in both cases. The *experiment* family is indicated as “historical”, referring to the historical runs explained in the previous section. The *ensemble member* is com-

posed by a triad of integers (r<N>i<M>p<L>) which refer to varying simulation conditions for each realization (member). N is the "*realization number*" : if the different members of one model vary only according to this integer N, it means that runs have been initialized with different, but equally realistic initial conditions ; the M corresponds to the "*initialization method indicator*" which indicates the different observational data sets or the different methods using observations that are employed as initial conditions. The L refers to the "*perturbed physics number*" which allows to distinguish between different realizations that have modified a particular set of model parameters. The <temporal subset> is restricted to the period 1979-2005.

The choice of the ensemble of models in Table 2.1 is justified by two reasons. First, our aim was to evaluate different snow variables and so, initially, we only focused on snow cover and snow water equivalent (SCE and SWE). Thus, we considered only the CMIP5 models which provided both characteristics. Later in the PhD, we began to use *in situ* measurements from the snow stations, which motivated us to form a new set of models including snow depth ; however, the models MPI-ESM-LR/P do not provide this variable. The risk of using an erroneous method to convert SWE to SND to include these models in the SND analysis has already been identified (Brown and Frei, 2007). Consequently, in the SND analysis the MPI-ESM-LR/P models do not appear. Secondly, we wanted to limit our study to an amount of models small enough to enable individual analysis. When using a large number of models, multimodel analysis is more suitable, but it is less evident to provide a catalog of individual model performance.

2.3 Observations

Generally, there are two fundamental ways to measure snow directly, from *in situ* snow stations and from remote sensing using satellites (e.g., Riggs *et al.*, 2006) or airborne LiDAR (e.g., Schaffhauser *et al.*, 2008). The main problem with *in situ* measurements is that they include intrinsic systematic human error (Woo and Marsh, 1978) and may not be accurately continuous in time. On the other hand, they are a unique record with precious information of snow characteristics. Remote sensing snow data coming from satellites, for instance, contain uncertainties related to the retrieval procedure such as the presence of clouds (Parajka and Blöschl, 2006). They are continuous in time, however, satellite snow products begin too late for our period of interest, except for the NOAA Climate Data Record (Estilow *et al.*, 2015). Reanalysis products are another source of snow infor-

mation considered here as an observational reference. However, they are also subject to intrinsic errors (e.g., Khan *et al.*, 2008; Dufour *et al.*, 2016; Wegmann *et al.*, 2017).

2.3.1 Snow Stations

Regular snow observations have been conducted all over the Eurasian continent from 1881 to 2013. This includes snow depth measurements and the amount of snow covering the visible area of meteorological stations, estimated on a scale of one to ten (10 to 100%; or zero in the absence of snow). Here we use the daily snow depth record over the former USSR (Union of Soviet Socialist Republics), which is composed of data from 600 stations, from the Russian Research Institute for Hydro-meteorological Information - World Data Center (RIHMI-WDC) (Bulygina *et al.*, 2011). Snow depth measurements have been conducted once a day using a graduated stake installed at a fixed point location within the station or by a wooden ruler, following the standard protocol from the World Meteorological Organization (WMO, McMichael *et al.*, 1996). Meteorological data sets are quality controlled before being stored at the RIHMI-WDC (Veselov, 2002). As the procedures of snow observation have changed over time (e.g., Meshcherskaya *et al.*, 1995), particular consideration has been taken to maintain the homogeneity in the data record. All information for the snow stations is available at http://meteo.ru/english/climate/snow.php.

2.3.2 NOAA CDR

The satellite-based weekly Snow Cover Extent dataset (Robinson *et al.*, 1993; Robinson and Frei, 2000; Estilow *et al.*, 2015) is the longest continuous record of snow cover extent, starting on 4th October 1966 and continuing at present. It is freely available at the NOAA (National Oceanic and Atmospheric Administration) National Center for Environmental Information (NCEI). It has been used in numerous studies (Déry and Brown, 2007; Derksen and Brown, 2012; Brown and Derksen, 2013; Gastineau *et al.*, 2017; Connolly *et al.*, 2019). Before 1972, the resolution of common meteorological satellites was around 4 km. From October 1972, VHRR (Very High Resolution Radiometer) provided imagery with an improved spatial resolution of 1 km, which was slightly reduced to 1.1 km in November 1978 with the replacement of the VHRR by the Advanced VHRR (AVHRR). From 1966 to 1999, snow maps were analyzed and interpreted by hand by experienced meteorologists from the NOAA who drew the boundaries of snow cover extension. Weekly maps were created in an 89 $\times$ 89 cell cartesian grid laid over a polar stereographic projection of the

Northern Hemisphere. The resolution of cells ranges from ≈ 10 700 to ≈ 41 800 km^2, with a spatial resolution of 190.5 km at 60°N. Each grid cell has a binary value displaying "1" when a cell has at least 50% of its surface covered with snow and "0" for all other cells, considered snow-free cells. Since 1999, this process has been automated by the Interactive Snow and Ice Mapping System (IMS, Ramsay, 1998) at the Global Snow Lab from Rutgers University. Thus, the early weekly snow cover analysis procedure changed with the introduction of IMS at much higher resolution (≈ 24 km). However, to maintain continuity, a pseudo-weekly snow chart has been created by drawing a map representative of the previous week each Sunday ; which is in agreement with Robinson (1993) who take the 5th day of the week as representative, with the first week starting on Tuesday, 4th October 1966.

NOAA maps are subject to limitations when overcast conditions, weak solar radiation or complex vegetation complicate the retrieval process. Robinson and Frei (2000) reanalyzed this data from 1961 to 1971, there were missing values mainly in autumn and the resolution was quite coarse. In spite of their limitations, the NOAA maps are trustworthy for continental-scale studies of snow cover variability (Wiesnet *et al.*, 1987) but caution should be taken at high latitudes and mountainous regions. Also, two studies (Wang *et al.*, 2005; Brown *et al.*, 2007) over northern Canada showed that NOAA CDR overestimates snow cover in spring and summer and tends to be uncoupled with temperature anomalies in July. It has been stated more recently that there is a bias in snow cover during October that has not been detected in other data records (Brown and Derksen, 2013), which in turn translates to an anomalous snow cover trend in October in Eurasia (Brown and Derksen, 2013; Estilow *et al.*, 2015).

2.3.3 CanSISE Ensemble Product

CanSISE Observation-Based Ensemble of Northern Hemisphere Terrestrial Snow Water Equivalent (Version 2) (Mudryk and Derksen, 2017) is a daily gridded terrestrial snow water equivalent (SWE) data set based on five component products :

1. *GlobSnow (Version 2)*, combined SWE product (Takala *et al.*, 2011) : Combines satellite-based passive microwave measurement with ground-based weather station in a data assimilation scheme spanning 1979-2012.

2. *ERA-Interim/Land reanalysis* (Balsamo *et al.*, 2012) : Global reanalysis of land-surface parameters with a horizontal resolution of ~ 80 km (T255) and a temporal resolution of 6 hours for the period from 1st January 1979 to 31st December 2010.

3. *MERRA reanalysis* (M. Rienecker *et al.*, 2011) : NASA atmospheric reanalysis using the Goddard Earth Observing System model (GEOS-5) and its associated assimilation system (DAS), Version 5.2.0 (Rienecker *et al.*, 2008). It provides hourly averages of land surface fields at a horizontal resolution of $2/3^\circ$ longitude by $1/2^\circ$ latitude from 1st January 1980 to present.

4. *CROCUS* snow pack model (Brun *et al.*, 1989, 1992) and updated by Vionnet *et al.* (2012) : SWE output from the CROCUS snow pack model, driven by ERA-Interim meteorology.

5. *GLDAS (Version 2)* (Rodell *et al.*, 2004; Rodell and Beaudoing, 2013) : SWE parameter from the Common Land Model (CLM) V2.0 model in the Global Land Data Assimilation System (GLDAS). The spatial resolution is 1° degree and range from January 1979 to present. The temporal resolution is 3-hourly.

Overall, the CanSISE product has a daily temporal resolution, $1.0^\circ \times 1.0^\circ$ spatial resolution and covers the period from 1st January 1981 to 31th December 2010. This product is available at https://nsidc.org/data/nsidc-0668.

2.3.4 Reanalyses

- **National Centers for Environmental Prediction (NCEP) Climate Forecast System Reanalysis (CFSR), "NCEP/CFSR"** (Saha *et al.*, 2010) is a 6-hourly product covering a 31 year-period from 1979 to 2010 and $0.5^\circ \times 0.5^\circ$ horizontal resolution. It includes a coupled atmosphere-ocean-land surface-sea ice system and direct assimilation of satellite radiances. The global atmosphere has a resolution of ~ 38 km (T382) with 64 levels, the ocean resolution is of 0.25° around the equator and 0.5° beyond the tropics, land surface models provides 4 levels and the sea ice model 3. The NCEP/CFSR reanalysis also includes changes in CO_2 and other trace gases, aerosols and solar variations. We used this data set for snow cover and it is available at https://rda.ucar.edu/datasets/ds093.0/.

- **NOAA-CIRES 20th Century Reanalysis version 2, "NOAAV2c"** (Compo *et al.*, 2011) which extends from 1851 to 2012 with an original temporal resolution of 6 hours and spatial resolution of $2.0^\circ \times 1.75^\circ$. It uses the coupled atmosphere-land model NCEP GFS

2008ex. It assimilates only surface pressure reports and uses observed monthly sea surface temperature and sea ice concentration fields as boundary conditions. The spectral resolution is T62 and the vertical resolution is composed of 28 hybrid sigma-pressure levels. From this data we analyzed snow cover and snow depth and it can be downloaded at http://www.esrl.noaa.gov/psd/data/gridded/data.20thC_ReanV2c.html.

- **Japanese 55-year Reanalysis, "JRA-55"** (Kobayashi *et al.*, 2015) conducted by the Japanese Meteorological Agency (JMA) ; extends back to 1958, coinciding with the establishment of the global radiosonde observing system. Snow depth is assimilated using snow stations data over the United States, Russia and Mongolia, which were supplied by UCAR (University Corporation for atmospheric research), RIHMI (Russian Research Institute of Hydrometeorological Information) and IMH (Institute of Meteorology and Hydrology), respectively. The spatial resolution is a regular latitude-longitude Gaussian grid 320 latitudes by 640 longitudes, nominally 0.5625° degree. The temporal resolution is 6-hourly. We used snow depth from this reanalysis which is available at https://rda.ucar.edu/datasets/ds628.0/.
- **ERA-20C, "ERA20c"** (Poli *et al.*, 2016) is the first atmospheric reanalysis from ECMWF (European Centre for Medium-Range Weather Forecasts) from 1900 to 2010. It assimilates observation of surface pressure and surface marine winds. The temporal resolution of the snow depth variable is 6-hourly. It is a coupled atmosphere/land-surface/ocean-waves model with 91 atmospheric levels (from surface to 0.01 hPa) and 4 soil layers. The horizontal spatial resolution is approximately 1.125° × 1.125° (spectral truncation T159). We used snow depth from this reanalysis which is available for download at https://apps.ecmwf.int/datasets/data/era20c-ofa/.

Data set	Spatial Resolution	Time coverage	References
Snow Stations (SND)	*In situ*	1881-2013	Bulygina *et al.* (2011)
NOAA CDR (SCE)	∼ 190.5km × 190.5km	1966 - Present	Robinson *et al.* (1993)
CanSISE (SWE)	1.0° × 1.0°	1981-2010	Mudryk and Derksen (2017)
NOAAV2c (SCE ; SND)	2.0° × 1.75°	1851-2012	Compo *et al.* (2011)
NCEP/CFSR(SCE)	0.5° × 0.5°	1979-Present	Saha *et al.* (2010)
JRA 55 (SND)	0.5625° × 0.5625°	1958-Present	Kobayashi *et al.* (2015)
ERA20c (SND)	1.125° × 1.125°	1900-2010	Poli *et al.* (2016)

TABLE 2.2 – Major characteristics of observational data sets compared in this study.

Chapter 3

Methodology

Contents

3.1 Overview

All data sets described in Chapter 2 are originally in different spatial and temporal resolutions. To provide an accurate intercomparison between data sets, it is necessary to convert them to compatible formats. This chapter explains briefly the data treatment preceding the analysis and how the domain restriction to an ice free land Arctic has been accomplished.

3.2 Spatial and temporal resolution

3.2.1 General procedure

In order to enable a grid-to-grid evaluation, we convert CMIP5 model output and reanalyses to compatible grids. The spatial resolution of CMIP5 models goes from relatively fine ($0.9^\circ \times 1.2^o$, CCSM4) to coarse ($2.8^o \times 2.8^o$, bcc-csm1-1). The reanalyses used in this study have grids ranging from $0.5^o \times 0.5^o$ in NCEP/CFSR to four times larger in NOAAV2c ($2.0^o \times 1.75^o$). For grid-to-grid evaluation, all snow fields from CMIP5 models (Table 2.1) are converted to a $1.0^o \times 1.0^o$ regular grid. An analogous procedure has been applied to all SCE reanalyses (NCAR/CFSR and NOAAV2c), the SWE satellite based product (CanSISE) and SND reanalyses (NOAAV2c, JRA-55 and ERA20c).

We have used the *cdo remapbil* operator (CDO : Climate Data Operator ; Schulzweida *et al.*, 2006) to conduct the bilinear interpolation (Table 3.1).

Data set	***Original spatial resolution***		
CanSISE (SWE)	$1.0° \times 1.0°$		
NCAR/CFSR (SCE)	$0.5° \times 0.5°$	$\xrightarrow{cdo\ remapbil}$	$1.0° \times 1.0°$
NOAAV2c (SCE ;SND)	$2.0° \times 1.75°$		
JRA-55 (SND)	$0.5625° \times 0.5625°$		
ERA20c (SND)	$1.125° \times 1.125°$		

Table 3.1 – Spatial resolution of different reference data sets.

The temporal resolution is dictated by the frequency of snow variables in CMIP5 models. Among the CMIP5 ensemble (Table 2.1), only few models provide daily resolution for snow characteristics (CanESM2, all versions of MIROC and MRI-CGCM3 ; https://esgf-node.llnl.gov). The majority of CMIP5 models dispense monthly snow output from the "LIMon" (Land Ice Monthly) CMOR2 table as mentioned in the previous chapter. Accordingly, we compute monthly means of the reference data sets using the *cdo monmean* operator (CDO : Climate Data Operator, Schulzweida *et al.*, 2006) as indicated in Table 3.2.

Data set	***Original temporal resolution***		
CanSISE (SWE)	daily		
NCAR CFSR (SCE)	6-hourly	$\xrightarrow{cdo\ monmean}$	monthly
NOAAV2c (SCE ;SND)	3-hourly		
JRA 55 (SND)	6-hourly		
ERA20c (SND)	6-hourly		

Table 3.2 – Temporal resolution of different reference data sets.

3.2.2 Particular cases

NOAA CDR is in a 89×89 cartesian grid laid over a polar stereographic projection (Robinson and Estilow, 2012). For this data we avoid interpolation, either spatial or temporal, in order to keep the data in its original binary format. Consequently, no grid-to-grid comparison is performed with this data. Nevertheless, we convert the weekly NOAA CDR to monthly resolution. As explained in Robinson (1993), a chart week is considered centered on the fifth day of the published chart week, being the most representative day of the week regarding snow chart boundaries. We consider a month by averaging all the chart weeks that fall in that particular month, without taking account the number of days that belong to the previous or the following month. For example, if the chart

week goes from 30th January to 5th of February, we consider this week as January regarding the first day as the reference date of the week (Figure 3.1). We choose this criterion to avoid weighting days of the week which will add some artificial character to the record. Also, because we will deal with two-month seasons, the possible missing days are not relevant compared with the monthly resolution of the CMIP5 ensemble.

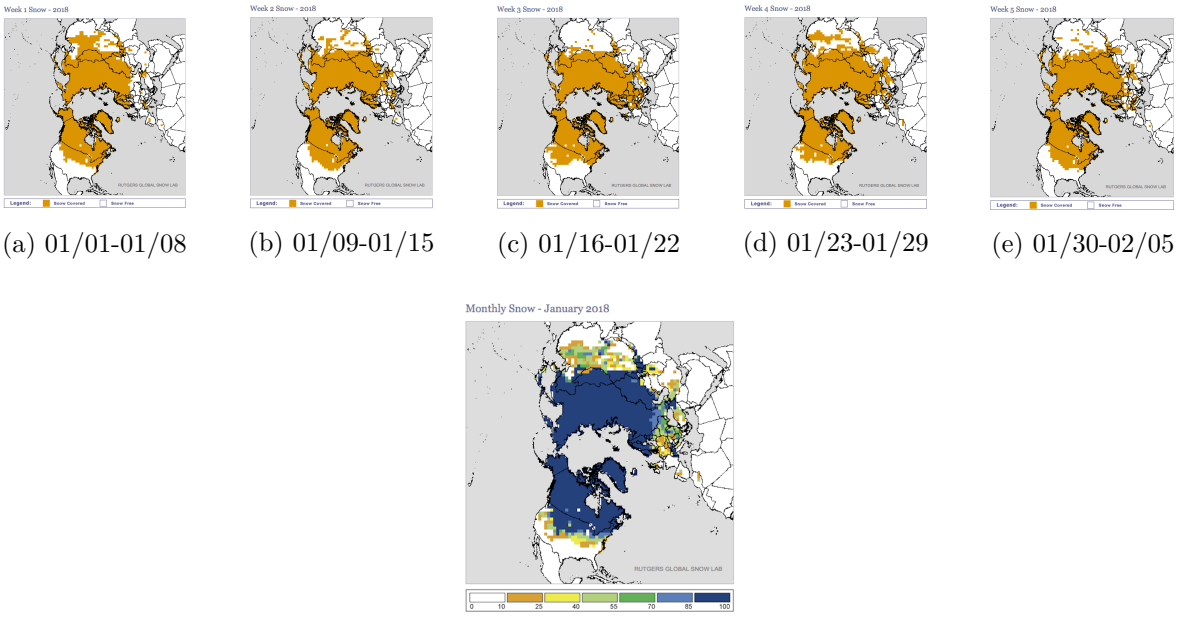

(a) 01/01-01/08 (b) 01/09-01/15 (c) 01/16-01/22 (d) 01/23-01/29 (e) 01/30-02/05

(f) January-2018

FIGURE 3.1 – Example of weekly to monthly conversion used in NOAA CDR. The snow field of January 2018 (f) is the result of averaging the five weeks (a to e). Figures are extracted from https://climate.rutgers.edu/snowcover/.

Snow Stations from the Russian Research Institute for Hydrometeorological Information - World Data Center (RIHMI-WDC, Bulygina *et al.*, 2011) provide a unique record of snow characteristics ; however, not all stations are continuous in time. The straightforward procedure is to examine the number of gaps of each station from 1979 to 2005 (Figure 3.2). A gap is defined as the absence of measurement in the record, i.e, when one date is missing in the station record. The values of "9999" meaning *"snow height's value is rejected or observations were not made"* (http://meteo.ru/english/climate/descrip2.htm) are not considered as gaps but are transformed to *NaN*.

For each of the 600 snow stations, we have computed the percentage of gaps considering the ratio of the number of absent data days to the total number of days in the period :

$$\%\,\text{of gaps} = \frac{\text{day gaps}}{\text{total days over period}}$$

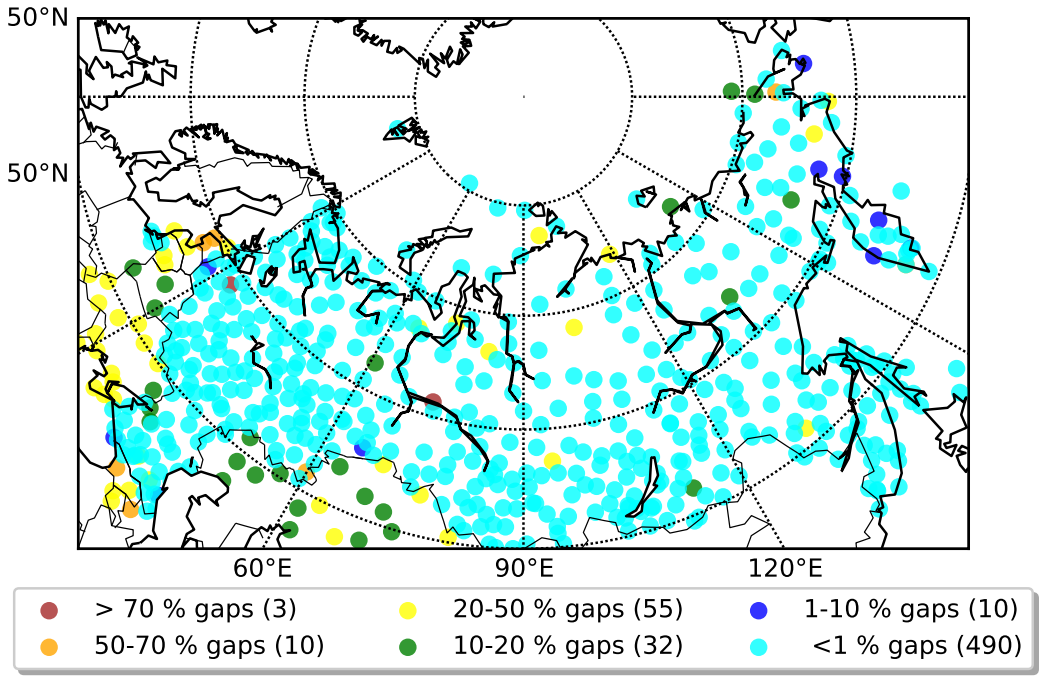

FIGURE 3.2 – Map of snow stations location and their classification depending on the percentage of gaps in the temporal record (in colors) for the period 1979-2005. The information about the coordinates and elevation of each station is described in http://meteo.ru/english/climate/snow.php.

There are 490 continuously running stations (less than 1% gaps) over 1979-2005 across the Russian territory. 10 snow stations have between 1 and 10% of gaps, 32 have 10-20% of gaps and 68 have more than 20% of absent days (Figure 3.2). We have selected the 490 stations (cyan) without gaps. In addition, as spatial density of snow stations is quite scarce in some regions of Eurasia (mainly in the northeast of Siberia), we have also kept stations with less that 10% gaps (dark blue). For instance, they can be used if the gaps appear to be in winter or summer, whereas during the mid-seasons of interest, temporal continuity prevails. Note that all snow stations shown in Figure 3.2 are located over the Russian territory (Figure 3.2). Since we only focus on Arctic land north of 50°N, we remove 66 snow stations from the total of 490 continuous stations

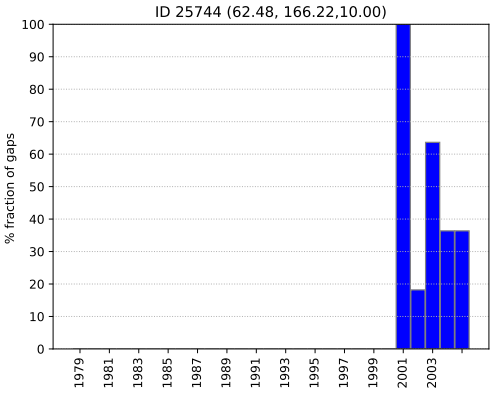

FIGURE 3.3 – Example of evaluation of number of gaps per year for the station ID 25744 at Kamenskoe. In the title is indicated identification number (ID), latitude, longitude and elevation (in meters).

that are situated south of the 50°N parallel as well as 2 stations with less than 10% of gaps. By doing so, we end up with 424 continuous polar snow stations in addition to 8 with between 1 and 10% gaps.

Of these last stations, we can consider seven of them as valid because the bulk of gaps is condensed in one year (ID 26258, 28661, 32389, 32583, 25954) or is out of the seasons of interest (ID 25594, 32411). There is only one dark blue station that is rejected because the number of gaps is quite elevated from 2000 to 2005 (ID 25744 ; Figure 3.3), maybe due to its replacement 7 km southwestwards in November 2002. Finally, we fill the gaps of the remaining stations with *NaN*. There is an area in the north of Siberia between the Yenisei and Lena Rivers with a scarce spatial coverage of snow stations (Figure 3.2). Unfortunately, the snow station "Essej" (ID 24105 ; yellow station to the west of the Yenisei River), which is located in a crucial enclave to cover this area, must be discarded as the record stopped in 1994.

We further restricted ourselves to snow stations displaying more than 70% of invalid or absent values in the seasonal time series. In this sense, when comparing against CMIP5 models, we do not produce any artificial bias. Consequently, 9 snow stations are removed. In total, we end up with 422 snow polar stations.

Two approaches can be used to compare *in situ* measurement with model grid cells. The first method consists in the averaging of the stations within particular model grid cell. This approach can be very effective if the distribution of stations is relatively homogeneous and sufficiently dense to cover all model grid cells. Unfortunately, the uneven spatial distribution of snow stations (Figure 3.2) and the coarse spatial resolution of general circulation models (Table 2.1) makes the "point to grid" method inconvenient for this case. The opposite approach consists in interpolating the model grid to the point locations. We used this method by performing a bilinear interpolation of the model and reanalysis climatological snow fields onto the location of snow stations. Figure 3.4 shows an example of the climatology of snow depth in March-April from the JRA-55 reanalysis in its original grid (Figure 3.4a) and the resulting interpolation to snow locations (Figure 3.4b). Note that there are some stations located overseas that show null values as they are out of the boundaries of snow land fields due to an ice-free land mask effect.

It is worth mentioning that while doing the interpolation with models and reanalyses, we do not include 19 snow stations. Snow climatological fields in models and reanalyses were defined in a domain restricted to 50°N and northward. When interpolating to a station located at 50°N, the

interpolation needs the information of the snow field at 49.5°N which is not defined inside the Arctic domain. Thus, for this particular analysis, we take into account only stations north of 50.5°N ; that is, in total, 403 snow stations.

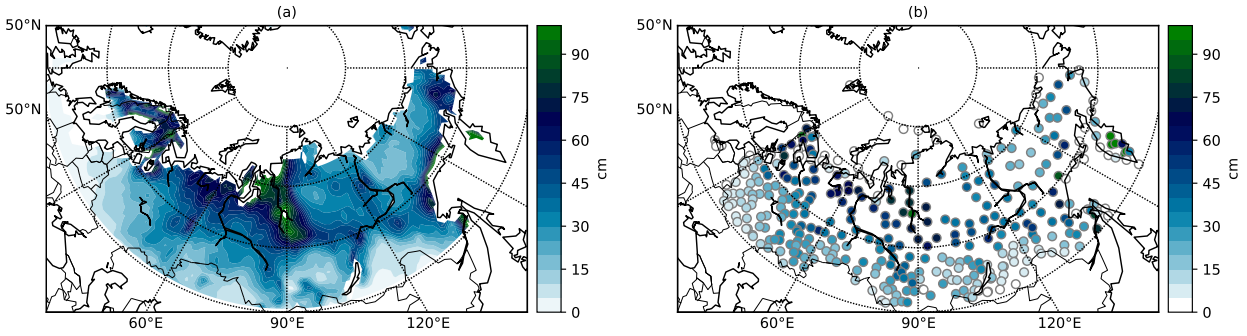

FIGURE 3.4 – (a) Climatology of snow depth in March-April during 1979-2005 from the JRA-55 reanalysis. (b) Same climatology but interpolated into the snow station point locations.

3.3 Ice-free land mask

The focus of this study is to evaluate snow in the terrestrial Arctic. It is therefore necessary to restrict our domain to an ice-free land surface. For that, we have used the variables *"sftlf"* (land area fraction) and *"sftgif"* (land ice area fraction) from the "fx" table of time-invariant fields on the atmospheric grid (https://cmip.llnl.gov/cmip5/docs/CMIP5_output_metadata_requirements.pdf). Even if some models include the land mask in the snow variable itself, in order to homogenize the analysis we have used the variables "sftlf" and "sftgif" of each CMIP5 model. We have applied two criteria to build the ice-free land mask (Table 3.3) : we selected those grid cells that contain 50% or more land fraction and less than 15% of permanent ice fraction. The main reason to apply these criteria is to exclude the permanent snow on ice in Greenland and glaciers, and the snow covering coastal sea ice, as well as the null values of the ocean.

Variable	**Standard name**	**Long name (Units)**	**Comment**	**Criteria of masking**
sftlf	land_area_fraction	Land Area Fraction (%)		< 50%
sftgif	land_ice_area_fraction	Fraction of Grid Cell Covered with Glacier (%)	(fraction of grid cell occupied by "permanent ice" (i.e., glaciers)	>15%

TABLE 3.3 – Criteria of ice-free land mask in CMIP5 models. Definition of variables extracted from the document "CMIP5_output_metadata_requirements.pdf" from https://cmip.llnl.gov/cmip5/docs/.

Even if some observational data sets produce their own land mask, they rarely provide an ice mask. For this reason, we decided to homogenize the masking procedure, as much as possible by choosing one mask for all data sets. We wish to find the most restrictive land-ice mask to ensures that we are not considering any area that would be masked in an other model. Figure 3.5 shows the ice-free land mask of all CMIP5 models (Table 2.1). We count the number of ice-free land cells on a $1.0° \times 1.0°$ grid for each of the model masks. Regarding the Arctic domain ($50°\text{N} - 90°\text{N}$), there is a total of 14400 (40 cells latitude $\times$ 360 cells longitude) grid cells ; if we consider only the terrestrial Arctic we find the number of cells of each CMIP5 models (Figure 3.6). As it is shown, the GISS-E2-R model is the most restrictive, having 4 965 ice-free land grid cells against 5 469 for MIROC5. This depends on several factors, for instance, the surface model, the definition of coastal areas or the spatial resolution. The singularity of GISS-E2-R masking is likely due to the representation of permanent ice in glaciers in the Alaska mountain range (Figure 3.5).

However, for the NOAA CDR data set we cannot apply this criteria as it is on a polar grid ; we decided not to do any interpolation to keep this data in its original binary format. NOAA CDR provides a binary land mask with the area of each grid that we can use for masking ocean grid cells, however, the ice mask is not provided. We applied July climatology (1979-2005) to generate a virtual "ice fraction mask". Using it, we masked the grid cells with more than 85% of snow cover, which is equivalent to less than 15% of the perennial snow fraction on ice as it is applied for CMIP5 models.

3.4 From fraction to binary

We convert the snow cover fraction climatology in CMIP5 models to a binary format following the satellite retrieval criterion from Robinson *et al.* (1993) for the NOAA CDR data set. The criterion specifies that if the grid contains a snow cover of 50% or more, we consider it as fully covered "1", otherwise the grid value is "0". To construct the binary field for the ensemble model, we first applied the conversion of SCE to binary form for the climatology field of each ensemble member (right-hand side of Figure 3.4). Thus, we set the grid cell to "1" if the SCE climatology value is superior to 50%, otherwise the grid cell is set to "0". Next, once we have computed all the binary climatologies for each of the model members, we estimate the value of the ensemble binary mean (left-hand side of Figure 3.5). For that, we set the grid cell to "1" if more than half of the ensemble members for a particular model reports "1", otherwise, the grid cell in the ensemble

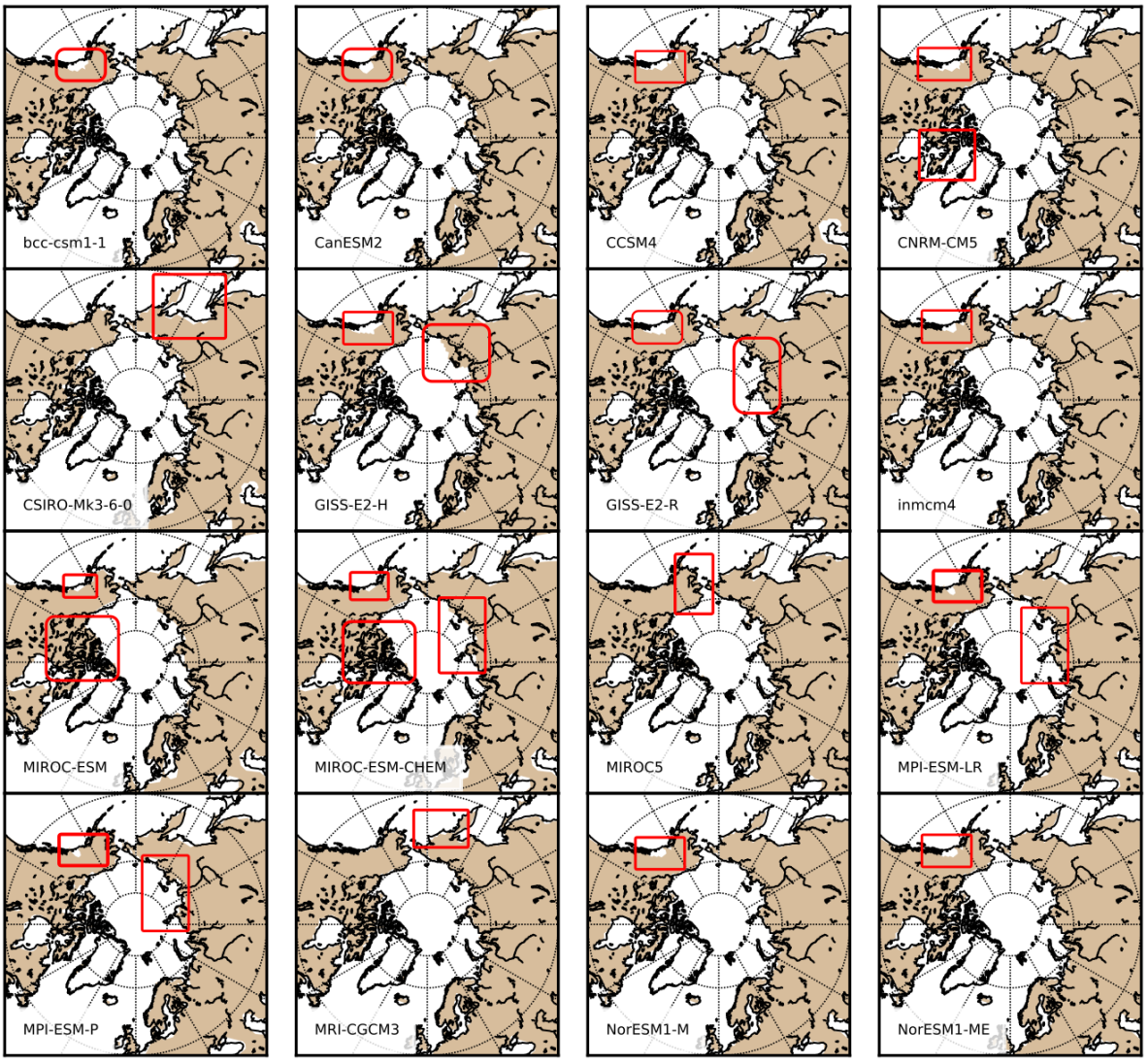

FIGURE 3.5 – Ice-free land mask for the Arctic domain (50°N – 90°N) of each of CMIP5 models from Table 2.1.

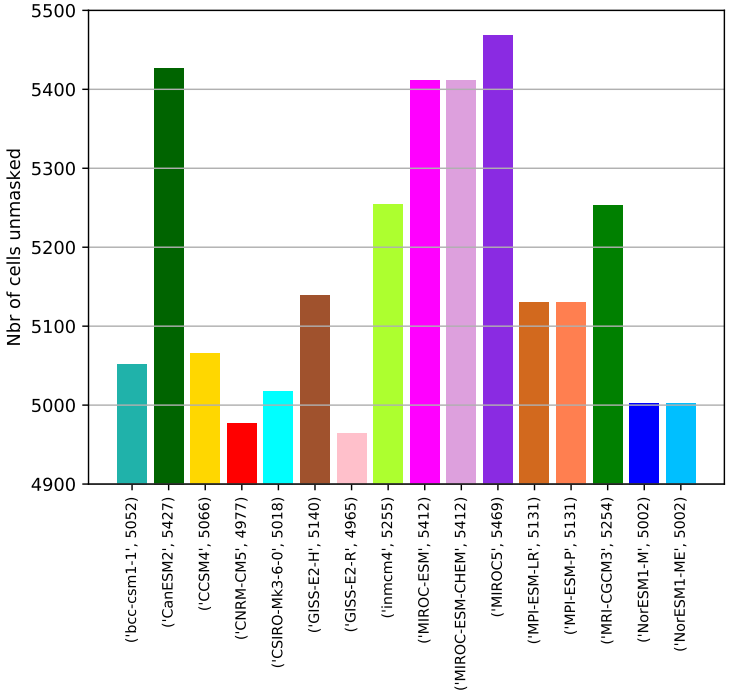

FIGURE 3.6 – Number of cells contained in the ice-free land Arctic domain ($50°\text{N} - 90°\text{N}$) in each of CMIP5 models from Table 2.1.

averaged model time series will be set to "0". In this manner, we obtain the binary field of the ensemble model (right-hand side of Figure 3.5).

- Model CMIP5-

Member 1	
50%	80%
20%	0%

$\Rightarrow$

Bin Member 1	
1	1
0	0

TABLE 3.4 – Criteria of conversion from snow fraction to binary.

Bin Member 1			**Bin Member 2**			**Bin Member 3**				**Bin Ensemble Mean**	
1	1	+	0	0	+	0	1	$\frac{1+0+0}{3} < 0,5$		0	1
0	0		0	1		0	1	$\Rightarrow$		0	1
								$\frac{0+1+1}{3} > 0,5$			

TABLE 3.5 – Criteria of ensemble binary averaging.

3.5 Statistical analysis of snow characteristics

3.5.1 Test for differences of mean for paired samples

When comparing differences in climatologies between models and observations, it is necessary to assess if these differences are significant or not at a certain level. Models and reference data sets can be considered as paired or "non-independent" samples as the values making up the two averages are "observed" simultaneously (Wilks, 2011). The size of model (n_1) and observation (n_2) samples should be equivalent. For example, the time series of snow depth displayed by the model and the particular reanalysis are computed at the same location and during the same period of time. When paired data of this kind are used in a two-sample sample Student's t test, the two different averages are generally correlated. The straightforward approach is to transform the problem to one-sample setting by analyzing differences between members of the $n_1 = n_2 = n$ (Wilks, 2011).

Let call x_1 to the model sample and x_2 to the observed sample, the size of each sample being equally $n_1 = n_2 = n$ pairs that can be considered as one-sample setting where

$$\Delta = x_1 - x_2$$

with sample mean

$$\bar{\Delta} = \frac{1}{n}\sum_{i=1}^{n}\Delta_i = \bar{x_1} - \bar{x_2}$$

The corresponding populations of delta will be $\mu_\Delta = \mu_f - \mu_o$ which is often zero under null hypothesis H_o. Then the test statistic for a Student's t-test corresponds to :

$$t_{score} = \frac{\bar{\Delta} - \mu_\Delta}{(s_\Delta^2/n)^{1/2}}$$

where s_Δ^2 is the sample variance of the n differences. Any joint variation in the pairs making up the difference $\Delta = x_f - x_o$ is also automatically accounted for in the sample variance s_Δ^2 of those differences (Wilks, 2011). We use this statistic to test the degree of significance of climatological differences. For example, the period for snow cover extent and snow depth is 1979-2005 (1981-2005 for SWE) which accounts for 27 years and thus, $n_1 = n_2 = 27$ pairs of data at 99% of confidence level from a two-tailed distribution, the corresponding t value is 2.771.

3.5.2 Statistical significance of linear trend

The detection and estimation of trends and their associated statistical significance are important aspects of climate research. Given the monthly time series of snow characteristics, we have computed linear trends to estimate the rate of snow change over the period 1979-2005 (1981-2005 for SWE). Prior to applying the linear regression, seasonal mean values over the period considered have been removed from the time series. Let consider the monthly time series of snow anomalies $y(x)$, where x is time period. The least squared linear regression estimate of the trend in $y(x)$, that is β, minimizes the squared differences between $y(x)$ and the fitting line $\widehat{y}(x)$:

$$\widehat{y}(x) = \alpha + \beta x + \epsilon$$

where x is known (time period), α and β are unknown and ϵ are the residuals. To test whether or not this trend is statistically significant, we have performed a Student t-test. The null hypothesis is that the regression coefficient β is zero given the uncertainty in estimating the trend.The residual of the regression ϵ_i are defined as

$$\widehat{\epsilon_i} = y_i - \widehat{y_i} = y_i - (\alpha + \beta x_i)$$

For statistically independent values of ϵ_i, the variance of β, s_β^2 is defined as

$$s_\beta^2 = \frac{s_\epsilon^2}{\sum_{i=1}^{n}(x_i - \bar{x})^2}$$

where s_ϵ^2, the variance of the residuals about the regression line, is given by :

$$s_e^2 = \frac{1}{n-2}\sum_{i=1}^{n}\widehat{\epsilon_i}^2$$

Thus, we can determined the t score for statistical significance by

$$t_{score} = \frac{\beta}{s_\beta}$$

which follows a t-distribution with n-2 degrees of freedom (Wilks, 2011). For example, for the snow cover trend over the Arctic during 1979 to 2005 (i.e., implying 27 years), the critical t value for a two-tail test with degrees of freedom equal to 25 and confidence level of 90% is 1.708.

3.5.3 Taylor Diagram

The Taylor diagram is a concise statistical summary of how well different patterns matches the observations (Taylor, 2001). This 2-D diagram provides the degree of correspondence between two fields by indicating the centered root mean squared error (RMS), the standard deviation σ and the correlation coefficient R between them. As described in Taylor (2001), let consider two variables f_n, the simulated field, and r_n, the observational reference which are defined by N discrete points. For example, we apply this analysis for the evaluation of snow time series with $N = 27$ years for snow cover and snow depth (25 years for SWE). The correlation R coefficient between simulated f and observed r field is :

$$R = \frac{\frac{1}{N}\sum_{n=1}^{N}(f_n - \bar{f})(r_n - \bar{r})}{\sigma_f \sigma_r}$$

Considering $\bar{f}$, and $\bar{r}$ as the mean values, and σ_f and σ_r the standard deviations of f and r. When apply to the time series diagram, $\bar{f}$ and $\bar{r}$ will refer to the seasonal climatology over the whole period. The correlation coefficient R reaches the maximum of 1 when for all n, $(f_n - \bar{f}) = \alpha(r_n - \bar{r})$ with $\alpha = cte > 0$; in this case, the two fields have the same centered pattern of variation, however, it is not possible to determine if they have the same amplitude of variation, which can be defined by their variances.

The statistic most frequently used to quantify difference between models and observation is the RMS difference E.

$$E = \left[\frac{1}{N}\sum_{n=1}^{N}(f_n - r_n)^2\right]^{1/2}$$

The differences between patterns can be isolated by considering differences between the means of the two fields, that is, the overall bias :

$$\bar{E} = \bar{f} - \bar{r}$$

and by the centered pattern RMS difference which is defined as :

$$E' = \left\{\frac{1}{N}\sum_{n=1}^{N}\left[(f_n - \bar{f}) - (r_n - \bar{r})\right]^2\right\}^{1/2}$$

The two components $\bar{E}$ and E' can be added quadratically to yield the full means square difference :

$$E^2 = \bar{E}^2 + E'^2$$

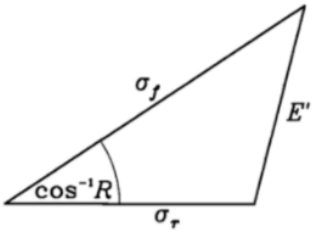

FIGURE 3.7 – Geometric relationship between the correlation coefficient R, the centered pattern RMS error E', and the standard deviations σ_f and σ_r of the test and reference fields, respectively Extracted from Taylor (2001).

As two patterns become more similar, the pattern of RMS approaches to zero. However, for a given E', it is impossible to distinguish if the error is due to differences in structure and phase or in the amplitude of variations.

The correlation coefficient R and the centered RMS E' quantify the correspondence between two patterns. Together with the information of fields variances (σ_f and σ_r), these four statistics are very useful to evaluate the differences between two patterns. The Taylor diagram is based on the relationship between the four statistical quantities following :

$$E'^2 = \sigma_f^2 + \sigma_r^2 - 2\sigma_f\sigma_r R$$

and which can be applied to the law of cosines :

$$c^2 = a^2 + b^2 - 2abcos\phi$$

where a, b, c, are the lengths of the sides of the triangle and ϕ the opposite angle to the side c (Figure 3.7).

Chapter 4

Spatial structure of snow characteristics

Contents

This chapter is devoted to the evaluation of the spatial distribution of snow characteristics over the Arctic in the mid-seasons. We investigate the representation of snow in CMIP5 models and in different data sets including reanalyses, satellite-based products and *in situ* measurements which have been described in Chapter 2. This chapter is divided into three main sections dedicated to the analysis of climatology, annual cycle and quantile statistics of snow characteristics, that are snow cover extent, snow water equivalent and snow depth. In some cases, we also include an additional analysis specific for a particular snow variable.

4.1 Climatology

4.1.1 Snow cover

Figure 4.1 shows the climatology of snow cover for the melting (Figure 4.1a) and the onset (Figure 4.1b) seasons for the period 1979-2005 from the NCEP/CFSR reanalysis. In this section, we consider NCEP/CFSR as the reference for SCE evaluation in the models due to its high spatial

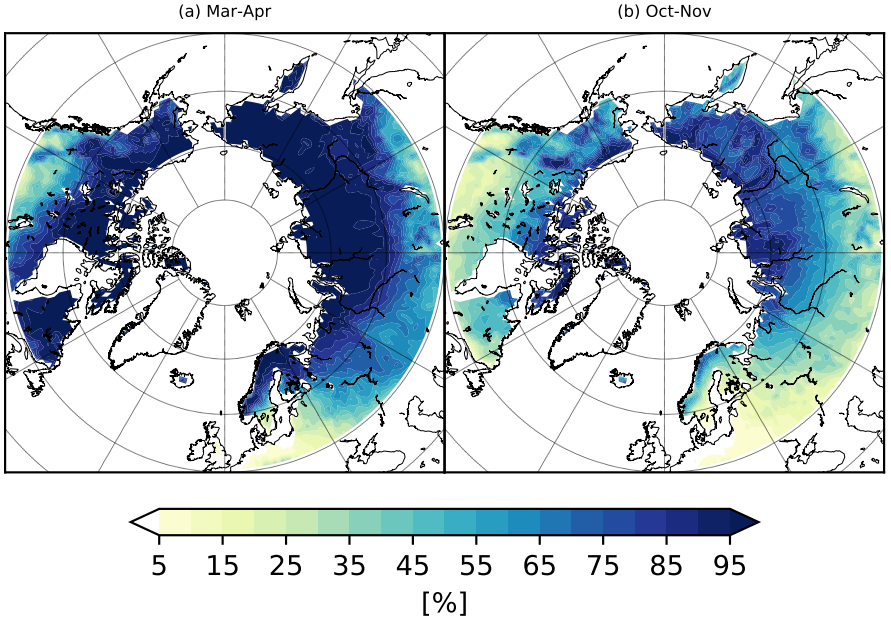

FIGURE 4.1 – Climatology of snow cover extent in March-April (a) and October-November (b) from the NCEP/CFSR reanalysis over the period 1979-2005.

resolution ($0.5° \times 0.5°$) compared to that displayed by NOAAV2c ($2.0° \times 1.75°$) (Table 2.2). Note that we do not include NOAA CDR in this analysis because of the incompatibility between grid projections as mentioned in Chapter 2.

In March-April (Figure 4.1a), complete snow cover (100%) is observed over the northern Eastern Eurasia as well as over Northern Canada and Alaska. Note that the areas covered by more than 80% of snow match well the areas of continuous permafrost (Brown *et al.*, 1997). In the southern part of Western Eurasia, snow has almost melted with SCE being around 15% whereas in Scandinavia, SCE values of 80-100% are observed northern of 60°N. Over North America, the decrease in SCE from north to south is more pronounced than over Eurasia in both seasons.

In October-November (Figure 4.1b), the maximum SCE (from 80% to 100%) is observed over Northern Alaska, the Canadian Archipelago and the northern part of Eastern Eurasia. Over North America, high values of SCE are observed in the Brooks mountain range in Alaska, in the Mackenzie Mountains in the northwest of Canada and over the Canadian Archipelago. In the Rocky Mountains in Western Canada, SCE values are around 50%. Over Eurasia, the maximum of SCE is observed over the northern part of Eastern Siberia with maxima of 90% to 100% over the Verkhoyansk, Chersky and Kolyma mountain ranges.

Differences of climatology

First, we assess the differences of climatology between both reanalyses, NCEP/CFSR and NOAAV2c, for spring and autumn from 1979 to 2005 (Figure 4.2). In March-April (Figure 4.2a), there is a good agreement over north central and far eastern Siberia as well as over east central Canada and over the Canadian Archipelago. By contrast, the mismatch occurs above the Eurasian Dry Land Band (EDLB, Groisman *et al.*, 2018) in Siberia with differences up to 50 p.p. [1] SCE east of the Lake Baikal. Additionally, NOAAV2c displays excess of SCE compared to NCEP/CFSR over the Rocky Mountains reaching 60 p.p. values. This local strong disagreement is likely due to a better resolved topography in NCEP/CFSR which makes it more sensitive to temperature changes that reduce SCE earlier in the season than NOAAV2c. In Scandinavia, differences are reversed and NCEP/CFSR estimates a slightly larger SCE than NOAAV2c but only by about 15 p.p. and very locally. Averaged over each of the subdomains NOAAV2c displays overestiamation by 6 p.p. in Eurasia and by 8 p.p. in North America in comparison with NCEP/CFSR (Tables B.2 and B.3, respectively). During the onset season (Figure 4.2b), NOAAV2c shows larger values of SCE than NCEP/CFSR over the whole terrestrial Arctic. Over North America differences are greater than in Eurasia, being of 15-20 p.p. in the southern part and 30-40 p.p. over the Canadian Archipelago ; however, averaged over North America, the discrepancy is only 12 p.p. (Table B.6). Differences across Eurasia cover the continent uniformly with NOAAV2c displaying less than 15 p.p. SCE exceeding NCEP/CFSR. On average the difference between both reanalyses over Eurasia is equal to 8 p.p. SCE (Table B.5). Overall, both reanalyses agree on the representation of SCE during the melting and onset seasons.

We now turn to the evaluation of snow cover climatology across the ensemble of CMIP5 models (Table 2.1) in the mid-seasons during the present period from 1979 to 2005. Figure 4.3 shows the differences between March-April SCE climatology in each of the selected CMIP5 models minus the NCEP/CFSR reanalysis. We can separate all models by three groups. The first group (bcc-csm1-1, CSIRO-Mk3-6-0 and both versions of MPI-ESM-LR/P ; Figure 4.3a,e,l,m) generally underestimates snow cover compared to NCEP/CFSR by almost 50 p.p. with the largest differences observed in the southern part of Western Eurasia. The second group (CanESM2, MIROC-ESM/-CHEM and MRI-

1. The arithmetic difference of two percentages is expressed in percentage points or percent points [pp] or [p.p.]. For example, if the model displays 80 % of SCE and the reanalysis, 30 % SCE, the difference is 50 p.p. not 50 % as this can induce to wrongly state that the model is doubling the value of the reanalysis.

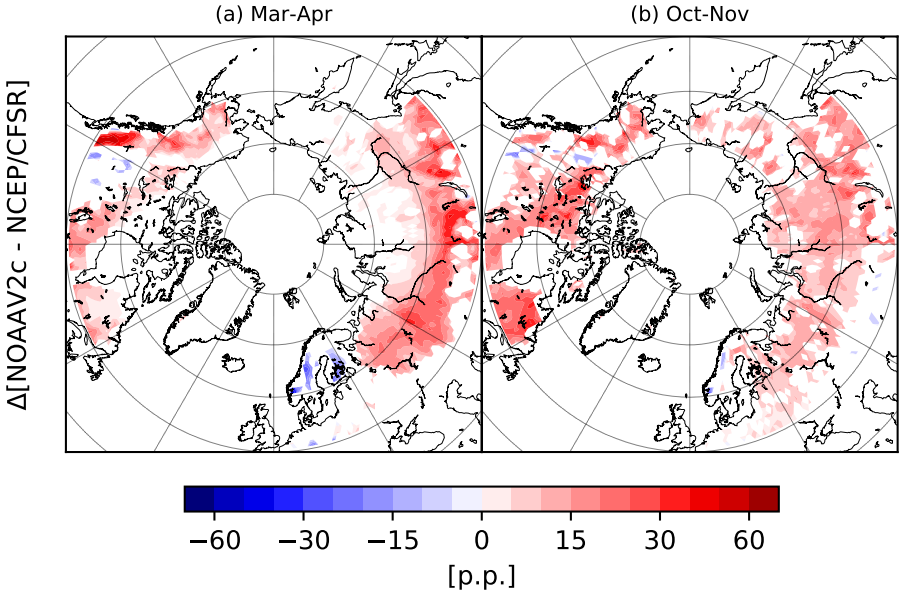

FIGURE 4.2 – Differences for March-April (a) and October-November (b) snow cover climatology of NOAAV2c minus NCEP/CFSR. Only differences with p-values less than 0.01 from the t-Student test are shown.

CGCM3 ; Figure 4.3b,i,j,n) broadly overestimates SCE with the largest differences observed in the Rocky Mountains (almost 60 p.p. by CanESM2). These four models show a zonal underestimation of 35 p.p. along the southern edge of Western Eurasia (Figure 4.3b,i,j), but smaller for MRI-CGCM3 being of 15 p.p. (Figure 4.3n). The third group (CNRM-CM5, GISS-E2-H/R and MIROC5 ; Figure 4.3d,f,g,k) demonstrates a dipole structure of differences with underestimation of SCE in the north and overestimation in the south, both being within 30 p.p. . The model inmcm4 (Figure 4.3h) shows overestimation in the south part of Eastern Eurasia from 15 p.p. to 40 p.p. and local differences of the opposite sign smaller than 30 p.p. in Western Canada. Similar patterns are shown by CCSM4 and NorESM1-M/ME (Figure 4.3c,o,p) with underestimation up to 30 p.p. in Western Eurasia and Eastern Canada, whereas in the south of Eastern Eurasia and west of Canada are characterized by an overestimation by 15 p.p. . The smallest differences are observed for both versions of NorESM1-M/ME (Figure 4.3o,p) and range from - 35 p.p. to 35 p.p. in the south of Eurasia and in the Rocky Mountains.

In the onset season, 7 of 16 models (bcc-csm1-1, CSIRO-Mk3-6-0, MIROC's and MPI's versions ; Figure 4.4a,e,i,j,k,l,m) show a general underestimation of SCE up to 60 p.p. over the whole terrestrial Arctic. In contrast, the models CCSM4, inmcm4, MRI-CGCM3 and NorESM1-M/ME (Figure 4.4c,h,n,o,p) demonstrate general overestimation of SCE over North America and Eastern Eurasia

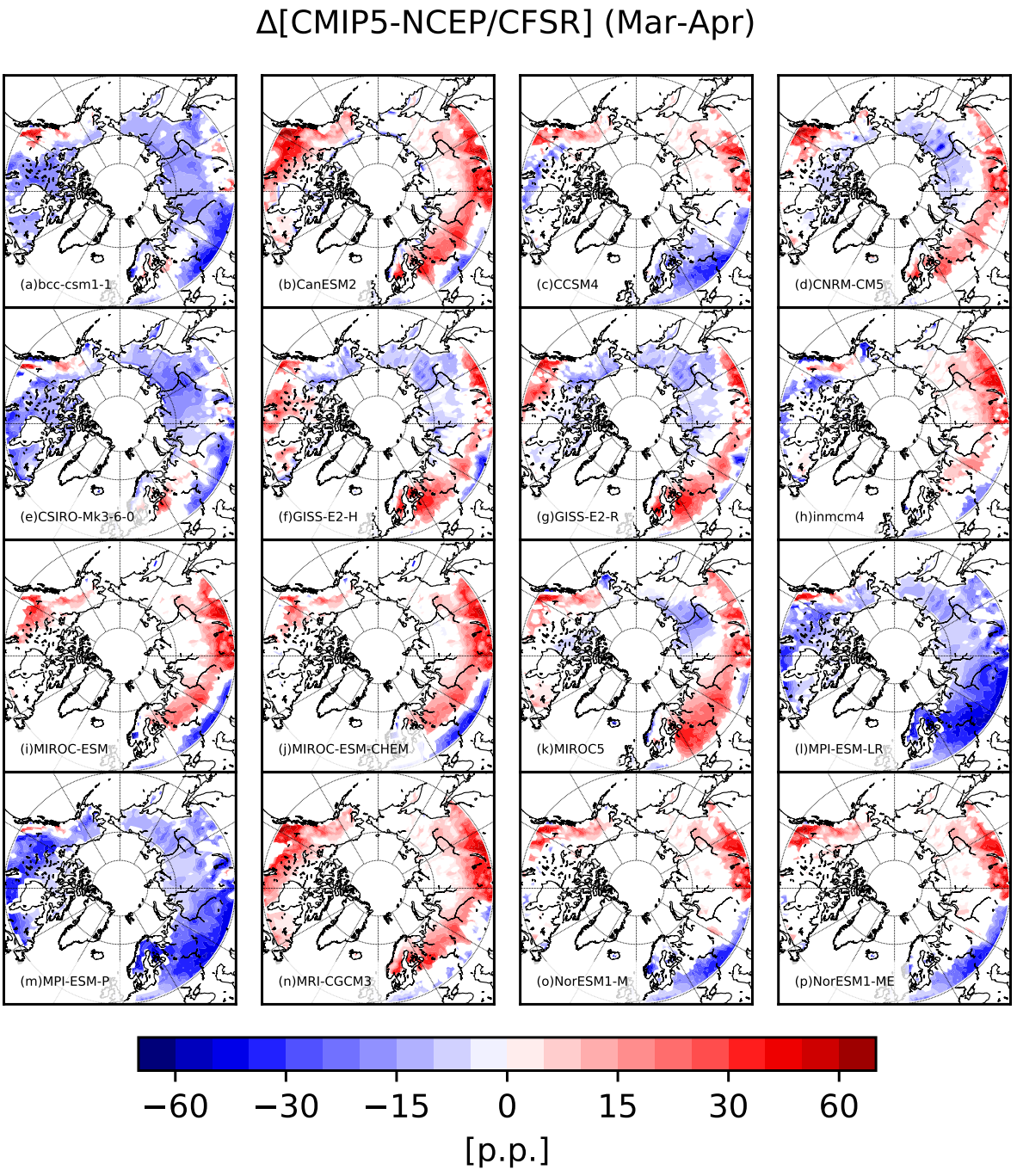

FIGURE 4.3 – Difference of March-April snow cover climatology of each ensemble CMIP5 minus NCEP/CFSR. Only differences with p-values less than 0.01 from the t-Student test are shown.

by 50-60 p.p. . GISS-E2-H/R (Figure 4.4f,g) exhibit overestimation in Western Eurasia and Eastern North America by 30 p.p. and underestimation in the coastal regions of East Siberian Sea and Bering Sea by 25 p.p. . The smallest differences are observed for CanESM2 and CNRM-CM5 (Figure 4.4b,c) and they show a good agreement with NCEP/CFSR especially in central Siberia.

The differences between CMIP5 models and the NOAAV2c reanalysis (not shown) are very similar to those found for NCEP/CFSR in terms of spatial patterns. However, NOAAV2c tends to slightly overestimate the SCE climatology of NCEP/CFSR (Figure 4.2). Therefore, when models have shown a positive (negative) bias compared to NCEP/CFSR, these differences are smaller (larger) in magnitude and less (more) significant when using NOAAV2c as reference.

Snow margin position

Figure 4.5 shows the position of the snow margin for spring (March-April) and autumn (October-November) for all the CMIP5 models and two reanalyses from 1979 to 2005. The position of the snow margin was defined as the 50% SCE contour. For both reanalyses, NOAAV2c and NCEP/CFSR, the snow margin position is computed directly by considering the contour of 50% SCE of the March-April and October-November climatologies for the period 1979-2005. We do not include NOAA CDR in this analysis because of the incompatibility between grid projections as mentioned in Chapter 2. To achieve comparability, we create binary fields for CMIP5 models with "1" attributed to all grids displaying March-April or October-November SCE $\geq$ 50% and with "0" for the remaining grid cells (further details in Chapter 3). To construct the binary field of each model with ensemble members, we first applied the conversion of SCE to binary form for each ensemble member and then set the grid cell to "1" if more than the half of the ensemble members for particular model report "1", otherwise, the grid cell in the ensemble averaged model was set to "0". By doing so, for each season, we obtain 16 binary fields corresponding to each of the CMIP5 models. To evaluate the agreement on position of the snow margin among CMIP5 models, we further counted the number of "1" for each season over the model ensemble. For example, value 4 in a grid cell implies that 4 out of 16 models display SCE $\geq$ 50%. If this grid cell is captured by the contour of the snow margin in the reanalyses, these 4 models are considered as representing the snow margin in agreement with the reanalyses.

Both reanalyses are in a better agreement with each other in spring (Figure 4.5a) than in autumn (Figure 4.5b). In March-April, the snow margins in both products match each other almost perfectly.

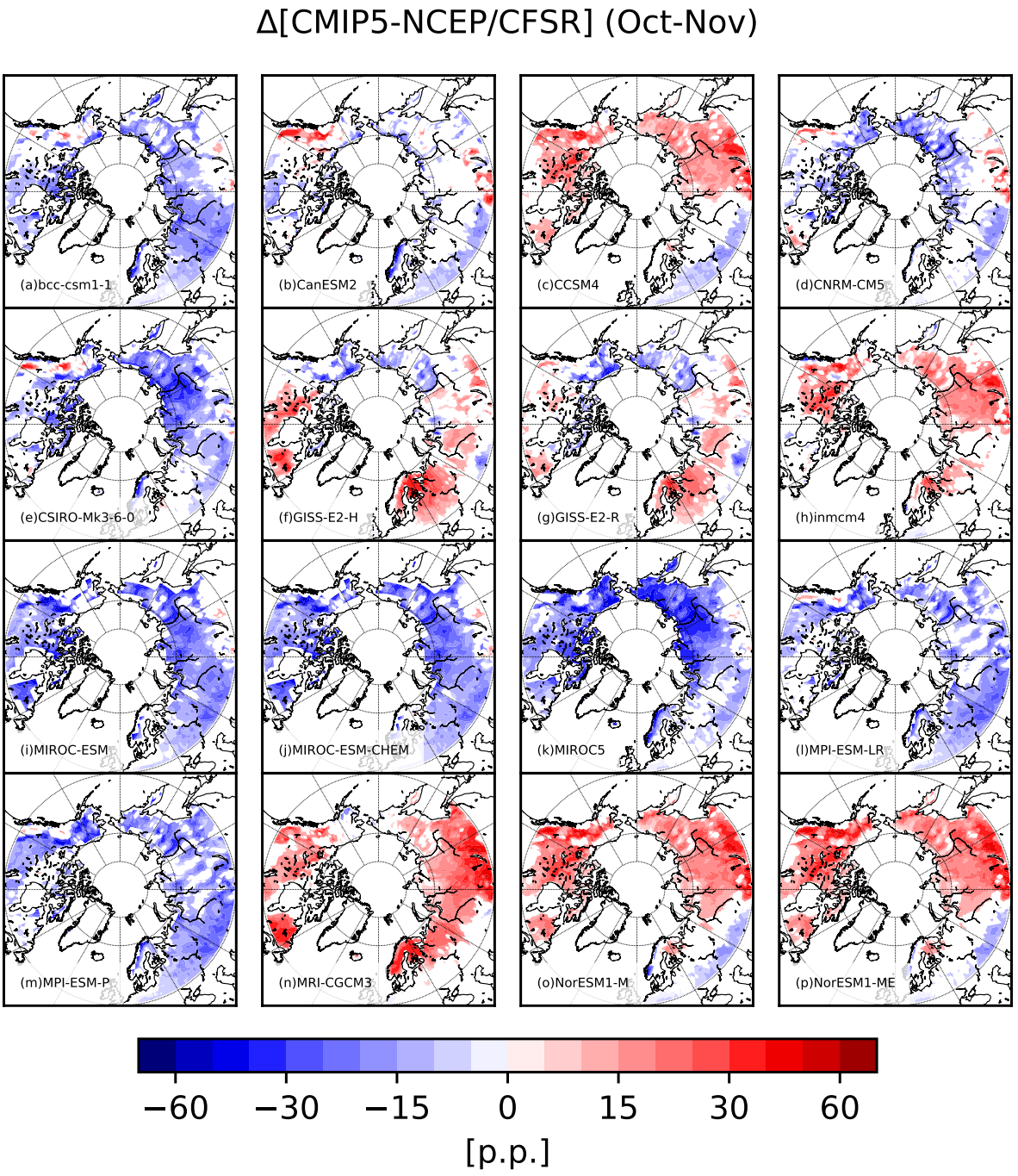

FIGURE 4.4 – Difference of October-November snow cover climatology of each ensemble CMIP5 minus NCEP/CFSR reanalysis. Only differences with p-values less than 0.01 from the t-Student test are shown.

However, in the onset season both reanalyses exhibit large spatial discrepancies with a deviation between the snow margins of about 10 degrees latitude. These discrepancies are more pronounced over North America than over Eurasia. This is due to a less intense onset of SCE in NOAAV2c than NCEP/CFSR, which is consistent with the faster rate of increase in SCE in NCEP/CFSR than in NOAAV2c in autumn (Figure 4.17c).

The position of the snow margin is also in a better agreement between different models and reanalyses during March-April rather than in October-November. This suggests that spatial discrepancies in the position of the snow margin are likely due to differences in starting time of melting season among CMIP5 models. The mismatch is accentuated in the south of Western Siberia, with only 3-4 models being consistent with the reanalyses. The snow margin over North America is more accurately represented with 10-12 models being in a close agreement with the reanalyses. In central and northern Eurasia, over Scandinavia, Canada and Alaska all models fit reasonably well with the reanalyses (Figure 4.5a). However, in autumn (Figure 4.5b), the agreement between the model data sets and reanalyses becomes less evident. Only three of 16 models show the snow margin close to that of NCEP/CFSR whereas 10 other models are closer to NOAAV2c. A reasonably good agreement across all data sets is identified only for the Siberian Plateau, the Verkhoyansk mountainous region and Northern Canada. The worse agreement in the position of snow margin is observed for the southern part of North America and for the region west of the Lake Baikal. Some disagreements observed in coastal areas are associated with different ice-land masks.

4.1.2 Snow water equivalent

Figure 4.6 shows the climatology of Arctic SWE in the melting season (Figure 4.6a) and in the onset season (Figure 4.6b) during 1981-2005 derived from the CanSISE ensemble product. In March-April (Figure 4.6a), the areas with high SWE include the Kamchatka Peninsula and the region east of the Yenisei River, where SWE amounts to 300 $\mathrm{kg\,m^{-2}}$. Also, high values of up to 210 $\mathrm{kg\,m^{-2}}$ are observed over the Ural and Kolyma Mountains as well as over Eastern Canada. The remaining part of the terrestrial Arctic is characterized by values around 50 $\mathrm{kg\,m^{-2}}$. In October-November (Figure 4.6b), SWE values are smaller compared to spring. Maximum values of up to 100 $\mathrm{kg\,m^{-2}}$ are observed east of the Yenisei River. All over the Arctic, SWE is around 20 $\mathrm{kg\,m^{-2}}$ with larger values up to 60 $\mathrm{kg\,m^{-2}}$ over the Verkhoyansk, Chersky and Kolyma mountain ranges. White areas in Figure 4.6 correspond to the land ice mask of the CanSISE ensemble product visible

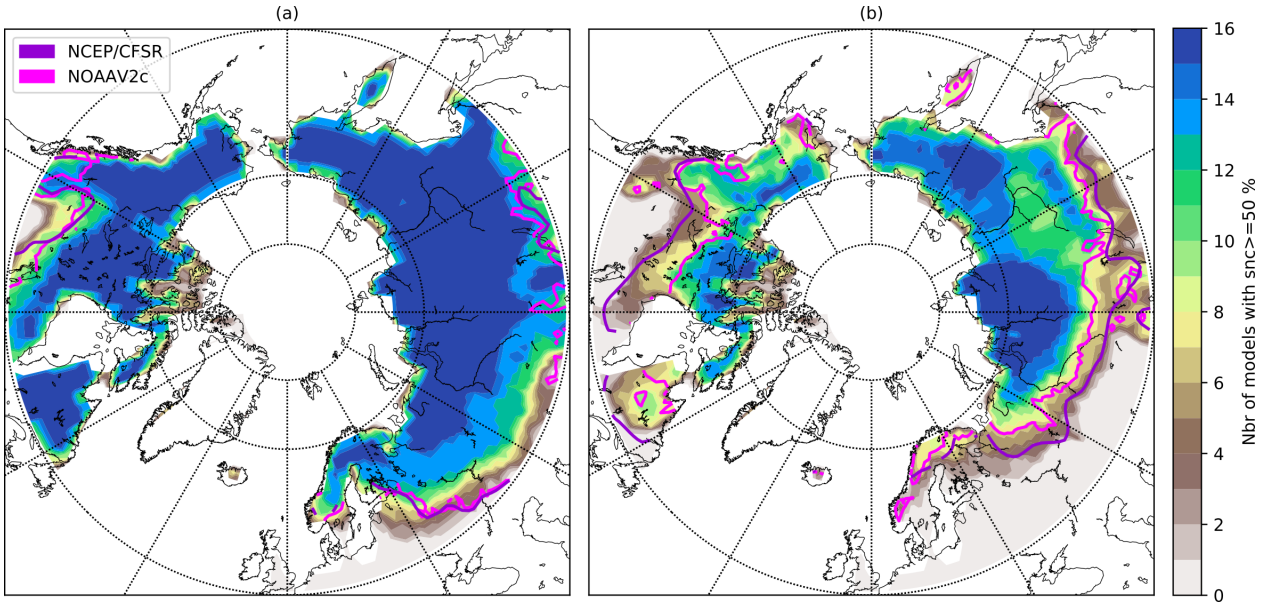

FIGURE 4.5 – The position of the snow margin is defined as the contourline of 50% snow cover fraction averaged over 1979-2005 in the NCEP/CFSR and NOAAV2c reanalyses (purple and pink lines, respectively) for (a) March-April and (b) October-November. The colorbar shows the number of CMIP5 models that display an ensemble seasonal mean of snow cover fraction equal or superior to 50%.

over the West Coast of Canada and Alaska as well as Scandinavia. This mask is originally from the MERRA reanalysis (M. Rienecker *et al.*, 2011) considering a grid cell masked when the land-ice fraction > 0 (*L. Mudryk, personal communication*). As mentioned in Chapter 3, this mask was not used for the analysis, instead the land-ice mask from GISS-E2-R was used.

Differences of climatology

We move to the evaluation of snow water equivalent climatology across CMIP5 models (Table 2.1) compared to the CanSISE ensemble product in the mid-seasons from 1981 to 2005.

Figure 4.7 shows the spatial patterns of differences in SWE spring climatology between CMIP5 models and CanSISE data for 1981-2005. There is an overall overestimation of SWE across nearly all CMIP5 models compared to the CanSISE ensemble product with differences ranging from 40 to 120 $\mathrm{kg\,m^{-2}}$ over most of Northern Eurasia and North America. Local underestimation up to -120 $\mathrm{kg\,m^{-2}}$ is observed in the majority of models in the delta of the Yenisei River and is especially pronounced in GISS-E2-H/R, MIROC-ESM/-CHEM and MIROC-5 (Figure 4.7f,g,i,j,k). This feature may result from the inability of models to capture the local cooling and moistening influence from the river that enhance the thickening of the snowpack. The pattern of underestimation of SWE

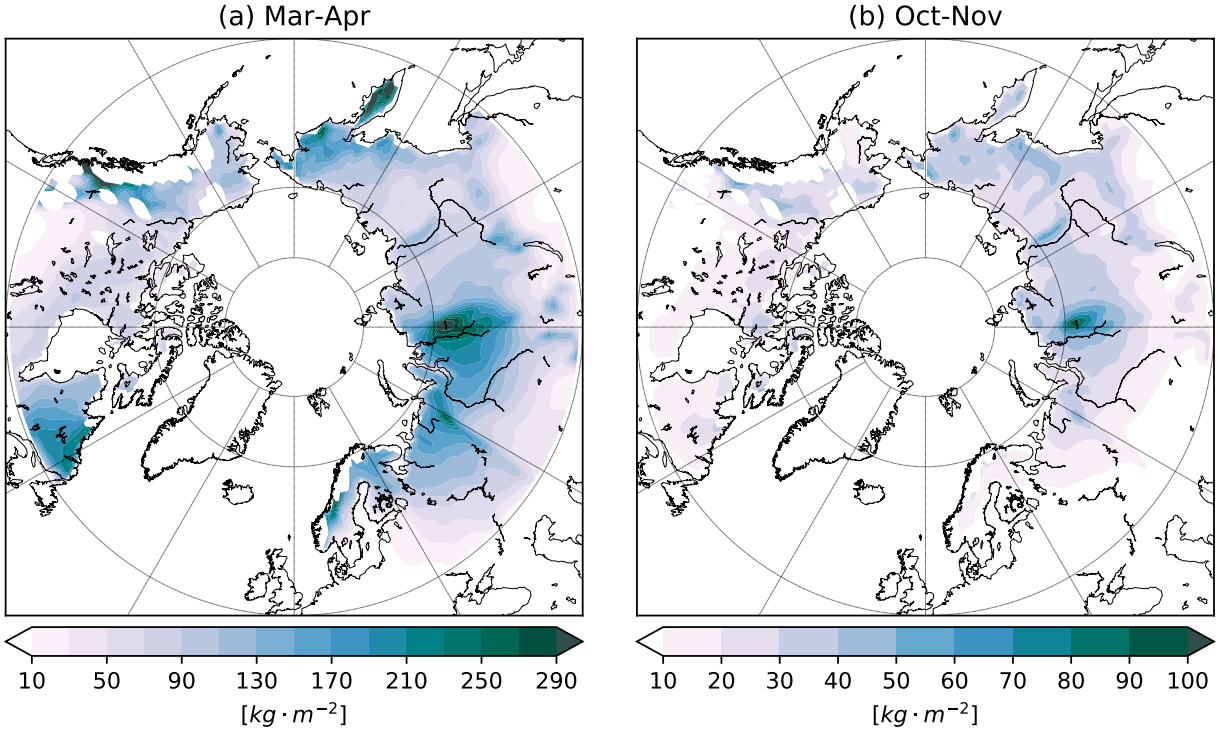

FIGURE 4.6 – Climatology of snow water equivalent in March-April (a) and October-November (b) from CanSISE product over the period 1981-2005.

over Western Eurasia is evident for CCSM4, CSIRO-Mk3-6-0, MPI-ESM-LR/P and NorESM1-M models. Among these, CSIRO-Mk3-6-0 demonstrates a pan-Arctic pattern of underestimation with differences around 26 kg m^{-2} (Table B.7, Figure 4.21).

The autumn differences between CanSISE and modeled SWE (Figure 4.8) are smaller compared to spring (by almost a factor of 3) with the strongest overestimation found for NorESM1-M and NorESM-ME (Figure 4.8o,p) and being up to 80 kg m^{-2} over the Far East of Eurasia. As for spring, CSIRO-Mk3-6-0 and MPI-ESM-LR/P show a broad underestimation of SWE which is stronger in Eurasia (Figure 4.8e,l,m). The relative differences are larger in spring than in autumn, which suggest that the discrepancies in the SWE representation are more related to the melting process, i.e., SWE changes in spring are more sensitive to temperature changes.

4.1.3 Snow depth

We consider the JRA-55 reanalysis as the reference data set above the other two reanalyses, ERA20c and NOAAV2c, for the evaluation of snow depth climatologies in CMIP5 models. This choice is justified by two reasons. First, we base our study on the results from Wegmann *et al.*

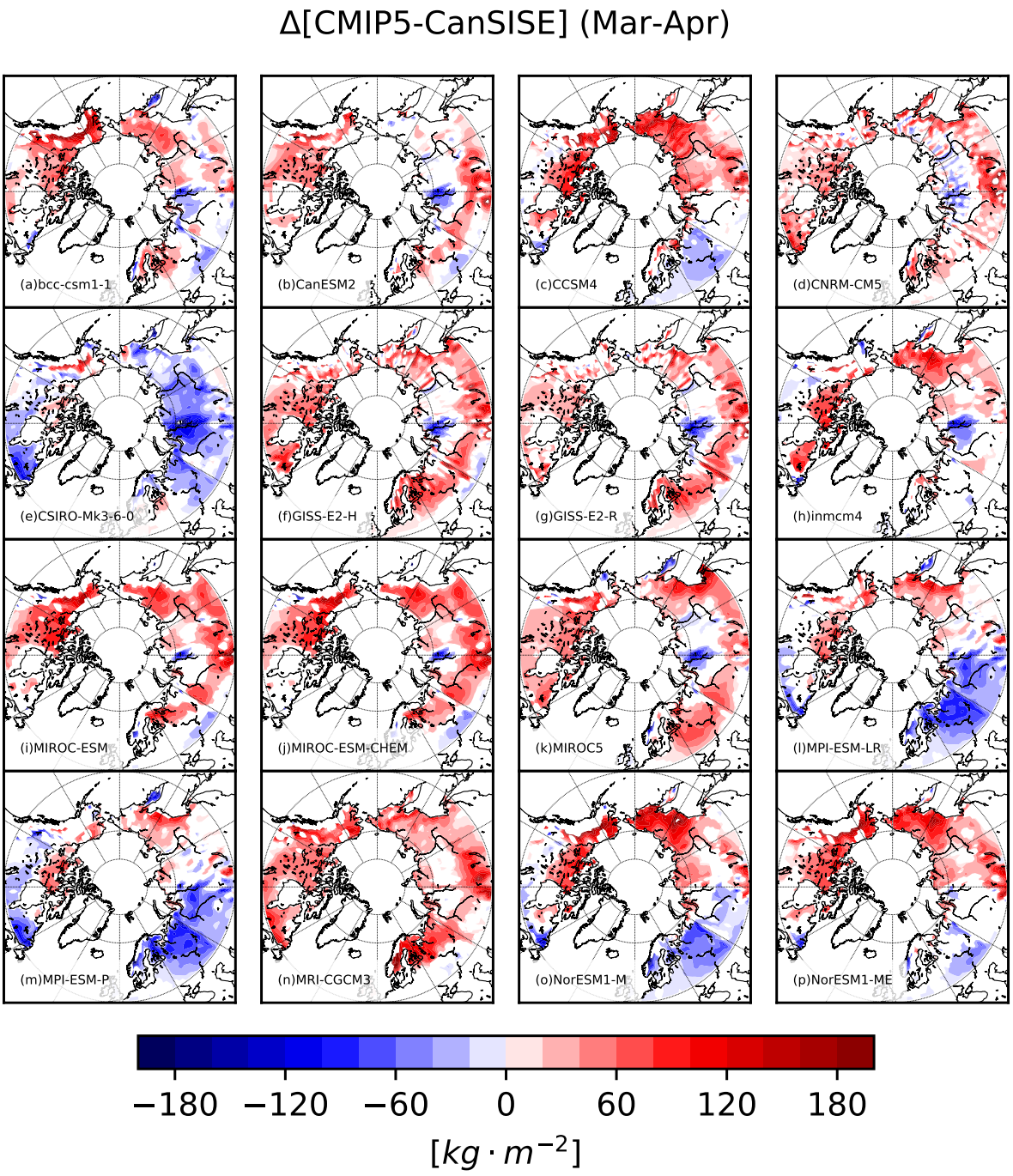

FIGURE 4.7 – Difference of March-April snow water equivalent climatology of each CMIP5 model minus CanSISE Ensemble product over the period 1981-2005. Only differences with p-values less than 0.01 from the t-Student test are shown.

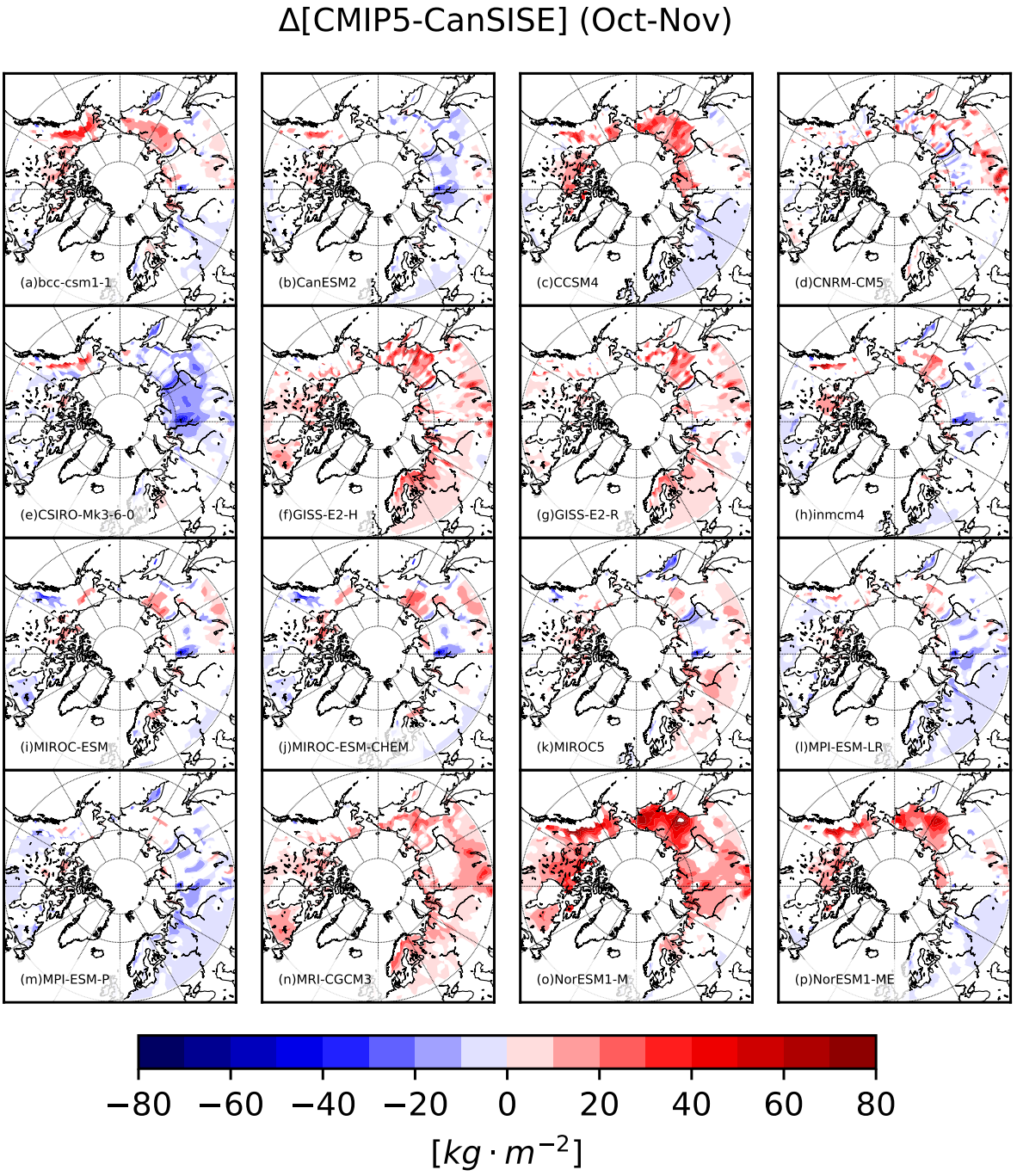

FIGURE 4.8 – Difference of October-November snow water equivalent climatology of each CMIP5 model minus CanSISE Ensemble product over the period 1981-2005. Only differences with p-values less than 0.01 from the t-Student test are shown.

(2017) who compared the snow depth representation in multiple reanalyses to the snow stations from RIHMI-WDC (Russian Research Institute of Hydro-meteorological Information-World Data Center) in April, October and November. The reanalyses evaluated can be divided in two families, namely, the European Center for Medium-Range Weather Forecasts (ECMWF ; ERA 20C, Poli *et al.*, 2016 ; ERA-Interim, Dee *et al.*, 2011 ; ERA-20C land and ERA-Interim land, Balsamo *et al.*, 2015) and the NOAA-CIRES Twentieth Century Reanalysis products (20CRv2 and 20CRv2c, Compo *et al.*, 2011). Wegmann *et al.* (2017) conclude that NOAAV2c (denoted 20CRv2c) shows generally larger values than the station data and that ERA20c displays the lowest values of snow depth among the six reanalyses evaluated. Our analysis shows similar results as in Wegmann *et al.* (2017) (Figure 4.14, 4.19) and we choose JRA-55 as the reference by the fact that it is a good compromise between ERA20c and NOAAV2c reanalyses. Second, one strength of JRA-55 is that it has the finest spatial resolution $\sim 0.56° \times 0.56°$ and assimilates *in situ* measurements (Kobayashi *et al.*, 2015).

Figure 4.9 shows the climatology of snow depth from the JRA-55 reanalysis during spring (Figure 4.9a) and autumn (Figure 4.9b) over the period 1979-2005. As expected, the snow depth spatial distribution in both seasons is very close to that of SWE (Figure 4.6) as the two variables represent snow accumulation on the ground and are directly related to each other (detailed explanation in Chapter 2).

In spring (Figure 4.9a), the highest values of snow depth (up to 150 cm) are observed in the east coast of the Laurentian Plateau in Canada and on a more region to region basis, over the Pacific Coast of Alaska and the Kamchatka Peninsula. Other centers of high snow accumulation are located over the delta of the Yenisei River and over Scandinavia with values from 70 to 90 cm. There is a clear positive gradient of snow accumulation towards the north, mainly in Canada ; but also, from the continent to the ocean over the Pacific Coast of Eurasia. This last feature is related to the presence of the Kolyma and Chersky mountain ranges which act as natural barriers for moisture coming from the ocean. Consequently, they favor snow accumulation on the Pacific Ocean side (as long as temperatures are below freezing). During the onset season (Figure 4.9b), snow depth values are smaller than in spring since the snow season has just started and accumulation has not yet occurred. The maximum values are located in the delta of the Yenisei River reaching 35 cm. In addition, relatively high snow accumulation is found over the Canadian Archipelago, north of Alaska and in the Kolyma and Chersky mountain ranges with values around 20 cm.

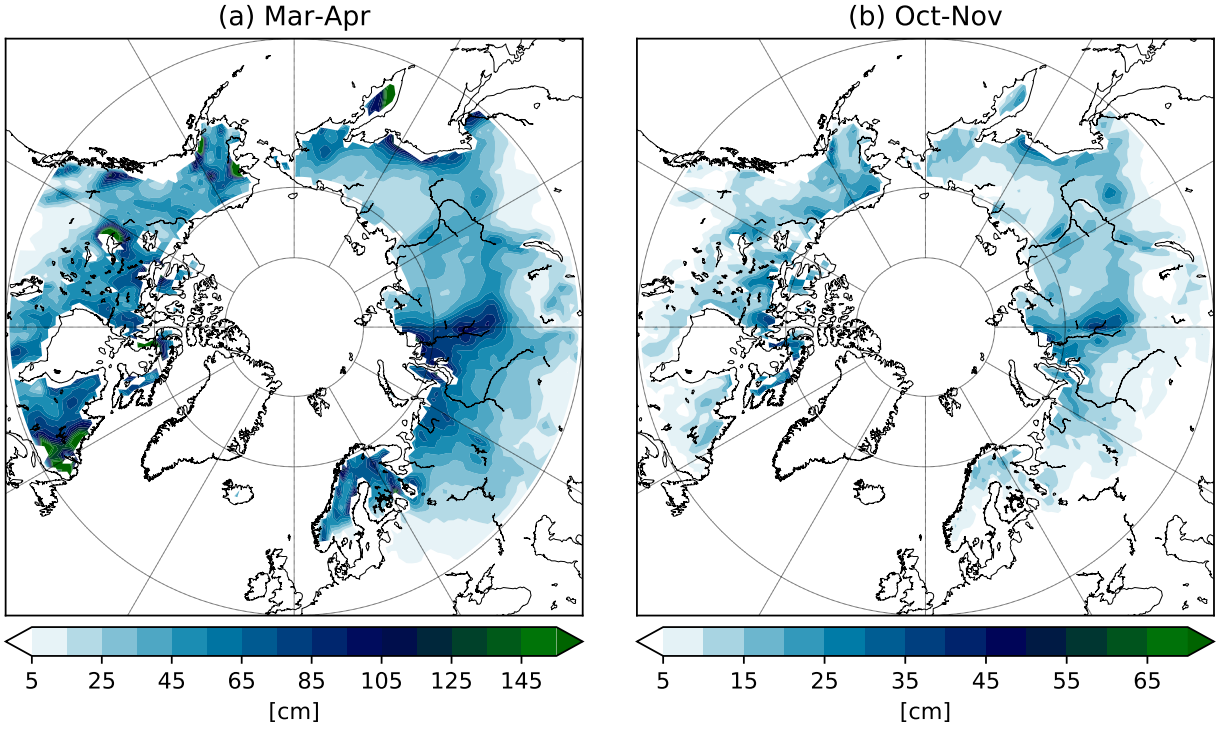

FIGURE 4.9 – Climatology of snow depth in March-April (a) and October-November (b) of the JRA-55 reanalysis over the period 1979-2005.

Differences of climatology

We first assess the difference of snow depth climatologies in ERA20c and NOAAV2c compared to JRA-55 in spring and autumn (Figure 4.10). The ERA20c reanalysis shows a general underestimation of snow depth over the whole terrestrial Arctic in both seasons. In spring (Figure 4.10a), maximum differences up to 60 cm are located in the coast of the Barents and Kara Seas and over the Ob and Yenisei Rivers. Smaller differences of 40-50 cm are found north of Canadian Archipelago. In autumn (Figure 4.10c), the magnitude of underestimation is smaller with the highest differences (up to 25 cm) located in the delta of the Yenisei River. NOAAV2c reanalysis displays an opposite sign of differences compared to ERA20c which is consistent with Wegmann *et al.* (2017). In spring (Figure 4.10b), NOAAV2c exhibits a general overestimation of snow depth, more remarkable across the Eurasian subdomain. The largest positive differences are located over Eastern Eurasia, particularly over the coast of Laptev Sea and east of the Lena River with values up to 60 cm. During the onset season (Figure 4.10d), differences are smaller in magnitude with values up to 30 cm and the centers of discrepancies are found over the same regions than in spring.

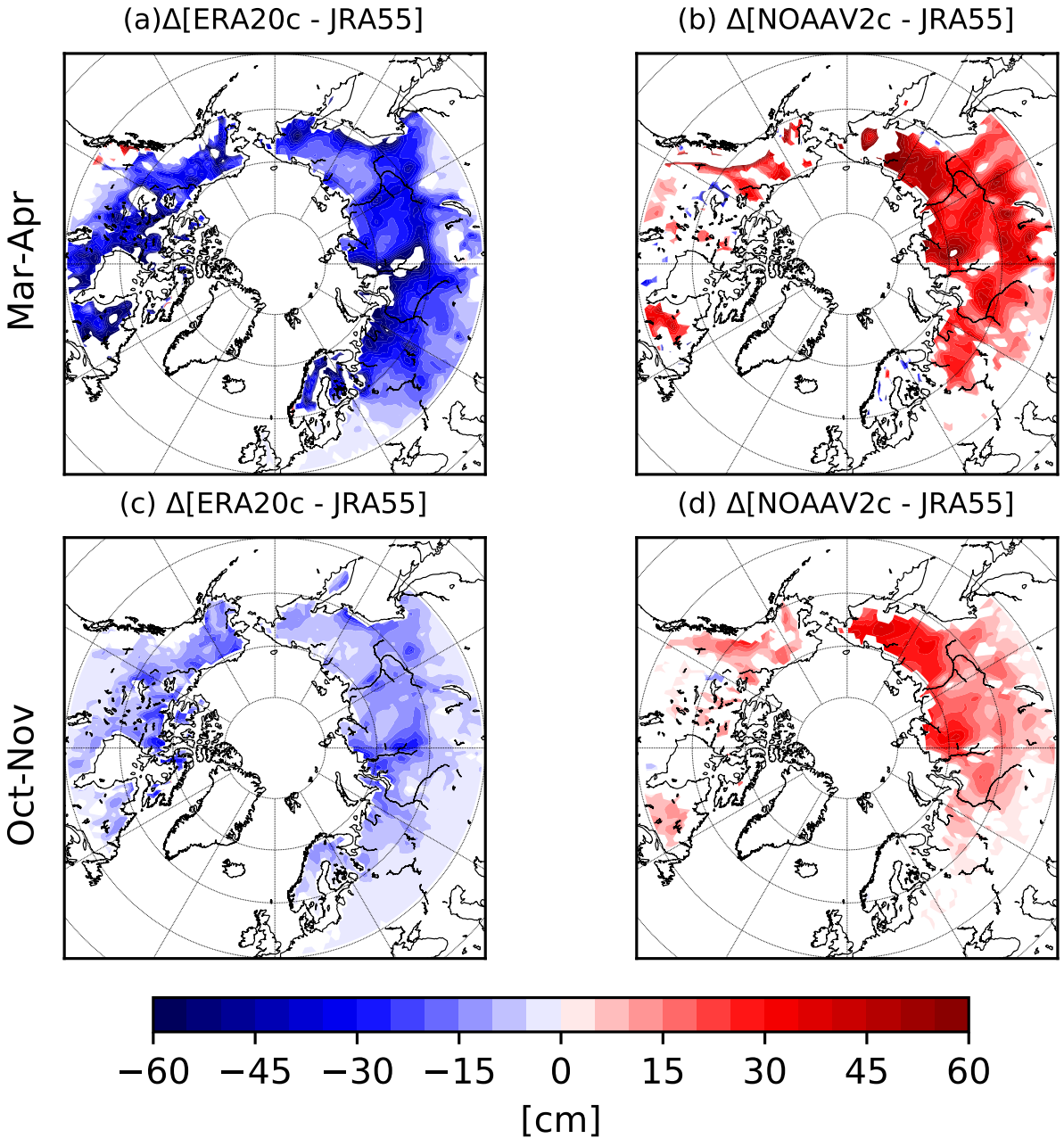

FIGURE 4.10 – Difference of March-April (a,b) and October-November (c,d) snow depth climatology of the reanalyses ERA20c (a,c) and NOAAV2c (b,d) minus JRA-55 over the period 1979-2005. Only differences with p-values less than 0.01 from the t-Student test are shown.

We now move to the evaluation of snow depth climatology across the CMIP5 ensemble compared to the JRA-55 reanalysis from 1979 to 2005. Differences of spring snow depth climatologies between CMIP5 models and JRA-55 reanalysis are shown in Figure 4.11. Three groups can be distinguished regarding the spatial pattern of discrepancies. The first group of models (bcc-csm1-1, CCSM4, NorESM1-M/ME ; Figure 4.11a,c,m,n) displays a large overestimation over the mountain ranges of the east coast of North America and over the northern part of Eastern Eurasia with differences up to 80 cm (almost the same value than the observed climatology ; Figure 4.9a). CSIRO-Mk3-6-0 and inmcm4 models (Figure 4.11e,h) can be considered as the second group and exhibits a general negative bias of SND across the terrestrial Arctic. The only local overestimation occurs over the Rocky and Mackenzie Ranges (up to 90 cm, CSIRO-Mk3-6-0) and over the Verkhoyansk Mountains (around 25 cm, inmcm4). The third group is formed by the remaining models (CanESM2, CNRM-CM5, GISS-E2-H/R, MIROCs, MRI-CGCM3 ; Figure 4.11b,d,f,g,i,j,k,l) and they all display a general positive bias of snow depth in Eurasia with regional significant differences. There is a zonal dipole of differences in models showing overestimation (underestimation) in the east (west) part of the North American Arctic. As for SWE, there is a common underestimation of snow accumulation over the delta of the Yenisei River, which may be related to the inability of CMIP5 models to capture the local snow-ice interaction (e.g., evaporation processes, blowing snow) around the river.

In autumn (Figure 4.12), discrepancies are smaller than in spring. Nevertheless, the models from the aforementioned first group (bcc-csm1-1, CCSM4, NorESM1-M/ME ; Figure 4.12a,c,m,n) still present a positive bias over the mountain ranges of the East Coast of North America and over the northern part of Eastern Eurasia with differences up to 45 cm, largely exceeding the observed snow depth climatology (Figure 4.9b). The models GISS-E2-H/R (Figure 4.12f,g) and MRI-CGCM3 (Figure 4.12l) show a general positive bias, mainly across Eurasia with differences around 5-20 cm. These discrepancies may be related to an earlier onset of snow compared to the observations (Figure 4.19e). The rest of models (CanESM2, CNRM-CM5, CSIRO-Mk3-6-0, inmcm4, MIROCs ; Figure 4.12b,d,e,h,i,j,k) show a general SND underestimation over the terrestrial Arctic with an exception over the mountain ranges in the West Coast of North America, where positive bias is present in some models (CanESM2, CNRM-CM5, CSIRO-Mk3-6-0, inmcm4 ; Figure 4.12b,d,e,h). Both versions of NorESM1-M/ME display a strong overestimation up to 40 cm over the mountain ranges of Eastern Eurasia and over the West Coast of North America (Figure 4.12m,n). Similarly

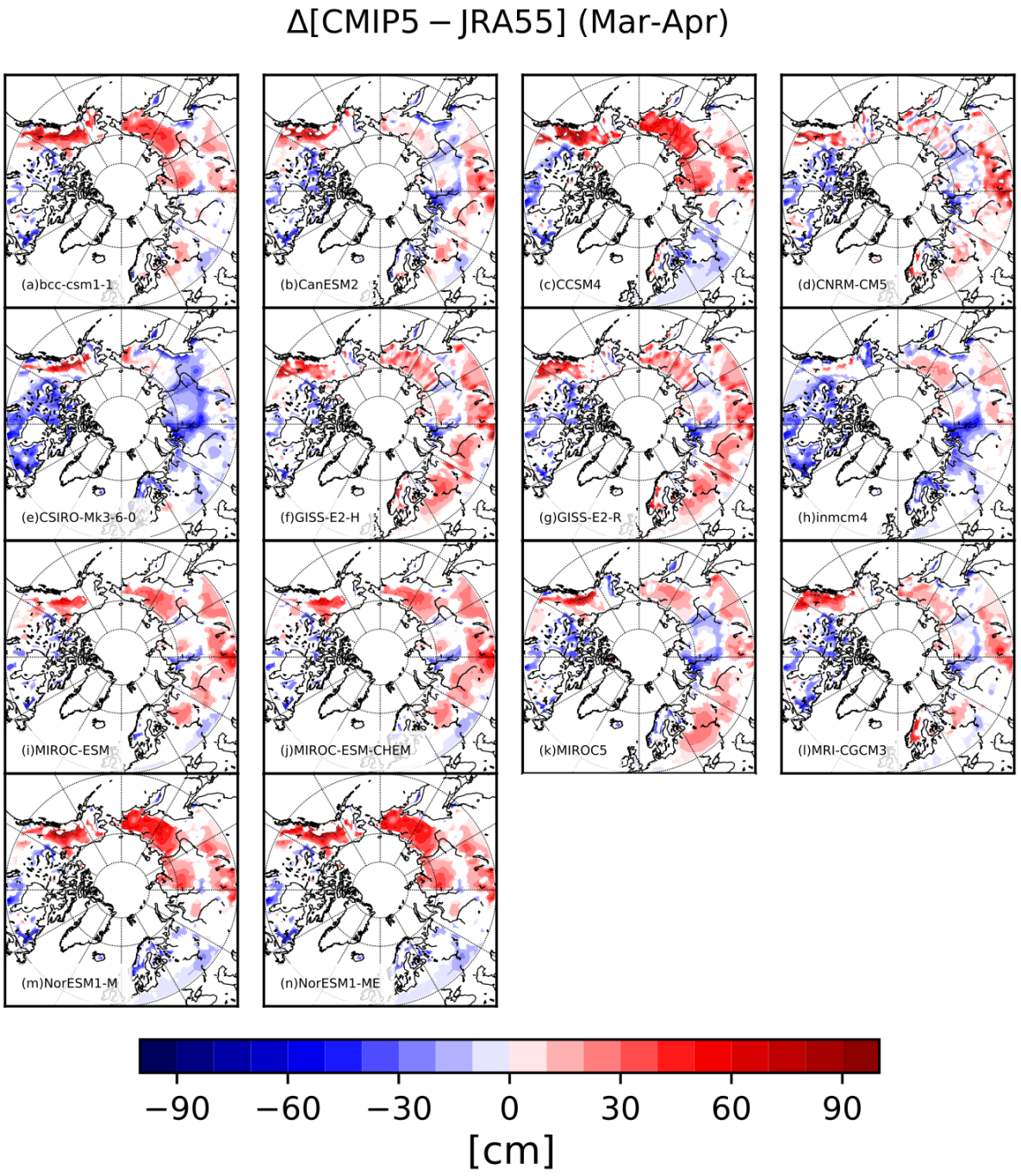

FIGURE 4.11 – Difference of March-April snow depth climatology of each ensemble CMIP5 model minus JRA-55 over the period 1979-2005. Only differences with p-values less than 0.01 from the t-Student test are shown.

to the SND spring pattern of differences and the bias found for SWE (Figure 4.7 and 4.8), CMIP5 models during the onset season also show a local underestimation of snow depth in the delta of the Yenisei River.

Comparison with *in situ* data

Figure 4.13 shows the SND climatology from snow stations of March-April (Figure 4.13a) and October-November (Figure 4.13b) during 1979-2005. Following the procedure explained in Chapter 3, here we account for a total of 422 snow stations.

In spring (Figure 4.13a), areas south of 55°N demonstrate snow depth values less than 10 cm implying that snow has already started receding. In contrast, the areas with higher values (up to 70 cm) include Northern Siberia, mainly the coast of the Barents and Kara Seas and the delta of the Ob and Yenisei Rivers. This local snow persistence may be related to the presence of sea ice and river ice promoting cold air temperature and moisture from evaporation, which favors the thickening of the snowpack. In the eastern part of Northern Eurasia, snow accumulation is substantial with the majority of stations showing more than 40 cm of snow depth. These snow stations are located in elevated areas where local conditions promote snowfall : high relief and moisture coming from the Pacific Ocean. Snow spatial distribution in autumn (Figure 4.13b) is more uniform than in spring. We can still distinguish a northern gradient of snow accumulation but less intense than in spring. Snow depth values are around 10-20 cm over the areas south of the 55° parallel and are up to 55 cm along the coast of Arctic Ocean. This snow pattern hints at two mechanisms sources of spatial differences, depending on the season. In spring, differences in snow distribution are related to local accumulation and temperature sensitivity. However, in autumn the snow spatial distribution is more uniform as it is dominated by a general atmospheric circulation pattern (e.g., NAO, AO, Hurrell *et al.*, 2003) rather than by local conditions.

In situ differences of climatology : from grid to point

We now turn to the evaluation of snow depth climatology in CMIP5 models and the three reanalyses (ERA20c, NOAAV2c and JRA-55) in spring and autumn (1979-2005) using *in situ* snow measurements (Figure 4.13). As explained in detail in Chapter 3, we have interpolated the climatological snow field of each model ensemble and reanalysis to the location of snow stations. We have

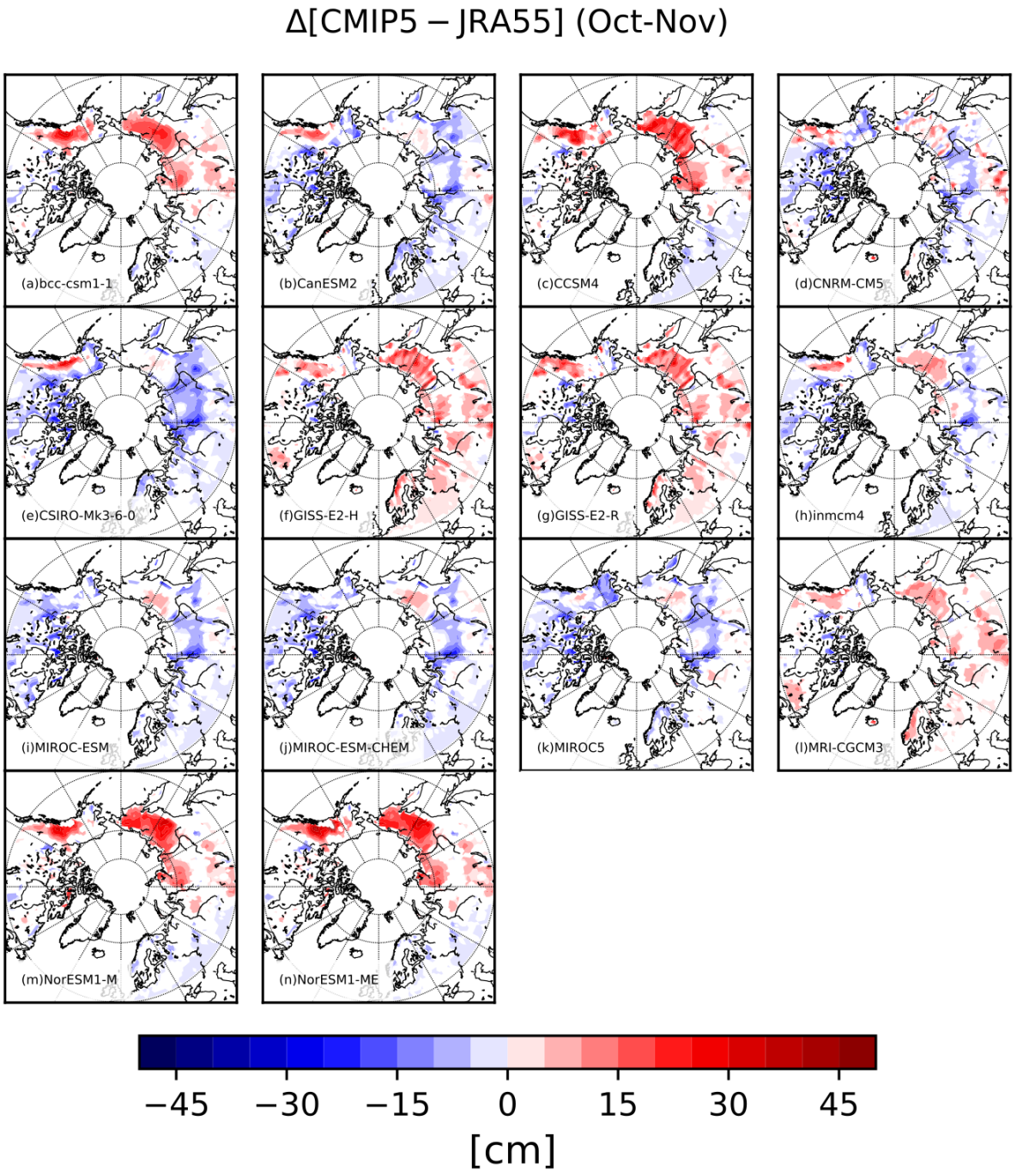

FIGURE 4.12 – Difference of October-November snow depth climatology of each ensemble CMIP5 model minus JRA-55 over the period 1979-2005. Only differences with p-values less than 0.01 from the t-Student test are shown.

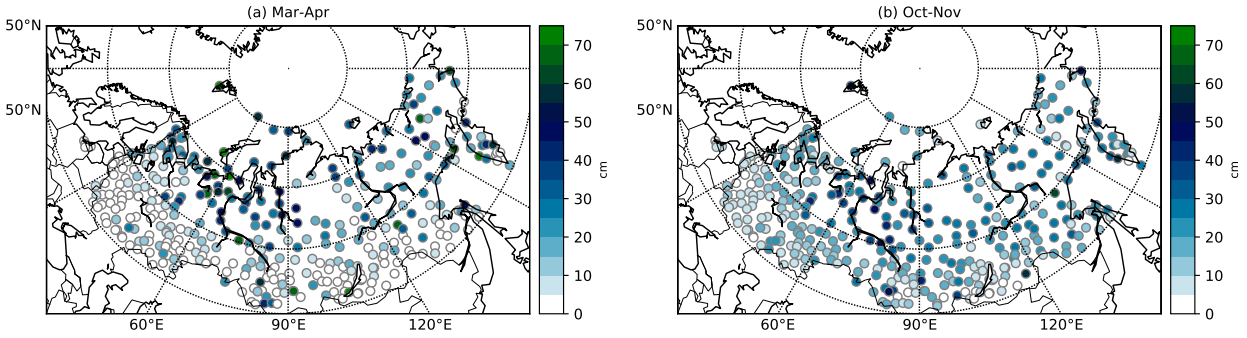

FIGURE 4.13 – Climatology of snow depth in March-April (a) and October-November (b) over the period 1979-2005 of snow stations from the Russian Research Institute for Hydro-meteorological Information - World Data Center (RIHMI-WDC).

used a bilinear interpolation instead of nearest point interpolation due to the uneven spatial distribution of snow stations and the coarse resolution of models and reanalyses. The stations overseas are not considered here as we only focus on Arctic land. For this particular *in situ* comparison, we show all differences without considering their degree of statistical significance in order to include as many stations as possible.

We first assess the differences in spring and autumn climatologies between reanalyses and snow stations (Figure 4.14). In spring (Figure 4.14a,b,c), the best agreement is found in JRA-55 over the eastern part of Eurasia with differences less than 10 cm in absolute value, whereas ERA20c and NOAAV2c display a positive bias of more than 45 cm, notably over the Kolyma Mountains. In central Siberia, around the 90°E meridian, the NOAAV2c reanalysis shows the highest overestimation being up to 40-45 cm, followed by JRA-55 displaying differences up to 15 cm in the north and a stronger disagreement close to the Altai Mountain Range ; lastly, ERA20c displays smaller differences of 20 cm all along the 90°E meridian. The western part of Eurasia is better reproduced by NOAAV2c with differences of 20 cm whereas in both ERA20c and JRA-55, the bias goes up to 40-45 cm north of 55°N parallel. In autumn, both ERA20c and NOAAV2c present a relatively good agreement with snow data in Eastern Eurasia. They both present a slight overestimation in the Far East up to 20 cm and an underestimation over the south of Eastern Eurasia with values not exceeding 20 cm. JRA-55 shows a general underestimation of snow depth compared to the *in situ* measurements with maximum discrepancies in the basin of the Ob River (up to 45 cm). In western Eurasia, all reanalyses present a similar bias with small discrepancies of 15 cm in the south and larger ones northwards.

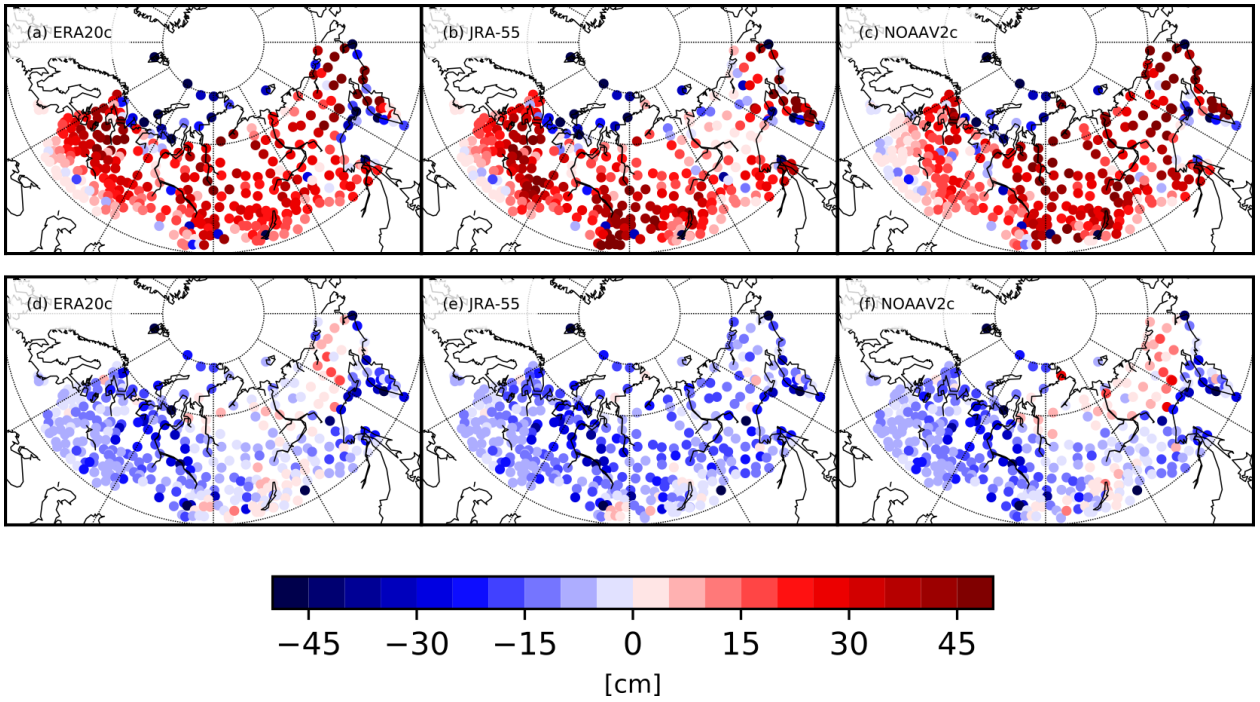

FIGURE 4.14 – Difference of March-April (a,b,c) and October-November (d,e,f) snow depth climatologies of the ERA20c (a,d), JRA-55 (b,e) and NOAAV2c (c,f) reanalyses minus snow stations over the period 1979-2005. All the reanalyses have been converted to station locations by bilinear interpolation.

To continue with the comparison, we calculated the differences of spring and autumn climatology between CMIP5 models and *in situ* snow data (Figure 4.15 and 4.16). In spring (Figure 4.15), there is a clear general overestimation of snow depth in CMIP5 models compared to snow stations. An exception is found in coastal areas, but we attribute this underestimation to the effect of models' land-mask. In Figure 4.11, we have compared the spring climatology in CMIP5 models to JRA-55 and we distinguished three different groups. The first group was bcc-csm1-1, CCSM4 and both versions of NorESM1-M/ME (Figure 4.11a,c,m,n). Here, the same pattern is displayed with a larger overestimation over the north of Eastern Siberia being more than 60 cm (Figure 4.15a,c,m,n). The second group, that was characterized by a negative bias (CSIRO-Mk3-6-0 and inmcm4 ; Figure 4.11e,h), here exhibits general positive differences but weaker than the other models, with values of 10-20 cm for most of the areas (Figure 4.15e,h). The remaining models display a general overestimation centered in the south central and western part of Eurasia (CanESM2, CNRM-CM5, GISS-E2-H/R, MIROC-ESM and MIROC5 ; Figure 4.15b,d,f,g,i,k). It is worth mentioning that there are a group of models (CCSM4, MIROC-ESM-/CHEM, MRI-CGCM3, NorESM1-M/ME ; Figure 4.15c,i,j,l,m,n) that are in relatively good agreement with snow stations over the south-west

of Eurasia, where snow starts to recede and thus, these models demonstrate a good timing of snow melting.

Figure 4.16 shows a general underestimation of snow depth in CMIP5 model compared to the snow *in situ* data in autumn. However, these discrepancies are smaller in absolute magnitude than for the melting season. We can distinguish a recurrent pattern in the models bcc-csm1-1, CCSM4 and NorESM1-M/ME (Figure 4.16a,c,m,n), which show higher than observed snow accumulation in the north of Eastern Eurasia and underestimation over the remaining land. To a lesser extent, this feature is also displayed by both versions of GISS-E2-H/R (Figure 4.16f,g). There is a local overestimation in the south of central Siberia (bcc-csm-1, CanESM2, CNRM-CM5, GISS-E2-H/R, MRI-CGCM3, NorESM1-M/ME ; Figure 4.16a,b,d,f,g,l,m,n), which may be related to an associated effect of orographic precipitation close to the Altai mountain range.

4.2 Annual Cycle

We turn now to the comparative analysis of the annual cycle of snow characteristics in CMIP5 models, reanalyses and observations for different Arctic regions. Spatial average across different Arctic subdomains of climatological monthly means of SCE and SND were computed over the 1979-2005 period, and those of SWE over the 1981-2005. We applied for each CMIP5 model its own land-ice mask and the GISS-E2-R mask to the reanalyses (NCEP/CFSR, NOAAV2c, ERA20c, JRA-55) and CanSISE product. For the NOAA CDR data set (which has a binary land mask but does not provide an ice mask), we applied the July SCE climatology (1979-2005) to generate a virtual “ice fraction mask”. Thus we masked the grid cells with more than 85 % SCE, which is equivalent to less than 15 % of perennial SCE on ice fraction as we had done with CMIP5. For reference, the ice-land masking procedure is described in detail in Chapter 3.

4.2.1 Snow cover

Figure 4.17 shows that for the whole Arctic (Figure 4.17a), the annual cycle of snow cover in both NCEP/CFSR and NOAAV2c is in good agreement with NOAA CDR with the largest differences not exceeding 10 p.p. . Between both reanalyses, the highest differences are only about 10 p.p. in May and they are observed in Eurasia. The multimodel mean generally reproduces the annual cycle compared to NOAA CDR with the largest discrepancies of up to 25 p.p. in October and November. The majority of the CMIP5 models tend to underestimate SCE throughout the year notably in

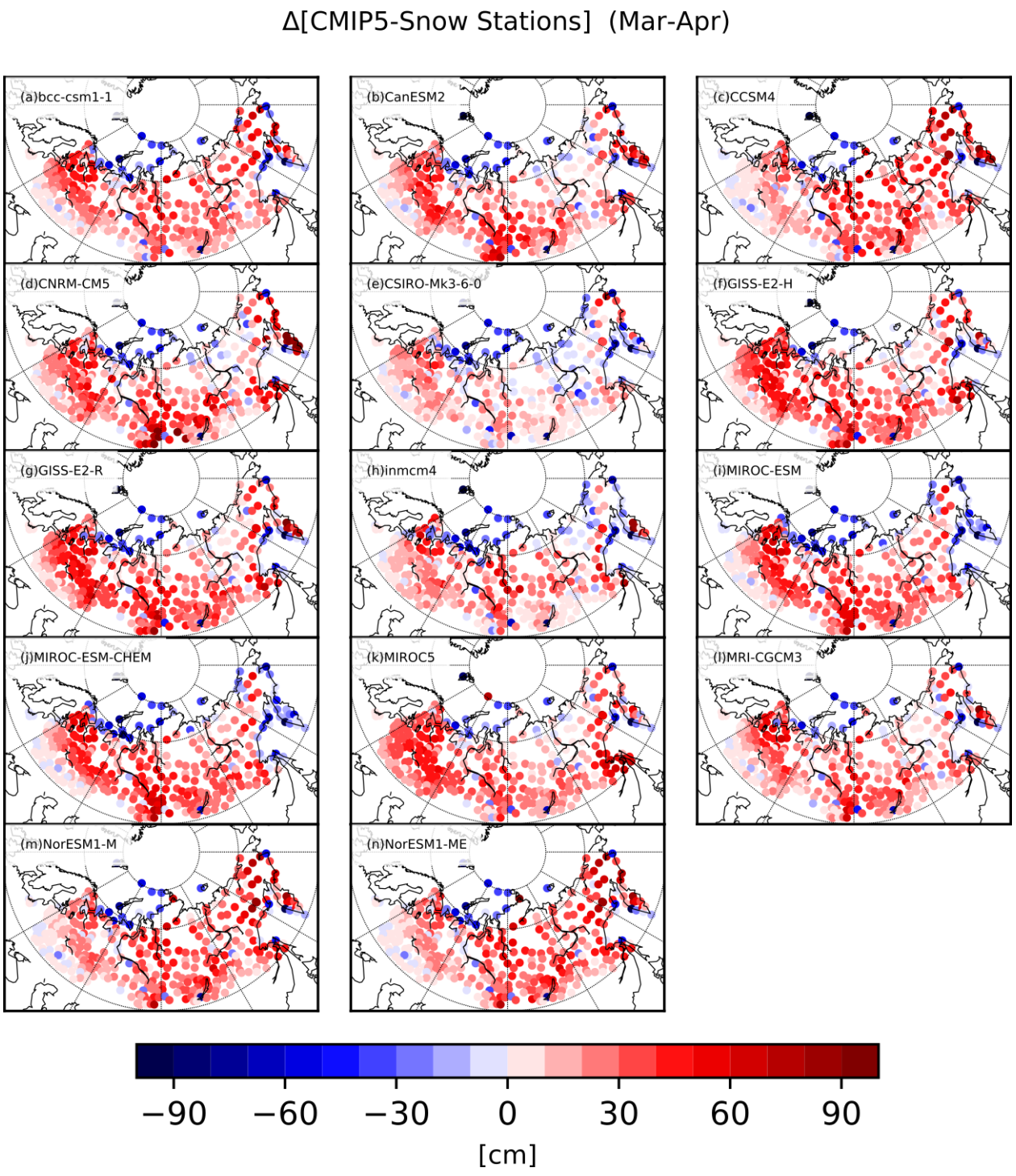

FIGURE 4.15 – Difference of March-April snow depth climatology of each ensemble CMIP5 model snow stations over the period 1979-2005. CMIP5 models have been converted to station locations by bilinear interpolation.

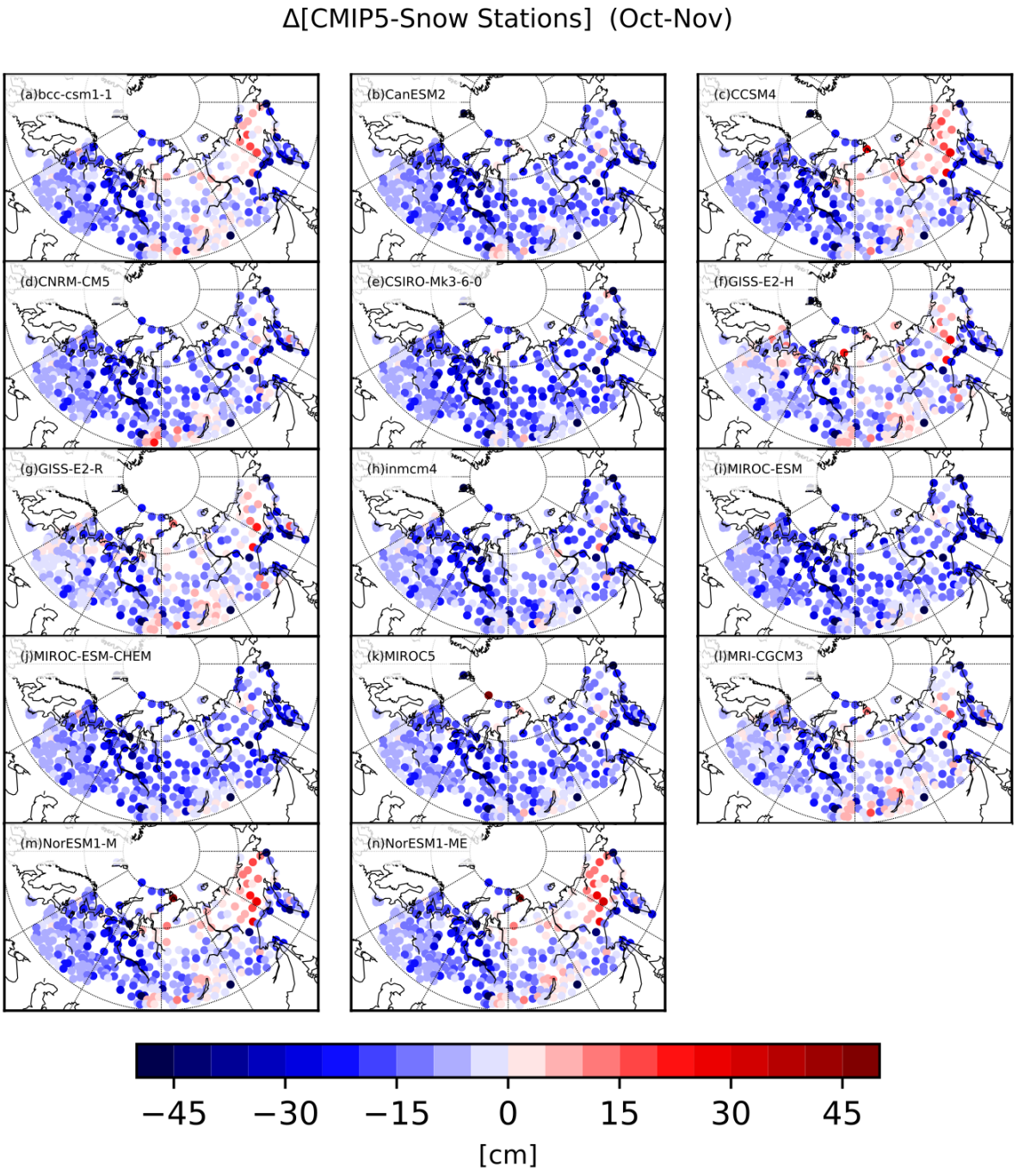

FIGURE 4.16 – Difference of October-November snow depth climatology of each ensemble CMIP5 model snow stations over the period 1979-2005. CMIP5 models have been converted to station locations by bilinear interpolation.

autumn and in winter (October to February). This underestimation is most distinct in North America (Figure 4.17c) while over Eurasia (Figure 4.17b) some models (CCSM4, MRI-CGCM3 and NorESM1-M/ME) match NOAA CDR quite closely with differences within 10 p.p. . The largest discrepancies with respect to observational data are identified in the MIROC versions during the months of October and November and over both sub-domains bordering on 40 p.p. (Figure 4.17b,c). When melting starts, discrepancies across the models are also evident. Considering the March-June period, MPI-ESM-LR/P, CSIRO-Mk3-6-0, bcc-csm1-1 and inmcm4 tend to underestimate SCE by up to 30 p.p in May, mainly in Eastern Eurasia (Figure 4.17d), and report complete snow melt in June. In contrast, the other models maintain some snow cover in July. This underestimation is mostly visible over North America being up to 40 p.p. in MPI-ESM-LR (Figure 4.17c). Other models (CanESM2, CNRM-CM5 and MRI-CGCM3) tend to slightly overestimate SCE by up to 10 p.p. in May primarily due to the Eurasia pattern (Figure 4.17b). During May-August period both versions of NorESM1-M/ME show an overestimation of SCE by up to 15 p.p. with respect to NOAA CDR, implying that these two models were not capable of completely melt the snow in summer, mainly over Eastern Eurasia (Figure 4.17e).

4.2.2 Snow water equivalent

Compared to SCE, the annual cycle of SWE (Figure 4.18) is characterized by a relatively stronger spread across the models and larger deviations from observations. There is a definite overestimation of SWE in CMIP5 models with respect to the CanSISE product. The multimodel mean shows a positive bias all along the annual cycle with the largest overestimation during March-May when differences for the whole Arctic amount to 40 $\mathrm{kg\,m^{-2}}$ (Figure 4.18a) reaching 65 $\mathrm{kg\,m^{-2}}$ in North America (Figure 4.18c) and 30 $\mathrm{kg\,m^{-2}}$ in Eurasia (Figure 4.18b), more specifically over the eastern part (Figure 4.18e). Considering the whole Arctic (Figure 4.18b), the largest differences are observed during the melting season, from March to June, reaching 20-30 $\mathrm{kg\,m^{-2}}$. Among CMIP5 models, the greatest SWE overestimation is in excess of 100 $\mathrm{kg\,m^{-2}}$ and occurs in April for MRI-CGCM3 (Figure 4.18a). The differences are larger over North America (Figure 4.18b) than over Eurasia (Figure 4.18c). Notably, there are three models (CSIRO-Mk3-6-0 and both versions of MPI-ESM-LR/P) that match fairly well the annual cycle of the CanSISE product for the whole Arctic and demonstrate differences in SWE from $-10\,\mathrm{kg\,m^{-2}}$ to $+20\,\mathrm{kg\,m^{-2}}$. For the period from August to September, when CanSISE is characterized by complete snow melt in the Arctic (Figure 4.18a),

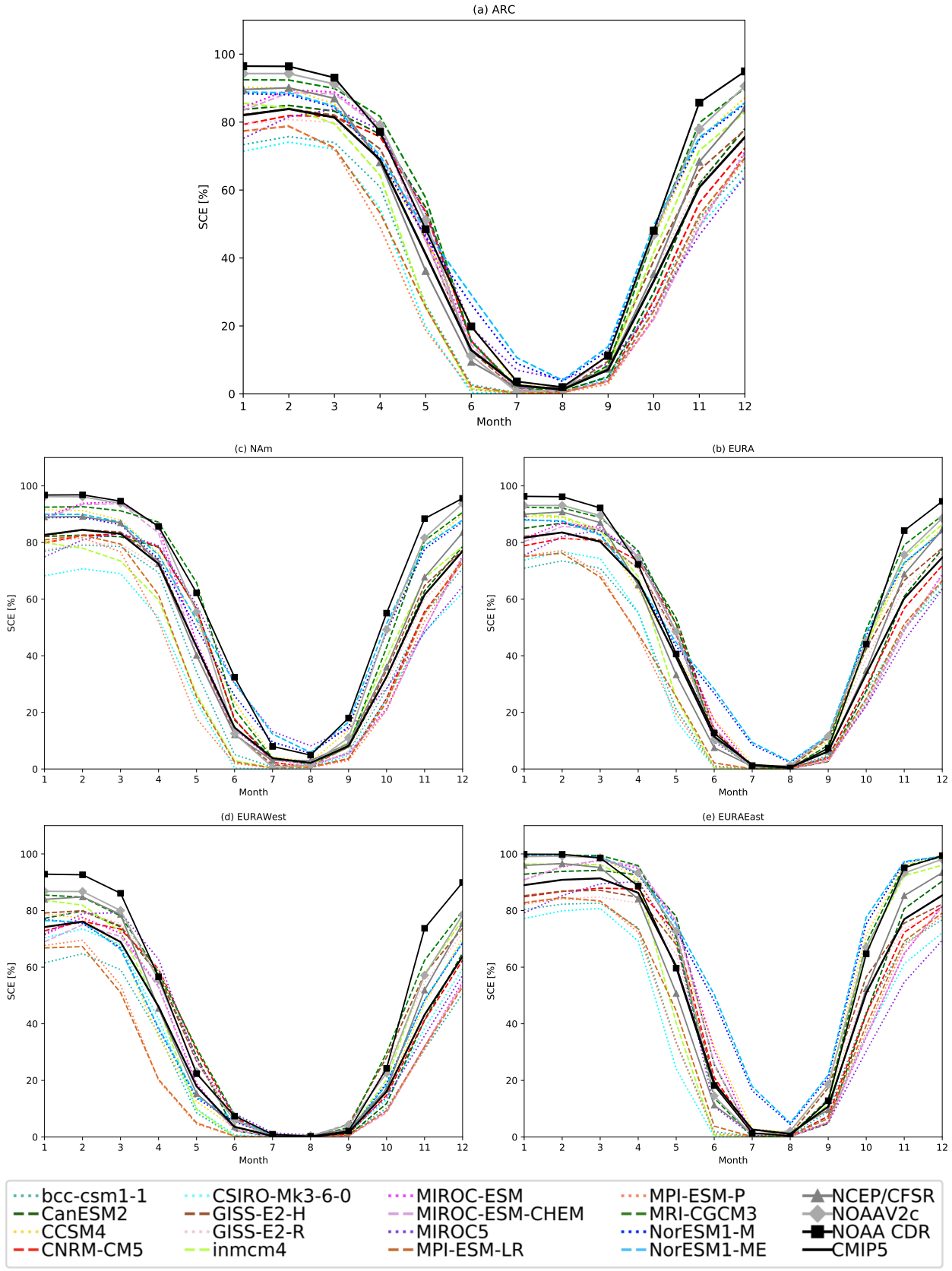

FIGURE 4.17 – Annual cycle of snow cover extent for CMIP5 models, the multimodel mean, reanalyses (NCEP/CFSR and NOAAV2c) and satellite-based NOAA CDR product over the ice-free land Arctic and subdomains computed from 1979 to 2005.

some models (MIROC5 and both NorESM1-M/ME) still show values up to 50 $\mathrm{kg\,m^{-2}}$ over North America (Figure 4.18c). During the snow season (January to May), nearly all models display large overestimation over all subdomains. The only exception is one group of models (MPI-ESM-LR/P, CSIRO-Mk3-6-0 and NorESM1-ME) that shows a negative bias over the western part of Eurasia (Figure 4.18d).

4.2.3 Snow depth

Figure 4.19 shows the annual cycle of snow depth over the Arctic and its subdomains for the period 1979-2005. It is characterized by a large spread similar to that of the annual cycle of SWE (Figure 4.18). The dispersion is more remarkable during the snow season (from December to June) over North America (Figure 4.19b). As found in section 4.1.3, the ERA20c reanalysis displays less overall snow depth than the other data sets. In addition to this negative bias, the amplitude of the seasonal cycle is widely underestimated, with only 20 cm of variation between summer and winter. Conversely, the NOAAV2c reanalysis is in a relatively good agreement with JRA-55 in terms of seasonal variability, with the former showing an amplitude of $\sim$ 70 cm, and $\sim$ 50 cm in the latter (Figure 4.19a). However, NOAAV2c overestimates SND compared to JRA-55 from November to April with differences around 20 cm in North America (Figure 4.19b) and up to 30 cm in Eastern Eurasia (Figure 4.19d). Hereafter, we consider the JRA-55 reanalysis as reference for the model evaluation of the SND annual cycle as we did in the previous section for the SND climatology.

Despite the individual model discrepancies, the multimodel mean is in good agreement with the JRA-55 reanalysis, mainly in the onset season (Figure 4.19a), differing no more than 10 cm throughout the annual cycle. The snow depth maximum displayed by the multimodel ensemble coincides with observations and it occurs in March. However, the rate of melting in JRA-55 is faster than the multimodel mean, notably in Eurasia (Figure 4.19c). JRA-55 melts snow almost in June, whereas, multimodel mean does it later in July. Over the Arctic (Figure 4.19a), there are four models (bcc-csm1-1, CCSM4 and both NorESM1-M/ME) that overestimate snow depth, by almost 20 cm during the winter and early spring. On the other hand, these four models capture adequately the peak of maximum snow accumulation in March. CNRM-CM5 and MRI-CGCM3 display a shift in the snow depth peak towards April. There are two models (CSIRO-Mk3-6-0, inmcm4) that show negative bias with values almost twice lower than those observed (Figure 4.19a). The highest discrepancies are demonstrated by inmcm4 in March, underestimating JRA-55 by 30-35 cm. The

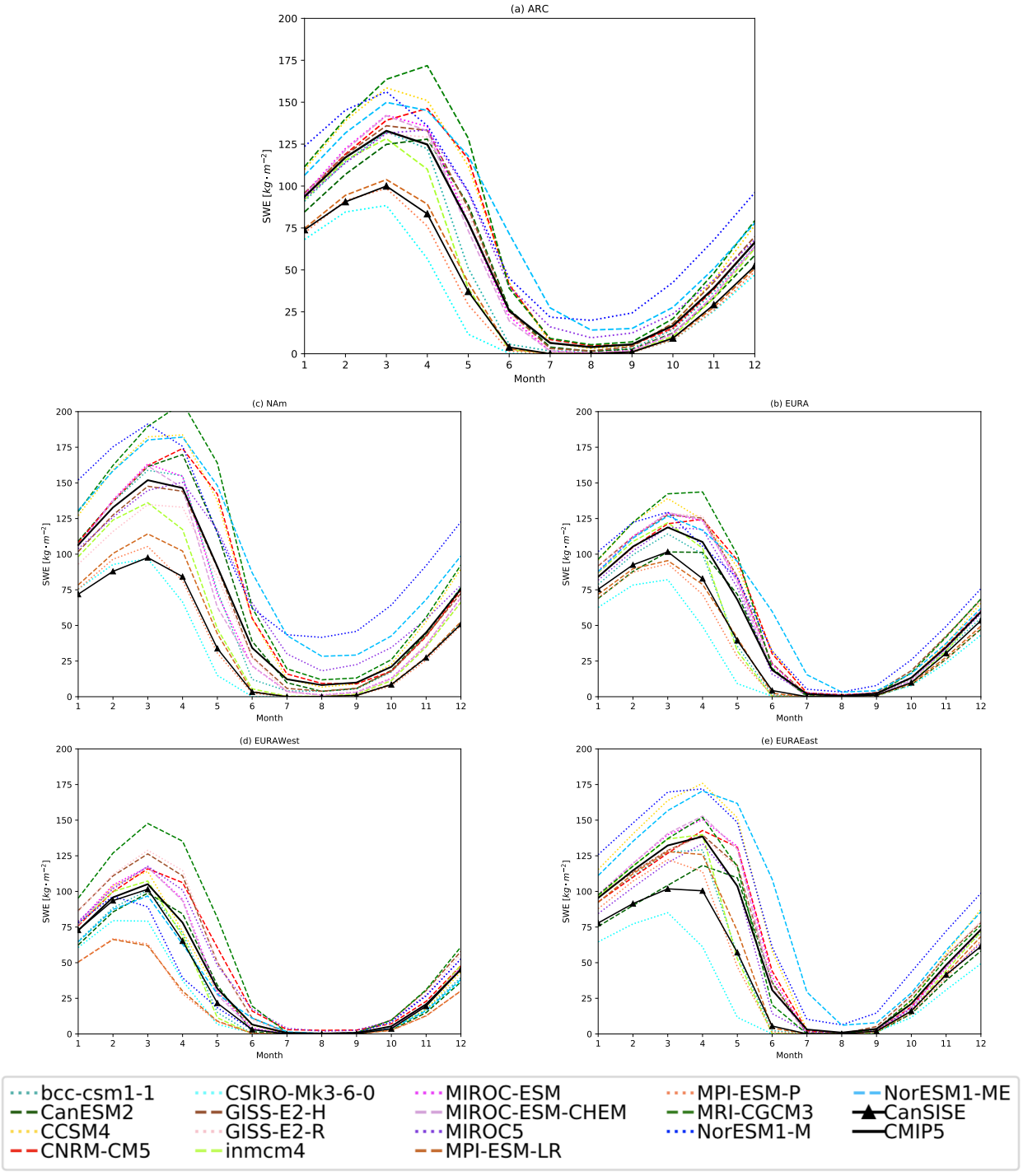

FIGURE 4.18 – Annual cycle of snow water equivalent for CMIP5 models, the multimodel mean and CanSISE ensemble over the ice-free land Arctic and subdomains computed from 1981 to 2005.

snow season period in Western Eurasia (Figure 4.19d) is shorter than in the eastern side (Figure 4.19e). This feature is identified across almost all CMIP5 models and it is clearly distinguishable in JRA-55. It consists in an early melting in March over the western part of Eurasia, and a later and slower snow offset over the eastern part starting in April ; also, snow onset occurs one month earlier in Eastern Eurasia (October) than in the western part (November).

4.3 Quantile statistics of the spatial average

Another view of the differences in snow characteristics climatology is given in Figures 4.20, 4.21 and 4.22. We present quantile statistics of the spatial average over the terrestrial Arctic for each snow variable in both seasons, March-April and October-November. For SCE and SND, the period considered is 1979-2005 and for SWE, 1981-2005. Each box represents the distributions of the seasonal time series for each ensemble model, for the multimodel ensemble and for the reference data sets. The horizontal line represents the spatial average, the filled rectangle is the interquartile range (IQR) from Q1 (25th percentile) to Q3 (75th percentile). The IQR provides information about the amplitude of snow interannual variability that will be addressed in the next chapter extensively.

4.3.1 Snow cover

Figure 4.20a shows a general underestimation of spring SCE by CMIP5 models compared to all reference data sets. This is evident in the multimodel mean value of 56% SCE while observations show an average around 83% (80% for NCEP/CFSR, 85% for NOAAV2c and 85% for NOAA CDR). Three models (bcc-csm1-1(a), CSIRO-Mk-3-6-0(e) and both versions of MPI-ESM-LR/P(l,m)) show a SNC mean value twice smaller than the reference data sets (44%(a), 37%(e), 39% and 34%(l,m)). This is in agreement with Figure 4.3 which identified these models (bcc-csm1-1, CSIRO-Mk-3-6-0, and both versions of MPI-ESM-LR/P) as negatively biased over the terrestrial Arctic. For the onset season (Figure 4.20b), the agreement between CMIP5 models and reference data is better than in spring. The multimodel mean, being 68%, is slightly above both reanalyses, reporting 56% and 62% in NCEP/CFSR and NOAAV2c respectively ; however, it lies within the range given by NOAA CDR (67%). The models CCSM4(c), inmcm4(h), MRI-CGCM3(n) and both versions of NorESM1-M/ME(o,p) are found to be above the observed range, with SCE values of 81%(c), 77%(h), 84%(n), 80%(o) and 81%(p). This is actually closer to the spring values rather than that

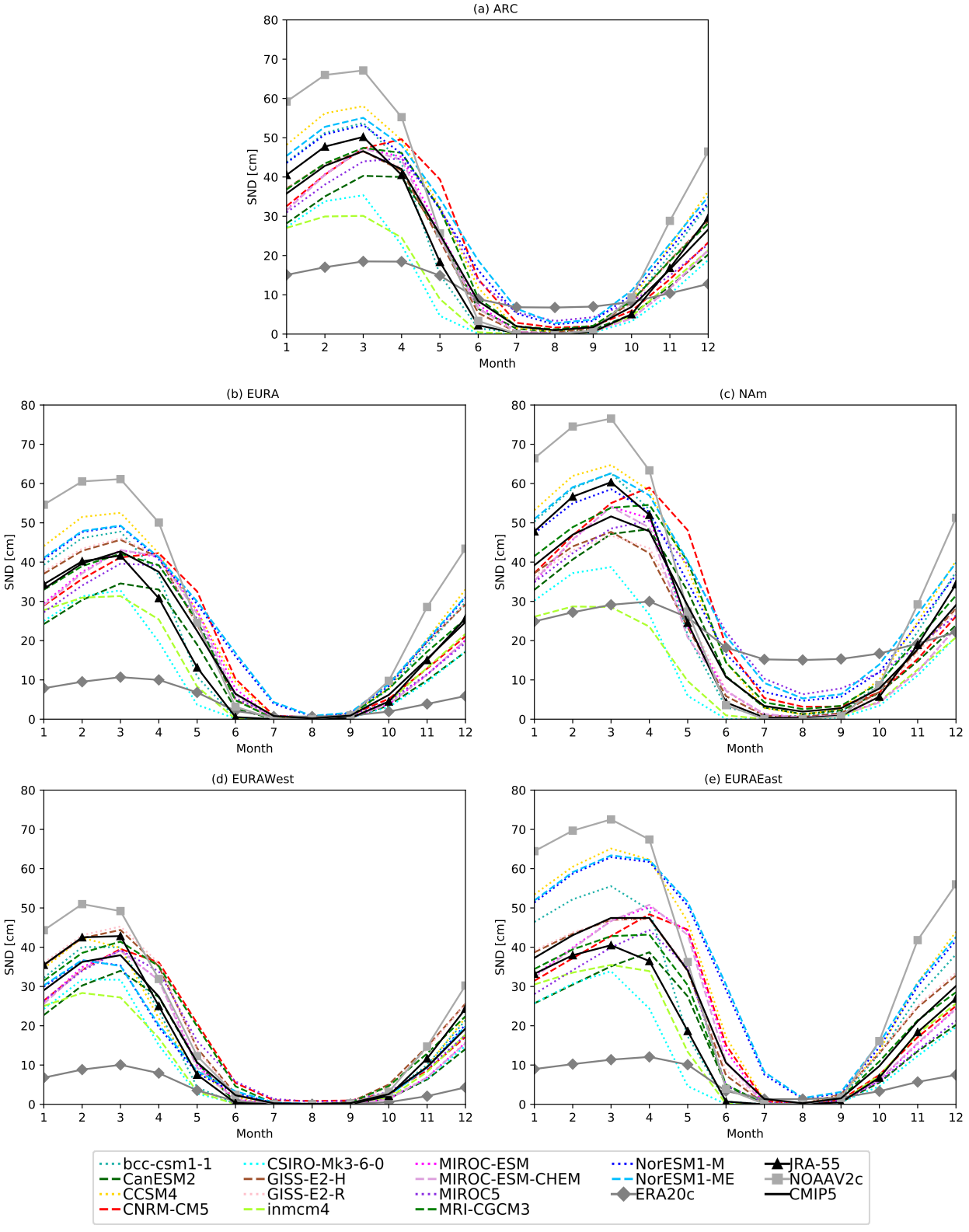

FIGURE 4.19 – Annual cycle of snow depth for CMIP5 models, the multimodel mean and reanalyses (ERA20c, JRA-55 and NOAAV2c) over the ice-free land Arctic and subdomains computed from 1979 to 2005.

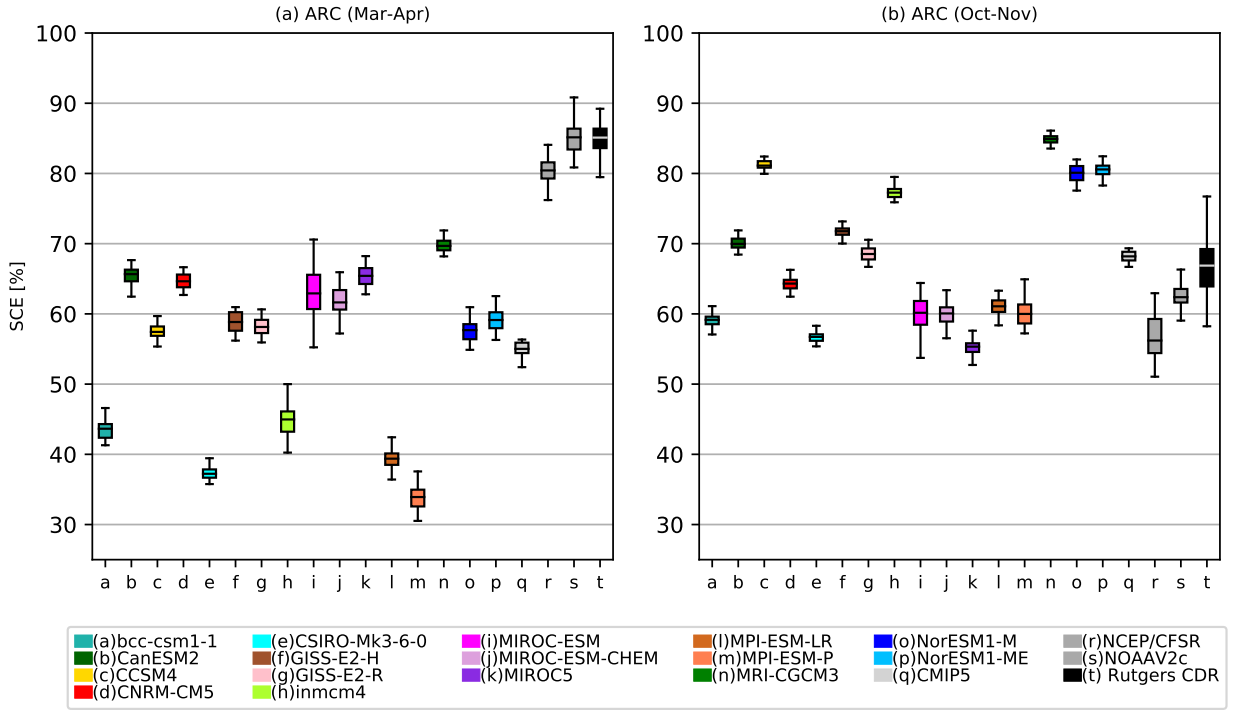

FIGURE 4.20 – Quantile statistics of the spatial average of snow cover for the CMIP5 models and the multimodel mean, the reanalyses (NCEP/CFSR and NOAAV2c) and the satellite data NOAA CDR for March-April (a) and October-November (b) over the terrestrial Arctic during 1979-2005.

from autumn. This overestimation is due to the representation of snow cover in Eastern Eurasia, as seen in Figure 4.4 for this group of models.

4.3.2 Snow water equivalent

Figure 4.21 exhibits a general overestimation of SWE in CMIP5 models since the multimodel mean amounts to a value of 99 $\mathrm{kg\,m^{-2}}$ whereas the CanSISE product displays 59 $\mathrm{kg\,m^{-2}}$. This feature was already manifested in Figure 4.7. The exception is CSIRO-Mk3-6-0(e) who shows the lowest average of 33 $\mathrm{kg\,m^{-2}}$. The models MPI-ESM-LR/P(l,m) capture the SWE average of the whole Arctic accurately (64 $\mathrm{kg\,m^{-2}}$, 50 $\mathrm{kg\,m^{-2}}$), however, this is the result of compensating errors (Figure 4.7l,m) : the positive/negative biases in east/west Eurasia and north/south of North America cancel out in the spatial mean. It is not surprising from Figure 4.18 that MRI-CGCM3(n) shows the highest value of SWE in spring at 148 $\mathrm{kg\,m^{-2}}$, that is 60% more that the reference. During the onset season (Figure 4.21b), CMIP5 models are in a better agreement with the CanSISE product, with values ranging from 40 to 60 $\mathrm{kg\,m^{-2}}$ in the majority of models, which is consistent with a multimodel mean of 52 $\mathrm{kg\,m^{-2}}$ and a SWE mean of 40 $\mathrm{kg\,m^{-2}}$ in CanSISE. As in spring,

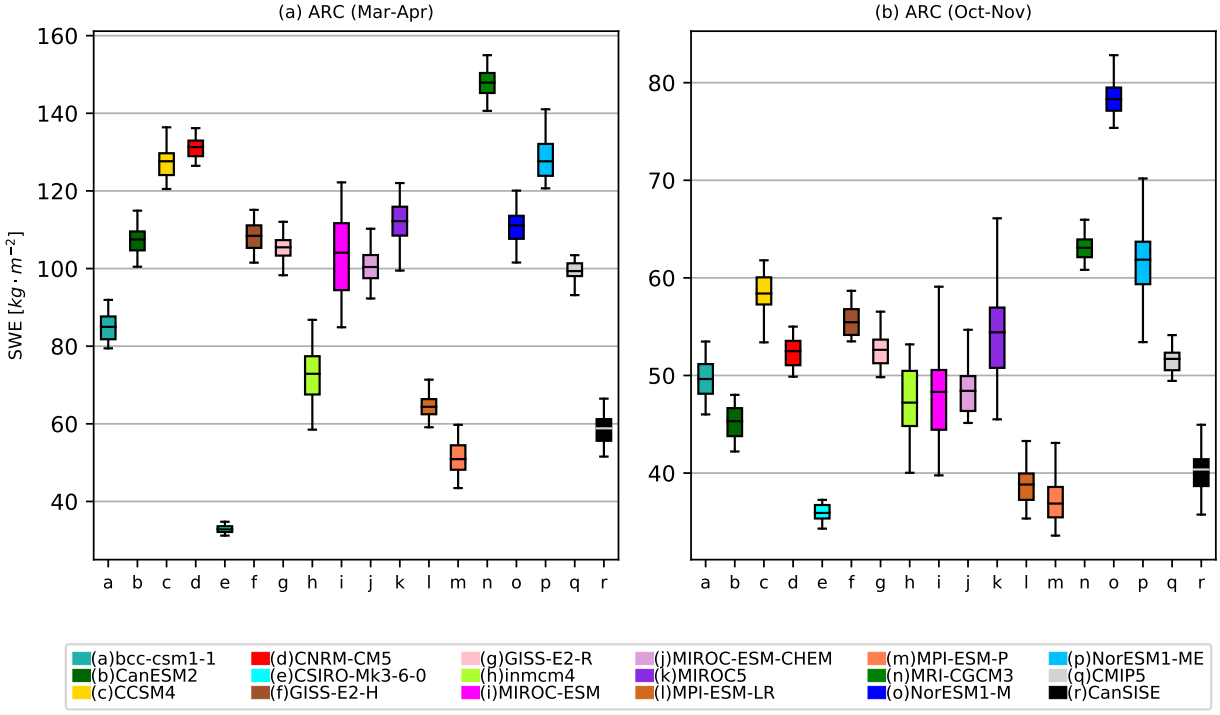

FIGURE 4.21 – Quantile statistics of the spatial average of snow water equivalent for the CMIP5 models and the multimodel mean, the CanSISE ensemble product for March-April(a) and October-November (b) over the terrestrial Arctic during 1981-2005

models CSIRO-Mk3-6-0(e) and MPI-ESM-LR/P(l,m) show the lowest values of SWE (36 kg m^{-2}, 39 kg m^{-2} and 37 kg m^{-2}, respectively). NorESM1-M gives the highest value of 78 kg m^{-2} due to the representation of SWE in Eastern Eurasia and Northern Canada (Figure 4.8). It is worth mentioning that the largest variability is found in MIROC-ESM(i), MIROC5(k) and NorESM1-ME(p) in autumn compared to the other CMIP5 models.

4.3.3 Snow depth

All reanalyses experience large discrepancies in spring SND average over the Arctic (Figure 4.22a). JRA-55 displays a mean of 29 cm which is surpassed by NOAAV2c, accounting with 37 cm. Consistent with Figure 4.17, ERA20c shows the lowest SND value, 17 cm. The interannual variability is particularly high in JRA-55 and NOAAV2c as seen by their IQR values. In Figure 4.22a, we found a good agreement between CMIP5 models and JRA-55 with the multimodel mean displaying a value of 34 cm. The only models that underestimate substantially JRA-55 and NOAAV2c are CSIRO-Mk3-6-0(e) and inmcm4(h), with values of 14 cm and 17 cm, respectively. This bias is not due to an early melt but to a general negative bias of SND, which is stronger in North America (Fi-

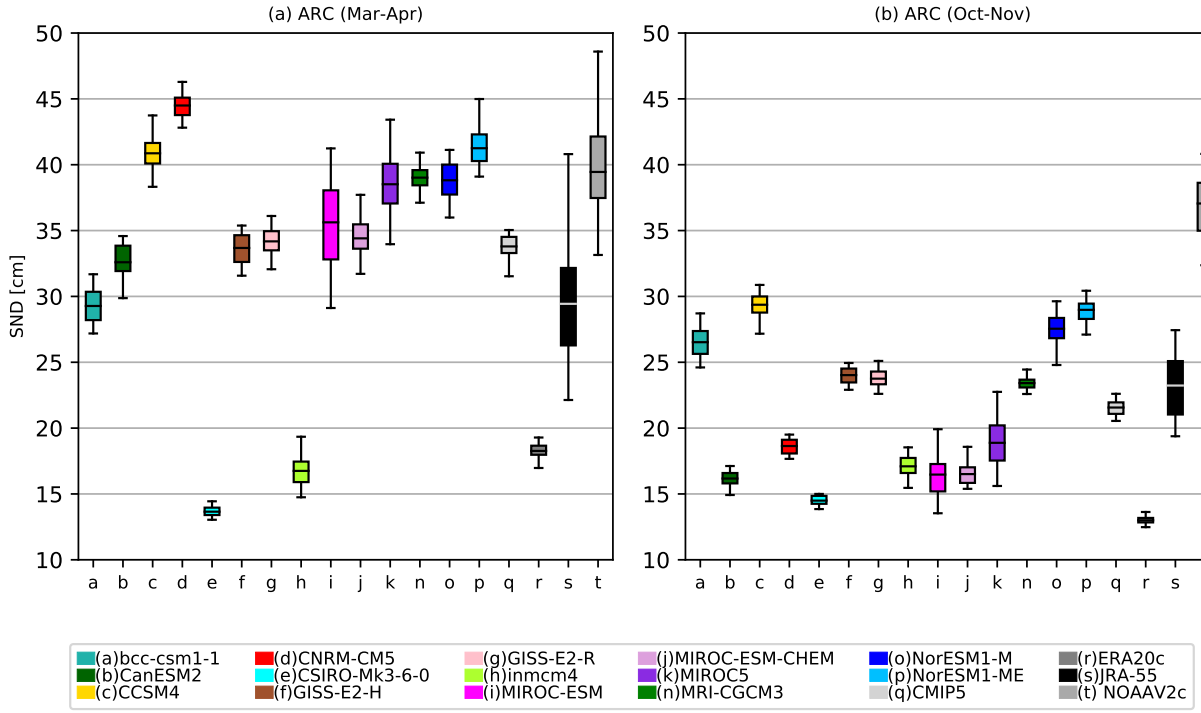

FIGURE 4.22 – Quantile statistics of the spatial average of snow depth for the CMIP5 models and the multimodel mean and the reanalyses (ERA20c, JRA-55 and NOAAV2c) for March-April (a) and October-November (b) over the terrestrial Arctic during 1979-2005.

gure 4.19b). In autumn, the discrepancies between reanalyses are still present. NOAAV2c exhibits the highest SND value (35 cm), almost close to the spring average. JRA-55's SND mean is 24 cm, twice as much as ERA20c. The agreement between CMIP5 and the reference data set improves in autumn (Figure 4.22b) compared to the other snow variables (Figures 4.20b and 4.21b). The multimodel mean SND averages 22 cm fitting almost perfectly with the JRA-55 reference. The models with higher SND in the onset season are bcc-csm1-1(a), CCSM4(c) and NorESM1-M/ME(o,p) (27 cm, 29 cm, 28 cm, 29 cm) because of an excess of accumulation in the northern part of Eastern Eurasia (Figures 4.11, 4.15 and 4.19d). As for SWE, the models MIROC-ESM(i), MIROC5(k) and NorESM1-ME(p) display a large variability compared to the other CMIP5 models.

4.4 Summary

We have investigated snow characteristics (SCE, SWE and SND) in the Arctic during spring and autumn in the historical runs of CMIP5 climate models and in different observational data sets – various reanalyses, one satellite-based product, an observation-based ensemble product and *in*

situ measurements. For SCE and SND variables, the period of study was 1979-2005 and for SWE the period was 1981-2005.

(i) Climatology :

- We have found that NOAAV2c displays higher SCE values than NCEP/CFSR in spring and autumn climatologies, they are nonetheless in relatively good agreement. The only discrepancies are located above the Eurasian Dry Land Band (EDLB, Groisman *et al.*, 2018) in Siberia and over the Rocky Mountains in spring and, in autumn, all over the terrestrial Arctic (but smaller in magnitude). CMIP5 models show three different patterns of SCE differences compared to NCEP/CFSR. The first group (bcc-csm1-1, CSIRO-Mk3-6-0 and MPI-ESM-LR/P) generally underestimates SCE, mainly in the south part of Eastern Eurasia. The second group (CanESM2, MIROC-ESM/-CHEM and MRI-CGCM3) displays a broad positive bias over the Rocky Mountains and a negative bias over the southern edge of Western Eurasia. The third group (CNRM-CM5, GISS-E2-H/R and MIROC5) is prone to underestimation in the north and overestimation in the south part of the Arctic. Lastly, the smallest significant differences are found for CCSM4 and NorESM1-M/ME with a negative bias over Western Eurasia and Eastern Canada whereas the south of Eastern Eurasia and Western Canada are characterized by a small positive bias. In autumn, 7 out of 16 models (bcc-csm1-1, CSIRO-Mk3-6-0, the MIROC and MPI versions) show a general underestimation of SCE over the whole terrestrial Arctic. In contrast, five other models (CCSM4, inmcm4, MRI-CGCM3 and NorESM1-M/ME) display a general overestimation, more marked over Eastern Eurasia and North America. GISS-E2-H/R presents a bias dipole with positive bias over Western Eurasia and Eastern Canada and a negative bias over Eastern Eurasia and Western Canada. The remaining models (CanESM2 and CNRM-CM5) show less significant SCE differences, and are generally the closest to observations
- The position of the snow margin is better captured by CMIP5 models in spring that in autumn. The best agreement is found over Eastern Eurasia and Western North America. During autumn, the CMIP5 ensemble has the snow margin shift considerably northward with only 4-6 out of 16 models matching the observations and overall agreement only occurs in Central Siberia.

- Differences of spring SWE climatology are characterized by an overall overestimation across nearly all CMIP5 models. The exception is CSIRO-Mk3-6-9 which displays a general underestimation over the whole Arctic; also, the models CCSM4, MPI-ESM-LR/P and NorESM1-M/E show a negative bias over Western Eurasia. The common feature in the CMIP5 ensemble is a local underestimation over the delta of the Yenisei River. In the onset season, differences are smaller in magnitude. The models NorESM1-M and NorESM1-ME stand out against the CMIP5 ensemble by presenting a strong bias over the Far East of Eurasia.

- There is a lack of agreement across reanalyses in representing SND climatology over the terrestrial Arctic in both seasons. ERA20c systematically reports the lowest values whereas NOAAV2c displays the largest accumulation. Discrepancies are stronger and more widespread in spring than in autumn, when they are concentrated almost only over Eastern Eurasia. Across CMIP5 models, we can distinguish three groups regarding the pattern of SND discrepancies. First group (bcc-csm1-1, CCSM4, NorESM1-M/ME) displays a large positive bias over the mountainous regions of Western North America and Eastern Eurasia. In contrast, the second group (CSIRO-Mk3-6-0 and inmcm4) displays a general overestimation over the whole Arctic. The remaining models (CanESM2, CNRM-CM5, GISS- E2-H/R, MIROCs, MRI-CGCM3) show a general overestimation with local significant differences; in particular, they are characterized by a negative bias over the Yenisei Delta. Discrepancies in autumn are smaller than in spring. A strong positive bias over Western North America and Eastern Eurasia prevails in the models from the first group (bcc-csm1-1, CCSM4, NorESM1-M/ME). GISS-E2-H/R and MRI-CGCM3 models show a general overestimation whereas the opposite is found in the rest of the CMIP5 ensemble (CanESM2, CNRM-CM5, CSIRO-Mk3-6-0, inmcm4, MIROCs).

  With respect to *in situ* snow measurements, we have found that reanalyses show a general overestimation in spring and underestimation in autumn. In spring, JRA-55 displays a good agreement in Eastern Eurasia, whereas the others show a strong overestimation. Over the southern edge of Western Eurasia, NOAAV2c shows the lowest bias which implies a good performance on the onset of the melting season. ERA20c shows a general positive bias compared to the snow stations. In autumn, ERA20c and NOAAV2c show a

relatively good agreement in Eastern Eurasia, however, they show a slightly positive bias over the northern part. JRA-55 displays a general underestimation with stronger values over the basin of the Ob River. Across CMIP5 models, we found a general positive bias over Eurasia. Some models show a negative bias over the Kamchatka Peninsula (MIROC-ESM/CHEM and CSIRO-Mk3-6-0). There is a group of models (CCSM4, MIROC-ESM-/CHEM, MRI-CGCM3, NorESM1-M/ME) that are in relatively good agreement with snow stations over south-west Eurasia implying a good timing of the start of the snow melt. In autumn, an overall underestimation is found across all CMIP5 models. The models bcc-csm1-1, CCSM4 and NorESM1-M/ME display a persistent positive bias of snow accumulation over the north of Eastern Eurasia.

(ii) Annual Cycle :

- There is a good agreement in the representation of the SCE annual cycle across the reference data sets. The observed annual cycle in SCE is relatively well captured by CMIP5 models in autumn but during the spring-summer season, most models tend to significantly underestimate SCE, especially over North America. Note that neither version NorESM1-M or NorESM1-ME is capable to completely melt snow in summer, mainly over Eastern Eurasia.
- The annual cycle in SWE is largely positively biased with respect to observations in most CMIP5 models. Nearly all models report persistent snow in summer months (mainly in North America), thus in contrast with observations. The large spread across the CMIP5 ensemble is substantial, especially over North America and Eastern Eurasia.
- The SND annual cycle displayed by the three reanalyses differs conspicuously. ERA20c shows the lowest values and it is not able to reproduce the seasonal variability accurately. NOAAV2c and JRA-55 are in better agreement, however, the former shows higher snow accumulation from November to April. The annual cycle of SND reported by CMIP5 models presents similar discrepancies with respect to observations as in the SWE annual cycle. The dispersion is remarkable during the snow accumulation season particularly in North America and Eastern Eurasia.

(iii) Quantile statistics of the spatial average :

- Reference data sets show similar SCE averages over the whole land Arctic in both seasons. However, in spring CMIP5 models generally underestimate the SCE average. Some models even display values twice too small. In autumn, there is better agreement with a slight tendency to overestimate.
- Regarding SWE averages, there is a large inconsistency between CMIP5 models and a general overestimation with respect to the observed reference, with only two out of sixteen models in accordance with observations. The dispersion is relatively smaller in autumn, however, the positive bias is still present.
- There is a general good agreement between CMIP5 models in SND in both seasons. However, the discrepancies between the different reanalyses are substantial.

Chapter 5

Temporal variability of snow characteristics

Contents

In this chapter, we evaluate the temporal variability of snow characteristics in spring and autumn throughout the historical period 1979-2005. First, snow interannual variability in CMIP5 models is compared to the different data sets. Second, linear trends in snow characteristics in CMIP5 models are considered. This is very important because CMIP5 models are extensively used to predict future climate and it is crucial to asses their fidelity in reproducing present snow trends.

5.1 Interannual variability of snow characteristics

We compare the characteristics of interannual variability of snow in CMIP5 models by means of a Taylor diagram representation (Taylor, 2001) of the time series of the snow variables spatially averaged over the Pan-Arctic in spring and autumn. The Taylor diagram is a concise statistical summary of how well different data sets match a reference (Taylor, 2001). This 2-D diagram provides the degree of correspondence between two time series by indicating the centered root mean squared error (RMS), the standard deviation σ or STD and the correlation coefficient R between them. In

practice, the STD is identified as the radial distance to the origin ; the distance to the reference point (star in x-axis) indicates the centered root-mean-squared error (RMS) and the azimuth gives the correlation coefficient R. We consider as observational reference the NOAA CDR for SCE, the CanSISE product for SWE and the JRA-55 reanalysis for SND.

5.1.1 Snow cover

The amplitude of interannual variability in both reanalyses (NCEP/CFSR and NOAAV2c) and NOAA CDR SCE are in a good agreement with each other in spring with standard deviations (STD) being 2.4% for NCEP/CFSR, 2.5% for NOAAV2c and 2.9% for NOAA CDR (Figure 5.1a). However, only the NOAAV2c reanalysis shows a positive and significant (at 95% level) correlation with NOAA CDR (R=0.58) and displays a centered RMS difference of 2.5% which is smaller compared to NCEP/CFSR (3.2%). Most of CMIP5 models show much smaller than observed STDs and practically no correlation on interannual scale with observations, except for bcc-csm1-1 and MIROC5 showing correlation of 0.42 and 0.37 (significant at the 95% level from the t-Student test).

During the onset season (Figure 5.1b), discrepancies with NOAA CDR are larger than in spring with centered RMS differences being greater for all models and reanalyses. The NCEP/CFSR reanalysis shows a similar magnitude of interannual variability as the NOAA CDR observational reference (4.8% and 4.5%, respectively). By contrast, the NOAAV2c reanalysis and the majority of CMIP5 models exhibit STDs of less than 2.5%, thus considerably smaller than in observations. Neither models nor reanalyses display a positive significant correlation with NOAA CDR, indeed, nearly all CMIP5 models correlate negatively.

5.1.2 Snow water equivalent

Spring SWE variability in CMIP5 models is characterized by a large spread (Figure 5.2a). The observed interannual variability (STD : 4.48 $\mathrm{kg\,m^{-2}}$) of SWE is well captured by CCSM4, MIROC-ESM and MPI-ESM-P (4.36 $\mathrm{kg\,m^{-2}}$, 4.46 $\mathrm{kg\,m^{-2}}$, 4.39 $\mathrm{kg\,m^{-2}}$, respectively). For the majority of models, the centered RMS differences are around 6 $\mathrm{kg\,m^{-2}}$. MIROC5, inmcm4 and NorESM1-ME models are characterized by the highest values of RMS ($\sim 7\,\mathrm{kg\,m^{-2}}$, $\sim 6.7\,\mathrm{kg\,m^{-2}}$ and $\sim 6.5\,\mathrm{kg\,m^{-2}}$). The model MIROC-ESM displays a STD in perfect agreement with CanSISE product. The lowest magnitude of interannual variability is found in CSIRO-Mk3-6-0 ($1.2\,\mathrm{kg\,m^{-2}}$) and is likely due to the relatively large number of ensemble members averaged (10 members, Table

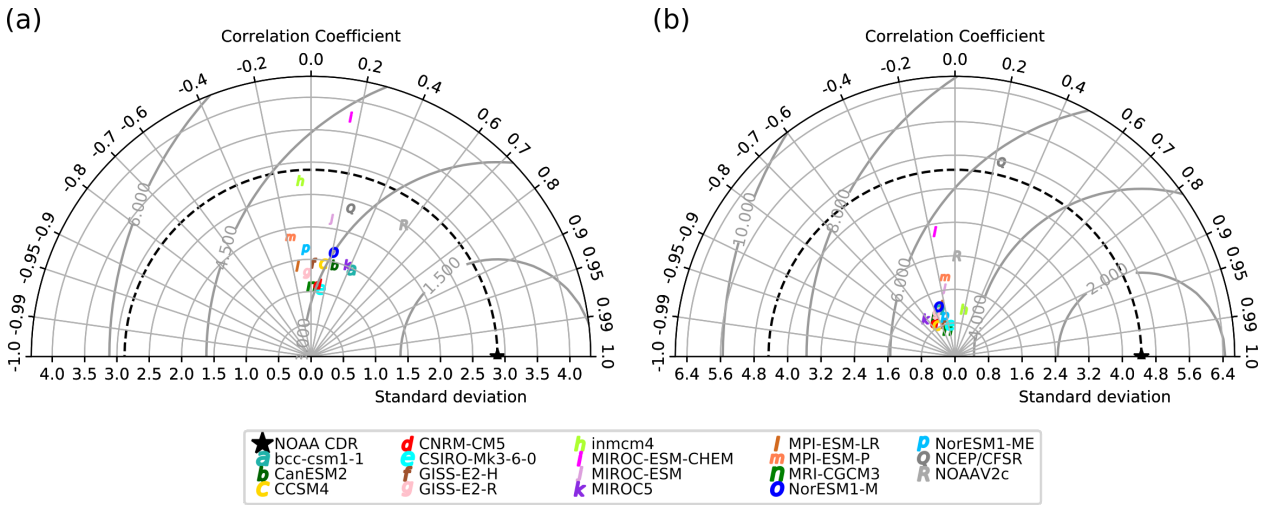

FIGURE 5.1 – Taylor diagram used in the evaluation of SCE time series over the Arctic in March-April (a) and in October-November (b) in CMIP5 models (a-p letters). The NCEP/CFSR (Q) and NOAAV2c (R) reanalyses are included versus the satellite-based NOAA CDR (black star). The radial distance to the origin indicates the standard deviation, the centered root-mean-squared error (RMS) is the distance to the reference point (star in x-axis) and the azimuth gives the correlation coefficient R.

2.1). The second lowest STD is displayed by CNRM-CM5 (2.72 $\mathrm{kg\,m^{-2}}$), also resulting from a 10 member average. MIROC-ESM-CHEM is not shown in Figure 5.2, as its STD of 10.25 $\mathrm{kg\,m^{-2}}$ was outside the bounds of the Taylor diagram. Only NorESM1-M display a significant positive correlation(R=0.42) with the CanSISE product.

In autumn, the spread of CMIP5 models is also remarkable (Figure 5.2b). The majority of CMIP5 models underestimate the magnitude of the interannual variability reported by the CanSISE product (2.7 $\mathrm{kg\,m^{-2}}$). By contrast, NorESM1-ME and all versions of MIROC yield STDs greater than 4 $\mathrm{kg\,m^{-2}}$; thus, they are considered outliers with respect to STDs and do not appear in Figure 5.2b. As for spring, the lowest amplitude of interannual variability is found in CSIRO-Mk3-6-0 (0.89 $\mathrm{kg\,m^{-2}}$). There is only one model (bcc-csm1-1) displaying a positive significant correlation of 0.39 with the observations.

5.1.3 Snow depth

Compared to the other snow characteristics, the interannual variability of SND seems to be better captured by CMIP5 models (Figure 5.3). Spring SND variability (Figure 5.3a) in JRA-55 and NOAAV2c reanalyses is in good agreement in both the amplitude (4.17 cm and 3.58 cm, respectively) and correlation (R=0.56). However, ERA20c is not able to correctly reproduce the

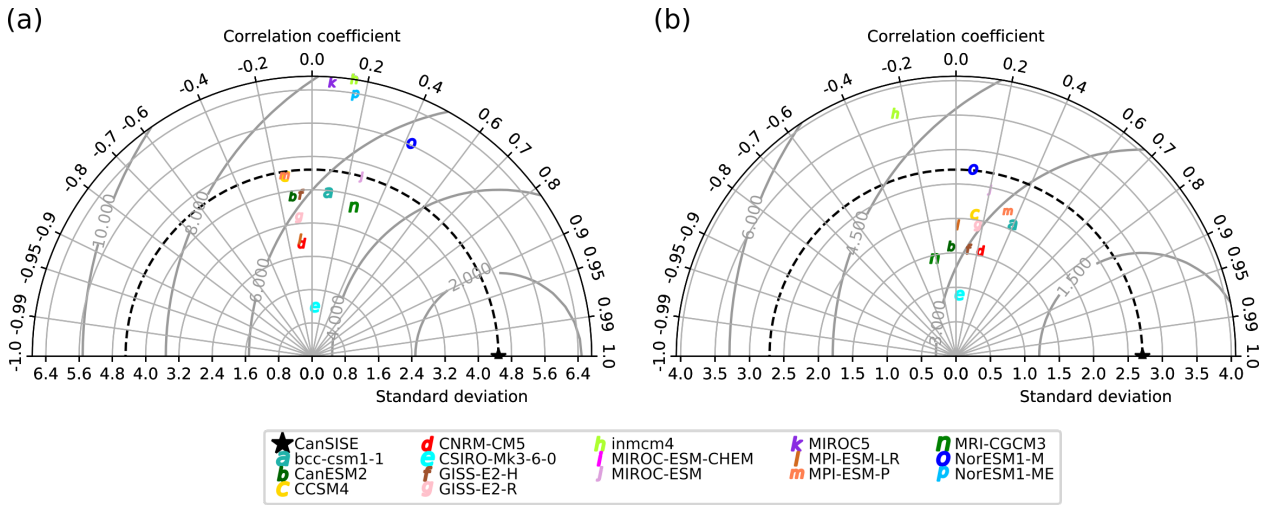

FIGURE 5.2 – Taylor diagram used in the evaluation of SWE time series over the Arctic in March-April (a) and in October-November (b) in CMIP5 models (a-p letters). CanSISE Ensemble product is used as reference (black star). The radial distance to the origin indicates the standard deviation, the centered root-mean-squared error (RMS) is the distance to the reference point (star in x-axis) and the azimuth gives the correlation coefficient R.

magnitude of interannual variability as it displays a very low STD of 0.59 cm, but a significant correlation with JRA-55 of 0.55. The amplitude of interannual variability is fairly simulated by only two models, MIROC-ESM-CHEM and MIROC5 (3.3 cm and 2.3 cm, respectively). MIROC5 is also characterized by giving rise to the lowest RMS, which indicates a relatively good agreement with the observational reference compared to the CMIP5 ensemble. The rest of the models displays an amplitude of interannual variability twice smaller than JRA-55, with a centered RMS around 4 cm. Half of the CMIP5 models show significant correlation (at 95% level) with JRA-55, which indicates a better performance in reproducing the interannual variability of snow depth than the other snow characteristics treated previously. These models are (lowest to highest correlation) : MIROC-ESM-CHEM (0.39), CNRM-CM5 (0.41), CSIRO-Mk3-6-0 (0.51), GISS-E2-H (0.51), NorESM1-M (0.53) and CanESM2 (0.62) and the highest correlation is found in MIROC5 (0.77).

The performance of CMIP5 in reproducing interannual variability in autumn is similar to spring (Figure 5.3b). However, the amplitude of interannual variability is smaller as evidenced by the STD of 2.45 cm in the JRA-55 reanalysis. NOAAV2c matches very well with JRA-55, reporting a STD of 2.65 cm and a significant correlation of 0.71. By contrast, the ERA20c reanalysis certainly underestimates the amplitude of interannual variability with a STD of 0.33 cm, less than all CMIP5 models. Despite that, ERA20c and JRA-55 correlate significantly (0.65). The models characterized by stronger variability are MIROC5 (1.86 cm), MIROC-ESM-CHEM (1.42 cm) and NorESM1-

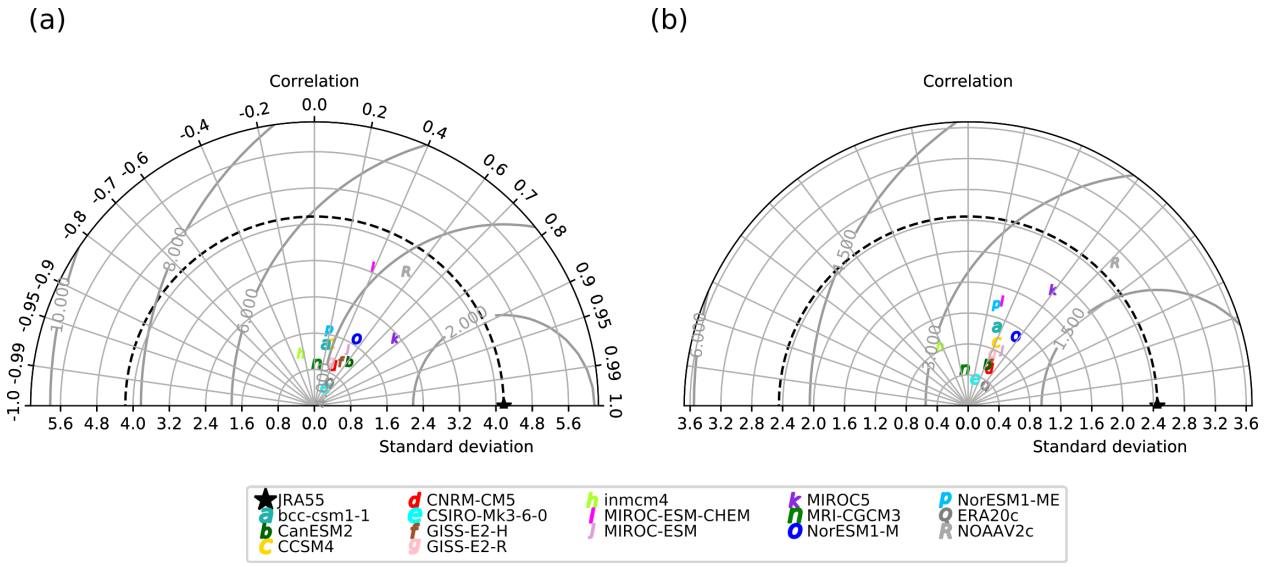

FIGURE 5.3 – Taylor diagram used in the evaluation of SND time series over the Arctic in March-April (a) and in October-November (b) in CMIP5 models(a-p letters). ERA20c (Q) and NOAAV2c (R) reanalyses are included versus the JRA-55 reanalysis (black star) considered here as reference. The radial distance to the origin indicates the standard deviation, the centered root-mean-squared error (RMS) is the distance to the reference point (star in x-axis) and the azimuth gives the correlation coefficient R.

ME (1.35 cm). For the majority of models, the centered RMS differences are around 2.2 cm. The only exception is the inmcm4 model showing the highest RMS of 3 cm and a negative significant correlation of -0.42. Eight out of the fourteen models show a positive significant correlation with JRA-55. Ordered by increasing correlation, these models are CCSM4 (0.41), CanESM2 (0.42), GISS-E2-R (0.43), GISS-E2-H (0.47), CNRM-CM5 (0.50), MIROC-ESM (0.52), NorESM1-M (0.56) and MIROC5 (0.59).

The low correlations found between SCE and SWE from CMIP5 and observations are not surprising considering the fundamental limitations of GCMs in reproducing interannual variability (Taylor *et al.*, 2012). Historical runs are initiated from a state in equilibrium with pre-industrial climate forcings simulated by the quasi-equilibrium control runs, the so-called “initial climate state”, which may not perfectly match to the observed climate state. For instance, the temporal evolution of climate system in the models will likely miss the impact of the unforced internal variations such as El Niño, the North Atlantic Oscillation (NAO), Atlantic Multidecadal Oscillation (AMO). In fact, among 16 models and a test at the 95% confidence level, it is very likely that there are one or two significant correlations across independent time series. Nonetheless, we consider that Taylor Diagram representation provides a very visible evaluation of STD and RMS in CMIP5 models. This

being said, reanalyses and satellite-based products are constrained by the real-time evolution of the climate and their mutual correlations in the Taylor diagram are relevant to evaluate them.

We have performed the same analysis but with detrended time series of snow characteristics (figure not shown) and we did not find any substantial differences. This can be explained by the weak trends displayed in CMIP5 models, as we shall see further. Actually, the significant correlations found in SND between CMIP5 models and observations are likely due to the anthropogenic forcing as they do not occur in the case for detrended time series.

5.2 Seasonal trend analysis

In this section, we evaluate the accuracy of CMIP5 models in reproducing interdecadal seasonal trends compared to the different snow data sets. The main target is to assess the robustness and to estimate the uncertainty in historical snow trends. For the analysis of trends in snow characteristics we evaluate CMIP5 model trends from individual model ensemble members, from the ensemble of a single model and from the multimodel ensemble mean. In total, we analyze 73 individual model realizations provided by 16 models (Table 2.1) for SCE and SWE and 68 individual simulations from 14 models for SND (without MPI-ESM-LR/P versions). We perform a similar analysis done by Stroeve *et al.* (2011) for the evaluation of Arctic sea ice trends in CMIP3 and CMIP5 models.

5.2.1 Snow cover

For the whole Arctic (Figure 5.4a), NCEP/CFSR shows an insignificant increase in spring SCE, disagreeing with NOAA CDR and NOAAV2c as both consistently display significantly negative trends of $-1.21 \pm 0.58\%$/dec and $-1,26 \pm 0.68\%$/dec, respectively (Figure 5.4a, Table B.1). The multimodel mean with a value of $-1.10 \pm 0.13\%$/dec falls in the range of estimates given by NOAA CDR and NOAAV2c. However, five models (inmcm4, MIROC-ESM-CHEM, MPI-ESM-LR, MRI-CGCM3 and NorESM1-ME) report SCE trends out of the observation range, but in only two of them (MIROC-ESM-CHEM and MPI-ESM-LR) those deviations are statistically significant (Table B.1). Considering individual ensemble members, 39 of 73 report significant trends consistently with observations. Remarkably, some models (bcc-csm1-1, CNRM-CM5, MIROC5 and NorESM1-M) demonstrate a quite strong spread in trend estimates across their ensemble members.

Among the reference data sets, only NOAA CDR is statistically significant at the 90% level displaying a decreasing trend of $-1.79 \pm 0.95\%$/dec over the Eurasian Arctic subdomain (Fi-

gure 5.4b, Table B.2). NCEP/CFSR and NOAAV2c report SCE trends of $-0.03 \pm 0.82\%$/dec and $-1.42 \pm 0.91\%$/dec, the latter being closer to the NOAA CDR estimate; however, none of them is significant at the 90% confidence level. The multimodel mean displays a negative trend slightly weaker than the observed value of $-1.01 \pm 0.17\%$/dec. There are 9 out of 16 model ensembles and almost half of the individual realizations that report significant trends inside the range implied by observations. The models bcc-csm1-1, inmcm4, MPI-ESM-LR/P and MRI-CGCM3 are out of the observed range and show no statistical significance neither in the ensemble nor in the member trends (the only exceptions are two members in bcc-csm1-1 and MPI-ESM-LR).

In North America (Figure 5.4c, Table B.3), all observational data sets display insignificant SCE trends in spring. The lowest p-value is found in NOAAV2c, being statistically significant at 78% (t-test), thus we consider it as reference for the analysis in the North American subdomain with its negative trend of $-0.87 \pm 0.71\%$/dec. NOAA CDR shows a weaker trend of $-0.33 \pm 0.76\%$/dec while NCEP/CFSR displays an increase in SCE of $+0.83 \pm 0.73\%$/dec. The multimodel mean ($-1.23 \pm 0.15\%$/dec) is statistically significant and lies in within the observed range. Nearly all the ensemble models fall inside the range given by NOAAV2c, however three of them (MPI-ESM-LR/P and NorESM1-M) are not statistically significant. The models GISS-E2-H, MIROC-ESM-CHEM and inmcm4 display SCE trends outside the observed range. Overall, there are 10 out 16 ensemble members and 15 out 73 individual realizations that show significant negative trends falling inside the observed range in North America.

In the onset season (Figure 5.4d, Table B.4), NOAA CDR displays a trend of $+3.28 \pm 0.91\%$/dec and is thus a clear outlier with respect to the other reference data sets. The unrealistic October trend estimated by NOAA CDR in the recent period has been already reported by Brown and Derksen (2013) and Estilow *et al.* (2015). NCEP/CFSR and NOAAV2c show SCE trends of $-1.61 \pm 1.15\%$/dec and $-0.76 \pm 0.59\%$/dec respectively, but they lack statistical significance. Consequently, we consider NCEP/CFSR as reference for model evaluation since it displays a p-value slightly lower than NOAAV2c (0.17 and 0.21, respectively). The multimodel mean shows an autumn SCE trend of $-0.72 \pm 0.12\%$/dec falling in the range given by NCEP/CFSR estimates. We also note generally weaker SCE trends in models respect to that from NCEP/CFSR. Thirteen of 16 models are within the observed SCE trend range. Considering individual ensemble members, 37 estimates fall into the range implied by observations, thus roughly 50% of individual model ensemble members present trends which are qualitatively consistent with observations. The lar-

gest spread across ensemble members is observed for bcc-csm1-1, CanESM2 and in both version of MPI-ESM-LR/P.

In Eurasia during autumn (Figure 5.4e, Table B.5), SCE trends in both NCEP/CFSR and NOAAV2c lack of statistical significance with values of $-1.83 \pm 1.40\%$/dec and $-0.36 \pm 0.80\%$/dec. The NCEP/CFSR reanalysis shows the lowest p-value, being statistically significant at 80% (t-test), so we consider it as reference in this comparison. The SCE trend in the multimodel mean is $-0.48 \pm 0.14\%$/dec, i.e. weaker than the reference. Half the models and 28% of individual realizations report significant decreasing trends lying inside the observed range. Note that, nearly all of these models and members report SCE trends weaker than the observed value.

The agreement between models and both reanalyses seems to be better over the North American Arctic for the autumn season (Figure 5.4f, Table B.6). Still, NOAA CDR is considered as outlier even if the trend reported here is slightly weaker than for Eurasia ($+2.62 \pm 0.12\%$/dec). NCEP/CFSR and NOAAV2c show SCE trends of $-1.35 \pm 0.27\%$/dec and $-1.38 \pm 1.17\%$/dec (respectively) but they lack statistical significance. Accordingly, we choose NCEP/CFSR as reference as it displays a p-value lower than NOAAV2c (0.27 and 0.18, respectively). The multimodel mean is quite close to the observed value of both reanalyses displaying a decreasing trend of $-1.05 \pm 0.13\%$/dec. All CMIP5 ensemble of single models report SCE significant trends inside the range implied by observations, and only two models are not significant (MPI-ESM-P and MRI-CGCM3). With respect to individual realizations, 25 out 73 are significant and lie within the observed range.

5.2.2 Snow water equivalent

In spring (Figure 5.5a, Table B.7), SWE in CanSISE product shows an insignificant downward tendency for the whole Arctic ($-1.09 \pm 1.25\,\mathrm{kg\,m^{-2}}$/dec). The multimodel model mean, however, shows a strong, negative and significant SWE trend of $-2.85 \pm 0.34\,\mathrm{kg\,m^{-2}}$/dec. Five models (bcc-csm1-1, CSIRO-Mk3-6-0, GISS-E2-R, MPI-ESM-LR and MRI-CGCM3) report trends in spring SWE falling in the range given by observations but only two of them are statistically significant (CSIRO-Mk3-6-0 and GISS-E2-R). Regarding individual ensemble members, only 5 of 73 significant SWE trends fall into the observed range (all belonging to CSIRO-Mk3-6-0 model). Thus, less than 7% of ensemble simulations are in agreement with the observed SWE trend in spring. The individual realizations of bcc-csm1-1, CNRM-CM5, MIROC5 and MRI-CGCM3 have the largest spread of trend estimates.

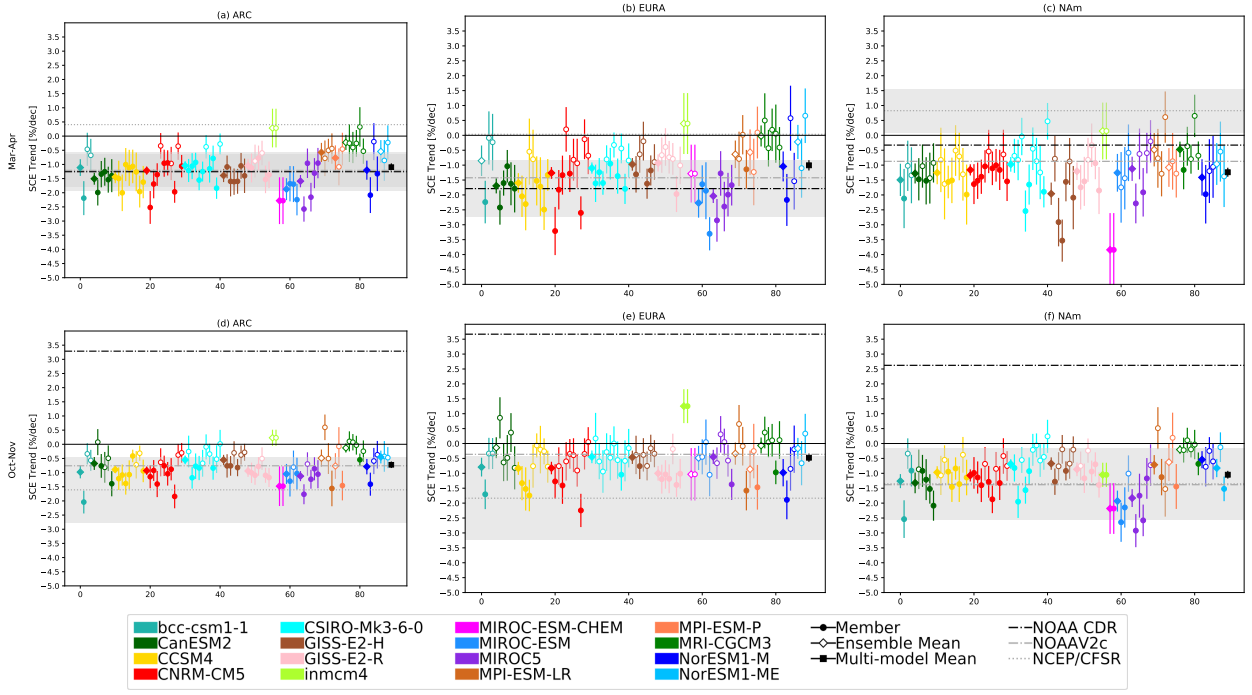

FIGURE 5.4 – SCE trend in March-April (top row) and October-November (bottom row) during 1979-2005 for the Arctic (a,c) and the subdomains of Eurasia (b,d) and North America (d,f). Trends are computed for each individual model realization (circle), the ensemble model mean (diamond) and the multimodel mean (black square). NCEP/CFSR and NOAAV2c and NOAA CDR are shown in horizontal lines. Shaded regions indicate the ±1 standard error of the trend in the reference data set. Filled markers indicates statistical significance at the 90% of confidence level (t-test). See text or tables in Annex B for statistical significance of the SCE trends in the reference data sets.

Over the Eurasian sector of the Arctic in spring (Figure 5.5b, Table B.8), the CanSISE product reports a weak and insignificant SWE trend of $-0.69 \pm 1.54\,\mathrm{kg\,m^{-2}}$/dec. The multimodel mean displays a strong significant trend of $-1.84 \pm 0.43\,\mathrm{kg\,m^{-2}}$/dec, lying inside the range given by observations. Thirteen ensemble models fall in the observed range, but only five of them (CanESM2, CCSM4, CNRM-CM5, CSIRO-Mk-3-6-0 and GISS-E2-H) are statistically significant. With respect to the individual realizations, there are only 4 (out of 73) members, all from CSIRO-Mk-3-6-0, that are significant and lie within the observed range.

During spring, North American SWE trends (Figure 5.5c, Table B.9) are characterized by a large spread in CMIP5 models compared to Eurasia. The CanSISE product displays a negative SWE trend of $-1.66 \pm 2.01\,\mathrm{kg\,m^{-2}}$/dec, but it is not statistically significant. The multimodel mean exhibits stronger than observed trend of $-4.23 \pm 1.03\,\mathrm{kg\,m^{-2}}$/dec falling out of the reference range. Three models report SWE trends inside the range implied by observations, but only two are significant (CSIRO-Mk-3-6-0 and GISS-E2-H). Just three individual realizations, from CSIRO-Mk-3-6-0 model, are significant and fall inside the observed range.

In the onset season (Figure 5.5d, Table B.10), most CMIP5 models show stronger negative trends in SWE compared to the CanSISE product which displays a weak and insignificant SWE trend of $-0.63 \pm 0.76\ \mathrm{kg\,m^{-2}}$/dec, while the multimodel mean trend is $-1.65 \pm 0.18\,\mathrm{kg\,m^{-2}}$/dec. Six out of 16 CMIP5 models (CanESM2, CSIRO-Mk3-6-0, GISS-E2-H/R and MPI-ESM-LR/P) fall inside the range given by observations, however, only two of them present significant trends (GISS-E2-H and MPI-ESM-LR). None of the individual model members simulate a significant SWE trend inside the range given by the CanSISE product (except for one member of CSIRO-Mk3-6-0). Also, we note that generally, the spread of individual members is smaller for autumn than spring, except for MIROC5 and MRI-CGCM3.

In Eurasia during the autumn season (Figure 5.5e, Table B.11), the majority of CMIP5 models show very weak SWE trends so does the CanSISE product which reports an insignificant decreasing trend of $-0.59 \pm 0.79\ \mathrm{kg\,m^{-2}}$/dec. The multimodel mean SWE trend of $-0.77 \pm 0.19\,\mathrm{kg\,m^{-2}}$/dec is very close to the observed value. There are six ensemble models showing significant SWE trends but only three (CCSM4, CNRM-CM5 and MPI-ESM-LR) fall inside the range given by observations. Across the individual model realizations none of them shows a significant SWE trend lying inside the observed range.

As for spring, the spread in SWE trend in autumn across CMIP5 models is higher in the North

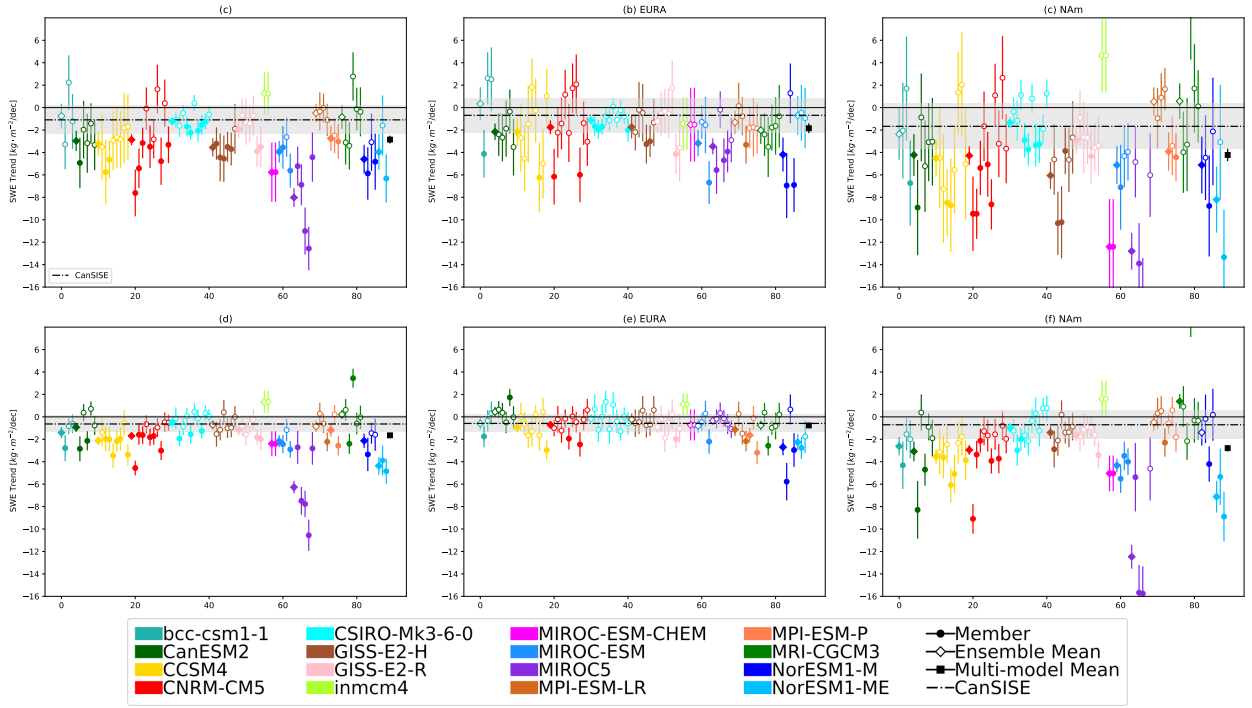

FIGURE 5.5 – SWE trend in March-April (top row) and October-November (bottom row) during 1981-2005 for the Arctic (a,c) and the subdomains of Eurasia (b,d) and North America (d,f). Trends are computed for each individual model realization (circle), the ensemble model mean (diamond) and the multimodel mean (black square). Shaded regions indicate the ±1 standard error of the trend in the CanSISE product. Filled markers indicated statistical significance at 90% of confidence level (t-test). See text or tables in Annex B for statistical significance of the SWE trends in the CanSISE product.

American Arctic sector (Figure 5.5f, Table B.12). The CanSISE product displays a decreasing and insignificant trend of $-0.70 \pm 1.25\,\mathrm{kg\,m^{-2}/dec}$. The SWE trend reported by the multimodel mean is outside the observed range with a value of $-2.79 \pm 0.28\,\mathrm{kg\,m^{-2}/dec}$. Six models display SWE trends inside the range implied by observations but only three of them are statistically significant (CSIRO-Mk3-6-0, GISS-E2-H/R). As for Eurasia, none of the individual members show significant trends lying inside the observed range.

5.2.3 Snow depth

We evaluate SND trends (1979-2005) in spring and autumn across the Arctic subdomains in CMIP5 models and in three reanalyses (ERA20c, JRA-55 and NOAAV2c) as seen in Figure 5.6. Discrepancies between the reference data sets are substantial ; mainly for ERA20c reanalysis which displays systematically very weak trends compared to the other reanalyses (JRA-55 and NOAAV2c). Wegmann *et al.* (2017) already reported the poor ability of ERA20c in reproducing SND trends in

Eurasia compared to *in situ* snow data. Therefore, for this diagnostics, the ERA20c reanalysis is considered as an additional or alternative data set to be evaluated, but not as a reference for model comparison.

Figure 5.6a shows spring Arctic SND trends displayed by CMIP5 models and the three reanalyses. The JRA-55 reanalysis shows a significant trend of -3.81 ± 0.72 cm/dec (Table B.13). This marked SND trend over the whole Arctic is due to local strong decreases found in some areas over the Rocky Mountains and Canadian Archipelago (Figure 5.10), which is demonstrated by a trend of -7.43 ± 1.6 cm/dec over the North American sector of one order greater than the SND trend reported using stations from Global Historical Climatology Network (GHCN). This SND trend value is only considered as an approximate reference since it has been computed for a longer period (1950-2013) and a smaller area, north of 60° latitude (Brown *et al.*, 2017). Therefore, we discard JRA-55 as reference for the whole Arctic spring SND trends (Figure 5.6a,b,c). Rather, we select the NOAAV2c reanalysis, which reports a SND trend of -1.74 ± 0.83 cm/dec statistically significant at 95%. ERA20c shows a weak but significant trend of -0.29 ± 0.14 cm/dec. With respect to NOAAV2c reanalysis, the multimodel mean (-0.95 ± 0.10 cm/dec) slightly underestimates the SND trend. Half of the ensemble models show a significant SND trend falling inside the range given by the NOAAV2c reanalysis. These models are CanESM2, CCSM4, CNRM-CM5, GISS-E2-H/R, MIROC-ESM-/CHEM and NorESM1-M. 30% of individual realizations display significant tendencies within the range implied by NOAAV2c.

In Eurasia during the melting season (Figure 5.6b, Table B.14), NOAAV2c is the only reference data set statistically significant at the 90% confidence level and displays a decrease in SND of -1.19 ± 0.16 cm/dec. The other two reanalyses, JRA-55 and ERA20c, exhibit trend values of -0.76 ± 0.55 cm/dec and -0.19 ± 0.16 cm/dec (respectively) but they lack statistical significance. The multimodel mean is slightly outside the range implied by observations, displaying a decreasing significant trend of -0.59 ± 0.12 cm/dec. There are six out of 14 models that present SND trend estimates inside the observed range, and five are statistically significant (CanESM2, CCSM4, MIROC-ESM, MIROC5 and NorESM1-M). There are only 25% of individual realizations that lie inside the range implied by observations. The largest spread in individual realization trends is found in CNRM-CM5 and MIROC5.

The JRA-55 reanalysis shows the best score of statistical significance compared to the other reanalyses in North America in spring (Figure 5.6c, Table B.15). However, as mentioned before, this

strong trend of -7.43 ± 1.6 cm/dec is unrealistic compared to *in situ* snow measurements (Brown *et al.*, 2017). The main contribution to this strong decreasing SND trend is located in elevated and northern areas over the Rocky Mountains and the Canadian Archipelago (Figure 5.10b). ERA20c reports a SND trend of -0.43 ± 0.26 cm/dec (statistically significant at 90%), but it is very weak compared to the *in situ* observations (Figure 5.12 ; Wegmann *et al.*, 2017). NOAAV2c shows a SND trend of -1.88 ± 1.51 cm/dec and is statistically significant at the 78% of confidence level. The multimodel mean is in good agreement with the NOAAV2c reference, reporting a decreasing trend of -1.42 ± 0.16 cm/dec. There are only three models (inmcm4, MIROC5 and MRI-CGCM4) out of the range implied by NOAAV2c but only one is statistically significant (MIROC5). The rest of CMIP5 models lie inside the observed range and are statistically significant (except bcc-csm1-1). There are 25 out of 68 individual realizations that agree with NOAAV2c and are statistically significant.

During the onset season (Figure 5.6d, Table B.16), JRA-55 displays a significant SND trend of -1.62 ± 0.52 cm/dec over the whole Arctic which is stronger than the other reanalyses. NOAAV2c shows almost a neutral trend of -0.09 ± 0.08 cm/dec and ERA20c one of -0.89 ± 0.64 cm/dec, however none of them are statistically significant. Thus, we consider JRA-55 as reference for evaluation of model autumn SND trends. The multimodel mean shows a weaker than observed trend with a value of -0.65 ± 0.07 cm/dec. Except for MRI-CGCM3, the rest of the ensemble models shows significant SND trends but none of them fall inside the range of JRA-55. There are only 8 out of 68 individual realizations that lie within the range given by the reference data set.

Over Eurasia in autumn (Figure 5.6e, Table B.17), SND trends are weak, almost neutral in the majority of CMIP5 models. JRA-55 shows a significant trend of -0.89 ± 0.42 cm/dec, stronger than NOAAV2c (-0.50 ± 0.61 cm/dec) and ERA20c (-0.09 ± 0.09 cm/dec), but none of them are statistically significant. The SND trend displayed of the multimodel mean is -0.30 ± 0.07 cm/dec, almost three times smaller than the reference. There are four models (bcc-csm1-1,GISS-E2-R and NorESM1-M/ME) that display SND trends within the range implied by JRA-55 and they are all statistically significant. Regarding individual realizations, there are 11 out 68 that lie inside the observed range and they are statistically significant at the 90% confidence level.

In the onset season, the spread of SND trends is larger in North America (Figure 5.6f, Table B.18) than in Eurasia. The only reanalysis displaying a significant SND trend is JRA-55, being of -2.48 ± 1.14 cm/dec, whereas NOAAV2c and ERA20c report weaker trends (-0.10 ± 0.14 cm/dec,

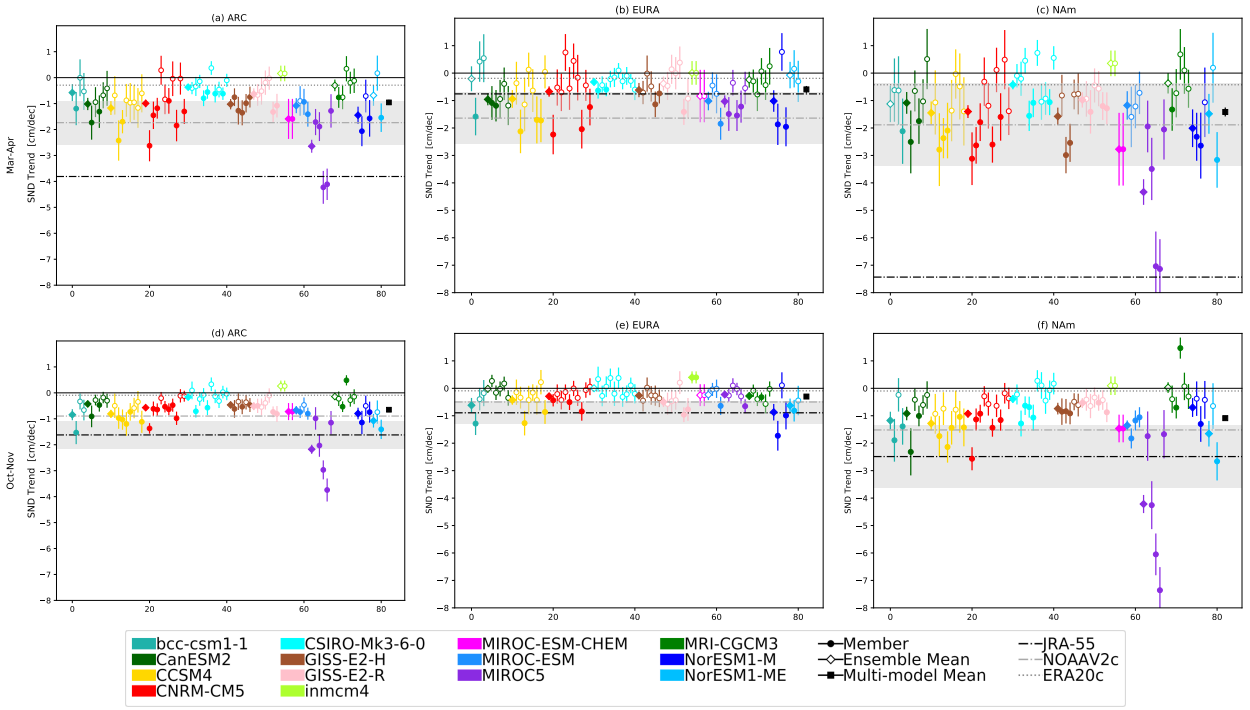

FIGURE 5.6 – SND trend in March-April (top row) and October-November (bottom row) during 1979-2005 for the Arctic (a,c) and the subdomains of Eurasia (b,d) and North America (d,f). Trends are computed for each individual model realization (circle), the ensemble model mean (diamond) and the multimodel mean (black square). ERA20c, JRA-55 and NOAAV2c trends are indicated in horizontal lines. Shaded regions indicate the ±1 standard error of the trend in the reference data set. Filled markers indicated statistical significance at 90% of confidence level (t-test). See text or tables in Annex B for statistical significance of the SND trends in the reference data sets.

-1.51 ± 1.12 cm/dec, respectively). The multimodel mean is quite close to the range implied by JRA-55 with a decreasing value of -1.09 ± 0.08 cm/dec. Only 3 out of 14 models (MIROC-ESM-/CHEM and NorESM1-ME) display significant SND trend inside the observed range. Fourteen out of 68 realizations are also significant and fall within the range implied by JRA-55 ; these simulations are from the aforementioned models in addition to members from bcc-csm1-1, CanESM2, CCSM4, CNRM-CM5 and MIROC5. It is worth mentioning the large spread of MIROC5 of SND trends in North America, which was already reported in Figure 5.6f for SWE trends.

5.3 Spatial trend pattern

The spatial patterns of linear trends in individual models are extremely noisy with trends of different signs coexisting in close proximity. In this section, we quantify the degree of consensus across the 16 models (14 models for SND) over linear trends in snow characteristics (Figure 5.8,5.9 and 5.11). For each grid cell, we compute the maximum number of models agreeing on the sign of

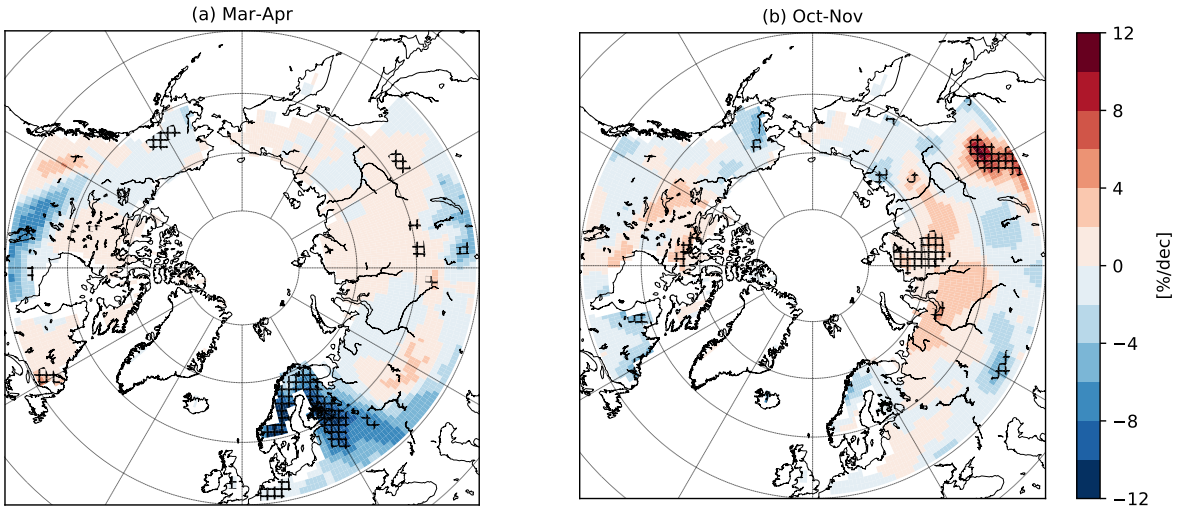

FIGURE 5.7 – Spatial SCE trend in March-April (a) and October-November (b) from the NOAAV2c reanalysis during the period 1979-2005. Statistically significant trends at 90% confidence level from the t-Student are hatched.

trend and on its significance. For instance, if in a particular cell 8 models show significant positive trends, 5 significant negative trends and 3 insignificant trends, this grid cell will hold "+8" value. If the numbers of models with positive and negative trends are equal, the grid cell is set to zero. For this analysis, we used the 80% significance level (t-test) for estimating statistical significance of individual trends rather than 90%, in order to increase the number of model trends considered for each grid cell.

5.3.1 Snow cover

To characterize SNC trends in CMIP5 models, we choose as reference the spatial trend pattern of NCEP/CFSR (Figure 5.8b,d) since NOAAV2c reanalysis shows very weak insignificant trends (Figure 5.7). NOAAV2c shows a localized significant decrease in SCE over Scandinavia of almost 8 cm/dec in spring (Figure 5.7a). During the onset season (Figure 5.7a), the areas with a positive significant SCE trend are located east of the Yenisei River (up to 4 cm/dec) and east of the Lake Baikal (around 10 cm/dec).

Figure 5.8b shows NCEP/CFSR trend pattern in SCE in spring. NCEP/CFSR exhibits significant positive trend over the eastern part of Siberia with a maximum up to +12%/dec observed east of the Lake Baikal. Positive SCE trends of +10-12%/dec are also observed over the mountain regions of the western part of North America. Most of Eastern Europe is characterized by significantly negative trends, amounting to −12%/dec over Eastern Scandinavia and south of the Ural

Mountains. The best agreement between CMIP5 models and observations is located over Western Eurasia where 8 to 12 models (out of 16) display significantly negative trends. Over the north of Eastern Eurasia, 4 to 8 models exhibit positive trends, in agreement with NCEP/CFSR. The North American pattern of negative trends is captured by 4 to 8 CMIP5 models, however, the CMIP5 ensemble does not capture the pattern of positive trends over the Rocky Mountains and over the Laurentian Plateau (Figure 5.8a).

During the onset season, NCEP/CFSR shows decreasing trends over Eastern Europe and north of the Eurasian Dry Land Band (EDLB, Groisman *et al.*, 2018) in Siberia. Over North America, negative trends in SCE (− 8-12%/dec) dominate over most regions except for the western mountainous regions (Figure 5.8d). Locally, positive trends (up to +12%/dec) are observed over the north of Eastern Eurasia in the Cherskly Mountain Range. The model ensemble demonstrates practically everywhere negative trends dominating over positive ones (Figure 5.8c). This coincides with NCEP/CFSR over Eastern Europe and north of EDLB in Siberia but not over the north of Eastern Eurasia and Western North America.

5.3.2 Snow water equivalent

A similar analysis is carried out for SWE during the period 1981-2005 (Figure 5.9). The CanSISE product shows very few locations with statistically significant trends in both seasons. In spring (Figure 5.9b), statistically significant decrease in SWE is observed in Northern Eurasia along the Arctic Ocean coast and a local increase is identified over the southern part of Western Siberia. In the onset season (Figure 5.9d), SWE in the CanSISE product demonstrates negative trends over northwestern Canada and the south part of Eastern Eurasia and locally positive trends over Northern Eurasia along the coast of the Arctic Ocean. In spring most models report primarily negative trends in SWE over Eastern Eurasia and primarily positive tendencies over Northern Siberia. In autumn (Figure 5.9c), the model ensemble reports negative trends nearly everywhere, with around 8 models showing downward SWE changes in North America and Western Eurasia. Eastern Eurasia is characterized by little consensus among CMIP5 models with estimates showing mostly insignificant trends and less than 4 models out of 16 demonstrating statistically significant trends.

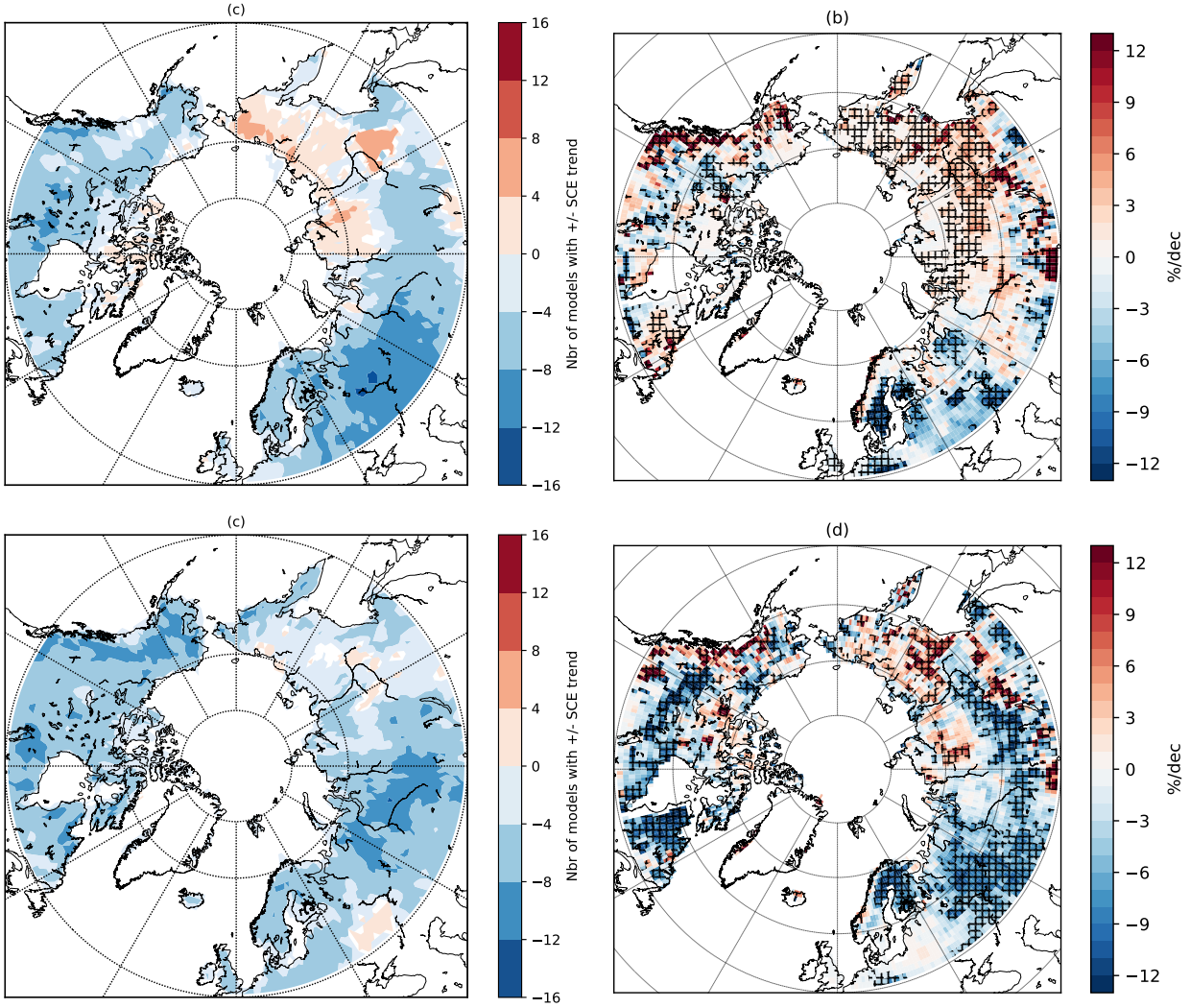

FIGURE 5.8 – (a,c) Number of CMIP5 models displaying a positive/negative SCE trend in March-April (a) and in October-November (c) during 1979-2005. Only SCE trends statistically significant at the 80% confidence level (t-Student test) are counted.(b,d) Spatial trend of SCE trend (%/dec) from NCEP/CFSR reanalysis in March-April(b) and October-November(d) during 1979-2005. Hatched regions indicate SCE trends statistically significant at the 90% confidence level (t-Student test).

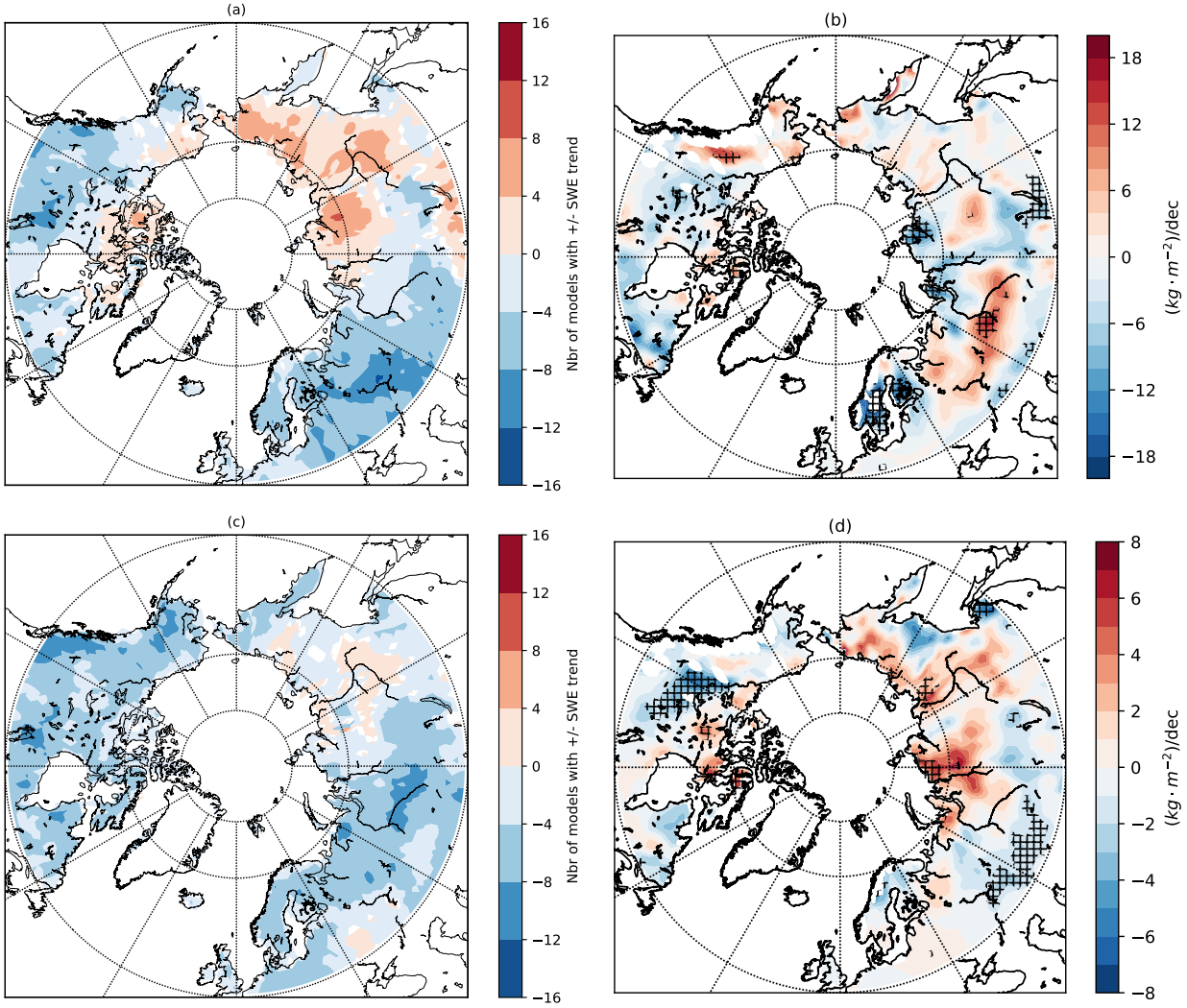

FIGURE 5.9 – (a,c) Number of CMIP5 models displaying a positive/negative SWE trend in March-April (a) and October-November (c) during 1981-2005.Only SWE trends statistically significant at the 80% confidence level (t-Student test). (b,d) Spatial trend of SWE trend (kg m^{-2})/dec) in March-April (b) and October-November (d) during 1981-2005 of CanSISE ensemble product. Hatched regions indicate SWE trends statistically significant at the 90% confidence level (t-Student test).

5.3.3 Snow depth

We assess the differences in SND spatial trends across the reanalyses (Figure 5.10). In spring (Figure 5.10a), ERA20c shows localized statistical significance over the east of the Canadian Archipelago and east of the Yenisei River, displaying increasing trends of less than + 1.5 cm/dec. Negative significant trends are located over Scandinavia with values as low as −2 cm/dec. During the onset season (Figure 5.10b), ERA20c displays a similar pattern of SND trend but twice smaller in magnitude than in spring. Two other regions, the south of Western Eurasia and west side of the Lake Baikal, show statistical significance, with decreasing trends of less than −1.0 cm/dec. The SND trends estimates in both seasons are very weak compared to the *in situ* data (Figure 5.12a ; Bulygina *et al.*, 2011; Wegmann *et al.*, 2017). Regarding the JRA-55 reanalysis, the statistical significance of the spring SND trends appears unusual, e.g., compared to the other data sets (Figure 5.10c). The Rocky Mountains, some areas north of Canada and over the Canadian Archipelago, and between the Ob and Yenisei Rivers experience steep negative trends of more than − 20-30 cm/dec. Very regional and positive strong SND trend can be fond in north of Alaska and along the coast of Okhotsk Sea with values up to + 30 cm/dec. During the onset season (Figure 5.10c), JRA-55 shows negative and significant SND trend along the coast of Hudson's Bay around −8 cm/dec and up to −12 cm/dec over the Canadian Archipelago. In Eurasia, there is a dipole of SND trends in the coast of the Kara Sea with a strong negative (positive) tendency in the west (east) of the Yenisei River reaching ± 12cm/dec of magnitude. JRA-55 underestimates SND trends over the Ob-Yenisei river basins as in its previous version JRA-25 (Khan *et al.*, 2008). Additionally, this trend is even sharper in spring and negative unlike snow stations (Figure 5.12a ; Bulygina *et al.*, 2011; Brown *et al.*, 2017).

The NOAAV2c reanalysis seems to be the best choice to characterize SND trends, being a good compromise between the other two reanalyses and it displays a fair agreement with snow station data (Figure 5.12 ; Wegmann *et al.*, 2017). In spring (5.11b), NOAAV2c shows statistically significant decreasing SND trends over central Canada, Scandinavia and west of the Lake Baikal with values ranging from −6 to −9 cm/dec. Positive trends are found over the south part of Eastern Eurasia in agreement with Bulygina *et al.* (2011), however the increase SND values over the Ob River observed by the latter are not reproduced in NOAAV2c. In autumn (5.11d), SND trends are weaker than in spring. Increasing significant trends are found over the north of the Canadian

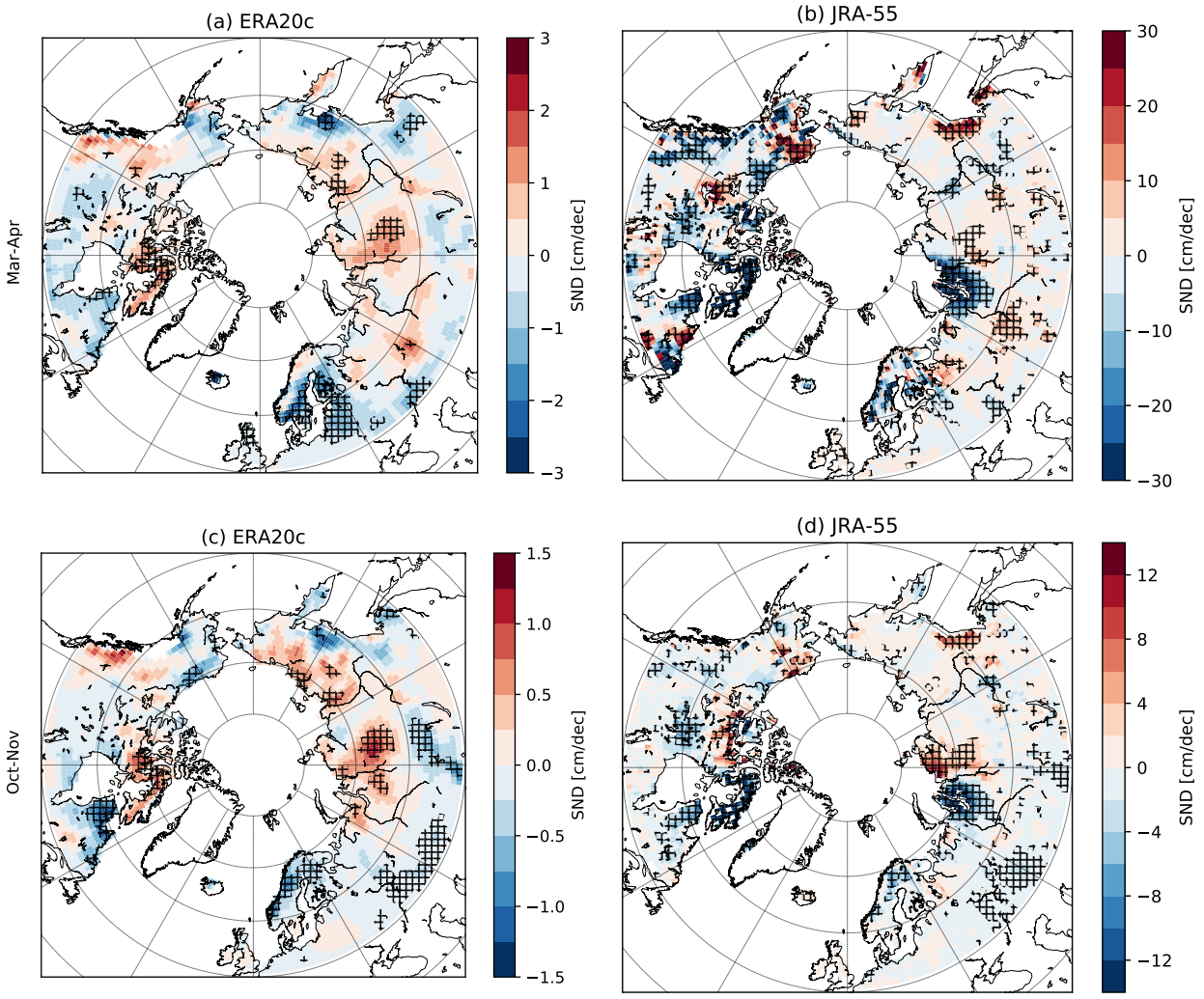

FIGURE 5.10 – Spatial SND trend in March-April (a,c) and October-November (b,d) from 1979-2005 from ERA20c (a,c) and JRA-55 (b,d) reanalyses. Statistical significant trends at the 90% confidence level from t-Student are hatched.

Archipelago and east of the Lake Baikal with values of +6 cm/dec. Over the north of the Laurentian Plateau, we found significant negative trends of – 4-5 cm/dec and weaker, but significant, over the south of Western Eurasia and north of the Lake Baikal. The negative(positive) SND trends found in east(west) of the Lake Baikal are also observed in the *in situ* snow data (Figure 5.12b).

Regarding CMIP5 SND trends, there is an almost indistinguishable match between the spatial pattern of SND trend and that of SWE trends in both seasons (Figure 5.9). In spring, 8 to 10 CMIP5 models report decreasing trends over Western Eurasia and North America. The agreement is reduced in the Eastern side of Eurasia with 4-6 models displaying positive trends (Figure 5.11a). This pattern corresponds relatively well with the SND trend distribution found in NOAAV2c except over the central part of Western Eurasia. During the onset season (Figure 5.11c), CMIP5 models show primarily negative trends over the whole Arctic. However, there are increasing SND trends in the south of the Lena River in 2-4 models. The best agreement is found over the Rocky Mountains with 8-12 models reporting negative trends. In general, the whole Arctic is characterized by little consensus among CMIP5 models with only 2-4 models displaying negative trends.

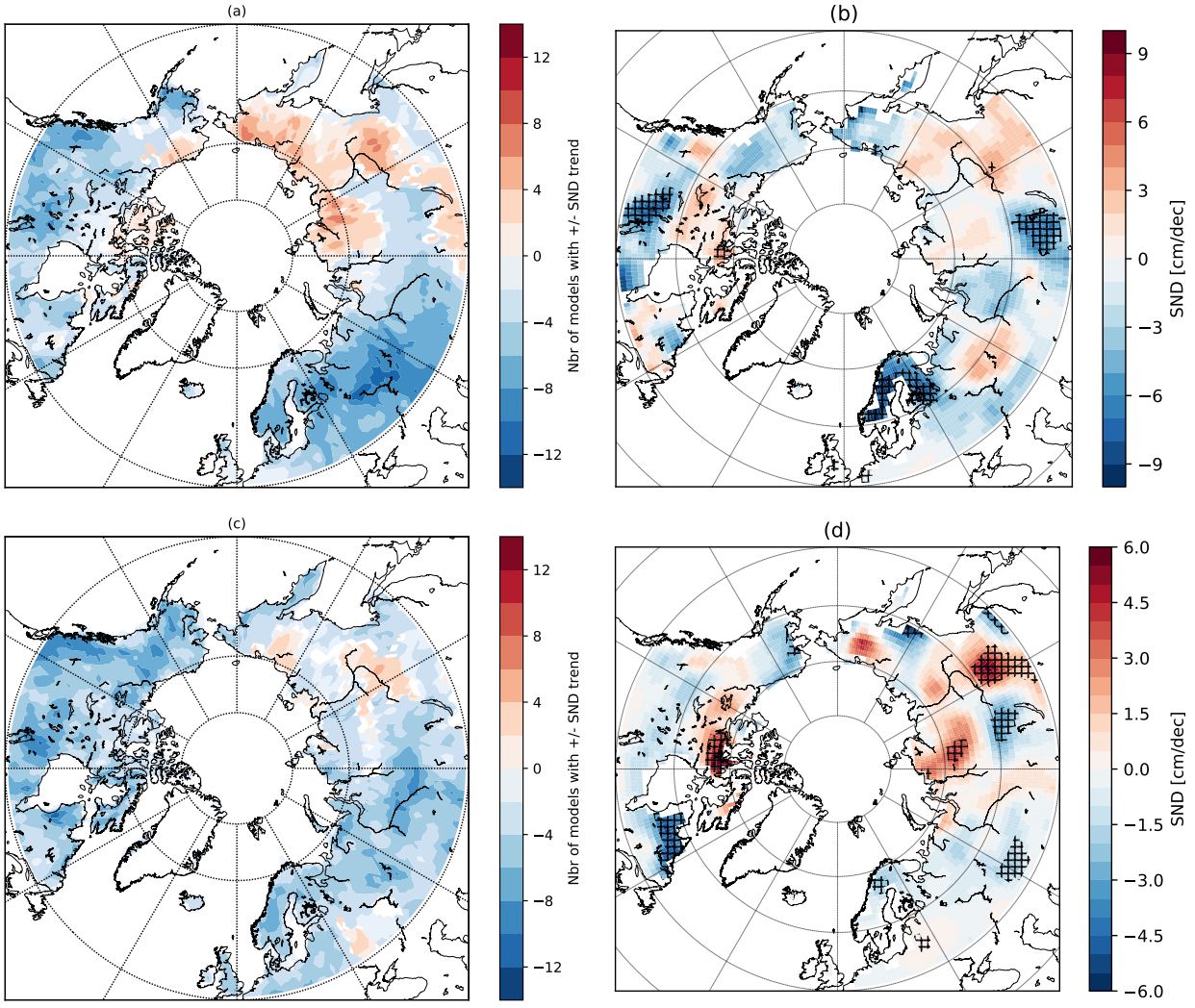

FIGURE 5.11 – (a,c) Number of CMIP5 models displaying a positive/negative SND trend in March-April (a) and in October-November (c) during 1979-2005. Only SND trends statistically significant at the 80% confidence level (t-Student test).(b,d) Spatial trend of SND trend (%/dec) from NOAAV2c reanalysis in March-April(b) and October-November(d) during 1979-2005. Hatched regions indicate SND trends statistically significant at the 90% confidence level (t-Student test).

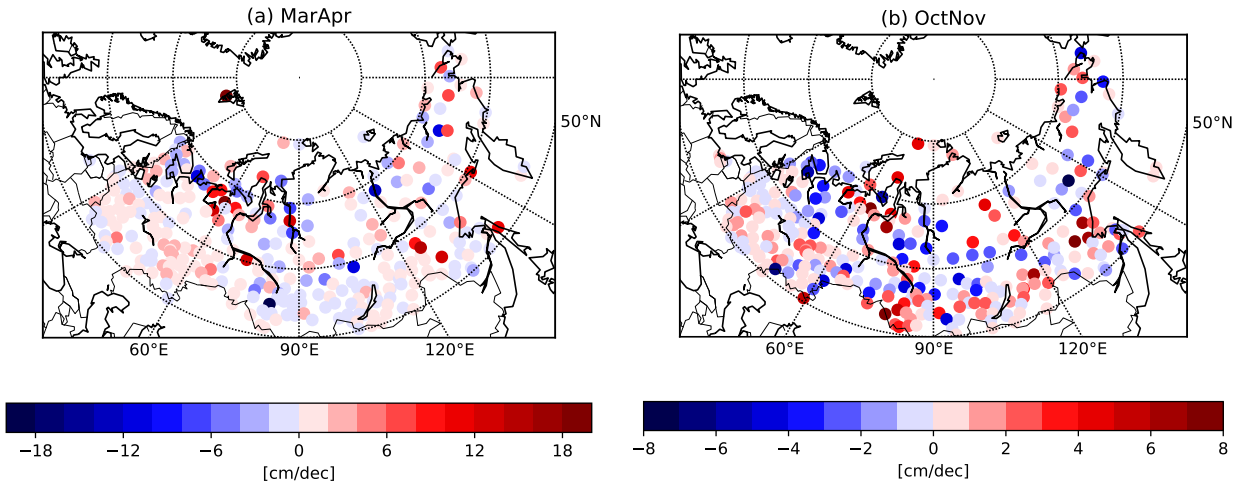

FIGURE 5.12 – Snow depth trends from snow stations in March-April (a) and October-November (b) from 1979-2005.

In situ measurements

We have computed the SND trends reported by 422 snow stations in spring and autumn over 1979-2005 following the criteria explained in Chapter 3. Figure 5.12 provides a realistic overview of SND temporal evolution that has been used as a reference to evaluate models and reanalyses. Note that we show all SND trends without considering their degree of statistical significance in order to include as many stations as possible to visualize the overall spatial SND trend pattern of Eurasia. During the melting season (Figure 5.12a), SND positive trends are located over the south of Western Eurasia and west of Lake Baikal of around 2-4 cm/dec . Decreasing trends are found south of the 90° meridian (< 2 cm/dec) and between the Ob and Yenisei Rivers (∼4 cm/dec). Over Eastern Eurasia, snow stations are quite scarce, however a prevalence of weak negative trends can be distinguished. In the onset season (Figure 5.12b), the SND trends are weaker than in spring. SND trends are negative in central Siberia and in the coast of Barents Sea (−6 cm/dec). Positive trends are found over the south of Siberia around the 90° meridian with values around +4-6 cm/dec. Over the south of western Eurasia, increasing trends are dominant (+2 cm/dec) ; however, when moving to 30° E parallel decreasing trend are found. Over the Far East, negative trends prevail over positive trends.

5.4 Summary

Characteristics of snow interannual variability and seasonal trends have been studied in spring and autumn across CMIP5 models and in different data sets – reanalyses, satellite-based products and *in situ* measurements. The period of study was from 1979 to 2005 for SCE and SND and from 1981 to 2005 for SWE.

(i) **Interannual variability :**

- Regarding SCE interannual variability, we have found that the reanalyses NCEP/CFSR and NOAAV2c are in good agreement with NOAA CDR in spring. However, most of CMIP5 ensemble underestimates the amplitude of interannual variability, being twice as small as in observations. During autumn, discrepancies are large between the reference data sets since NOAAV2c displays smaller standard deviation (STD) than NCEP/CFSR and NOAA CDR ; as well as CMIP5 models that still underestimate the amplitude of interannual variability. In addition, both reanalyses correlates negatively with NOAA CDR.
- SWE interannual variability is characterized by a large spread in both seasons. In terms of spring STD, three models (CCSM4, MIROC-ESM and MPI-ESM-P) agree with the CanSISE product. Four other models (MIROC5, inmcm4 and NorESM1-ME, MIROC-ESM-CHEM) show larger amplitude of interannual variability than CanSISE product. The rest of CMIP5 ensemble underestimate the reference STD, with the lowest value found in CSIRO-Mk3-6-0 model. In autumn, the spread in CMIP5 models is also distinct. The majority of models underestimate the amplitude of interannual variability. There are also four outliers among the models (NorESM1-ME and all versions of MIROCs), with considerably larger STDs than in observations.
- The interannual variability of SND is better captured by CMIP5 models compared to the other variables. In spring, JRA-55 and NOAAV2c agree in terms of STD and correlation whereas ERA20c displays lower STD but a significant correlation with JRA-55. There are two models (MIROC-ESM-CHEM and MIROC5) that accurately reproduce the amplitude of interannual variability. The rest of CMIP5 ensemble underestimates the observed STD by a factor of two. Similar results are found for autumn, in particular,

a good agreement between JRA-55 and NOAAV2C reanalyses, but an underestimation of STD is found in ERA20c. CMIP5 ensemble displays lower STD values than JRA-55, the models MIROC5, MIROC-ESM-CHEM and NorESM1-ME being the closest to the reference data set.

(**ii**) **Seasonal trend analysis :**

- Pan-Arctic SCE trends in spring across reference data sets present some discrepancies since the NCEP/CFSR reanalysis shows almost neutral and even increasing (in North America) values whereas NOAA CDR and NOAAV2c are in relatively good agreement, mainly for Eurasia. More than half of the ensemble models agree with NOAA CDR and NOAAV2, displaying a general decrease of spring SCE. In autumn, NOAA CDR displays an unrealistic positive trend being higher in Eurasia than in North America. NCEP/CFSR and NOAAV2c display decreasing SCE trends and are in better agreement in North America, but both trends lack statistical significance. Overall almost all CMIP5 models are able to reproduce the pan-Arctic trends in autumn.
- Observed SWE trends over the Arctic lack statistical significance in both seasons. In spring, CMIP5 models report a large spread in SWE trends, namely in the North American sector. Over the Pan-Arctic, less than 30% of models display significant trends inside the range implied by CanSISE product. During the onset season, CMIP5 models show stronger than observed decreasing trends. As in spring, the spread is larger in North America. There are around three ensemble models approximating the SWE trend of CanSISE product in any Arctic subdomain and very few individual realizations ; but almost no trend is significant.
- The SND trends over the Arctic reported by the three reanalyses differ substantially. ERA20c displays very weak trends in both seasons. During spring, the SND trend observed in JRA-55 is unrealistically strong in North America, one order of magnitude larger than the *in situ* measurements (Brown *et al.*, 2017). Compared to NOAAV2c reanalysis, CMIP5 models generally underestimate the magnitude of the SND trend all over the Arctic. In autumn, JRA-55 and NOAAV2c are in better agreement than in spring. Nearly all models from the CMIP5 ensemble show weaker SND trends as evidenced by the multimodel mean being out of the observed range over the Pan-Arctic subdomains.

As for SWE trends, the spread in North American sector is quite large compared to Eurasia.

(**iii**) **Spatial trend pattern :**

- NOAAV2c SCE trends are very weak and only locally significant compared to NCEP/CFSR. The latter is in a good agreement with CMIP5 models, displaying decreasing trends over Western Eurasia (8-12 models) and over North America (4-8 models) and increasing trend over the north part of Eastern Eurasia (4-8 models). However, CMIP5 ensemble does not capture the observed positive trend over the Rocky Mountains. In autumn, models demonstrate practically everywhere more frequent negative than positive trends, which is in agreement with SCE trend pattern from NCEP/CFSR. However, mismatches occur in the Far East of Eurasia and along the West Coast of North America.
- SWE trends computed from CanSISE show very few locations with statistically significant trends in spring and autumn. The CMIP5 trends for spring form a pattern of primarily negative trends over North America and Western Eurasia, and primarily positive trends over Eastern Eurasia. During the onset season, in around 8 of the CMIP5 models, negative trends dominate, except over the Lena Delta.
- Assessment of SND in reanalyses shows that, in spring, ERA20c reports very weak trends whereas JRA-55 displays strong trends one order of magnitude larger ; in both cases, statistically significant trends are very local. NOAAV2c show significant SND decrease over central Canada, Scandinavia and east of Lake Baikal. The best agreement between CMIP5 models (8-12 models) is found in North America and, to a lesser degree in Western Eurasia. Over Eastern Eurasia, CMIP5 models (4-6 models) report positive SND trends ; so does the reference but without statistical significance. In autumn, NOAAV2c reports significant positive trends north of the Canadian Archipelago, east of the Yenisei River and south of the Lena River. Very few locations show decreasing significant trends such as north of the Laurentian Plateau, east of the Lake Baikal and south of the Ural Mountains. CMIP5 ensemble (8-12 models) displays primarily decreasing trends throughout the terrestrial Arctic, the best fit to the observations is found in the West Coast of North America. 2-4 models report positive trends over the south of the Lena catchment in agreement with NOAAV2c.

Chapter 6

Conclusions and perspectives

We have investigated snow characteristics in the Arctic during spring and autumn in the historical runs of CMIP5 climate models and in different observational data sets – various reanalyzes, a satellite-observed product, an observation-based ensemble product and *in situ* measurements. For the SCE and SND variables the period of study was 1979-2005 and for SWE the period was 1981-2005. The main characteristics of each individual model from the CMIP5 ensemble are indicated in tables (6.1,6.2,6.3,6.4) as well as of each reference data set (Table 6.5).

We identified three groups of CMIP5 models according to their representation of SCE : models broadly overestimating observational SCE (up to 60 p.p. regionally), models underestimating observed climatological SCE (the strongest differences between 40-50 p.p.) and those showing overestimation over the northern regions and underestimation in the southern regions of the Arctic. Differences are especially marked in the melting season but also pronounced during autumn. For SWE, we identified a pan-Arctic overestimation in most CMIP5 models except for CSIRO-Mk3-6-0 and MPI-ESM-LR/P, who show either general underestimation or an east-west (underestimation-overestimation) pattern over Eurasia. Again, these patterns are most pronounced during the melting season, when positive biases may be of the same order as the mean values. Three groups of CMIP5 models can be identified with respect to SND : models displaying a large overestimation (up to 80 cm locally), models underestimating SND throughout the Arctic and finally, those exhibiting a general positive bias in Eurasia and a positive-negative bias pattern in the eastern-western part of North America. In autumn, differences are smaller than in spring and the pattern slightly changes. We can distinguish three different groups : models showing a general negative bias, models with a strong positive bias centered in Eastern Eurasia and models generally overestimating the observed SND climatology. For the particular case of Eurasia, the comparison of CMIP5 models and SND reanalyses with snow stations reveals a clear overestimation in spring and an underestimation in autumn with respect to the *in situ* measurements.

The position of the snow margin is better captured by CMIP5 models in the spring season with the best agreement found in Eastern Eurasia and Western North America. During autumn, the CMIP5 ensemble identifies a considerable northward shift of the snow margin and the overall agreement only occurs in Central Siberia, whereas, there are only 4-6 out of 16 models matching the location of the observed snow margin.

The observed annual cycle of SCE is relatively well captured by CMIP5 models in autumn, but during the spring-summer season, most models tend to significantly underestimate SCE, especially over North America. At the same time, the annual cycle of SWE is largely positively biased with respect to observations in most CMIP5 models, indicating persistent snow in summer months, thus contradicting observations. The annual cycle of SND reported by CMIP5 models presents similar discrepancies with respect to observations as SWE annual cycle. The dispersion is remarkably high during the snow accumulation season notably in North America and Eastern Eurasia.

We found that spring SCE averaged over the whole terrestrial Arctic is generally underestimated by CMIP5 models, to the point where some models are 50% lower than observations. In autumn, there is better agreement with a slight tendency for overestimation. For SWE, there is a large inconsistency between CMIP5 models and an overestimation with respect to the observed reference, with only two out of sixteen models in accordance with the observations. The dispersion is smaller in autumn, however, the positive bias still exists. CMIP5 models show a general good agreement in SND in both seasons. However, the discrepancies between the different reanalyses are substantial.

We found that the interannual variability of all snow characteristics is significantly underestimated in most CMIP5 models compared to observations. The SWE variable shows the largest discrepancies among CMIP5 models regarding the amplitude of interannual variability. With respect to Pan-Arctic interdecadal variability, most CMIP5 models show weakly negative (partially significant) trends in SCE, mainly in spring. The spread in SWE trends in CMIP5 models is quite large, notably in North America in both seasons. Generally, CMIP5 models show slightly stronger than observed trends in spring and autumn that are statistically significant, which is not the case for the observational data set. With respect to SND, CMIP5 models report weaker trends than the observational reference and they are particularly inconsistent over North America.

Regionally, the CMIP5 ensemble captures relatively well the observational trend pattern in all snow characteristics in spring over Eurasia, but SWE and SND show no consistency with the regional trend patterns in autumn in both continents. However, the discrepancies found between

the spatial pattern of observed trends in SCE and SND hampers to designate a reference data set for such a model evaluation.

In agreement with previous studies (Brutel-Vuilmet *et al.*, 2013; Mudryk *et al.*, 2014), we found that the SCE annual cycle is relatively well captured by CMIP5 models compared to the three different reference data sets used. Nevertheless, the significant overestimation and the large spread of SWE on the Northern Hemisphere reported by Roesch (2006) in the previous generation of models has not been reduced in CMIP5 models. Regional differences in snow cover duration in autumn (Peng *et al.*, 2013; Brown *et al.*, 2017; Liston and Hiemstra, 2011) are the likely cause of the spatial differences in the position of the snow margin in the onset season in both reanalyses and models.

In spring, we have found that SCE discrepancies in CMIP5 models are located over the southern part of the Arctic, where temperature changes are substantial and may favor snow to recede. This is consistent with the inability of CMIP5 models to capture the temperature sensitivity of snow cover (Fletcher *et al.*, 2012; Brutel-Vuilmet *et al.*, 2013; Thackeray *et al.*, 2016). Conversely, during the onset season, we have found a more spatially uniform pattern of SCE differences. In fact, snow onset is highly coupled with variability in regional precipitation and surface temperature, as both are need to initiate snow cover (Mudryk *et al.*, 2017; Ye, 2019). The accumulation and persistence of snow are linked to atmospheric modes of variability such as North Atlantic Oscillation (NAO) and Arctic Oscillation (AO) (Bamzai, 2003; Cohen *et al.*, 2012; Liu *et al.*, 2012). This suggests that discrepancies found on the onset, as well as during the snow accumulation (December to February), are more related to atmospheric circulation rather than temperature.

With regard to snow tendencies, we have found that in both spring and autumn, CMIP5 snow characteristics display negative but weaker-than-observed trends, consistent to previous studies at North Hemispheric scale (Brutel-Vuilmet *et al.*, 2013; Mudryk *et al.*, 2014; Connolly *et al.*, 2019). In addition, an interesting feature was that both CMIP5 and reference data sets report stronger trends in snow accumulation (SWE and SND) over North America than over Eurasia. This is consistent with the findings of Biancamaria *et al.* (2011) based on satellite data and Park *et al.* (2012) using both *in situ* data and an hydrological and biogeochemical model. In fact, Biancamaria *et al.* (2011) related this pattern of variations to a difference in regional climate conditions between both Arctic subdomains. Indeed, snow depth in Eurasia is linked to the Arctic Oscillation and Atlantic Multi-decadal Oscillation (AMO) whereas in North America, snow depth accumulation is influenced by

the Pacific North American (PNA) pattern and AMO. However, there exist some deficiencies in the reproductibility of these atmospheric modes in the CMIP5 ensemble (Ning and Bradley, 2016; Davini and Cagnazzo, 2014), which may make the reproduction of the snow-atmosphere coupling more difficult (e.g., Furtado *et al.*, 2015; Gastineau *et al.*, 2017). We suggest that the mismatches found in snow accumulation, mainly in trends and the overall overestimation of SWE and SND throughout the snow season, can be linked to an inadequate representation of atmospheric internal variability and snow-atmosphere coupling. This is consistent with the low interannual variability found in CMIP5 models (Figures 5.1,5.2 and 5.3) and the internal limitations of CMIP5 models (Taylor *et al.*, 2012). Our study highlights the need for a deeper understanding of atmospheric variability and snow in the CMIP5 ensemble and their relation to the dominant atmospheric circulation patterns of Northern Hemisphere (e.g. AO, NAO and PNA). Their role can be investigated with the help of EOF (Empirical Orthogonal Function) analysis following Popova (2007).

We confirm that the October trend of NOAA CDR is an outlier compared to the other data sources, as previously reported (Brown and Derksen, 2013; Estilow *et al.*, 2015). The discrepancies found in SND and SCE trends among the reference data sets encourages us to strongly recommend a multi-data set approach to evaluate snow characteristics in models. Using one single reference can induce to an incorrect model evaluation as it is sensitive to the choice of the reference data set (e.g., Gómez-Navarro *et al.*, 2012). This is the case of Connolly *et al.* (2019) who identified an artificial bias in autumn SCE trends in CMIP5 models using only the NOAA CDR data set as reference, while in fact, it is the observation which is not realistic. When considering multiple data sets (Mudryk *et al.*, 2015) or an ensemble product (CanSISE, Mudryk and Derksen, 2017), we can hope to overcome the limitations of individual data sets and get access to the real climate state.

Overall, the lack of agreement found among the ensemble of models in the spatial distribution of Arctic snow, as well as, in the reproductibility of snow trends questions the robustness of future projections (Hinzman *et al.*, 2013). Climate projections cannot follow the pace of polar amplification and the associated snow-albedo feedback (Derksen and Brown, 2012; Déry and Brown, 2007; Hernández-Henríquez *et al.*, 2015; Qu and Hall, 2013). In the context of a warmer and wetter Arctic (Screen and Simmonds, 2013; Bintanja and Selten, 2014), the future impact of snow on the surface albedo (Thackeray *et al.*, 2018), circulations patterns (Rydzik and Desai, 2014), permafrost (Biskaborn *et al.*, 2019) and water supply (Mankin *et al.*, 2015) among many other consequences (Callaghan *et al.*, 2011a), should be consider as high priority. More targeted

simulations of ESM-SnowMIP (Krinner *et al.*, 2018) and the new generation of models (Eyring *et al.*, 2016) will broaden our knowledge of snow-climate interactions and increase our confidence in future projections and mitigation scenarios in the context of polar amplification. We hope that our assessment of snow representation in CMIP5 models serve as a standard to evaluate the next generation of CMIP6 ensemble and also, to provide valuable information for climate community when using these snow-related variables from CMIP5 historical output.

Data set		**bcc-csm1-1**	**CanESM2**	**CCSM4**	**CNRM-CM5**
SCE	*Clim.*	Negative bias	• Overestimation MA • Best fit (ON)	Dipole Pattern *	• Positive bias over the Northern ARC • Overestimation South • Best fit in ON
	Trends	Low interannual variability (EURA)	Lack stat. significance in EURA (ON)	Large intermember spread (EURA)	Large intermember spread (EURA)
SWE	*Clim.*	• General positive bias • Negative bias over Yenisei River	• General positive bias • Negative bias over Yenisei River	Dipole Pattern *	• General positive bias • Negative bias over Yenisei River
	Trends	Lack stat. significance (except in NAm-ON)	Large intermember spread (NAm)	• Interannual variability as ref. (MA) • Large intermember spread	Large intermember spread
SND	*Clim.*	Dipole Pattern*	General negative bias (ON)	Dipole Pattern*	General negative bias (ON)
	Trends	Lack stat. significance (MA)	Large intermember spread (NAm-MA)	Large intermember spread (NAm-MA)	Large intermember spread (NAm-MA)

TABLE 6.1 – Main characteristics of the spatial structure and temporal variability of snow representation in individual CMIP5 models. * *Dipole Pattern* : Overestimation over Western North America and Eastern Eurasia and underestimation over Eastern North America and Western Eurasia. "MA" and "ON" refer to March-April and October-November. The abbreviations for the Arctic and its subdomains are indicated in Table 1.1.

Data set		**CSIRO-Mk3-6-0**	**GISS-E2-H**	**GISS-E2-R**	**inmcm4**
SCE	*Clim.*	Negative bias	Opposite Dipole Pattern*	Opposite Dipole Pattern*	• Negative bias (MA) • Positive bias (ON)
	Trends	• Large intermember spread (NAm-MA) • Lack stat. significance (EURA-ON)	Large intermember spread (NAm-MA)	Lack stat. significance across members (EURA-MA)	• Interannual variability as ref. • Positive trends (≠)
SWE	*Clim.*	Negative bias	• General positive bias • Negative bias over Yenisei River	• General positive bias • Negative bias over Yenisei River	• General positive bias • Negative bias over Yenisei River
	Trends	Lack stat. significance (EURA-ON)	Lack stat. significance (ON)	Lack stat. significance in members	• High interannual variability • Positive (not stat. sig.) (≠)
SND	*Clim.*	Negative bias	General positive bias	General positive bias	Negative bias (MA)
	Trends	• Large intermember spread (NAm-MA) • Lack stat. significance (EUR-ON)	Large intermember spread (NAm-MA)	Lack stat. significance (EURA-MA)	• Negative Correlation • Positive trends (≠) (not stat. sig.)

TABLE 6.2 – Main characteristics of the spatial structure and temporal variability of snow representation in individual CMIP5 models (continuation).* *Dipole Pattern* : Overestimation over Western North America and Eastern Eurasia and underestimation over Eastern North America and Western Eurasia. "MA" and "ON" refer to March-April and October-November. The abbreviations for the Arctic and its subdomains are indicated in Table 1.1. The symbol (≠) means that this model presents an opposite behavior to CMIP5 ensemble (and to the observations).

Data set		MIROC-ESM-CHEM	MIROC-ESM	MIROC5	MPI-ESM-LR
SCE	*Clim.*	• Zonal positive bias Southern Eurasia(MA) • Negative bias (ON)	Zonal positive bias Southern Eurasia (MA) • Negative bias (ON)	• Zonal positive bias Southern Eurasia (MA) • Negative bias (ON)	Negative bias
	Trends	• High interannual variability • Strong trend in NAm ; insig. in EURA	Moderate intermember spread	Very large intermember spread (NAm)	Lack stat. significance
SWE	*Clim.*	• General positive bias • Negative bias over Yenisei River	• General positive bias • Negative bias over Yenisei River	• General positive bias • Negative bias over Yenisei River	Negative bias EURAWest
	Trends	• Very high interannual variability • Strong trend in NAm ; insig. in EURA	Interannual variability as ref.	• High interannual variability • Very large intermember spread (NAm)	Lack stat. significance
SND	*Clim.*	• General positive bias • Negative bias over Yenisei River	• General positive bias • Negative bias over Yenisei River	• General positive bias • Negative bias over Yenisei River	X X X
	Trends	• Interannual variability close to ref. (MA) • Strong trend in NAm ; insig. in EURA		• Interannual variability close to ref. (ON) • Very large intermember spread (NAm)	X X X

TABLE 6.3 – Main characteristics of the spatial structure and temporal variability of snow representation in individual CMIP5 models (continuation).* *Dipole Pattern* : Overestimation over Western North America and Eastern Eurasia and underestimation over Eastern North America and Western Eurasia. "MA" and "ON" refer to March-April and October-November. The abbreviations for the Arctic and its subdomains are indicated in Table 1.1

Data set		**MPI-ESM-P**	**MRI-CGCM3**	**NorESM1-M**	**NorESM1-ME**
SCE	*Clim.*	Negative bias	Positive bias	• Best fit (MA) • Towards a positive bias (ON) • Unable to melt snow in summer	• Best fit (MA) • Towards a positive bias (ON) • Unable to melt snow in summer
	Trends	Lack stat. significance	Lack stat. significance	• Large intermember spread(EURA-MA)	• Large intermember spread(EURA-MA) • Lack stat. significance (MA)
SWE	*Clim.*	Negative bias	Positive bias	Dipole Pattern*	Dipole Pattern*
	Trends	• Interannual variability close to ref. (MA) • Lack stat. significance (ON)	Lack stat. significance	• Very high interannual variability • Large intermember spread (NAm)	• High interannual variability (as ref. in ON) • Large intermember spread (NAm)
SND	*Clim.*	X X X	Best fit (ON)	Dipole Pattern*	Dipole Pattern*
	Trends	X X X	Lack stat. significance	Moderate intermember spread (EURA)	• Large intermember spread (NAm) • Lack stat. significance (EURA-Ma)

TABLE 6.4 – Main characteristics of the spatial structure and temporal variability of snow representation in individual CMIP5 models (continuation).* *Dipole Pattern* : Overestimation over Western North America and Eastern Eurasia and underestimation over Eastern North America and Western Eurasia. "MA" and "ON" refer to March-April and October-November. The abbreviations for the Arctic and its subdomains are indicated in Table 1.1.

Data set		NOAA CDR	NCEP/CFSR	NOAAV2c	JRA-55	ERA20c
SCE	*Clim.*		Slight underestimation (compared to ref.)	Slight underestimation (compared to ref.)		
	Trend	Unrealistic positive trend ON (≠)	• Interannual variability close to ref. • Positive trend in NAm MA(≠)	• Interannual variability close to ref. (MA) • Low in ON • Lack of stat. sig.		
SND	*Clim.*			• High accumulation in EURAEast • Consistent with *in situ* in EURAWest (MA)	Consistent with in situ in EURAEast	• Low values • Inability to reproduce annual cycle
	Trend			• Interannual variability as ref.	• Unrealistic trend in NAm MA • Very strong regional trends	• Low interannual variability • Poor ability to reproduce trends

TABLE 6.5 – Main characteristics of the spatial structure and temporal variability of snow variables in different data sets. *Note* : (≠) refers to an unrealistic value or an opposite behavior against the other data sets. NOAA CDR and JRA-55 are considered as reference (*ref.*) unless otherwise stated.

Annexe A

GREENICE Experiments

At the beginning of my 2nd PhD year, I conducted a scientific stay at Bjerknes Centre for Climate Research (Bergen, Norway) with a student grant from of GREENICE Project to work with Dr. Noel Keenslyside, Dr. Fumiaki Ogawa and Dr. Ho Nam Cheung. GREENICE is a multidisciplinary project that focus on the "Impacts of Sea-Ice and Snow-Cover Changes on Climate, Green Growth and Society" (https://greenice.w.uib.no/about/). The aim of this visit was to learn more about the features of snow representation in climate models using an example of two atmospheric circulation models : Community Atmosphere Model (CAM4) and the Whole Atmosphere Community Climate Model (WACCM).

A.1 Introduction

Arctic sea ice extent has declined significantly under recent global warming (e.g., Comiso *et al.*, 2008; Cavalieri and Parkinson, 2012; Serreze and Barry, 2011) with a direct impact on the climate system (Vihma, 2014; Gao *et al.*, 2015; Koenigk *et al.*, 2019). Particular attention has been paid to the influence of sea ice reduction in the Barents-Kara Seas region onto the wintertime cooling trend over the Eurasian continent, the so-called "Warm Arctic, Cold Continents" teleconnection pattern (e.g., Cohen *et al.*, 2013; Inoue *et al.*, 2012; Mori *et al.*, 2014; Wegmann *et al.*, 2018). Concomitantly, observational and modeling studies have associated sea ice reduction over the Eastern Arctic with increase in snowfall over Siberia (Deser *et al.*, 2010; Orsolini *et al.*, 2011; Cohen *et al.*, 2012, 2013; Ghatak *et al.*, 2012; Liu *et al.*, 2012; Li and Wang, 2012; Wegmann *et al.*, 2015). However, the processes underlying both teleconnections are still unclear (e.g., Wegmann *et al.*, 2018). Ogawa *et al.* (2018) shed light onto this debate by performing coordinated experiments with six atmospheric circulation forced by observed sea ice and sea surface temperature. Their main conclusion was that the impact of recent sea ice reduction is confined to the lower troposphere at high latitudes in winter, and it does not significantly lead to Siberian cooling. Instead, they argue that atmospheric internal

dynamics could have played a major role in the observed wintertime Siberian temperature trends. In this annex we show some exploratory results for snow cover from the two models' experiments described in Ogawa *et al.* (2018).

A.2 Data

We have analyzed simulations of the recent 33 years (1982-2014) from two atmospheric circulations models forced by prescribed sea surface temperature (SST) and sea ice concentration (SIC) from National Oceanic and Atmospheric Administration (NOAA) Optimum Interpolation 1/ Degree Daily Surface Temperature Analysis version 2, AVHRR-only product (Reynolds *et al.*, 2007, http://www.ncdc.noaa.gov/sst/index.php). The first atmospheric model employed is the Community Atmosphere Model (CAM4, Neale *et al.*, 2013) with a horizontal resolution of $0.9° \times 1.25°$ and 26 vertical levels from surface to 3 hPa. We refer to it as "low top" model and it is the atmospheric component of the general circulation model of CCSM4 (Gent *et al.*, 2011, Table 2.1). The second model is the Whole Atmosphere Community Climate Model (WACCM, Marsh *et al.*, 2013) and it displays the same horizontal resolution as CAM4, but a higher vertical resolution of 66 levels up to 0.000006 hPa, thus it is considered as "high top" model. Two different experiments were carried out to distinguish the impact of sea ice (SIC) and sea surface temperatures (SST). The experiments were repeated using different initial conditions to provide 20 member realizations for each of model. Daily varying SIC is prescribed in both experiments. In the first experiment ("SST-SIC-EXP") daily varying SST conditions are prescribed, whereas daily climatological SST computed from the NOAA data is prescribed in the second experiment ("SIC-EXP"). See Ogawa *et al.* (2018) for further details of simulations and experiments. We analyzed the snow cover output (SCE) from these simulations. We restrict the domain to an ice-free land Arctic north of 50°N. The mask from the coupled model CCSM4 (Gent *et al.*, 2011, Table 2.1) has been applied considering only grid cells with more or equal to 50% of land fraction and less than 15% of permanent ice (Figure 3.3).

A.3 Results

A.3.1 Spatial distribution of snow cover

Differences in climatology between the four simulations are computed for winter (December-January-February), spring (March-April) and autumn (October-November) seasons for the period

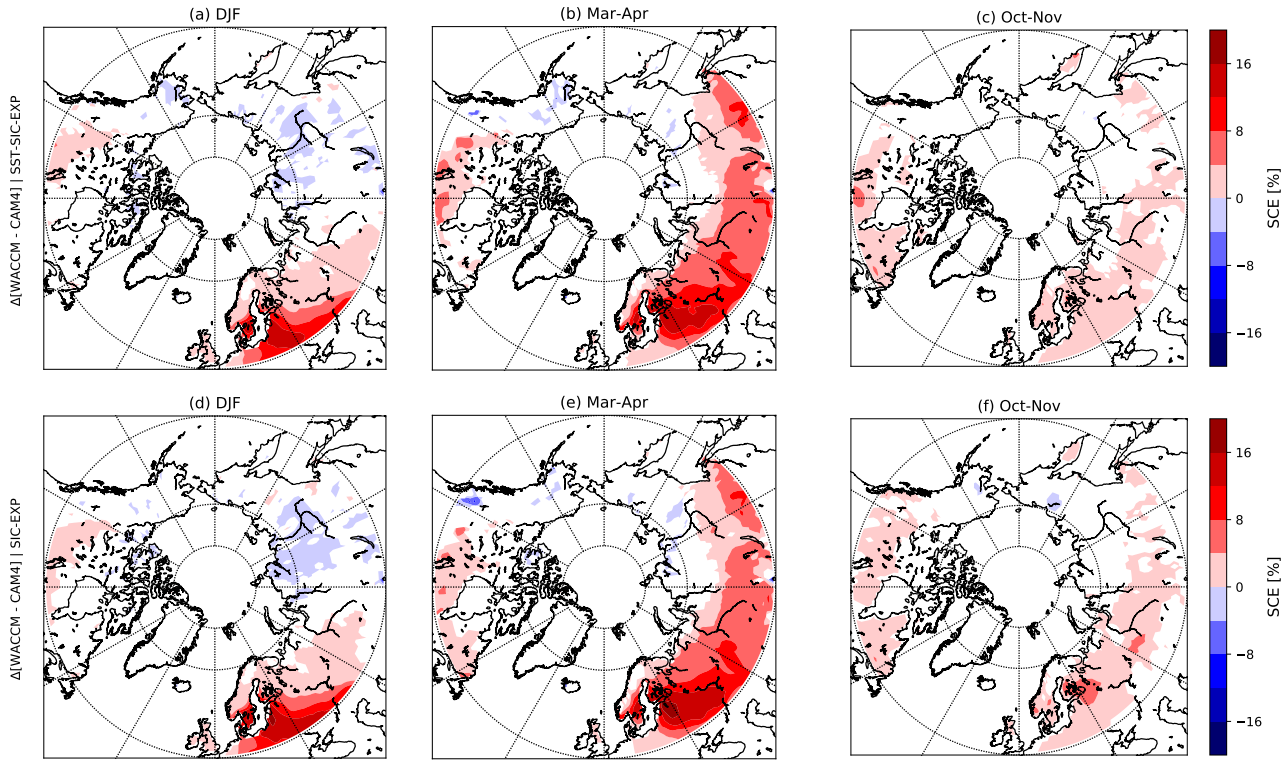

FIGURE A.1 – Difference of snow cover climatology (1982-2014) of December-January-February (a,d), March-April (b,e) and October-November (c,f) of WACCM minus CAM4 atmospheric model simulations of SST-SIC-EXP (a,b,c) and SIC-EXP (d,e,f) experiments. Only differences with p-values less than 0.10 from the t-Student test are shown.

from 1982 to 2014. We have found that climatological differences between experiments SST-SIC-EXP and SIC-EXP for the same model (CAM4 or WACCM) are not statistically significant (at 90% confidence level) for any of the seasons considered (not shown). Conversely, Figure A.1 shows that differences between "high-top" and "low-top" models are significant, notably for spring. In winter (Figure A.1a,d), WACCM slightly overestimates SCE in comparison with CAM4 over central Canada (differences are less than 4 p.p.). Over Eastern Eurasia differences are larger with maximum differences of 8-12 p.p. over south of the Baltic Sea. Negative differences are located in the surroundings of the Lena River, notably in SIC-EXP, meaning that CAM4 displays up to 4 p.p. excess of SCE compared to WACCM. In March-April (Figure A.1b,e), positive differences between WACCM and CAM4 up to 12-14 p.p. are found over Western Eurasia for both experiments. Over central Canada and the Laurentian Plateau differences are significantly smaller (about 4 p.p.) but still positive. For autumn (Figure A.1c,f), both models show the best agreement, with slightly positive differences up to 4 p.p. over the southern part of Canada and east-central Eurasia.

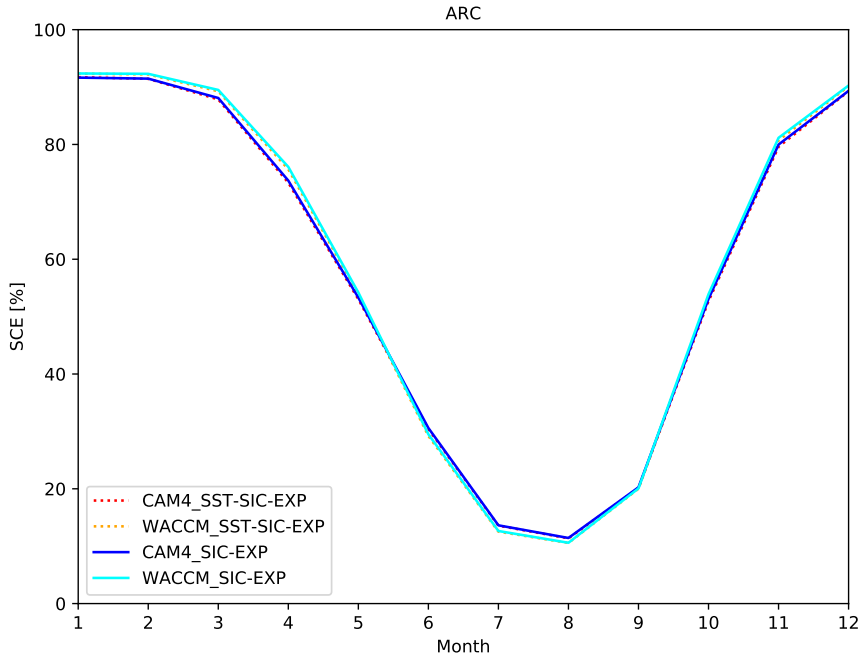

FIGURE A.2 – Annual cycle of Arctic snow cover (1982-2014) of simulations from SST-SIC-EXP and SIC-EXP from CAM4 ("low-top") and WACCM ("high-top") atmospheric models.

Annual cycle of Arctic SCE is very well reproduced by the four simulations and different lines are almost indistinguishable from each other (Figure A.2). Interestingly, in all cases the atmospheric models CAM4 and WACCM do not melt snow cover during summer displaying values of 10-15% in July and August ; while the coupled model CCSM4 reproduces SCE annual cycle consistently with observations (Figure 4.17). We suggest that the inability to fully melt snow in summer in CAM4 and WACCM is due to the lack of coupling with a land surface model which controls the heat balance at the surface necessary for melting (Equation 2.1).

Figure A.3 shows the quantile statistics of spatial SCE averaged over the land Arctic during the period 1982-2014 for winter (December-January-February), spring (March-April) and autumn (October-November) seasons. It is difficult to make a clear separation across the simulations as discrepancies in SCE average are almost negligible being less than 2 p.p. for all considered seasons. As expected, we found that the amplitude of interannual variability is slightly larger in simulations from SST-SIC-EXP, where both SST and SIC are prescribed with daily variations, than in simulation from SIC-EXP, where SST are set to daily climatology (IQRs in Figure A.3).

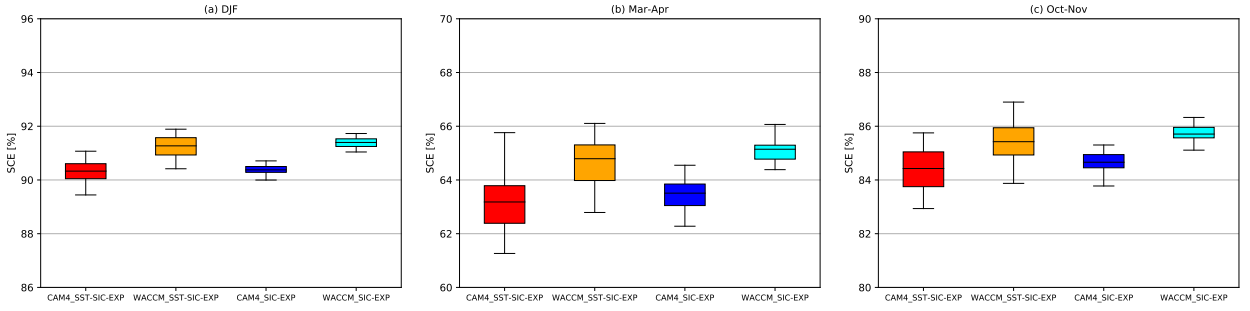

FIGURE A.3 – Quantile statistics of the spatial average for snow cover of simulations from SST-SIC-EXP and SIC-EXP from CAM4 "low-top" and WACCM "high-top" atmospheric models for winter DJF (a), March-April (b) and October-November (c) over the land Arctic during 1982-2014. Horizontal line represents the spatial average, filled rectangle is the interquartil range (IQR) from Q1 (25th percentile) to Q3 (75th percentile). The IQR provides information about the amplitude of snow interannual variability.

A.3.2 Seasonal trends of snow cover

Figure A.4 shows the time series of Arctic SCE average from the four simulations for three seasons during 1982-2014. As seen in figure A.1 and A.3, simulations using WACCM atmospheric model have systematically larger SCE throughout the period. During winter, SCE time series shows the lowest amplitude of interannual variability, whereas in spring larger variations are observed.

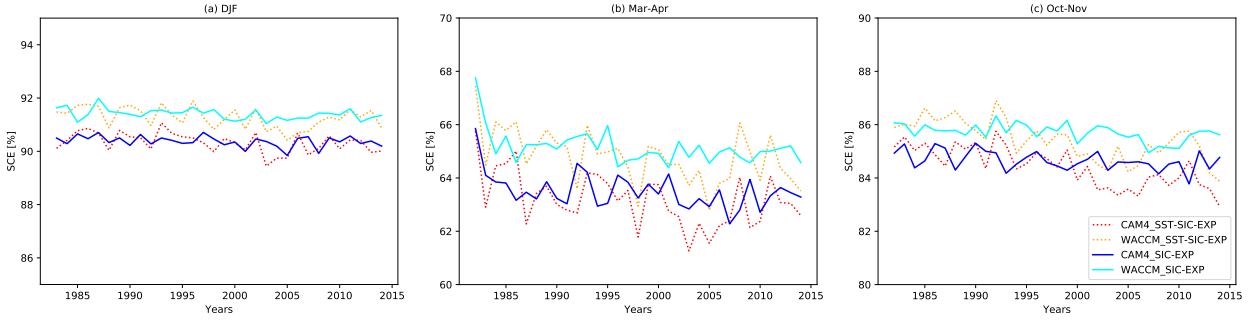

FIGURE A.4 – Time series of Arctic snow cover (1982-2014) of simulations from EXP1 and EXP2 from CAM4 ("low-top") and WACCM ("high-top") atmospheric models in December-January-February (a), March-April (b) and October-November (c).

We calculated also linear trends of averaged Arctic SCE for four simulations (Figure A.5). During winter (Figure A.5a, Table A.1), SCE trends are weaker compared to the other seasons. Stronger trends are displayed by simulations from SST-SIC-EXP experiment showing $-0.17 \pm 0.07\%$/dec and $-0.18 \pm 0.07\%$/dec using CAM4 and WACCM, respectively. Weaker,but still significant, trends are found in SIC-EXP being of $-0.07 \pm 0.04\%$/dec in CAM4 and $-0.09 \pm 0.04\%$/dec in WACCM. In spring (Figure A.5b,Table A.2), SCE trends from CAM4 and WACCM are $-0.30 \pm 0.11\%$/dec and

$-0.31 \pm 0.10\%$/dec in experiment SIC-EXP. While stronger significant SCE trends are found in SST-SIC-EXP of $-0.51 \pm 0.16\%$/dec and $-0.55 \pm 0.16\%$/dec in CAM4 and WACCM, respectively.

The differences in autumn SCE trends between both experiments are larger than in spring (Figure A.5c). In SST-SIC-EXP, both models shows stronger trends of $-0.60 \pm 0.08\%$/dec and $-0.55 \pm 0.10\%$/dec close to the SCE trends displayed by CCSM4 ($-0.89 \pm 0.12\%$/dec) but for 1979-2005. By contrast, SIC-EXP displays weaker trends of $-0.16 \pm 0.06\%$/dec in CAM4 and $-0.16 \pm 0.05\%$/dec in WACCM. From the larger discrepancies of SCE trends in autumn compared to the other seasons we can conclude that the onset of snow cover is more affected by summer sea ice reduction than the snow accumulation (winter) or melting snow seasons (spring).

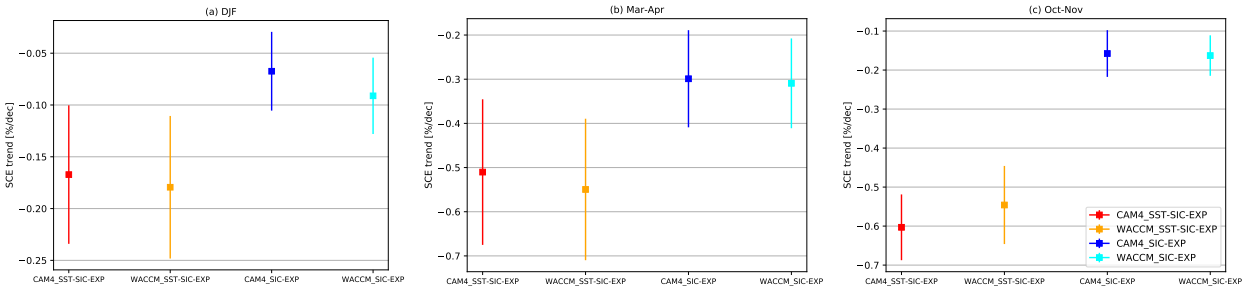

FIGURE A.5 – Snow cover trends of Arctic snow cover (1982-2014) of simulations from SST-SIC-EXP and SIC-EXP from CAM4 ("low-top") and WACCM ("high-top") atmospheric models in December-January-February (a), March-April (b) and October-November (c). All SCE trends are statistically significant at the 90% confidence level from the t-Student test.

ARC DJF

Model and experiment	μ [%]	σ_μ[%]	T [%/dec]	σ_T[%/dec]	p-value
CAM4_SST-SIC-EXP	90.33	0.37	-0.17	0.07	0.02
WACCM_SST-SIC-EXP	91.27	0.38	-0.18	0.07	0.01
CAM4_SIC-EXP	90.37	0.20	-0.07	0.04	0.09
WACCM_SIC-EXP	91.40	0.20	-0.09	0.04	0.02

TABLE A.1 – Winter (December-January-February) Arctic SCE mean (i.e., μ), standard deviation (i.e., σ_μ), trend (i.e., T), standard error (i.e., σ_T) and p-value from the trend (1982-2014) from SST-SIC-EXP and SIC-EXP simulations using CAM4 and WACCM atmospheric models.

ARC Mar-Apr

Model and experiment	μ [%]	σ_μ[%]	T [%/dec]	σ_T[%/dec]	p-value
CAM4_SST-SIC-EXP	63.18	1.00	-0.51	0.16	0.004
WACCM_SST-SIC-EXP	64.79	1.00	-0.55	0.16	0.002
CAM4_SIC-EXP	63.51	0.65	-0.30	0.11	0.011
WACCM_SIC-EXP	65.14	0.61	-0.31	0.10	0.005

TABLE A.2 – Spring (March-April) Arctic SCE mean (i.e., μ), standard deviation (i.e., σ_μ), trend (i.e., T), standard error (i.e., σ_T) and p-value from the trend (1982-2014) from SST-SIC-EXP and SIC-EXP simulations using CAM4 and WACCM atmospheric models.

ARC Oct-Nov

Model and experiment	μ [%]	σ_μ[%]	T [%/dec]	σ_T[%/dec]	p-value
CAM4_SST-SIC-EXP	84.43	0.73	0.60	0.08	e-08
WACCM_SST-SIC-EXP	85.42	0.74	-0.55	0.10	e-06
CAM4_SIC-EXP	84.66	0.35	-0.16	0.06	0.013
WACCM_SIC-EXP	85.71	0.32	-0.16	0.05	0.0037

TABLE A.3 – Autumn (October-November) Arctic SCE mean (i.e., μ), standard deviation (i.e., σ_μ), trend (i.e., T), standard error (i.e., σ_T) and p-value from the trend (1982-2014) from SST-SIC-EXP and SIC-EXP simulations using CAM4 and WACCM atmospheric models.

Figure A.6 shows the spatial patterns of SCE trends. For the first experiment SST-SIC-EXP, snow cover trends in winter are significantly weaker compared to the other seasons (Figure A.5a,b). Slightly positive SCE trends are located in central-east Eurasia and Northern Canada with values less than 1%/dec in both models (Figure A.5a,b). In spring, simulations from CAM4 and WACCM show decreasing significant SCE trends (at the 90% confidence level) over the western and southern part of Eurasia up to 4%/dec over Scandinavia (Figure A.6c,d). Positive significant SCE trends are found locally in central Canada in CAM4, but are not significant in WACCM. During the onset season (Figure A.6e,f), SCE decreasing trends cover almost the whole land Arctic, except over the east part of North America. Maxima SCE trends are located in Scandinavia with values up to 5%/dec. Regarding the second experiment SIC-EXP, winter SCE trends performed are almost indistinguishable from SST-SIC-EXP (Figure A.7a,b). In contrast, for spring and autumn, we have found that SCE trends reported in simulations from SIC-EXP are not statistically significant (Figure A.7c,d,e,f). Significant trends only appear locally in some parts of Western Eurasia in WACCM with values of 2%/dec in spring (Figure A.7a,b). In autumn (Figure A.7c,d), SCE trends of less than 1.5%/dec are located over the Canadian Archipelago and central Siberia.

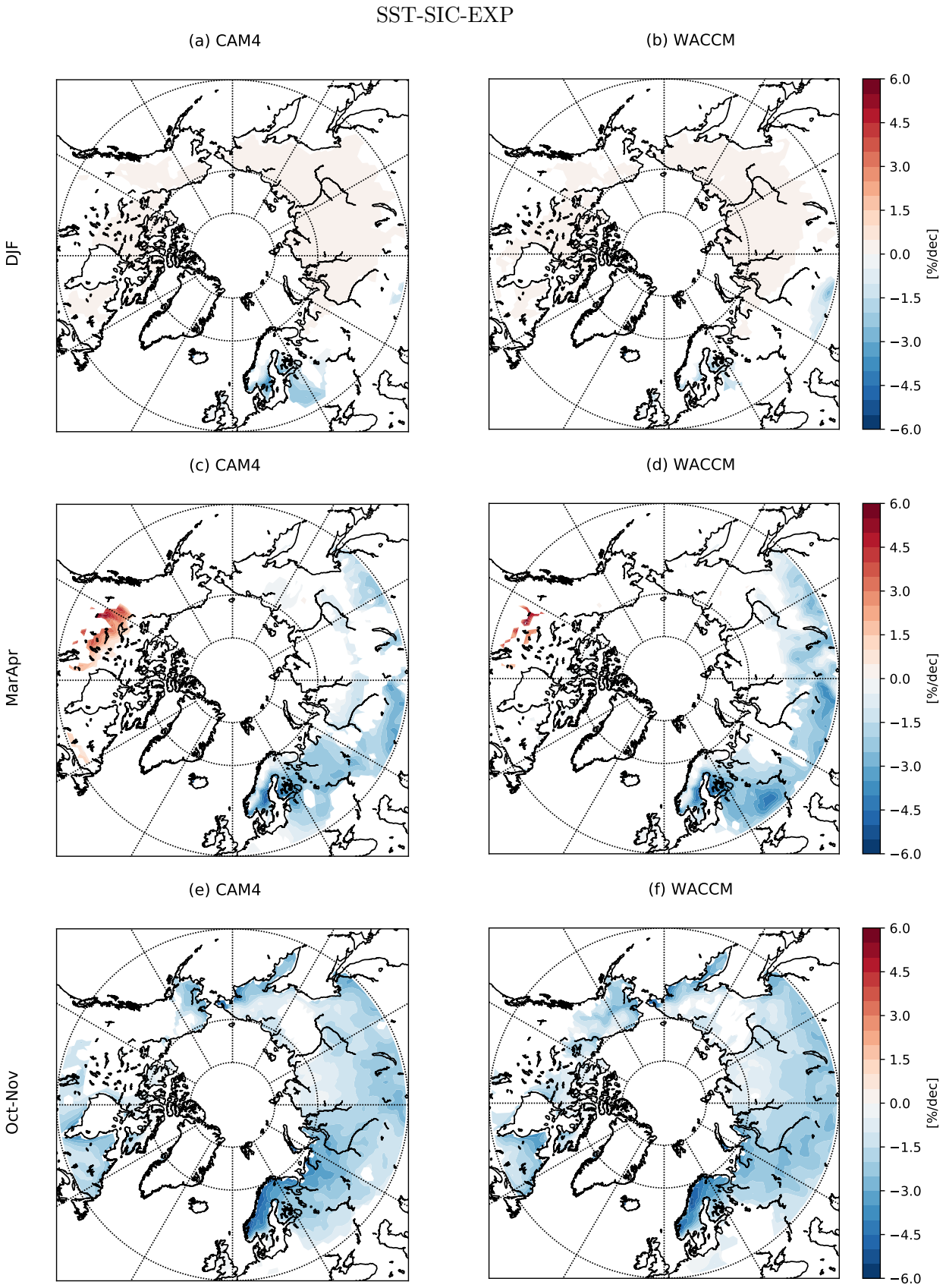

FIGURE A.6 – Spatial Arctic snow cover trends (1982-2014) of simulations from SST-SIC-EXP using CAM4 ("low-top") and WACCM ("high-top") atmospheric models in December-January-February (a,b), March-April (c,d) and October-November (e,f). Only statistically significant trends at the 90% confidence level from the t-Student test are shown.

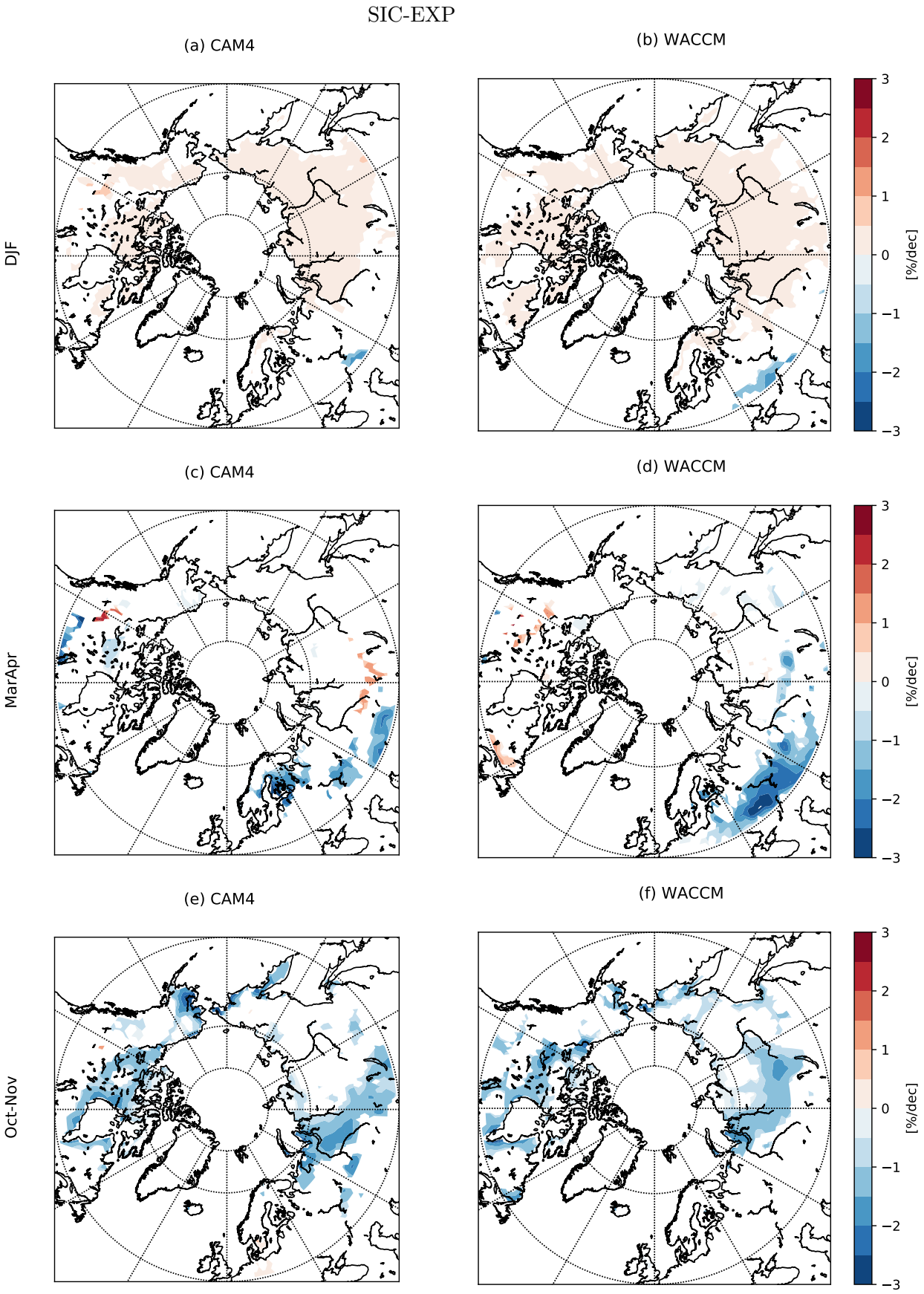

FIGURE A.7 – Spatial Arctic snow cover trends (1982-2014) of simulations from SIC-EXP using CAM4 ("low-top") and WACCM ("high-top") atmospheric models in December-January-February (a,b), March-April (c,d) and October-November (e,f). Only statistically significant trends at the 90% confidence level from the t-Student test are shown.

A.4 Conclusions

We have analyzed the snow cover variable from two different modeling experiments using two atmospheric models CAM4 ("low-top") and WACCM ("high-top"). In the first experiment (SST-SIC-EXP) daily varying SIC and SST conditions were prescribed, whereas in the second experiment (SIC-EXP), SST was prescribed to daily climatology. Simulations expand from 1982 to 2014 and the seasons considered were winter (December-January-February), spring (March-April) and autumn(October-November).

We have found that climatological differences between both experiments, SST-SIC-EXP and SIC-EXP, are not statistically significant for any season. However, SCE climatology in "high-top" (WACCM) and "low-top" (CAM4) differs significantly with the strongest discrepancies found in spring corresponding to the peak of maximum snow accumulation (Figure 4.18 and 4.19). The higher SCE climatology in WACCM than in CAM4 may be related to the ability of the "high-top" model to better capture stratosphere variability and thus, being able to accurately reproduce the frequency of stratospheric warming events. They are associated to cold air outbreaks (Kolstad *et al.*, 2010) and to increase of precipitation and moisture transport (*Ziuliaeva et al. in preparation*), thus providing favorable conditions for snowfall. This is consistent with Charlton-Perez *et al.* (2013) who found that "low-top" models from CMIP5 ensemble strongly underestimate the frequencies of major sudden stratospheric warming events, reproducing less than half the frequency of events observed in the reanalysis data and in the "high- top" models.

SCE annual cycle is almost indistinguishable across all simulations. It is interesting that, in all cases, the simulations are not able to melt snow in summer displaying values of 10-15% during July-August, whereas the coupled model CCSM4 reproduces accurately the observed SCE annual cycle (Figure 4.17). This is likely due to absence of a land surface model which is crucial for the heat balance at the surface necessary for melting (M_e in Equation 2.1). Ogawa *et al.* (2018) did not observe any significant cooling trend in 2 m temperature over Siberia, neither SST-SIC-EXP nor SIC-EXP ; instead, SST-SIC-EXP displayed a strong warming trend during 1982-2014 (~ 0.5°C/dec). The connection to the temperature trends found in Ogawa *et al.* (2018) may be related with the negative SCE trends displayed in spring (Figure A.6), that is, the warming found in SST-SIC-EXP in winter may promote an early melt in spring.

The next step would be to conduct a similar procedure for snowfall variable and to apply a

regression analysis using September sea ice anomalies as in Ghatak *et al.* (2012). Another analysis to be conducted is to investigate the different patterns of variability from individual realizations (members) in both snow cover and snowfall as has already been presented by Ogawa *et al.* (2018).

Annexe B

Tables

ARC-MarApr

Data sets	μ [%]	σ_μ [%]	T [%/dec]	σ_T [%/dec]	p-value
bcc-csm1-1	43.65	1.44	-1.11	0.30	0.00
CanESM2	65.66	1.43	-1.51	0.21	0.00
CCSM4	57.43	1.41	-1.44	0.22	0.00
CNRM-CM5	64.64	1.10	-1.22	0.14	0.00
CSIRO-Mk3-6-0	37.23	1.02	-1.04	0.16	0.00
GISS-E2-H	58.84	1.41	-1.39	0.23	0.00
GISS-E2-R	58.14	1.26	-1.05	0.25	0.00
inmcm4	44.97	2.67	0.28	0.68	0.68
MIROC-ESM	62.92	3.67	-2.28	0.83	0.01
MIROC-ESM-CHEM	61.63	2.10	-1.87	0.39	0.00
MIROC5	65.42	1.50	-1.59	0.22	0.00
MPI-ESM-LR	39.38	1.38	-0.58	0.34	0.10
MPI-ESM-P	33.92	1.83	-0.77	0.44	0.09
MRI-CGCM3	69.69	1.06	-0.22	0.27	0.41
NorESM1-M	57.69	1.61	-1.20	0.34	0.00
NorESM1-ME	59.13	1.62	-0.54	0.40	0.19
NCEP/CFSR	80.43	2.31	0.41	0.59	0.50
NOAAV2c	85.14	2.44	-1.21	0.58	0.05
NOAA CDR	85.11	2.83	-1.26	0.68	0.08
CMIP5	55.02	1.00	-1.10	0.13	0.00

TABLE B.1 – Spring (March-April) Arctic SCE mean (i.e., μ), standard deviation (i.e., σ_μ), trend (i.e., T), standard error (i.e., σ_T) and p-value from the trend for the period 1979-2005.

EURA-MarApr					
Data sets	μ [%]	σ_μ [%]	T [%/dec]	σ_T [%/dec]	p-value
bcc-csm1-1	38.12	2.10	-0.85	0.51	0.11
CanESM2	64.07	1.65	-1.70	0.25	0.00
CCSM4	51.99	1.78	-1.60	0.33	0.00
CNRM-CM5	62.40	1.25	-1.26	0.20	0.00
CSIRO-Mk3-6-0	36.23	1.13	-1.10	0.19	0.00
GISS-E2-H	59.18	1.12	-0.97	0.21	0.00
GISS-E2-R	58.47	1.33	-0.93	0.29	0.00
inmcm4	46.47	3.99	0.40	1.02	0.70
MIROC-ESM	61.54	3.91	-1.28	0.97	0.20
MIROC-ESM-CHEM	61.58	2.61	-2.27	0.49	0.00
MIROC5	62.51	1.83	-2.04	0.23	0.00
MPI-ESM-LR	36.66	1.87	-0.64	0.46	0.18
MPI-ESM-P	33.19	3.02	-0.57	0.77	0.47
MRI-CGCM3	64.10	1.38	-0.02	0.35	0.95
NorESM1-M	54.42	2.12	-1.04	0.50	0.05
NorESM1-ME	55.27	2.24	-0.22	0.57	0.70
NCEP/CFSR	77.46	3.20	0.03	0.82	0.97
NOAAV2c	82.17	3.73	-1.42	0.91	0.13
NOAA CDR	82.25	3.94	-1.79	0.95	0.07
CMIP5	52.89	1.03	-1.01	0.17	0.00

TABLE B.2 – Spring (March-April) Eurasian subdomain SCE mean (i.e., μ), standard deviation (i.e., σ_μ), trend (i.e., T), standard error (i.e.,σ_T) and p-value from the trend for the period 1979-2005.

NAm-MarApr

Data sets	μ [%]	σ_μ [%]	T [%/dec]	σ_T [%/dec]	p-value
bcc-csm1-1	51.80	2.41	-1.49	0.54	0.01
CanESM2	67.56	1.65	-1.28	0.34	0.00
CCSM4	64.11	1.79	-1.26	0.39	0.00
CNRM-CM5	67.51	1.16	-1.16	0.19	0.00
CSIRO-Mk3-6-0	38.56	1.22	-0.97	0.25	0.00
GISS-E2-H	58.39	2.11	-1.96	0.37	0.00
GISS-E2-R	57.68	1.48	-1.21	0.29	0.00
inmcm4	43.09	3.72	0.14	0.95	0.88
MIROC-ESM	65.09	5.66	-3.84	1.23	0.00
MIROC-ESM-CHEM	61.72	2.65	-1.26	0.63	0.06
MIROC5	68.46	1.81	-1.12	0.41	0.01
MPI-ESM-LR	43.47	2.21	-0.48	0.56	0.40
MPI-ESM-P	35.01	2.67	-1.08	0.65	0.11
MRI-CGCM3	76.49	1.08	-0.47	0.26	0.08
NorESM1-M	61.95	2.61	-1.41	0.61	0.03
NorESM1-ME	64.15	2.84	-0.96	0.70	0.18
NCEP/CFSR	83.80	2.91	0.83	0.73	0.27
NOAAV2c	89.82	2.83	-0.87	0.71	0.23
NOAA CDR	90.13	2.96	-0.33	0.76	0.67
CMIP5	57.81	1.13	-1.24	0.15	0.00

TABLE B.3 – Spring (March-April) North American subdomain SCE mean (i.e., μ), standard deviation (i.e., σ_μ), trend (i.e., T), standard error (i.e.,σ_T) and p-value from the trend for the period 1979-2005.

ARC-OctNov

Data sets	μ [%]	σ_μ [%]	T [%/dec]	σ_T [%/dec]	p-value
bcc-csm1-1	59.16	1.15	-0.98	0.22	0.00
CanESM2	69.97	1.03	-0.68	0.23	0.01
CCSM4	81.12	0.84	-0.89	0.12	0.00
CNRM-CM5	64.31	0.92	-0.93	0.15	0.00
CSIRO-Mk3-6-0	56.72	0.74	-0.55	0.16	0.00
GISS-E2-H	71.77	0.82	-0.55	0.18	0.01
GISS-E2-R	68.53	1.09	-0.94	0.21	0.00
inmcm4	77.27	1.12	0.23	0.29	0.43
MIROC-ESM	60.16	2.96	-1.48	0.70	0.04
MIROC-ESM-CHEM	60.06	1.60	-1.05	0.35	0.01
MIROC5	55.33	1.12	-1.12	0.18	0.00
MPI-ESM-LR	61.08	1.24	-0.49	0.30	0.12
MPI-ESM-P	59.99	1.86	-0.77	0.45	0.10
MRI-CGCM3	84.91	0.64	-0.13	0.16	0.43
NorESM1-M	80.10	1.22	-0.79	0.27	0.01
NorESM1-ME	80.57	0.95	-0.45	0.23	0.06
NCEP/CFSR	56.20	4.66	-1.61	1.15	0.18
NOAAV2c	62.38	2.36	-0.76	0.59	0.21
NOAA CDR	66.88	4.37	3.29	0.91	0.00
CMIP5	68.19	0.72	-0.72	0.12	0.00

TABLE B.4 – Autumn (October-November) Arctic SCE mean (i.e., μ), standard deviation (i.e., σ_μ), trend (i.e., T), standard error (i.e.,σ_T) and p-value from the trend for the period 1979-2005.

EURA-OctNov

Data sets	μ [%]	σ_μ [%]	T [%/dec]	σ_T [%/dec]	p-value
bcc-csm1-1	56.68	1.37	-0.79	0.31	0.02
CanESM2	69.33	1.37	-0.14	0.35	0.69
CCSM4	78.46	1.07	-0.83	0.22	0.00
CNRM-CM5	64.33	1.04	-0.82	0.21	0.00
CSIRO-Mk3-6-0	57.78	0.90	-0.45	0.21	0.05
GISS-E2-H	72.30	0.94	-0.46	0.22	0.05
GISS-E2-R	70.01	1.24	-1.00	0.25	0.00
inmcm4	80.65	2.42	1.25	0.57	0.04
MIROC-ESM	58.77	3.52	-1.03	0.88	0.25
MIROC-ESM-CHEM	58.72	1.62	-0.48	0.41	0.24
MIROC5	54.36	0.99	-0.45	0.24	0.07
MPI-ESM-LR	58.85	1.47	-0.34	0.37	0.37
MPI-ESM-P	58.10	2.52	-0.86	0.62	0.18
MRI-CGCM3	84.31	1.05	-0.07	0.27	0.81
NorESM1-M	78.29	1.94	-0.98	0.46	0.04
NorESM1-ME	78.43	1.38	-0.16	0.35	0.65
NCEP/CFSR	53.51	5.61	-1.84	1.39	0.20
NOAAV2c	60.46	3.11	-0.36	0.80	0.65
NOAA CDR	64.11	4.81	3.67	0.99	0.00
CMIP5	67.46	0.66	-0.48	0.14	0.00

TABLE B.5 – Autumn (October-November) Eurasian subdomain SCE mean (i.e., μ), standard deviation (i.e., σ_μ), trend (i.e., T), standard error (i.e.,σ_T) and p-value from the trend for the period 1979-2005.

NAm-OctNov

Data sets	μ [%]	σ_μ [%]	T [%/dec]	σ_T [%/dec]	p-value
bcc-csm1-1	62.81	1.34	-1.26	0.24	0.00
CanESM2	70.74	1.70	-1.32	0.35	0.00
CCSM4	84.38	1.10	-0.97	0.21	0.00
CNRM-CM5	64.29	1.15	-1.07	0.20	0.00
CSIRO-Mk3-6-0	55.33	0.83	-0.69	0.16	0.00
GISS-E2-H	71.06	0.97	-0.67	0.21	0.00
GISS-E2-R	66.53	1.12	-0.86	0.23	0.00
inmcm4	73.04	1.78	-1.05	0.41	0.02
MIROC-ESM	62.33	3.73	-2.18	0.85	0.02
MIROC-ESM-CHEM	62.16	2.04	-1.93	0.35	0.00
MIROC5	56.36	1.84	-1.83	0.30	0.00
MPI-ESM-LR	64.42	1.38	-0.71	0.32	0.04
MPI-ESM-P	62.84	2.52	-0.62	0.64	0.33
MRI-CGCM3	85.65	0.61	-0.21	0.15	0.18
NorESM1-M	82.45	1.19	-0.54	0.29	0.07
NorESM1-ME	83.36	1.35	-0.82	0.31	0.01
NCEP/CFSR	59.26	4.78	-1.35	1.20	0.27
NOAAV2c	65.40	4.02	-1.38	1.00	0.18
NOAA CDR	71.73	5.00	2.62	1.17	0.03
CMIP5	69.23	0.96	-1.05	0.13	0.00

Table B.6 – Autumn (October-November) North American subdomain SCE mean (i.e., μ), standard deviation (i.e., σ_μ), trend (i.e., T), standard error (i.e., σ_T) and p-value from the trend for the period 1979-2005.

ARC-MarApr

Data sets	μ [kg m^{-2}]	σ_μ [kg m^{-2}]	T [kg m^{-2}/dec]	σ_T [kg m^{-2}/dec]	p-value
bcc-csm1-1	84.98	3.87	-0.76	1.11	0.50
CanESM2	107.50	3.80	-2.97	0.91	0.00
CCSM4	127.64	4.28	-3.23	1.04	0.00
CNRM-CM5	131.28	2.67	-2.86	0.49	0.00
CSIRO-Mk3-6-0	32.82	1.16	-1.22	0.22	0.00
GISS-E2-H	108.44	3.82	-3.55	0.82	0.00
GISS-E2-R	105.47	3.27	-1.91	0.86	0.04
inmcm4	72.89	6.60	1.26	1.89	0.51
MIROC-ESM	104.07	10.05	-5.76	2.65	0.04
MIROC-ESM-CHEM	100.40	4.37	-3.93	0.96	0.00
MIROC5	112.21	6.47	-8.02	0.84	0.00
MPI-ESM-LR	64.39	2.78	-0.49	0.80	0.54
MPI-ESM-P	50.91	4.30	-2.75	1.10	0.02
MRI-CGCM3	147.91	3.64	-0.85	1.04	0.42
NorESM1-M	111.10	5.52	-4.59	1.28	0.00
NorESM1-ME	127.63	6.23	-3.96	1.60	0.02
CanSISE	58.84	4.39	-1.09	1.25	0.39
CMIP5	99.35	2.38	-2.85	0.34	0.00

TABLE B.7 – Spring (March-April) Arctic SWE mean (i.e., μ), standard deviation (i.e., σ_μ), trend (i.e., T), standard error (i.e., σ_T) and p-value from the trend for the period 1981-2005.

EURA-MarApr

Data sets	μ [kg m^{-2}]	σ_μ [kg m^{-2}]	T [kg m^{-2}/dec]	σ_T [kg m^{-2}/dec]	p-value
bcc-csm1-1	65.32	5.12	0.33	1.48	0.82
CanESM2	85.13	2.99	-2.16	0.74	0.01
CCSM4	103.82	4.53	-2.17	1.23	0.09
CNRM-CM5	109.22	2.52	-1.75	0.63	0.01
CSIRO-Mk3-6-0	27.68	1.07	-1.13	0.20	0.00
GISS-E2-H	103.00	3.71	-1.74	1.01	0.10
GISS-E2-R	103.26	3.45	-1.23	0.96	0.22
inmcm4	66.03	8.23	-1.45	2.36	0.55
MIROC-ESM	100.04	11.45	-1.52	3.30	0.65
MIROC-ESM-CHEM	99.63	4.64	-3.17	1.17	0.01
MIROC5	93.87	3.51	-3.45	0.71	0.00
MPI-ESM-LR	58.05	3.69	-1.32	1.03	0.21
MPI-ESM-P	48.12	6.42	-1.81	1.82	0.33
MRI-CGCM3	117.09	4.46	-2.02	1.22	0.11
NorESM1-M	91.23	6.03	-4.19	1.51	0.01
NorESM1-ME	102.68	6.05	-0.70	1.74	0.69
CanSISE	59.03	5.37	-0.69	1.55	0.66
CMIP5	85.89	2.01	-1.84	0.44	0.00

TABLE B.8 – Spring (March-April) Eurasian subdomain SWE mean (i.e., μ), standard deviation (i.e., σ_μ), trend (i.e., T), standard error (i.e., σ_T) and p-value from the trend for the period 1981-2005.

NAm-MarApr

Data sets	μ [kg m^{-2}]	σ_μ [kg m^{-2}]	T [kg m^{-2}/dec]	σ_T [kg m^{-2}/dec]	p-value
bcc-csm1-1	113.98	8.06	-2.36	2.28	0.31
CanESM2	142.52	7.11	-4.22	1.86	0.03
CCSM4	156.65	6.51	-4.51	1.63	0.01
CNRM-CM5	159.44	4.20	-4.28	0.82	0.00
CSIRO-Mk3-6-0	39.61	1.88	-1.35	0.47	0.01
GISS-E2-H	115.97	6.01	-6.06	1.19	0.00
GISS-E2-R	108.71	4.58	-2.91	1.18	0.02
inmcm4	81.47	11.83	4.65	3.28	0.17
MIROC-ESM	110.39	17.20	-12.41	4.25	0.01
MIROC-ESM-CHEM	101.60	6.90	-5.12	1.68	0.01
MIROC5	131.41	10.84	-12.80	1.64	0.00
MPI-ESM-LR	72.23	4.46	0.53	1.28	0.68
MPI-ESM-P	54.36	6.53	-3.91	1.70	0.03
MRI-CGCM3	185.43	5.50	0.57	1.59	0.72
NorESM1-M	137.01	9.52	-5.12	2.54	0.06
NorESM1-ME	160.18	11.77	-8.20	2.94	0.01
CanSISE	58.57	7.08	-1.67	2.02	0.42
CMIP5	116.93	3.60	-4.22	0.56	0.00

Table B.9 – Spring (March-April) North American subdomain SWE mean (i.e., μ), standard deviation (i.e., σ_μ), trend (i.e., T), standard error (i.e., σ_T) and p-value from the trend for the period 1981-2005.

ARC-OctNov

Data sets	μ [kg m^{-2}]	σ_μ [kg m^{-2}]	T [kg m^{-2}/dec]	σ_T [kg m^{-2}/dec]	p-value
bcc-csm1-1	49.64	2.03	-1.41	0.51	0.01
CanESM2	45.32	1.57	-0.93	0.41	0.03
CCSM4	58.40	2.03	-2.11	0.39	0.00
CNRM-CM5	52.49	1.54	-1.69	0.27	0.00
CSIRO-Mk3-6-0	35.91	0.87	-0.50	0.23	0.04
GISS-E2-H	55.45	1.53	-0.71	0.42	0.10
GISS-E2-R	52.63	1.88	-1.19	0.48	0.02
inmcm4	47.22	3.56	1.33	0.99	0.19
MIROC-ESM	48.31	4.22	-2.40	1.11	0.04
MIROC-ESM-CHEM	48.42	2.41	-2.17	0.53	0.00
MIROC5	54.42	4.91	-6.27	0.56	0.00
MPI-ESM-LR	38.83	1.87	-0.84	0.51	0.11
MPI-ESM-P	36.88	2.18	-1.18	0.58	0.05
MRI-CGCM3	63.08	1.42	0.21	0.41	0.61
NorESM1-M	78.30	2.67	-2.13	0.63	0.00
NorESM1-ME	61.87	4.17	-4.37	0.79	0.00
CanSISE	40.36	2.65	-0.63	0.76	0.41
CMIP5	51.70	1.35	-1.65	0.18	0.00

Table B.10 – Autumn (October-November) Arctic SWE mean (i.e., μ), standard deviation (i.e., σ_μ), trend (i.e., T), standard error (i.e., σ_T) and p-value from the trend for the period 1981-2005.

EURA-OctNov

Data sets	μ [kg m^{-2}]	σ_μ [kg m^{-2}]	T [kg m^{-2}/dec]	σ_T [kg m^{-2}/dec]	p-value
bcc-csm1-1	42.93	1.96	-0.59	0.55	0.30
CanESM2	36.13	1.59	0.44	0.45	0.34
CCSM4	49.93	1.53	-0.93	0.40	0.03
CNRM-CM5	47.67	1.16	-0.71	0.30	0.03
CSIRO-Mk3-6-0	32.90	0.98	-0.14	0.28	0.62
GISS-E2-H	54.53	1.79	-0.21	0.52	0.69
GISS-E2-R	53.60	2.07	-0.89	0.57	0.13
inmcm4	44.91	3.48	1.12	0.98	0.27
MIROC-ESM	46.13	4.81	-0.72	1.38	0.61
MIROC-ESM-CHEM	46.35	2.21	-0.79	0.62	0.21
MIROC5	44.96	1.23	-0.34	0.35	0.34
MPI-ESM-LR	37.99	2.14	-1.13	0.57	0.06
MPI-ESM-P	36.43	2.59	-1.64	0.67	0.02
MRI-CGCM3	54.23	1.67	-0.75	0.46	0.11
NorESM1-M	61.11	3.18	-2.69	0.73	0.00
NorESM1-ME	48.39	2.96	-2.26	0.71	0.00
CanSISE	41.27	2.76	-0.59	0.79	0.47
CMIP5	46.14	0.87	-0.77	0.19	0.00

TABLE B.11 – Autumn (October-November) Eurasian subdomain SWE mean (i.e., μ), standard deviation (i.e., σ_μ), trend (i.e., T), standard error (i.e., σ_T) and p-value from the trend for the period 1981-2005.

NAm-OctNov

Data sets	μ [kg m^{-2}]	σ_μ [kg m^{-2}]	T [kg m^{-2}/dec]	σ_T [kg m^{-2}/dec]	p-value
bcc-csm1-1	59.54	3.41	-2.62	0.82	0.00
CanESM2	59.69	3.79	-3.08	0.89	0.00
CCSM4	68.70	3.47	-3.54	0.68	0.00
CNRM-CM5	58.65	2.62	-2.95	0.44	0.00
CSIRO-Mk3-6-0	39.91	1.62	-0.98	0.42	0.03
GISS-E2-H	56.73	2.22	-1.40	0.57	0.02
GISS-E2-R	51.20	2.28	-1.62	0.57	0.01
inmcm4	50.11	5.72	1.60	1.62	0.33
MIROC-ESM	51.73	6.60	-5.04	1.59	0.00
MIROC-ESM-CHEM	51.67	3.76	-4.33	0.61	0.00
MIROC5	64.33	9.72	-12.47	1.06	0.00
MPI-ESM-LR	39.86	2.56	-0.49	0.73	0.51
MPI-ESM-P	37.43	3.12	-0.61	0.89	0.50
MRI-CGCM3	73.86	2.48	1.38	0.66	0.05
NorESM1-M	100.71	4.13	-1.40	1.16	0.24
NorESM1-ME	79.45	7.08	-7.12	1.41	0.00
CanSISE	39.07	4.38	-0.70	1.26	0.58
CMIP5	58.97	2.23	-2.79	0.28	0.00

Table B.12 – Autumn (October-November) North American SWE mean (i.e., μ), standard deviation (i.e., σ_μ), trend (i.e., T), standard error (i.e., σ_T) and p-value from the trend for the period 1981-2005.

ARC-MarApr

Data sets	μ [cm]	σ_μ [cm]	T [cm / dec]	σ_T [cm/ dec]	p-value
bcc-csm1-1	29.27	1.35	-0.58	0.33	0.09
CanESM2	32.59	1.21	-1.02	0.24	0.00
CCSM4	40.87	1.38	-1.17	0.27	0.00
CNRM-CM5	44.50	0.95	-0.99	0.14	0.00
CSIRO-Mk3-6-0	13.65	0.45	-0.37	0.09	0.00
GISS-E2-H	33.68	1.11	-1.02	0.20	0.00
GISS-E2-R	34.18	0.99	-0.63	0.22	0.01
inmcm4	16.75	1.18	0.16	0.30	0.60
MIROC-ESM	35.62	3.25	-1.59	0.77	0.05
MIROC-ESM-CHEM	34.41	1.41	-1.08	0.29	0.00
MIROC5	38.52	2.28	-2.64	0.25	0.00
MRI-CGCM3	39.02	0.90	-0.30	0.22	0.19
NorESM1-M	38.82	1.71	-1.45	0.33	0.00
NorESM1-ME	41.25	1.65	-0.68	0.40	0.10
ERA20c	18.27	0.58	-0.29	0.14	0.04
JRA-55	29.44	4.09	-3.81	0.72	0.00
NOAAV2c	39.45	3.51	-1.74	0.83	0.05
CMIP5	33.80	0.84	-0.95	0.10	0.00

Table B.13 – Spring (March-April) Arctic SND mean (i.e., μ), standard deviation (i.e., σ_μ), trend (i.e., T), standard error (i.e., σ_T) and p-value from the trend for the period 1979-2005.

EURA-MarApr

Data sets	μ [cm]	σ_μ [cm]	T [cm / dec]	σ_T [cm/ dec]	p-value
bcc-csm1-1	23.76	1.78	-0.21	0.45	0.65
CanESM2	25.99	1.12	-0.96	0.21	0.00
CCSM4	34.88	1.46	-0.94	0.32	0.01
CNRM-CM5	37.40	0.90	-0.67	0.19	0.00
CSIRO-Mk3-6-0	11.68	0.44	-0.32	0.09	0.00
GISS-E2-H	33.24	1.12	-0.62	0.26	0.03
GISS-E2-R	33.64	1.04	-0.38	0.25	0.15
inmcm4	16.84	1.68	0.01	0.43	0.99
MIROC-ESM	34.45	3.78	-0.84	0.96	0.39
MIROC-ESM-CHEM	34.17	1.53	-1.02	0.34	0.01
MIROC5	32.36	1.18	-1.03	0.22	0.00
MRI-CGCM3	32.16	1.14	-0.24	0.29	0.41
NorESM1-M	34.97	1.72	-1.02	0.39	0.02
NorESM1-ME	35.59	1.88	-0.07	0.48	0.88
ERA20c	8.66	0.65	-0.19	0.16	0.25
JRA-55	21.98	2.21	-0.76	0.55	0.18
NOAAV2c	36.07	3.90	-1.64	0.95	0.10
CMIP5	30.08	0.67	-0.59	0.13	0.00

TABLE B.14 – Spring (March-April) Eurasian subdomain SND mean (i.e., μ), standard deviation (i.e., σ_μ), trend (i.e., T), standard error (i.e., σ_T) and p-value from the trend for the period 1979-2005.

NAm-MarApr

Data sets	μ [cm]	σ_μ [cm]	T [cm / dec]	σ_T [cm/ dec]	p-value
bcc-csm1-1	37.41	2.73	-1.12	0.66	0.10
CanESM2	40.51	1.76	-1.09	0.40	0.01
CCSM4	48.16	1.98	-1.45	0.42	0.00
CNRM-CM5	53.56	1.42	-1.40	0.23	0.00
CSIRO-Mk3-6-0	16.27	0.73	-0.42	0.17	0.02
GISS-E2-H	34.28	1.75	-1.58	0.32	0.00
GISS-E2-R	34.91	1.33	-0.98	0.28	0.00
inmcm4	16.64	1.84	0.35	0.47	0.45
MIROC-ESM	37.47	5.60	-2.77	1.33	0.05
MIROC-ESM-CHEM	34.79	2.21	-1.18	0.52	0.03
MIROC5	44.97	3.84	-4.33	0.47	0.00
MRI-CGCM3	47.37	1.48	-0.37	0.37	0.33
NorESM1-M	43.83	3.10	-2.01	0.69	0.01
NorESM1-ME	48.64	3.06	-1.48	0.73	0.05
ERA20c	31.27	1.05	-0.43	0.26	0.11
JRA-55	38.28	8.56	-7.43	1.62	0.00
NOAAV2c	44.76	6.06	-1.88	1.51	0.22
CMIP5	38.49	1.27	-1.42	0.16	0.00

Table B.15 – Spring (March-April) North American subdomain SND mean (i.e., μ), standard deviation (i.e., σ_μ), trend (i.e., T), standard error (i.e., σ_T) and p-value from the trend for the period 1979-2005.

ARC-OctNov

Data sets	μ [cm]	σ_μ [cm]	T [cm / dec]	σ_T [cm/ dec]	p-value
bcc-csm1-1	26.52	1.06	-0.84	0.21	0.00
CanESM2	16.17	0.58	-0.43	0.12	0.00
CCSM4	29.37	0.88	-0.81	0.16	0.00
CNRM-CM5	18.64	0.54	-0.57	0.08	0.00
CSIRO-Mk3-6-0	14.49	0.35	-0.16	0.08	0.06
GISS-E2-H	24.02	0.60	-0.46	0.12	0.00
GISS-E2-R	23.76	0.71	-0.51	0.15	0.00
inmcm4	17.10	0.84	0.26	0.21	0.22
MIROC-ESM	16.47	1.40	-0.72	0.33	0.04
MIROC-ESM-CHEM	16.51	0.82	-0.67	0.16	0.00
MIROC5	18.88	1.83	-2.18	0.18	0.00
MRI-CGCM3	23.42	0.46	-0.14	0.11	0.23
NorESM1-M	27.55	1.07	-0.80	0.22	0.00
NorESM1-ME	28.98	1.32	-1.07	0.26	0.00
ERA20c	13.00	0.33	-0.09	0.08	0.26
JRA-55	23.23	2.40	-1.62	0.53	0.00
NOAAV2c	37.06	2.60	-0.89	0.64	0.18
CMIP5	21.56	0.57	-0.65	0.07	0.00

Table B.16 – Autumn (October-November) Arctic SND mean (i.e., μ), standard deviation (i.e., σ_μ), trend (i.e., T), standard error (i.e., σ_T) and p-value from the trend for the period 1979-2005.

EURA-OctNov

Data sets	μ [cm]	σ_μ [cm]	T [cm / dec]	σ_T [cm/ dec]	p-value
bcc-csm1-1	24.24	1.15	-0.62	0.27	0.03
CanESM2	13.53	0.52	-0.02	0.13	0.89
CCSM4	26.73	0.75	-0.43	0.17	0.02
CNRM-CM5	16.98	0.43	-0.29	0.09	0.01
CSIRO-Mk3-6-0	13.35	0.39	0.00	0.10	0.97
GISS-E2-H	24.52	0.55	-0.26	0.13	0.05
GISS-E2-R	24.60	0.80	-0.50	0.18	0.01
inmcm4	17.40	0.91	0.40	0.22	0.08
MIROC-ESM	15.71	1.56	-0.25	0.40	0.54
MIROC-ESM-CHEM	15.74	0.78	-0.23	0.20	0.25
MIROC5	15.44	0.45	-0.23	0.11	0.04
MRI-CGCM3	21.34	0.52	-0.28	0.12	0.03
NorESM1-M	25.35	1.35	-0.87	0.30	0.01
NorESM1-ME	25.67	1.11	-0.63	0.26	0.02
ERA20c	4.86	0.35	-0.09	0.09	0.30
JRA-55	20.36	1.76	-0.89	0.42	0.04
NOAAV2c	35.35	2.39	-0.50	0.61	0.42
CMIP5	20.04	0.36	-0.30	0.07	0.00

TABLE B.17 – Autumn (October-November) Eurasian subdomain SND mean (i.e., μ), standard deviation (i.e., σ_μ), trend (i.e., T), standard error (i.e., σ_T) and p-value from the trend for the period 1979-2005.

NAm-OctNov

Data sets	μ [cm]	σ_μ [cm]	T [cm / dec]	σ_T [cm/ dec]	p-value
bcc-csm1-1	29.90	1.54	-1.17	0.32	0.00
CanESM2	19.34	1.19	-0.92	0.25	0.00
CCSM4	32.58	1.40	-1.28	0.25	0.00
CNRM-CM5	20.75	0.89	-0.93	0.14	0.00
CSIRO-Mk3-6-0	16.01	0.64	-0.39	0.14	0.01
GISS-E2-H	23.35	1.01	-0.74	0.21	0.00
GISS-E2-R	22.61	0.82	-0.54	0.18	0.01
inmcm4	16.72	1.32	0.09	0.34	0.78
MIROC-ESM	17.67	2.27	-1.46	0.50	0.01
MIROC-ESM-CHEM	17.71	1.27	-1.35	0.18	0.00
MIROC5	22.48	3.53	-4.22	0.33	0.00
MRI-CGCM3	25.95	0.75	0.03	0.19	0.89
NorESM1-M	30.42	1.44	-0.70	0.34	0.05
NorESM1-ME	33.29	2.23	-1.65	0.47	0.00
ERA20c	24.02	0.55	-0.10	0.14	0.49
JRA-55	26.65	4.85	-2.49	1.14	0.04
NOAAV2c	39.75	4.54	-1.52	1.12	0.19
CMIP5	23.49	0.91	-1.09	0.09	0.00

TABLE B.18 – Autumn (October-November) North American SND mean (i.e., μ), standard deviation (i.e., σ_μ), trend (i.e., T), standard error (i.e., σ_T) and p-value from the trend for the period 1979-2005.

List of figures

References

ACIA (2004). Impacts of a Warming Arctic-Arctic Climate Impact Assessment. *Impacts of a Warming Arctic-Arctic Climate Impact Assessment, by Arctic Climate Impact Assessment, pp. 144. ISBN 0521617782. Cambridge, UK : Cambridge University Press, December 2004.*, page 144.

Alexander, M. A., Tomas, R., Deser, C., and Lawrence, D. M. (2010). The atmospheric response to projected terrestrial snow changes in the late twenty-first century. *Journal of Climate*, **23**(23), 6430–6437.

Armstrong, R. L. and Brun, E. (2008). *Snow and climate : physical processes, surface energy exchange and modeling*. Cambridge University Press.

Arora, V., Scinocca, J., Boer, G., Christian, J., Denman, K., Flato, G., Kharin, V., Lee, W., and Merryfield, W. (2011). Carbon emission limits required to satisfy future representative concentration pathways of greenhouse gases. *Geophysical Research Letters*, **38**(5).

Arrhenius, S. (1896). XXXI. On the influence of carbonic acid in the air upon the temperature of the ground. *The London, Edinburgh, and Dublin Philosophical Magazine and Journal of Science*, **41**(251), 237–276.

Balsamo, G., Albergel, C., Beljaars, A., Boussetta, S., Brun, E., Cloke, H. L., Dee, D., Dutra, E., Pappenberger, F., de Rosnay, P., Sabater, J., Stockdale, T., and Vitart, F. (2012). ERA-Interim/Land : A global land-surface reanalysis based on ERA-Interim meteorological forcing. (13), 25.

Balsamo, G., Albergel, C., Beljaars, A., Boussetta, S., Brun, E., Cloke, H., Dee, D., Dutra, E., Muñoz-Sabater, J., Pappenberger, F., *et al.* (2015). ERA-Interim/Land : a global land surface reanalysis data set. *Hydrology and Earth System Sciences*, **19**(1), 389–407.

Bamzai, A. (2003). Relationship between snow cover variability and Arctic Oscillation index on a hierarchy of time scales. *International Journal of Climatology : A Journal of the Royal Meteorological Society*, **23**(2), 131–142.

Barichivich, J., Briffa, K. R., Myneni, R. B., Osborn, T. J., Melvin, T. M., Ciais, P., Piao, S., and Tucker, C. (2013). Large-scale variations in the vegetation growing season and annual cycle of atmospheric CO2 at high northern latitudes from 1950 to 2011. *Global change biology*, **19**(10), 3167–3183.

Barnett, T. P., Adam, J. C., and Lettenmaier, D. P. (2005). Potential impacts of a warming climate on water availability in snow-dominated regions. *Nature*, **438**(7066), 303.

Bentsen, M., Bethke, I., Debernard, J. B., Iversen, T., Kirkevåg, A., Seland, Ø., Drange, H., Roelandt, C., Seierstad, I. A., Hoose, C., and Kristjánsson, J. E. (2013). The Norwegian Earth System Model, NorESM1-M Part 1 : Description and basic evaluation of the physical climate. *Geoscientific Model Development*, **6**(3), 687–720.

Berghuijs, W., Woods, R., and Hrachowitz, M. (2014). A precipitation shift from snow towards rain leads to a decrease in streamflow. *Nature Climate Change*, **4**(7), 583.

Berghuijs, W. R., Woods, R. A., Hutton, C. J., and Sivapalan, M. (2016). Dominant flood generating mechanisms across the United States. *Geophysical Research Letters*, **43**(9), 4382–4390.

Biancamaria, S., Cazenave, A., Mognard, N. M., Llovel, W., and Frappart, F. (2011). Satellite-based high latitude snow volume trend, variability and contribution to sea level over 1989/2006. *Global and Planetary Change*, **75**(3-4), 99–107.

Bintanja, R. and Selten, F. (2014). Future increases in Arctic precipitation linked to local evaporation and sea-ice retreat. *Nature*, **509**(7501), 479.

Biskaborn, B. K., Smith, S. L., Noetzli, J., Matthes, H., Vieira, G., Streletskiy, D. A., Schoeneich, P., Romanovsky, V. E., Lewkowicz, A. G., Abramov, A., *et al.* (2019). Permafrost is warming at a global scale. *Nature communications*, **10**(1), 264.

Bokhorst, S., Pedersen, S. H., Brucker, L., Anisimov, O., Bjerke, J. W., Brown, R. D., Ehrich, D., Essery, R. L. H., Heilig, A., Ingvander, S., Johansson, C., Johansson, M., Jónsdóttir, I. S., Inga, N., Luojus, K., Macelloni, G., Mariash, H., McLennan, D., Rosqvist, G. N., Sato, A., Savela, H., Schneebeli, M., Sokolov, A., Sokratov, S. A., Terzago, S., Vikhamar-Schuler, D., Williamson, S., Qiu, Y., and Callaghan, T. V. (2016). Changing Arctic snow cover : A review of recent

developments and assessment of future needs for observations, modelling, and impacts. *Ambio*, **45**(5), 516–537.

Brown, J., Ferrians Jr, O., Heginbottom, J., and Melnikov, E. (1997). *Circum-Arctic map of permafrost and ground-ice conditions*. US Geological Survey Reston, VA.

Brown, R. and Derksen, C. (2013). Is Eurasian October snow cover extent increasing ? *Environmental Research Letters*, **8**(2), 024006.

Brown, R., Derksen, C., and Wang, L. (2007). Assessment of spring snow cover duration variability over northern Canada from satellite datasets. *Remote Sensing of Environment*, **111**(2-3), 367–381.

Brown, R., Schuler, D. V., Bulygina, O., Derksen, C., Luojus, K., Mudryk, L., Wang, L., and Yang, D. (2017). Arctic terrestrial snow cover. *AMAP 2017 Snow, Water, Ice and Permafrost in the Arctic (SWIPA) 2017*, page 269.

Brown, R. D. (2000). Northern Hemisphere snow cover variability and change, 1915–97. *Journal of climate*, **13**(13), 2339–2355.

Brown, R. D. and Braaten, R. O. (1998). Spatial and temporal variability of Canadian monthly snow depths, 1946–1995. *Atmosphere-Ocean*, **36**(1), 37–54.

Brown, R. D. and Frei, A. (2007). Comment on "Evaluation of surface albedo and snow cover in AR4 coupled models" by A. Roesch. *Journal of Geophysical Research : Atmospheres*, **112**(D22).

Brown, R. D. and Mote, P. W. (2009). The Response of Northern Hemisphere Snow Cover to a Changing Climate. *Journal of Climate*, **22**(8), 2124–2145.

Brun, E., Martin, E., Simon, V., Gendre, C., and Coleou, C. (1989). An energy and mass model of snow cover suitable for operational avalanche forecasting. *Journal of Glaciology*, **35**(121), 333–342.

Brun, E., David, P., Sudul, M., and Brunot, G. (1992). A numerical model to simulate snow-cover stratigraphy for operational avalanche forecasting. *Journal of Glaciology*, **38**(128), 13–22.

Brun, E., Martin, E., and Spiridonov, V. (1997). Coupling a multi-layered snow model with a GCM. *Annals of Glaciology*, **25**, 66–72.

Brutel-Vuilmet, C., Ménégoz, M., and Krinner, G. (2013). An analysis of present and future seasonal Northern Hemisphere land snow cover simulated by CMIP5 coupled climate models. *The Cryosphere*, **7**(1), 67–80.

Bulygina, O., Groisman, P. Y., Razuvaev, V., and Korshunova, N. (2011). Changes in snow cover characteristics over Northern Eurasia since 1966. *Environmental Research Letters*, **6**(4), 045204.

Bulygina, O. N., Razuvaev, V. N., and Korshunova, N. N. (2009). Changes in snow cover over Northern Eurasia in the last few decades. *Environmental Research Letters*, **4**(4), 045026.

Callaghan, T. V., Johansson, M., Brown, R. D., Groisman, P. Y., Labba, N., and Radionov, V. (2011a). Changing snow cover and its impacts.

Callaghan, T. V., Johansson, M., Brown, R. D., Groisman, P. Y., Labba, N., Radionov, V., Bradley, R. S., Blangy, S., Bulygina, O. N., Christensen, T. R., *et al.* (2011b). Multiple effects of changes in Arctic snow cover. *Ambio*, **40**(1), 32–45.

Cavalieri, D. J. and Parkinson, C. L. (2012). Arctic sea ice variability and trends, 1979-2010. *The Cryosphere*, **6**(4), 881.

Cayan, D. R., Kammerdiener, S. A., Dettinger, M. D., Caprio, J. M., and Peterson, D. H. (2001). Changes in the onset of spring in the western United States. *Bulletin of the American Meteorological Society*, **82**(3), 399–416.

Charlton-Perez, A. J., Baldwin, M. P., Birner, T., Black, R. X., Butler, A. H., Calvo, N., Davis, N. A., Gerber, E. P., Gillett, N., Hardiman, S., *et al.* (2013). On the lack of stratospheric dynamical variability in low-top versions of the CMIP5 models. *Journal of Geophysical Research : Atmospheres*, **118**(6), 2494–2505.

Ciais, P., Sabine, C., Bala, G., Bopp, L., Brovkin, V., Canadell, J., Chhabra, A., DeFries, R., Galloway, J., Heimann, M., *et al.* (2014). Carbon and other biogeochemical cycles. In *Climate change 2013 : the physical science basis. Contribution of Working Group I to the Fifth Assessment Report of the Intergovernmental Panel on Climate Change*, pages 465–570. Cambridge University Press.

Cohen, J. and Rind, D. (1991). The effect of snow cover on the climate. *Journal of Climate*, **4**(7), 689–706.

Cohen, J., Barlow, M., Kushner, P. J., and Saito, K. (2007). Stratosphere–troposphere coupling and links with Eurasian land surface variability. *Journal of Climate*, **20**(21), 5335–5343.

Cohen, J., Jones, J., Furtado, J. C., and Tziperman, E. (2013). Warm Arctic, cold continents : A common pattern related to Arctic sea ice melt, snow advance, and extreme winter weather. *Oceanography*, **26**(4), 150–160.

Cohen, J., Ye, H., and Jones, J. (2015). Trends and variability in rain-on-snow events. *Geophysical Research Letters*, **42**(17), 7115–7122.

Cohen, J. L., Furtado, J. C., Barlow, M. A., Alexeev, V. A., and Cherry, J. E. (2012). Arctic warming, increasing snow cover and widespread boreal winter cooling. *Environmental Research Letters*, **7**(1), 014007.

Collier, M., Jeffrey, S. J., Rotstayn, L. D., Wong, K., Dravitzki, S., Moseneder, C., Hamalainen, C., Syktus, J., Suppiah, R., Antony, J., *et al.* (2011). The CSIRO-Mk3. 6.0 Atmosphere-Ocean GCM : participation in CMIP5 and data publication. In *International Congress on Modelling and Simulation–MODSIM*.

Collins, M., Knutti, R., Arblaster, J., Dufresne, J.-L., Fichefet, T., Friedlingstein, P., Gao, X., Gutowski, W. J., Johns, T., Krinner, G., *et al.* (2013). Long-term climate change : projections, commitments and irreversibility. In *Climate Change 2013-The Physical Science Basis : Contribution of Working Group I to the Fifth Assessment Report of the Intergovernmental Panel on Climate Change*, pages 1029–1136. Cambridge University Press.

Comiso, J. C., Parkinson, C. L., Gersten, R., and Stock, L. (2008). Accelerated decline in the Arctic sea ice cover. *Geophysical research letters*, **35**(1).

Compo, G. P., Whitaker, J. S., Sardeshmukh, P. D., Matsui, N., Allan, R. J., Yin, X., Gleason, B. E., Vose, R. S., Rutledge, G., Bessemoulin, P., BrÃ¶nnimann, S., Brunet, M., Crouthamel, R. I., Grant, A. N., Groisman, P. Y., Jones, P. D., Kruk, M. C., Kruger, A. C., Marshall, G. J., Maugeri, M., Mok, H. Y., Nordli, Ø., Ross, T. F., Trigo, R. M., Wang, X. L., Woodruff, S. D., and Worley, S. J. (2011). The Twentieth Century Reanalysis Project. *Quarterly Journal of the Royal Meteorological Society*, **137**(654), 1–28.

Connolly, R., Connolly, M., Soon, W., Legates, D. R., Cionco, R. G., Velasco Herrera, V., *et al.* (2019). Northern Hemisphere Snow-Cover Trends (1967–2018) : A Comparison between Climate Models and Observations. *Geosciences*, **9**(3), 135.

Cook, B. I., Bonan, G. B., Levis, S., and Epstein, H. E. (2008). The thermoinsulation effect of snow cover within a climate model. *Climate dynamics*, **31**(1), 107–124.

Davini, P. and Cagnazzo, C. (2014). On the misinterpretation of the North Atlantic Oscillation in CMIP5 models. *Climate dynamics*, **43**(5-6), 1497–1511.

Dee, D. P., Uppala, S., Simmons, A., Berrisford, P., Poli, P., Kobayashi, S., Andrae, U., Balmaseda, M., Balsamo, G., Bauer, d. P., *et al.* (2011). The ERA-Interim reanalysis : Configuration and performance of the data assimilation system. *Quarterly Journal of the royal meteorological society*, **137**(656), 553–597.

Derksen, C. and Brown, R. (2012). Spring snow cover extent reductions in the 2008–2012 period exceeding climate model projections. *Geophysical Research Letters*, **39**(19).

Déry, S. J. and Brown, R. D. (2007). Recent Northern Hemisphere snow cover extent trends and implications for the snow-albedo feedback. *Geophysical Research Letters*, **34**(22).

Deser, C., Tomas, R., Alexander, M., and Lawrence, D. (2010). The seasonal atmospheric response to projected Arctic sea ice loss in the late twenty-first century. *Journal of Climate*, **23**(2), 333–351.

Dewey, K. F. (1977). Daily maximum and minimum temperature forecasts and the influence of snow cover. *Monthly Weather Review*, **105**(12), 1594–1597.

Domine, F., Barrere, M., and Sarrazin, D. (2016). Seasonal evolution of the effective thermal conductivity of the snow and the soil in high Arctic herb tundra at Bylot Island, Canada. *The Cryosphere*, **10**(6), 2573.

Douville, H., Royer, J.-F., and Mahfouf, J.-F. (1995). A new snow parameterization for the Meteo-France climate model. *Climate Dynamics*, **12**(1), 21–35.

Douville, H., Peings, Y., and Saint-Martin, D. (2017). Snow-(N)AO relationship revisited over the whole twentieth century. *Geophysical Research Letters*, **44**(1), 569–577.

Dufour, A., Zolina, O., and Gulev, S. K. (2016). Atmospheric Moisture Transport to the Arctic : Assessment of Reanalyses and Analysis of Transport Components. *Journal of Climate*, **29**(14), 5061–5081.

Edenhofer, O., Pichs-Madruga, R., Sokona, Y., Farahani, E., Kadner, S., Seyboth, K., Adler, A., Baum, I., Brunner, S., Eickemeier, P., Kriemann, B., Savolainen, J., S.Schlömer, von Stechow, C., Zwickdl, T., and Minx, J. (2014). Mitigation of climate change. *Contribution of Working Group III to the Fifth Assessment Report of the Intergovernmental Panel on Climate Change*, **1454**.

Essery, R. (2013). Large-scale simulations of snow albedo masking by forests. *Geophysical Research Letters*, **40**(20), 5521–5525.

Estilow, T. W., Young, A. H., and Robinson, D. A. (2015). A long-term Northern Hemisphere snow cover extent data record for climate studies and monitoring. *Earth System Science Data*, **7**(1), 137–142.

Eyring, V., Bony, S., Meehl, G. A., Senior, C. A., Stevens, B., Stouffer, R. J., and Taylor, K. E. (2016). Overview of the Coupled Model Intercomparison Project Phase 6 (CMIP6) experimental design and organization. *Geoscientific Model Development*, **9**(5), 1937–1958.

Field, C., Barros, V., Dokken, D., Mach, K., Mastrandrea, M., Bilir, T., Chatterjee, M., Ebi, K., Estrada, Y., Genova, R., Girma, B., Kissel, E., Levy, A., Mastrandrea, S. M. P., White, L., *et al.* (2014). *Climate change 2014–Impacts, adaptation and vulnerability : Regional aspects*. Cambridge University Press.

Flanner, M. G., Shell, K. M., Barlage, M., Perovich, D. K., and Tschudi, M. (2011). Radiative forcing and albedo feedback from the Northern Hemisphere cryosphere between 1979 and 2008. *Nature Geoscience*, **4**(3), 151.

Flato, G., Marotzke, J., Abiodun, B., Braconnot, P., Chou, S. C., Collins, W., Cox, P., Driouech, F., Emori, S., Eyring, V., *et al.* (2013). Evaluation of climate models. In *Climate change 2013 : the physical science basis. Contribution of Working Group I to the Fifth Assessment Report of the Intergovernmental Panel on Climate Change*, pages 741–866. Cambridge University Press.

Fletcher, C. G., Zhao, H., Kushner, P. J., and Fernandes, R. (2012). Using models and satellite observations to evaluate the strength of snow albedo feedback. *Journal of Geophysical Research : Atmospheres*, **117**(D11), n/a–n/a.

Fletcher, C. G., Thackeray, C. W., and Burgers, T. M. (2015). Evaluating biases in simulated snow albedo feedback in two generations of climate models. *Journal of Geophysical Research : Atmospheres*, **120**(1), 12–26.

Francis, J. and Skific, N. (2015). Evidence linking rapid Arctic warming to mid-latitude weather patterns. *Philosophical Transactions of the Royal Society A : Mathematical, Physical and Engineering Sciences*, **373**(2045), 20140170.

Furtado, J. C., Cohen, J. L., Butler, A. H., Riddle, E. E., and Kumar, A. (2015). Eurasian snow cover variability and links to winter climate in the CMIP5 models. *Climate dynamics*, **45**(9-10), 2591–2605.

Gao, Y., Sun, J., Li, F., He, S., Sandven, S., Yan, Q., Zhang, Z., Lohmann, K., Keenlyside, N., Furevik, T., *et al.* (2015). Arctic sea ice and Eurasian climate : a review. *Advances in Atmospheric Sciences*, **32**(1), 92–114.

Gastineau, G., García-Serrano, J., and Frankignoul, C. (2017). The Influence of Autumnal Eurasian Snow Cover on Climate and Its Link with Arctic Sea Ice Cover. *Journal of Climate*, **30**(19), 7599–7619.

Gent, P. R., Danabasoglu, G., Donner, L. J., Holland, M. M., Hunke, E. C., Jayne, S. R., Lawrence, D. M., Neale, R. B., Rasch, P. J., Vertenstein, M., Worley, P. H., Yang, Z.-L., and Zhang, M. (2011). The Community Climate System Model Version 4. *Journal of Climate*, **24**(19), 4973–4991.

Ghatak, D., Deser, C., Frei, A., Gong, G., Phillips, A., Robinson, D. A., and Stroeve, J. (2012). Simulated Siberian snow cover response to observed Arctic sea ice loss, 1979–2008. *Journal of Geophysical Research : Atmospheres*, **117**(D23).

Giorgetta, M. A., Jungclaus, J., Reick, C. H., Legutke, S., Bader, J., Böttinger, M., Brovkin, V., Crueger, T., Esch, M., Fieg, K., *et al.* (2013). Climate and carbon cycle changes from 1850 to

2100 in MPI-ESM simulations for the Coupled Model Intercomparison Project phase 5. *Journal of Advances in Modeling Earth Systems*, **5**(3), 572–597.

Gómez-Navarro, J., Montávez, J., Jerez, S., Jiménez-Guerrero, P., and Zorita, E. (2012). What is the role of the observational dataset in the evaluation and scoring of climate models ? *Geophysical Research Letters*, **39**(24).

Gouttevin, I., Menegoz, M., Dominé, F., Krinner, G., Koven, C., Ciais, P., Tarnocai, C., and Boike, J. (2012). How the insulating properties of snow affect soil carbon distribution in the continental pan-Arctic area. *Journal of Geophysical Research : Biogeosciences*, **117**(G2), n/a–n/a.

Groisman, P. and Davies, T. (2001). Snow cover and the climate system Snow Ecology ed HG Jones, JW Pomeroy, DA Walker and RW Hoham.

Groisman, P., Shugart, H., Kicklighter, D., Henebry, G., Tchebakova, N., Maksyutov, S., Monier, E., Gutman, G., Gulev, S., Qi, J., *et al.* (2017). Northern Eurasia Future Initiative (NEFI) : facing the challenges and pathways of global change in the twenty-first century. *Progress in Earth and Planetary Science*, **4**(1), 41.

Groisman, P., Bulygina, O., Henebry, G., Speranskaya, N., Shiklomanov, A., Chen, Y., Tchebakova, N., Parfenova, E., Tilinina, N., Zolina, O., *et al.* (2018). Dryland belt of Northern Eurasia : contemporary environmental changes and their consequences. *Environmental Research Letters*, **13**(11), 115008.

Groisman, P. Y., Karl, T. R., Knight, R. W., and Stenchikov, G. L. (1994). Changes of snow cover, temperature, and radiative heat balance over the Northern Hemisphere. *Journal of Climate*, **7**(11), 1633–1656.

Henderson, G. R., Peings, Y., Furtado, J. C., and Kushner, P. J. (2018). Snow–atmosphere coupling in the Northern Hemisphere. *Nature Climate Change*, page 1.

Hernández-Henríquez, M. A., Déry, S. J., and Derksen, C. (2015). Polar amplification and elevation-dependence in trends of Northern Hemisphere snow cover extent, 1971–2014. *Environmental Research Letters*, **10**(4), 044010.

Hinzman, L. D., Deal, C. J., McGuire, A. D., Mernild, S. H., Polyakov, I. V., and Walsh, J. E. (2013). Trajectory of the Arctic as an integrated system. *Ecological Applications*, **23**(8), 1837–1868.

Hobbs, P. V. (1974). Physics of ice. *Clarendon, Oxford*.

Holland, M. M., Finnis, J., Barrett, A. P., and Serreze, M. C. (2007). Projected changes in Arctic Ocean freshwater budgets. *Journal of Geophysical Research : Biogeosciences*, **112**(G4).

Hurrell, J. W., Kushnir, Y., Ottersen, G., and Visbeck, M. (2003). An overview of the North Atlantic oscillation. *Geophysical Monograph-American Geophysical Union*, **134**, 1–36.

Inoue, J., Hori, M. E., and Takaya, K. (2012). The role of Barents Sea ice in the wintertime cyclone track and emergence of a warm-Arctic cold-Siberian anomaly. *Journal of Climate*, **25**(7), 2561–2568.

IPA (2008). International Permafrost Association. https://ipa.arcticportal.org/. [Online access].

Jarraud, M. (2008). Guide to meteorological instruments and methods of observation (WMO-No. 8). *World Meteorological Organisation : Geneva, Switzerland*.

Kapnick, S. B. and Delworth, T. L. (2013). Controls of Global Snow under a Changed Climate. *Journal of Climate*, **26**(15), 5537–5562.

Kattsov, V. M. and Walsh, J. E. (2000). Twentieth-century trends of Arctic precipitation from observational data and a climate model simulation. *Journal of Climate*, **13**(8), 1362–1370.

Khan, V., Holko, L., Rubinstein, K., and Breiling, M. (2008). Snow cover characteristics over the main Russian river basins as represented by reanalyses and measured data. *Journal of Applied Meteorology and Climatology*, **47**(6), 1819–1833.

Kobayashi, S., Ota, Y., Harada, Y., Ebita, A., Moriya, M., Onoda, H., Onogi, K., Kamahori, H., Kobayashi, C., Endo, H., *et al.* (2015). The JRA-55 reanalysis : General specifications and basic characteristics. *Journal of the Meteorological Society of Japan. Ser. II*, **93**(1), 5–48.

Koenigk, T., Gao, Y., Gastineau, G., Keenlyside, N., Nakamura, T., Ogawa, F., Orsolini, Y., Semenov, V., Suo, L., Tian, T., *et al.* (2019). Impact of Arctic sea ice variations on winter temperature anomalies in northern hemispheric land areas. *Climate Dynamics*, **52**(5-6), 3111–3137.

Kolstad, E. W., Breiteig, T., and Scaife, A. A. (2010). The association between stratospheric weak polar vortex events and cold air outbreaks in the Northern Hemisphere. *Quarterly Journal of the Royal Meteorological Society*, **136**(649), 886–893.

Koven, C. D., Riley, W. J., and Stern, A. (2013). Analysis of Permafrost Thermal Dynamics and Response to Climate Change in the CMIP5 Earth System Models. *Journal of Climate*, **26**(6), 1877–1900.

Krinner, G., Derksen, C., Essery, R., Flanner, M., Hagemann, S., Clark, M., Hall, A., Rott, H., Brutel-Vuilmet, C., Kim, H., *et al.* (2018). ESM-SnowMIP : assessing snow models and quantifying snow-related climate feedbacks. *Geoscientific Model Development*, **11**, 5027–5049.

Lafaysse, M., Cluzet, B., Dumont, M., Lejeune, Y., Vionnet, V., and Morin, S. (2017). A multiphysical ensemble system of numerical snow modelling. *The Cryosphere*, **11**(3), 1173–1198.

Lawrence, D. M. and Slater, A. G. (2009). The contribution of snow condition trends to future ground climate. *Climate Dynamics*, **34**(7-8), 969–981.

Lemke, P., Ren, J., Alley, R. B., Allison, I., Carrasco, J., Flato, G., Fujii, Y., Kaser, G., Mote, P., Thomas, R. H., *et al.* (2007). Observations : changes in snow, ice and frozen ground.

Li, F. and Wang, H. (2012). Autumn sea ice cover, winter Northern Hemisphere annular mode, and winter precipitation in Eurasia. *Journal of Climate*, **26**(11), 3968–3981.

Liston, G. E. (2004). Representing subgrid snow cover heterogeneities in regional and global models. *Journal of climate*, **17**(6), 1381–1397.

Liston, G. E. and Hiemstra, C. A. (2011). The changing cryosphere : Pan-Arctic snow trends (1979–2009). *Journal of Climate*, **24**(21), 5691–5712.

Liu, J., Curry, J. A., Wang, H., Song, M., and Horton, R. M. (2012). Impact of declining Arctic sea ice on winter snowfall. *Proceedings of the National Academy of Sciences*, **109**(11), 4074–4079.

M. Rienecker, M., J. Suarez, M., Gelaro, R., Todling, R., Bacmeister, J., Liu, E., G. Bosilovich, M., Schubert, S., Takacs, L., Kim, G.-K., Bloom, S., Chen, J., Collins, D., Conaty, A., Da Silva, A., Gu, W., Joiner, J., D. Koster, R., Lucchesi, R., and Woollen, J. (2011). MERRA : NASA's Modern-Era Retrospective analysis for Research and Applications. *Journal of Climate*, **24**, 3624–3648.

Ma, J., Chadwick, R., Seo, K.-H., Dong, C., Huang, G., Foltz, G. R., and Jiang, J. H. (2018).

Responses of the tropical atmospheric circulation to climate change and connection to the hydrological cycle. *Annual Review of Earth and Planetary Sciences*, **46**, 549–580.

Magnusson, J., Wever, N., Essery, R., Helbig, N., Winstral, A., and Jonas, T. (2015). Evaluating snow models with varying process representations for hydrological applications. *Water Resources Research*, **51**(4), 2707–2723.

Mahanama, S., Livneh, B., Koster, R., Lettenmaier, D., and Reichle, R. (2012). Soil moisture, snow, and seasonal streamflow forecasts in the United States. *Journal of Hydrometeorology*, **13**(1), 189–203.

Manabe, S. (1969). Climate and the ocean circulation. *Mon. Wea. Rev*, **97**(11), 739–774.

Mankin, J. S., Viviroli, D., Singh, D., Hoekstra, A. Y., and Diffenbaugh, N. S. (2015). The potential for snow to supply human water demand in the present and future. *Environmental Research Letters*, **10**(11), 114016.

Marsh, D. R., Mills, M. J., Kinnison, D. E., Lamarque, J.-F., Calvo, N., and Polvani, L. M. (2013). Climate change from 1850 to 2005 simulated in CESM1 (WACCM). *Journal of climate*, **26**(19), 7372–7391.

Marzeion, B., Cogley, J. G., Richter, K., and Parkes, D. (2014). Attribution of global glacier mass loss to anthropogenic and natural causes. *Science*, **345**(6199), 919–921.

Maurer, E. P., Rhoads, J. D., Dubayah, R. O., and Lettenmaier, D. P. (2003). Evaluation of the snow-covered area data product from MODIS. *Hydrological Processes*, **17**(1), 59–71.

McGuire, A. D., Koven, C., Lawrence, D. M., Clein, J. S., Xia, J., Beer, C., Burke, E., Chen, G., Chen, X., Delire, C., *et al.* (2016). Variability in the sensitivity among model simulations of permafrost and carbon dynamics in the permafrost region between 1960 and 2009. *Global Biogeochemical Cycles*, **30**(7), 1015–1037.

McMichael, A. J., Haines, A., Slooff, R., *et al.* (1996). Climate change and human health : an assessment prepared by a task group on behalf of the World Health Organization, the World Meteorological Organization and the United Nations Environment Programme. In *Climate change*

and human health : an assessment prepared by a Task Group on behalf of the World Health Organization, the World Meteorological Organization and the United Nations Environment Programme. OMS.

Meehl, G. A., Boer, G. J., Covey, C., Latif, M., and Stouffer, R. J. (2000). The coupled model intercomparison project (CMIP). *Bulletin of the American Meteorological Society*, **81**(2), 313–318.

Meehl, G. A., Covey, C., McAvaney, B., Latif, M., and Stouffer, R. J. (2005). Overview of the coupled model intercomparison project. *Bulletin of the American Meteorological Society*, **86**(1), 89–93.

Meehl, G. A., Goddard, L., Murphy, J., Stouffer, R. J., Boer, G., Danabasoglu, G., Dixon, K., Giorgetta, M. A., Greene, A. M., Hawkins, E., *et al.* (2009). Decadal prediction : can it be skillful ? *Bulletin of the American Meteorological Society*, **90**(10), 1467–1486.

Mernild, S., Lipscomb, W., Bahr, D., Radić, V., and Zemp, M. (2013). Global glacier changes : a revised assessment of committed mass losses and sampling uncertainties. *The Cryosphere*, **7**(5), 1565–1577.

Meshcherskaya, A., Belyankina, I., and Golod, M. (1995). Snow depth monitoring in the main corn belt of the former Soviet Union during the period of instrumental observations. *Izv. Acad. Sci. USSR, Ser. Geogr*, **5**, 101–110.

Min, S.-K., Zhang, X., Zwiers, F. W., and Agnew, T. (2008). Human influence on Arctic sea ice detectable from early 1990s onwards. *Geophysical Research Letters*, **35**(21).

Mishra, V., Cherkauer, K. A., and Shukla, S. (2010). Assessment of drought due to historic climate variability and projected future climate change in the midwestern United States. *Journal of Hydrometeorology*, **11**(1), 46–68.

Mori, M., Watanabe, M., Shiogama, H., Inoue, J., and Kimoto, M. (2014). Robust Arctic sea-ice influence on the frequent Eurasian cold winters in past decades. *Nature Geoscience*, **7**(12), 869.

Moss, R. H., Edmonds, J. A., Hibbard, K. A., Manning, M. R., Rose, S. K., Van Vuuren, D. P., Carter, T. R., Emori, S., Kainuma, M., Kram, T., *et al.* (2010). The next generation of scenarios for climate change research and assessment. *Nature*, **463**(7282), 747.

Mouginot, J., Rignot, E., Bjørk, A. A., van den Broeke, M., Millan, R., Morlighem, M., Noël, B., Scheuchl, B., and Wood, M. (2019). Forty-six years of Greenland Ice Sheet mass balance from 1972 to 2018. *Proceedings of the National Academy of Sciences*, **116**(19), 9239–9244.

Mudryk, L., Kushner, P., and Derksen, C. (2014). Interpreting observed Northern Hemisphere snow trends with large ensembles of climate simulations. *Climate dynamics*, **43**(1-2), 345–359.

Mudryk, L., Derksen, C., Kushner, P., and Brown, R. (2015). Characterization of Northern Hemisphere snow water equivalent datasets, 1981–2010. *Journal of Climate*, **28**(20), 8037–8051.

Mudryk, L. R. and Derksen, C. (2017). CanSISE Observation-Based Ensemble of Northern Hemisphere Terrestrial Snow Water Equivalent, Version 2. *Bulletin of the American Meteorological Society*.

Mudryk, L. R., Kushner, P. J., Derksen, C., and Thackeray, C. (2017). Snow cover response to temperature in observational and climate model ensembles. *Geophysical Research Letters*, **44**(2), 919–926.

Musselman, K. N., Clark, M. P., Liu, C., Ikeda, K., and Rasmussen, R. (2017). Slower snowmelt in a warmer world. *Nature Climate Change*, **7**(3), 214.

Najafi, M. R., Zwiers, F. W., and Gillett, N. P. (2016). Attribution of the spring snow cover extent decline in the Northern Hemisphere, Eurasia and North America to anthropogenic influence. *Climatic Change*, **136**(3-4), 571–586.

Neale, R. B., Richter, J., Park, S., Lauritzen, P. H., Vavrus, S. J., Rasch, P. J., and Zhang, M. (2013). The mean climate of the Community Atmosphere Model (CAM4) in forced SST and fully coupled experiments. *Journal of Climate*, **26**(14), 5150–5168.

Ning, L. and Bradley, R. S. (2016). NAO and PNA influences on winter temperature and precipitation over the eastern United States in CMIP5 GCMs. *Climate dynamics*, **46**(3-4), 1257–1276.

Niu, G.-Y. and Yang, Z.-L. (2007). An observation-based formulation of snow cover fraction and its evaluation over large North American river basins. *Journal of Geophysical Research : Atmospheres*, **112**(D21).

Ogawa, F., Keenlyside, N., Gao, Y., Koenigk, T., Yang, S., Suo, L., Wang, T., Gastineau, G., Nakamura, T., Cheung, H. N., *et al.* (2018). Evaluating impacts of recent Arctic sea ice loss on the northern hemisphere winter climate change. *Geophysical Research Letters*, **45**(7), 3255–3263.

Orsolini, Y. J., Kindem, I., and Kvamstø, N. (2011). On the potential impact of the stratosphere upon seasonal dynamical hindcasts of the North Atlantic Oscillation : a pilot study. *Climate dynamics*, **36**(3-4), 579–588.

Parajka, J. and Blöschl, G. (2006). Validation of MODIS snow cover images over Austria. *Hydrology and Earth System Sciences Discussions*, **3**(4), 1569–1601.

Park, H., Yabuki, H., and Ohata, T. (2012). Analysis of satellite and model datasets for variability and trends in Arctic snow extent and depth, 1948–2006. *Polar Science*, **6**(1), 23–37.

Parkinson, C. L. and Comiso, J. C. (2013). On the 2012 record low Arctic sea ice cover : Combined impact of preconditioning and an August storm. *Geophysical Research Letters*, **40**(7), 1356–1361.

Peings, Y. and Douville, H. (2010). Influence of the Eurasian snow cover on the Indian summer monsoon variability in observed climatologies and CMIP3 simulations. *Climate dynamics*, **34**(5), 643–660.

Peings, Y., Saint-Martin, D., and Douville, H. (2012). A numerical sensitivity study of the influence of Siberian snow on the northern annular mode. *Journal of Climate*, **25**(2), 592–607.

Peng, G. and Meier, W. N. (2018). Temporal and regional variability of Arctic sea-ice coverage from satellite data. *Annals of Glaciology*, **59**(76pt2), 191–200.

Peng, S., Piao, S., Ciais, P., Friedlingstein, P., Zhou, L., and Wang, T. (2013). Change in snow phenology and its potential feedback to temperature in the Northern Hemisphere over the last three decades. *Environmental Research Letters*, **8**(1), 014008.

Poli, P., Hersbach, H., Dee, D. P., Berrisford, P., Simmons, A. J., Vitart, F., Laloyaux, P., Tan, D. G., Peubey, C., Thépaut, J.-N., *et al.* (2016). ERA-20C : An atmospheric reanalysis of the twentieth century. *Journal of Climate*, **29**(11), 4083–4097.

Popova, V. (2007). Winter snow depth variability over northern Eurasia in relation to recent

atmospheric circulation changes. *International Journal of Climatology : A Journal of the Royal Meteorological Society*, **27**(13), 1721–1733.

Prabhu, A., Oh, J., Kim, I.-w., Kripalani, R., Mitra, A., and Pandithurai, G. (2017). Summer monsoon rainfall variability over North East regions of India and its association with Eurasian snow, Atlantic Sea Surface temperature and Arctic Oscillation. *Climate Dynamics*, **49**(7-8), 2545–2556.

Qu, X. and Hall, A. (2007). What Controls the Strength of Snow-Albedo Feedback ? *Journal of Climate*, **20**(15), 3971–3981.

Qu, X. and Hall, A. (2013). On the persistent spread in snow-albedo feedback. *Climate Dynamics*, **42**(1-2), 69–81.

Räisänen, J. (2008). Warmer climate : less or more snow ? *Climate Dynamics*, **30**(2-3), 307–319.

Ramsay, B. H. (1998). The interactive multisensor snow and ice mapping system. *Hydrological Processes*, **12**(10-11), 1537–1546.

Rawlins, M. A., Steele, M., Holland, M. M., Adam, J. C., Cherry, J. E., Francis, J. A., Groisman, P. Y., Hinzman, L. D., Huntington, T. G., Kane, D. L., *et al.* (2010). Analysis of the Arctic system for freshwater cycle intensification : Observations and expectations. *Journal of Climate*, **23**(21), 5715–5737.

Reynolds, R. W., Smith, T. M., Liu, C., Chelton, D. B., Casey, K. S., and Schlax, M. G. (2007). Daily high-resolution-blended analyses for sea surface temperature. *Journal of Climate*, **20**(22), 5473–5496.

Rienecker, M. M., Suarez, M., Todling, R., Bacmeister, J., Takacs, L., Liu, H., Gu, W., Sienkiewicz, M., Koster, R., Gelaro, R., *et al.* (2008). The GEOS-5 Data Assimilation System : Documentation of Versions 5.0. 1, 5.1. 0, and 5.2. 0.

Riggs, G. A., Hall, D. K., and Salomonson, V. V. (2006). MODIS snow products user guide to collection 5. *Digital Media*, **80**(6), 1–80.

Robinson, D. and Estilow, T. (2012). Program : NOAA Climate Date Record (CDR) of Northern Hemisphere (NH) Snow Cover Extent (SCE), Version 1. NOAA National Climatic Data Center.

Robinson, D. A. (1993). Monitoring northern hemisphere snow cover. In *Snow Watch*, volume 92, pages 1–25.

Robinson, D. A. and Frei, A. (2000). Seasonal variability of Northern Hemisphere snow extent using visible satellite data. *The Professional Geographer*, **52**(2), 307–315.

Robinson, D. A., Dewey, K. F., and Heim Jr, R. R. (1993). Global snow cover monitoring : An update. *Bulletin of the American Meteorological Society*, **74**(9), 1689–1696.

Rodell, M. and Beaudoing, H. K. (2013). GLDAS Noah Land Surface Model l4 Monthly 0.25× 0.25 Degree Version 2.0. *Goddard Earth Sciences Data and Information Services Center : Greenbelt, MD, USA*.

Rodell, M., Houser, P. R., Jambor, U., Gottschalck, J., Mitchell, K., Meng, C.-J., Arsenault, K., Cosgrove, B., Radakovich, J., Bosilovich, M., Entin, J. K., Walker, J. P., Lohmann, D., and Toll, D. (2004). The Global Land Data Assimilation System. *Bulletin of the American Meteorological Society*, **85**(3), 381–394.

Roesch, A. (2006). Evaluation of surface albedo and snow cover in AR4 coupled climate models. *Journal of Geophysical Research : Atmospheres*, **111**(D15).

Romanovsky, V. and Osterkamp, T. (1997). Thawing of the active layer on the coastal plain of the Alaskan Arctic. *Permafrost and Periglacial processes*, **8**(1), 1–22.

Rydzik, M. and Desai, A. R. (2014). Relationship between snow extent and midlatitude disturbance centers. *Journal of Climate*, **27**(8), 2971–2982.

Saha, S., Moorthi, S., Pan, H.-L., Wu, X., Wang, J., Nadiga, S., Tripp, P., Kistler, R., Woollen, J., Behringer, D., Liu, H., Stokes, D., Grumbine, R., Gayno, G., Wang, J., Hou, Y.-T., ya Chuang, H., Juang, H.-M. H., Sela, J., Iredell, M., Treadon, R., Kleist, D., Delst, P. V., Keyser, D., Derber, J., Ek, M., Meng, J., Wei, H., Yang, R., Lord, S., van den Dool, H., Kumar, A., Wang, W., Long, C., Chelliah, M., Xue, Y., Huang, B., Schemm, J.-K., Ebisuzaki, W., Lin, R., Xie, P., Chen, M., Zhou, S., Higgins, W., Zou, C.-Z., Liu, Q., Chen, Y., Han, Y., Cucurull, L., Reynolds, R. W., Rutledge, G., and Goldberg, M. (2010). The NCEP Climate Forecast System Reanalysis. *Bulletin of the American Meteorological Society*, **91**(8), 1015–1058.

Schaffhauser, A., Adams, M., Fromm, R., Jörg, P., Luzi, G., Noferini, L., and Sailer, R. (2008). Remote sensing based retrieval of snow cover properties. *Cold Regions Science and Technology*, **54**(3), 164–175.

Schmidt, G. A., Ruedy, R., Hansen, J. E., Aleinov, I., Bell, N., Bauer, M., Bauer, S., Cairns, B., Canuto, V., Cheng, Y., Del Genio, A., Faluvegi, G., Friend, A. D., Hall, T. M., Hu, Y., Kelley, M., Kiang, N. Y., Koch, D., Lacis, A. A., Lerner, J., Lo, K. K., Miller, R. L., Nazarenko, L., Oinas, V., Perlwitz, J. P., Perlwitz, J., Rind, D., Romanou, A., Russell, G. L., Sato, M., Shindell, D. T., Stone, P. H., Sun, S., Tausnev, N., Thresher, D., and Yao, M.-S. (2006). Present day atmospheric simulations using GISS ModelE : Comparison to in-situ, satellite and reanalysis data. *J. Climate*, **19**, 153–192.

Schulzweida, U., Kornblueh, L., and Quast, R. (2006). CDO user's guide. *Climate data operators, Version*, **1**(6).

Schuur, E. A., Bockheim, J., Canadell, J. G., Euskirchen, E., Field, C. B., Goryachkin, S. V., Hagemann, S., Kuhry, P., Lafleur, P. M., Lee, H., *et al.* (2008). Vulnerability of permafrost carbon to climate change : Implications for the global carbon cycle. *BioScience*, **58**(8), 701–714.

Schuur, E. A., McGuire, A. D., Schädel, C., Grosse, G., Harden, J., Hayes, D. J., Hugelius, G., Koven, C. D., Kuhry, P., Lawrence, D. M., *et al.* (2015). Climate change and the permafrost carbon feedback. *Nature*, **520**(7546), 171.

Screen, J. A. and Simmonds, I. (2013). Exploring links between Arctic amplification and mid-latitude weather. *Geophysical Research Letters*, **40**(5), 959–964.

Senan, R., Orsolini, Y. J., Weisheimer, A., Vitart, F., Balsamo, G., Stockdale, T. N., Dutra, E., Doblas-Reyes, F. J., and Basang, D. (2016). Impact of springtime Himalayan–Tibetan Plateau snowpack on the onset of the Indian summer monsoon in coupled seasonal forecasts. *Climate Dynamics*, **47**(9-10), 2709–2725.

Serreze, M. C. and Barry, R. G. (2011). Processes and impacts of Arctic amplification : A research synthesis. *Global and planetary change*, **77**(1-2), 85–96.

Serreze, M. C. and Barry, R. G. (2014). *The Arctic climate system*. Cambridge University Press.

Serreze, M. C. and Hurst, C. M. (2000). Representation of mean Arctic precipitation from NCEP–NCAR and ERA reanalyses. *Journal of Climate*, **13**(1), 182–201.

Serreze, M. C. and Stroeve, J. (2015). Arctic sea ice trends, variability and implications for seasonal ice forecasting. *Philosophical Transactions of the Royal Society A : Mathematical, Physical and Engineering Sciences*, **373**(2045), 20140159.

Sherstyukov, B., Sherstyukov, A., and Groisman, P. Y. (2008). Impact of surface air temperature and snow cover depth on the upper soil temperature variations in Russia. In *AGU Fall Meeting Abstracts*.

Sicart, J.-E., Pomeroy, J., Essery, R., and Bewley, D. (2006). Incoming longwave radiation to melting snow : observations, sensitivity and estimation in northern environments. *Hydrological processes*, **20**(17), 3697–3708.

Singh, D., Flanner, M., and Perket, J. (2015). The global land Cryosphere Radiative Effect during the MODIS era. *The Cryosphere Discussions*, **9**, 3925–3957.

Slater, A. G., Schlosser, C. A., Desborough, C., Pitman, A., Henderson-Sellers, A., Robock, A., Vinnikov, K. Y., Entin, J., Mitchell, K., Chen, F., *et al.* (2001). The representation of snow in land surface schemes : Results from PILPS 2 (d). *Journal of Hydrometeorology*, **2**(1), 7–25.

Slater, A. G., Lawrence, D. M., and Koven, C. D. (2017). Process-level model evaluation : a snow and heat transfer metric. *The Cryosphere (Online)*, **11**(2).

Stewart, I. T. (2009). Changes in snowpack and snowmelt runoff for key mountain regions. *Hydrological Processes : An International Journal*, **23**(1), 78–94.

Streletskiy, D., Anisimov, O., and Vasiliev, A. (2015). Permafrost degradation. In *Snow and Ice-Related Hazards, Risks and Disasters*, pages 303–344. Elsevier.

Stroeve, J. C., Maslanik, J., Serreze, M. C., Rigor, I., Meier, W., and Fowler, C. (2011). Sea ice response to an extreme negative phase of the Arctic Oscillation during winter 2009/2010. *Geophysical Research Letters*, **38**(2).

SWIPA (2011). *Snow, Water, Ice and Permafrost in the Arctic (SWIPA) : Climate Change and the Cryosphere.* Arctic Monitoring and Assessment Programme (AMAP).

SWIPA (2017). Snow, Water, Ice and Permafrost in the Arctic (SWIPA) ; Summary for Policy-makers.

Takala, M., Luojus, K., Pulliainen, J., Derksen, C., Lemmetyinen, J., Kärnä, J.-P., Koskinen, J., and Bojkov, B. (2011). Estimating northern hemisphere snow water equivalent for climate research through assimilation of space-borne radiometer data and ground-based measurements. *Remote Sensing of Environment*, **115**(12), 3517 – 3529.

Taylor, K. E. (2001). Summarizing multiple aspects of model performance in a single diagram. *Journal of Geophysical Research : Atmospheres*, **106**(D7), 7183–7192.

Taylor, K. E., Balaji, V., Hankin, S., Juckes, M., Lawrence, B., and Pascoe, S. (2011). CMIP5 data reference syntax (DRS) and controlled vocabularies. *Program for Climate Model Diagnosis and Intercomparison*.

Taylor, K. E., Stouffer, R. J., and Meehl, G. A. (2012). An overview of CMIP5 and the experiment design. *Bulletin of the American Meteorological Society*, **93**(4), 485–498.

Terzago, S., von Hardenberg, J., Palazzi, E., and Provenzale, A. (2014). Snowpack changes in the Hindu Kush–Karakoram–Himalaya from CMIP5 global climate models. *Journal of Hydrometeorology*, **15**(6), 2293–2313.

Thackeray, C. W., Fletcher, C. G., and Derksen, C. (2015). Quantifying the skill of CMIP5 models in simulating seasonal albedo and snow cover evolution. *Journal of Geophysical Research : Atmospheres*, **120**(12), 5831–5849.

Thackeray, C. W., Fletcher, C. G., Mudryk, L. R., and Derksen, C. (2016). Quantifying the Uncertainty in Historical and Future Simulations of Northern Hemisphere Spring Snow Cover. *Journal of Climate*, **29**(23), 8647–8663.

Thackeray, C. W., Qu, X., and Hall, A. (2018). Why Do Models Produce Spread in Snow Albedo Feedback ? *Geophysical Research Letters*.

Van den Broeke, M. R., Enderlin, E. M., Howat, I. M., Kuipers Munneke, P., Noël, B. P., Jan Van De Berg, W., Van Meijgaard, E., and Wouters, B. (2016). On the recent contribution of the Greenland ice sheet to sea level change. *The Cryosphere*, **10**(5), 1933–1946.

Vavrus, S. (2007). The role of terrestrial snow cover in the climate system. *Climate Dynamics*, **29**(1), 73–88.

Veselov, V. (2002). PC archives of the State Data Holding and technology of their organization. *Proc. RIHMI-WDC*, **170**, 16–30.

Vihma, T. (2014). Effects of Arctic Sea Ice Decline on Weather and Climate : A Review. *Surveys in Geophysics*, **35**(5), 1175–1214.

Vincent, L., Zhang, X., Brown, R., Feng, Y., Mekis, E., Milewska, E., Wan, H., and Wang, X. (2015). Observed trends in Canada's climate and influence of low-frequency variability modes. *Journal of Climate*, **28**(11), 4545–4560.

Vionnet, V., Brun, E., Morin, S., Boone, A., Faroux, S., Le Moigne, P., Martin, E., and Willemet, J. (2012). The detailed snowpack scheme Crocus and its implementation in SURFEX v7. 2. *Geoscientific Model Development*, **5**, 773–791.

Voldoire, A., Sanchez-Gomez, E., y Mélia, D. S., Decharme, B., Cassou, C., Sénési, S., Valcke, S., Beau, I., Alias, A., Chevallier, M., Déqué, M., Deshayes, J., Douville, H., Fernandez, E., Madec, G., Maisonnave, E., Moine, M.-P., Planton, S., Saint-Martin, D., Szopa, S., Tyteca, S., Alkama, R., Belamari, S., Braun, A., Coquart, L., and Chauvin, F. (2012). The CNRM-CM5.1 global climate model : description and basic evaluation. *Climate Dynamics*, **40**(9-10), 2091–2121.

Volodin, E., A. Dianskii, N., and Gusev, A. (2010). Simulating present-day climate with the INMCM4.0 coupled model of the atmospheric and oceanic general circulations. *Izvestiya, Atmospheric and Oceanic Physics*, **46**, 414–431.

Walsh, J. E. and Ross, B. (1988). Sensitivity of 30-day dynamical forecasts to continental snow cover. *Journal of Climate*, **1**(7), 739–754.

Wang, L., Sharp, M., Brown, R., Derksen, C., and Rivard, B. (2005). Evaluation of spring snow covered area depletion in the Canadian Arctic from NOAA snow charts. *Remote Sensing of Environment*, **95**(4), 453–463.

Wang, L., Derksen, C., Brown, R., and Markus, T. (2013). Recent changes in pan Arctic melt onset from satellite passive microwave measurements. *Geophysical Research Letters*, **40**(3), 522–528.

Watanabe, M., Suzuki, T., O'ishi, R., Komuro, Y., Watanabe, S., Emori, S., Takemura, T., Chikira, M., Ogura, T., Sekiguchi, M., *et al.* (2010). Improved climate simulation by MIROC5 : mean states, variability, and climate sensitivity. *Journal of Climate*, **23**(23), 6312–6335.

Watanabe, S., Hajima, T., Sudo, K., Nagashima, T., Takemura, T., Okajima, H., Nozawa, T., Kawase, H., Abe, M., Yokohata, T., Ise, T., Sato, H., Kato, E., Takata, K., Emori, S., and Kawamiya, M. (2011). MIROC-ESM 2010 : model description and basic results of CMIP5-20c3m experiments. *Geoscientific Model Development*, **4**(4), 845–872.

Wegmann, M., Orsolini, Y., Vázquez, M., Gimeno, L., Nieto, R., Bulygina, O., Jaiser, R., Handorf, D., Rinke, A., Dethloff, K., *et al.* (2015). Arctic moisture source for Eurasian snow cover variations in autumn. *Environmental Research Letters*, **10**(5), 054015.

Wegmann, M., Orsolini, Y., Dutra, E., Bulygina, O., Sterin, A., and Brönnimann, S. (2017). Eurasian snow depth in long-term climate reanalyses.

Wegmann, M., Orsolini, Y., and Zolina, O. (2018). Warm Arctic- cold Siberia : comparing the recent and the early 20th-century Arctic warmings. *Environmental Research Letters*, **13**(2), 025009.

Westerling, A. L., Hidalgo, H. G., Cayan, D. R., and Swetnam, T. W. (2006). Warming and earlier spring increase western US forest wildfire activity. *science*, **313**(5789), 940–943.

Wiesnet, D., Ropelewski, C., Kukla, G., and Robinson, D. (1987). A discussion of the accuracy of NOAA satellite-derived global seasonal snow cover measurements. *Large Scale Effects of Seasonal Snow Cover*, **166**, 291–304.

Wilks, D. S. (2011). *Statistical methods in the atmospheric sciences*, volume 100. Academic press.

Woo, M.-K. (1980). Hydrology of a Small Lake in the Canadian High Arctic. *Arctic and Alpine Research*, **12**(2), 227–235.

Woo, M.-K. and Marsh, P. (1978). Analysis of error in the determination of snow storage for small high Arctic basins. *Journal of Applied Meteorology*, **17**(10), 1537–1541.

Wu, T., Li, W., Ji, J., Xin, X., Li, L., Wang, Z., Zhang, Y., Li, J., Zhang, F., Wei, M., *et al.* (2013). Global carbon budgets simulated by the Beijing Climate Center Climate System Model for the last century. *Journal of Geophysical Research : Atmospheres*, **118**(10), 4326–4347.

Wu, X., Che, T., Li, X., Wang, N., and Yang, X. (2018). Slower snowmelt in spring along with climate warming across the Northern Hemisphere. *Geophysical Research Letters*, **45**(22), 12–331.

Xu, L. and Dirmeyer, P. (2013). Snow–Atmosphere Coupling Strength. Part II : Albedo Effect Versus Hydrological Effect. *Journal of Hydrometeorology*, **14**(2), 404–418.

Ye, K. (2019). Interannual variability of March snow mass over Northern Eurasia and its relation to the concurrent and preceding surface air temperature, precipitation and atmospheric circulation. *Climate Dynamics*, **52**(5-6), 2813–2836.

Yukimoto, S., Adachi, Y., Hosaka, M., Sakami, T., Yoshimura, H., Hirabara, M., Tanaka, T. Y., Shindo, E., Tsujino, H., Deushi, M., *et al.* (2012). A new global climate model of the Meteorological Research Institute : MRI-CGCM3 model description and basic performance. *Journal of the Meteorological Society of Japan. Ser. II*, **90**, 23–64.

Zhang, T., Osterkamp, T. E., and Stamnes, K. (1996). Influence of the depth hoar layer of the seasonal snow cover on the ground thermal regime. *Water Resources Research*, **32**(7), 2075–2086.

Zhang, T., Wang, T., Krinner, G., Wang, X., Gasser, T., Peng, S., Piao, S., and Yao, T. (2019). The weakening relationship between Eurasian spring snow cover and Indian summer monsoon rainfall. *Science Advances*, **5**(3), eaau8932.

Zhong, X., Zhang, T., Kang, S., Wang, K., Zheng, L., Hu, Y., and Wang, H. (2018). Spatiotemporal variability of snow depth across the Eurasian continent from 1966 to 2012. *The Cryosphere*, **12**(1), 227–245.